R/V Mirai Cruise Report

MR19-03C

Arctic Challenge for Sustainability (ArCS)

Arctic Ocean, Bering Sea and North Pacific

28 September 2019 – 10 November 2019

Japan Agency for Marine-Earth Science and Technology (JAMSTEC)

Contents

1. Cruise Summary

1.1 Objectives

In recent years, sea-ice freeze-up has been delayed over both the northern Bering Sea and the Chukchi Sea during autumn, causing decline in Arctic sea-ice extent in autumn and winter. The decreased sea-ice extent leads to changes in the atmosphere, ocean and ecosystem of the Arctic region that affect not only the regional but also the global climate.

The objectives of this cruise were as follows:

(1) To quantify ongoing changes in the atmosphere, sea ice, ocean and ecosystem, including wave characteristics and the environmental chemical cycle during autumn
(2) To understand the processes of and interactions between the atmosphere, sea ice, ocean and ecosystem
(3) To investigate the influence of Arctic Ocean change on global climate during autumn

In addition to the above, the Multidisciplinary drifting Observatory for the Study of Arctic Climate (MOSAiC) expedition commenced in September 2019, during which year-round measurements will be obtained by the German icebreaker Polarstern. The combination of MOSAiC and our cruise provides a great opportunity to investigate differences in atmospheric and oceanographic structures between areas of sea ice and open water.

1.2 Basic information

|	
Cruise ID:	MR19-03C
Name of vessel:	R/V Mirai
	L x B x D 118.02 m x 19.0 m x 13.2 m
	Gross Tonnage: 8,706 tons
	Call Sign JNSR
Title of the cruise:	Arctic Challenge for Sustainability (ArCS)
Undertaking institute:	Japan Agency for Marine-Earth Science and Technology (JAMSTEC)
Chief scientist:	Kazutoshi Sato (Kitami Institute of Technology)
Cruise period:	27 September 2019 – 10 November 2019
Ports of call:	27 September 2019, Sekinehama (departure from port)
	29 September 2019, Hachinohe (arrival in and departure from port)
	10 November 2019, Hachinohe (arrival in port)
Research area:	The North Pacific Ocean, Bering Sea and Arctic Ocean
Research Map:	
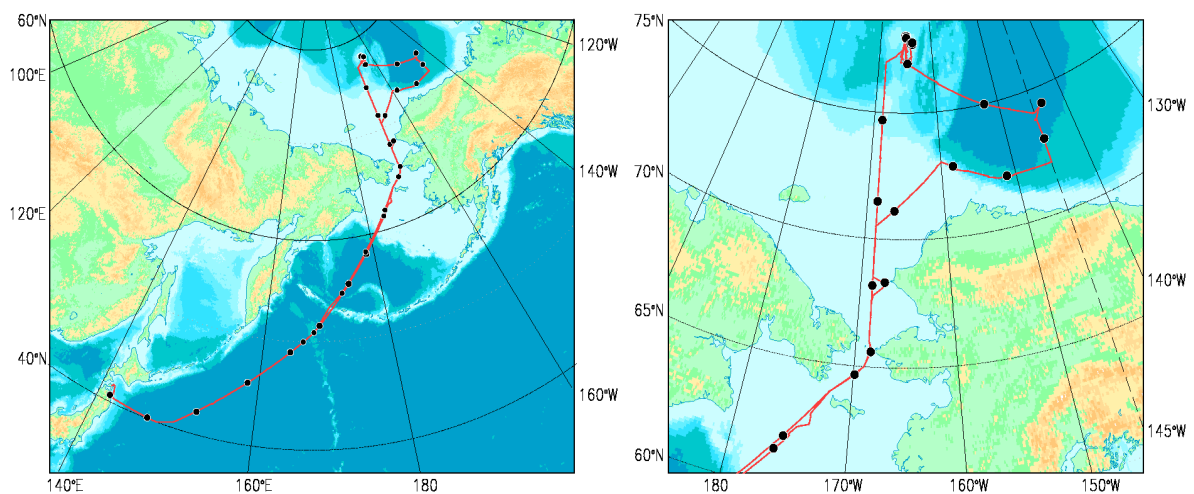
Figure 1.2: Cruise track and location points at 00UTC for each day of MR19-03C.

1.3 Atmospheric and Oceanographic Overview during the cruise

Meteorological and oceanographic observations were conducted in the North Pacific Ocean, Bering Sea and Arctic Ocean onboard the R/V Mirai from 28 September 2019 to 10 November 2019 as part of the Arctic Challenge for Sustainability (ArCS) project (Figure 1.2). During this cruise, the R/V Mirai was able to enter the northern Chukchi Sea (78.2°N) because the sea-ice extent during October in the Arctic Ocean (particularly the Chukchi and Beaufort seas) was at its lowest minimum level since 2002. Based on NCEP CFSR reanalysis data, a negative sea-ice concentration anomaly was found over the Chukchi Sea in comparison with the early 2000s (Figure 1.3-1 left). The monthly averaged sea surface temperature (SST) was abnormally high (>2 °C) over the northern Chukchi Sea (Figure 1.3-1 right) during October, suggesting that delay in freezing in the northern Chukchi Sea was likely.
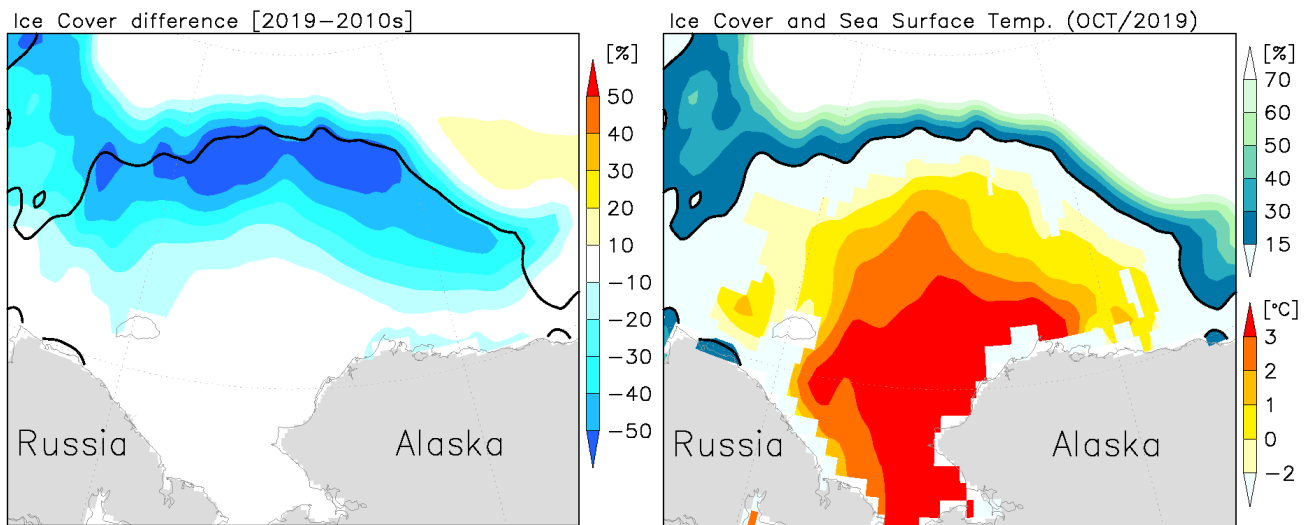

Figure 1.3-1: (Left) Map of difference in ice cover between 2019 and the 2010s during October (shaded) with ice area exceeding 15% in October 2019 (contour). (Right) Map of averaged ice cover and sea surface temperature during October 2019 derived from NCEP CFSR reanalysis data.

We performed conductivity–temperature–depth (CTD) observations to investigate the vertical structure of the ocean and to sample water across the Arctic Ocean (Table 1.3). In conjunction with the CTD observations, zooplankton samples were also collected using plankton nets. Over the southern Chukchi Sea, a Smith–McIntyre sampler was used to collect sea bottom sediments. Tethered-balloon observations were conducted to measure vertical profiles of particle number concentration, BC mass concentration and particle size distribution over the Pacific and Arctic oceans. Over the sea-ice area, surface temperature and the distribution of sea ice were monitored by drone observations. To measure wave heights and upper-ocean currents, drifting buoys were deployed over the Canada Basin and near Barrow.

Following wave buoy deployments over ice-free and ice-covered regions in the Canada Basin on 13 October, we performed a daily repeat section over the northern Chukchi Sea (Figure 1.3-2). This repeat section included stations in the marginal ice zone (MIZ) and in the open-water zone. Each day, we had one station in the MIZ and three–four stations in the open-water zone. The position of the MIZ station varied daily due to sea-ice advance/retreat. During the period of the repeat section, CTD, plankton and cloud particle sensor (CPS) observations were conducted in the open-water area during nighttime every day. Tethered-balloon and drone observations were performed over the MIZ when the wind speed was weaker than approximately 5 m/s. Radiosonde observations were conducted at 6-h intervals.
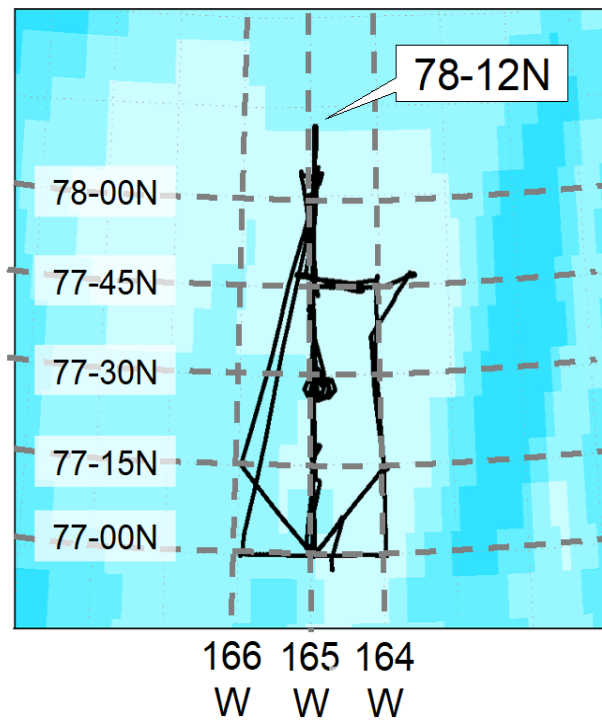
Figure 1.3-2: Map of repeat section.
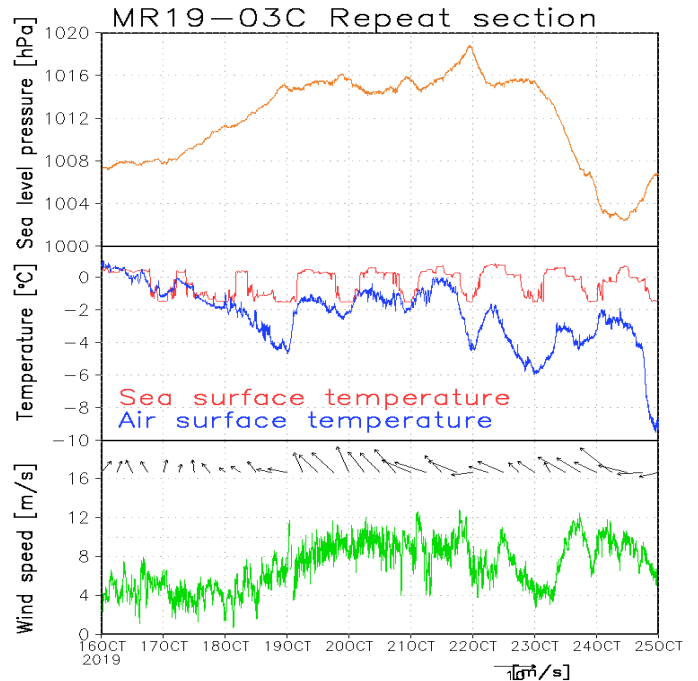
Figure 1.3-3: Time series of sea level pressure, air/sea surface temperatures and wind speeds, observed by the RV Mirai during the repeat section.

There were two weather regimes during the repeat section (Figure 1.3-3). The first was characterized by a moderate southerly wind and high surface air temperatures (around -2 °C) from the open-water area (16–22 October). On the first day of the repeat section, small ice floes were found in the northern part (around 78°N) of the repeat section (Figure 1.3-4). However, warm air advection reduced sea-ice formation. The second weather regime was characterized by a moderate southwesterly wind with low surface air temperatures (around -4 °C) from the sea-ice area (23–25 October). Overall, this repeat section provided unique opportunities to understand the recent delay in freezing during early autumn.

In undertaking this challenging cruise, precise weather and sea-ice forecasts were necessary for safe navigation and valuable observing activities. This cruise was supported by operational forecasts provided by the ECMWF and ECCC as a part of the Year of Polar Prediction (YOPP). In addition, the Japanese National Institute of Polar Research (NIPR) has developed the Vessel Navigation Unit support System (VENUS) that allows forecast data to be received and processed automatically onboard a ship. To determine appropriate observation points and to manage the cruise schedule, the chief scientist used these useful sources of information, particularly near the sea-ice area.

Figure 1.3-4: Photos taken at northernmost point in the marginal ice zone for each day (left to right: 16, 17, 18 and 19 November 2019) during the repeat section.

Table 1.3: List of observation points of MR19-03C

Sta. no for schedule	Information						Activities						
							CTD	XCTD	RINKO	NORPAC net	Ring net	Closing net	Sediments net
sta. 000		50	0.00	N	166	7.63	E	○ (000-1,2)		○ (000)			
sta. 001		62	0.60	N	175	3.60	W						
sta. 002		62	3.00	N	175	12.60	W						
sta. 003		62	13.14	N	174	52.62	W						
sta. 004		62	23.40	N	174	34.20	W						
sta. 005		62	28.08	N	174	4.98	W						
sta. 006		62	33.60	N	173	33.00	W						
sta. 007		62	47.22	N	173	30.00	W						
sta. 008		63	2.00	N	173	27.60	W						
sta. 009		63	16.80	N	173	4.80	W						
sta. 010		63	36.24	N	172	35.46	W						
FP-1		64	40.13	N	169	55.15	W			○ (001)	○			○
sta. 011		65	38.00	N	168	28.00	W	○ (001)			○			
sta. 012		66	0.00	N	168	45.00	W	○ (002)						
sta. 013		66	30.00	N	168	45.00	W	○ (003)			○			
sta. 014		67	0.00	N	168	45.00	W	○ (004)			○		○	○
sta. 015		67	30.00	N	168	45.00	W		○					
sta. 016		68	0.00	N	168	45.00	W		○					
FT-1		68	9.91	N	168	45.38	W			○ (002)				
sta. 017		68	30.00	N	168	45.00	W		○					
sta. 018		69	0.00	N	168	45.00	W	○ (005)			○			○
sta. 019		69	30.00	N	168	45.00	W	○ (006)			○			
sta. 020		70	0.00	N	168	45.00	W	○ (007)						
sta. 021		70	30.00	N	168	45.00	W	○ (008)			○		○	○
sta. 022		71	0.00	N	167	0.00	W		○					
FT-2		71	6.54	N	166	30.65	W			○ (003)				
sta. 023		71	30.00	N	165	15.00	W		○					
sta. 024		72	0.00	N	163	30.00	W	○ (009)			○		○	○

sta. 025		72	30.00	N	161	45.00	W	○ (010)			○		
sta. 026		73	0.00	N	160	0.00	W	○ (011)			○		
sta. 027		72	50.00	N	158	45.00	W						
FT-3		72	46.90	N	158	22.49	W			○ (004)			
sta. 028		72	40.00	N	157	30.00	W						
sta. 029		72	30.00	N	156	15.00	W	○ (012)			○		
sta. 030		72	20.00	N	155	0.00	W	○ (013)			○		
sta. 031		72	10.00	N	153	45.00	W	○ (014)			○		
sta. 032		72	0.00	N	152	30.00	W						
FT-4		72	0.62	N	151	17.73	W			○ (005)			
sta. 033		72	0.00	N	150	0.00	W						
sta. 034		72	0.00	N	147	30.00	W	○ (015)	○		○		
sta. 035		72	0.00	N	145	0.00	W	○ (016)			○		
FT-5		72	58.53	N	144	55.52	W			○ (006)			
sta. 036		73	0.00	N	145	0.00	W						
sta. 037		74	0.00	N	145	0.00	W						
FT-6		74	20.08	N	143	30.89	W			○ (007)			
FP-2		74	46.09	N	150	30.13	W	○ (017)			○		○
FT-7		74	59.96	N	152	16.15	W			○ (008)			
FP-3		76	27.95	N	161	38.51	W	○ (018)			○		
sta. 038		76	30.00	N	165	0.00	W						
FT-8		76	57.80	N	164	45.19	W			○ (009)			
sta. 39-1	Repaeat Day 1	77	0.00	N	165	0.00	W	○ (019-1)			○	○	
sta. 40-1	Repaeat Day 1	77	15.00	N	165	0.00	W	○ (020-1)					
FP-4	Repaeat Day 1	77	15.10	N	164	59.48	W			○ (010)			
FT-9 (MIZ-1)	Repaeat Day 1	78	3.94	N	164	56.89	W			○ (011)	○	○	
FP-5	Repaeat Day 1	77	53.38	N	164	59.98	W			○ (012)			

8

sta. 40-2	Repaeat Day 2	77	15.00	N	165	0.00	W	○ (020-2)				○	○
sta. 41-1	Repaeat Day 2	77	30.00	N	165	0.00	W	○ (021-1)					
sta. 42-1	Repaeat Day 2	77	45.00	N	165	0.00	W	○ (022-1)				○	
FT-10 (MIZ-2)	Repaeat Day 2	78	0.28	N	164	59.05	W			○ (013)		○	○
FP-6	Repaeat Day 2	77	45.12	N	165	0.00	W			○ (014)			
sta. 40-3	Repaeat Day 3	77	15.00	N	165	0.00	W	○ (020-3)				○	○
sta. 41-2	Repaeat Day 3	77	30.00	N	165	0.00	W	○ (021-2)					
sta. 42-2	Repaeat Day 3	77	45.00	N	165	0.00	W	○ (022-2)				○	
FP-7	Repaeat Day 3	78	2.13	N	164	58.49	W	○ (022-2)					
FT-11 (MIZ-3)	Repaeat Day 3	78	3.87	N	165	10.12	W	○ (023)		○ (015)		○	○
FP-8	Repaeat Day 3	77	45.21	N	164	59.79	W			○ (016)			
sta. 39-2	Repaeat Day 4	77	0.00	N	165	0.00	W	○ (019-2)				○	○
sta. 40-4	Repaeat Day 4	77	15.00	N	165	0.00	W	○ (020-4)					
sta. 41-3	Repaeat Day 4	77	30.00	N	165	0.00	W	○ (021-3)				○	
FT-12 (MIZ-4)	Repaeat Day 4	78	3.06	N	164	59.60	W			○ (017)		○	○
FP-9	Repaeat Day 4	77	45.16	N	165	0.32	W			○ (018)			
sta. 39-3	Repaeat Day 5	77	0.00	N	165	0.00	W	○ (019-3)				○	○
sta. 40-5	Repaeat Day 5	77	15.00	N	165	0.00	W	○ (020-5)					
sta. 41-4	Repaeat Day 5	77	30.00	N	165	0.00	W	○ (021-4)				○	
FP-10	Repaeat Day 5	77	44.98	N	164	59.95	W			○ (019)			
FT-13 (MIZ-5)	Repaeat Day 5	78	0.92	N	164	58.44	W			○ (020)		○	○
sta. 043	Repaeat Day 6	77	15.00	N	166	0.00	W	○ (024)				○	○
sta. 39-4	Repaeat Day 6	77	0.00	N	165	0.00	W	○ (019-4)				○	○
sta. 40-6	Repaeat Day 6	77	15.00	N	165	0.00	W	○ (020-6)					
sta. 41-5	Repaeat Day 6	77	30.00	N	165	0.00	W	○ (021-5)					

FP-11	Repaeat Day 6	77	44.87	N	164	59.98	W			○ (021)			
FT-14 (MIZ-6)	Repaeat Day 6	78	1.55	N	164	57.64	W			○ (022)	○	○	
sta. 044	Repaeat Day 7	77	0.00	N	166	0.00	W	○ (025)			○	○	
sta. 39-5	Repaeat Day 7	77	0.00	N	165	0.00	W	○ (019-5)			○	○	
sta. 40-7	Repaeat Day 7	77	15.00	N	165	0.00	W	○ (020-7)					
sta. 41-6	Repaeat Day 7	77	30.00	N	165	0.00	W	○ (021-6)					
FP-12	Repaeat Day 7	77	44.96	N	165	0.00	W			○ (023)			
FT-15 (MIZ-7)	Repaeat Day 7	77	46.14	N	164	5.42	W			○ (024)	○	○	
sta. 045	Repaeat Day 8	77	0.00	N	164	0.00	W	○ (026)			○	○	
sta. 39-6	Repaeat Day 8	77	0.00	N	165	0.00	W	○ (019-6)			○	○	
sta. 40-8	Repaeat Day 8	77	15.00	N	165	0.00	W	○ (020-8)					
sta. 41-7	Repaeat Day 8	77	30.00	N	165	0.00	W	○ (021-7)					
FP-13	Repaeat Day 8	77	44.98	N	165	0.31	W			○ (025)			
FT-16 (MIZ-8)	Repaeat Day 8	77	47.02	N	163	35.81	W			○ (026)	○	○	
sta. 046	Repaeat Day 9	77	15.00	N	164	0.00	W	○ (027)			○	○	
sta. 39-7	Repaeat Day 9	77	0.00	N	165	0.00	W	○ (019-7)			○	○	
sta. 40-9	Repaeat Day 9	77	15.00	N	165	0.00	W	○ (020-9)					
sta. 41-8	Repaeat Day 9	77	30.00	N	165	0.00	W	○ (021-8)					
FP-14	Repaeat Day 9	77	44.99	N	165	0.32	W			○ (027)			
FT-17 (MIZ-9)	Repaeat Day 9	77	47.62	N	163	40.60	W			○ (028)	○	○	
sta. 046		77	15.00	N	164	0.00	W						
sta. 047		77	30.00	N	168	45.00	W						
sta. 048		77	15.00	N	168	45.00	W						
sta. 049		77	0.00	N	168	45.00	W	○ (028)			○	○	
sta. 050		76	0.00	N	168	45.00	W		○				
sta. 051		75	0.00	N	168	45.00	W						
FT-18		74	41.30	N	168	45.66	W			○ (029)	○		

sta. 052		74	0.00	N	168	45.00	W	○ (029)			○	○	
sta. 053		73	30.00	N	168	45.00	W	○ (030)					
sta. 054		73	0.00	N	168	45.00	W	○ (031)			○	○	
sta. 055		72	30.00	N	168	45.00	W	○ (032)					
sta.056		72	0.00	N	168	45.00	W			○ (030-1, 2)	○		
sta.057 (FT-19)		71	30.00	N	168	45.00	W			○ (031)			
sta. 058		71	0.00	N	168	45.00	W			○ (032)	○	○	
sta. 059		70	30.00	N	168	45.00	W	○ (033)					
sta. 060		70	0.00	N	168	45.00	W	○ (034)			○	○		○
sta. 061		69	30.00	N	168	45.00	W	○ (035)			○	○	
sta. 062		69	0.00	N	168	45.00	W	○ (036)			○	○	
sta. 063		68	30.00	N	168	45.00	W			○ (033)	○	○	
FT-20		68	18.12	N	167	23.01	W			○ (034)			
sta. 064		68	18.00	N	166	56.10	W				○		
sta. 065		68	14.52	N	167	7.32	W						
sta. 066		68	11.10	N	167	18.48	W						
sta. 067		68	7.68	N	167	29.70	W						
sta. 068		68	0.78	N	167	52.02	W	○ (037)			○	○		○
sta. 069		67	53.88	N	168	14.10	W						
sta. 070		67	46.98	N	168	36.12	W	○ (038)			○	○		○
sta. 071		67	30.00	N	168	45.00	W	○ (039)			○		
sta. 072		67	0.00	N	168	45.00	W	○ (040)			○		
sta. 073		66	30.00	N	168	45.00	W	○ (041)					
sta. 074		66	0.00	N	168	45.00	W			○ (035)			
FT-21		65	36.85	N	168	28.79	W			○ (036)			
sta. 000-2		50	0.00	N	166	7.63	E	○ (000-3,4)	○	○ (037)			

11

1.4 List of participants

Table 1.4: List of participants of MR19-03C

No.	Name	Organization	Position
1	Kazutoshi Sato	Kitami Institute of Technology (KIT)	Assistant professor
2	Akihiko Murata	Japan Agency for Marine-Earth Science and Technology (JAMSTEC)	Superior researcher
3	Jun Inoue	National Institute of Polar Research (NIPR)	Associate professor
4	Jumpei Yamamoto	Tokyo University of Marine Science and Technology	Graduate student
5	Rio Maya	Tokyo University of Marine Science and Technology	Project researcher
6	Eri Yoshizawa	Korea Polar Research Institute	Research scientist
7	Tsubasa Kodaira	The University of Tokyo	Assistant professor
8	Ryo Kusakawa	The University of Tokyo	Graduate student
9	Eun Yae Son	The University of Tokyo	Graduate student
10	Kohei Matsuno	Hokkaido University	Assistant professor
11	Koki Tokuhiro	Hokkaido University	Graduate student
12	Fumihiko Kimura	Hokkaido University	Graduate student
13	Nao Sato	Hokkaido University	Graduate student
14	Hotaek Park	Japan Agency for Marine-Earth Science and Technology (JAMSTEC)	Senior scientist
15	Fumikazu Taketani	Japan Agency for Marine-Earth Science and Technology (JAMSTEC)	Senior scientist
16	Taro Maruo	Japan Agency for Marine-Earth Science and Technology (JAMSTEC) / University of Kobe	Research student / Graduate student
17	Minoru Hamana	Japan Agency for Marine-Earth Science and Technology (JAMSTEC)	Research scientist
18	Ryo Oyama	Nippon Marine Enterprises, Ltd. (NME)	Technical staff
19	Souichiro Sueyoshi	Nippon Marine Enterprises, Ltd. (NME)	Technical staff
20	Shinya Okumura	Nippon Marine Enterprises, Ltd. (NME)	Technical staff
21	Kazuho Yoshida	Nippon Marine Enterprises, Ltd. (NME)	Technical staff
22	Yutaro Murakami	Nippon Marine Enterprises, Ltd. (NME)	Technical staff
23	Masanori Enoki	Marine Works Japan Ltd. (MWJ)	Technical staff
24	Jun Matsuoka	Marine Works Japan Ltd. (MWJ)	Technical staff
25	Masahiro Orui	Marine Works Japan Ltd. (MWJ)	Technical staff
26	Shinichiro Yokogawa	Marine Works Japan Ltd. (MWJ)	Technical staff
27	Keitaro Matsumoto	Marine Works Japan Ltd. (MWJ)	Technical staff
28	Hiroshi Hoshino	Marine Works Japan Ltd. (MWJ)	Technical staff
29	Atsushi Ono	Marine Works Japan Ltd. (MWJ)	Technical staff
30	Tomomi Sone	Marine Works Japan Ltd. (MWJ)	Technical staff
31	Erii Irie	Marine Works Japan Ltd. (MWJ)	Technical staff
32	Yuko Miyoshi	Marine Works Japan Ltd. (MWJ)	Technical staff
33	Mikio Kitada	Marine Works Japan Ltd. (MWJ)	Technical staff
34	Shinsuke Toyota	Marine Works Japan Ltd. (MWJ)	Technical staff
35	Shungo Oshitani	Marine Works Japan Ltd. (MWJ)	Technical staff
36	Rio Kobayashi	Marine Works Japan Ltd. (MWJ)	Technical staff
37	Kanako Yoshida	Marine Works Japan Ltd. (MWJ)	Technical staff
38	Tun Htet Aung	Marine Works Japan Ltd. (MWJ)	Technical staff
39	David Snider	Martech Polar Consulting Ltd.	Ice Navigator

2. Meteorology

2.1 GPS Radiosonde

(1) Personnel

Jun Inoue	NIPR	- Principle Investigator (PI)
Kazutoshi Sato	KIT	
Jumpei Yamamoto	Tokyo University of Marine Science and Technology	
Hotaek Park	JAMSTEC	
Taro Maruo	JAMSTEC	
Ryo Oyama	NME	
Shinya Okumura	NME	
Kazuho Yoshida	NME	
Yutaro Murakami	NME	
Soichiro Sueyoshi	NME	

(2) Objectives

To understand the thermodynamic structure of the boundary layer, as well as the characteristics of migratory cyclones and anticyclones, GPS radiosonde observations were performed from 12 UTC 30 September 2019 to 00 UTC 1 November 2019. The data obtained will be used mainly for studies of clouds, validation both of reanalysis data and of satellite analyses, as well as data assimilation. The data were also used during the cruise for briefing information with regard to drone flights (Section 2.6) and tethered-balloon launches (Section 2.10.2).

(3) Parameters

Temperature, Humidity, Pressure, Wind speed and direction.

(4) Instruments and Methods

Two types of GPS radiosonde were used: the Vaisala RS41-SG for 00 and 12 UTC launches, and the Vaisala RS41-SGP for 06 and 18 UTC launches. The observing frequency over the Arctic Ocean (north of the Bering Strait) was four times per day (00, 06, 12 and 18 UTC), while that over other areas (i.e., the Bering Sea and North Pacific Ocean) was twice per day (00 and 12 UTC). The software (MW41 Vaisala Sounding System; version 2.11.0), processor (SPS311), GPS antenna (GA20), UHF antenna (RB21) and balloon launcher (ASAP) used were all from Vaisala Oyj. Prior to launch, the humidity, air temperature and pressure sensors were calibrated using the calibrator system (RI41 and PTB330, Vaisala). In cases when the wind relative to the ship was not appropriate for launch, the handy launch method was selected. For every launch, a Totex 350 g balloon was used.

Several simultaneous observations were performed with CPS sondes (Section 2.2), mainly during the night (e.g., 06 UTC), which are identified in the remarks in Table 2.1 as "CPS exp." Most data were entered into the Global Telecommunication System (GTS) though the Japan Meteorological Agency immediately after each observation and thus were available for use in operational weather forecasts.

(5) Station list

Table 2.1 summarizes the log of the GPS radiosonde observations. Raw data were recorded in binary format during ascent. ASCII data were converted from raw data.

(6) Preliminary results

The locations of all radiosonde observations performed during the cruise are shown in Figure 2.1-1. A time–height cross section of observed air temperature and wind during the cruise is shown in Figure 2.1-2.

During 16–25 October, a daily repeat section was undertaken to elucidate the differences in atmospheric and oceanic characteristics between the MIZ and the open-ocean zone. During the repeat period, radiosonde observations were conducted near the MIZ at 00 UTC (at the northernmost point in the section), while observations at the southernmost location were performed at 18 UTC.

During most of the period, conditions were characterized by southerly winds associated with low pressure systems over the Bering Sea, enhancing the intrusion of warm air masses into the north of the Chukchi Sea. The tropopause height was recorded at 11 km (abnormally high for this season) at 78°N over the MIZ. On the final day of the repeat section (25 October), strong northerly winds prevailed bringing relatively cold air from the northern sea-ice region.

(7) Data archive

   The data obtained during the cruise will be submitted to the Data Management Group of JAMSTEC, and they will be made available to the public via the "Data Research System for Whole Cruise Information in JAMSTEC (DARWIN)" on the JAMSTEC website (http://www.godac.jamstec.go.jp/darwin/e)

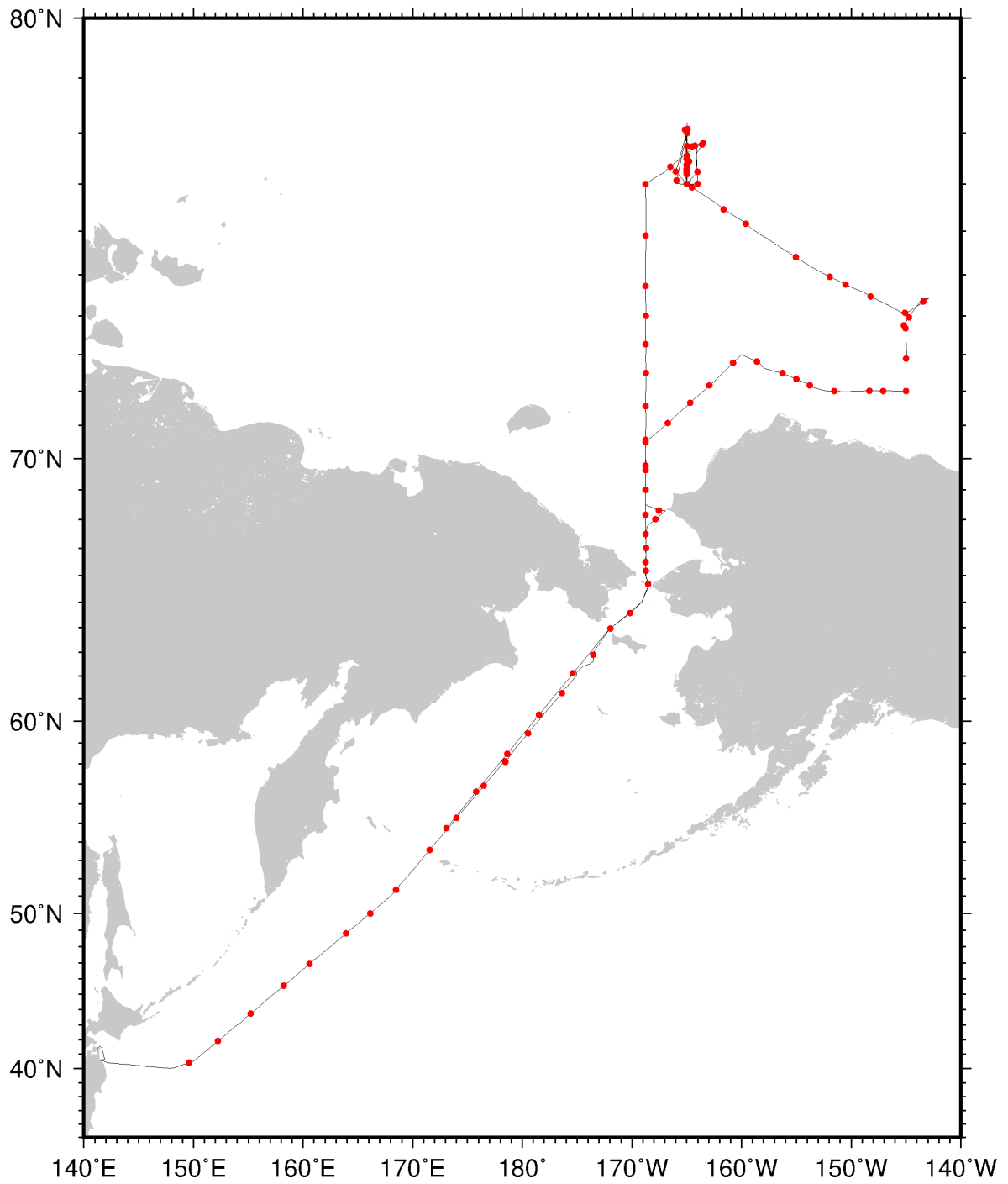# GPS radiosonde observation point

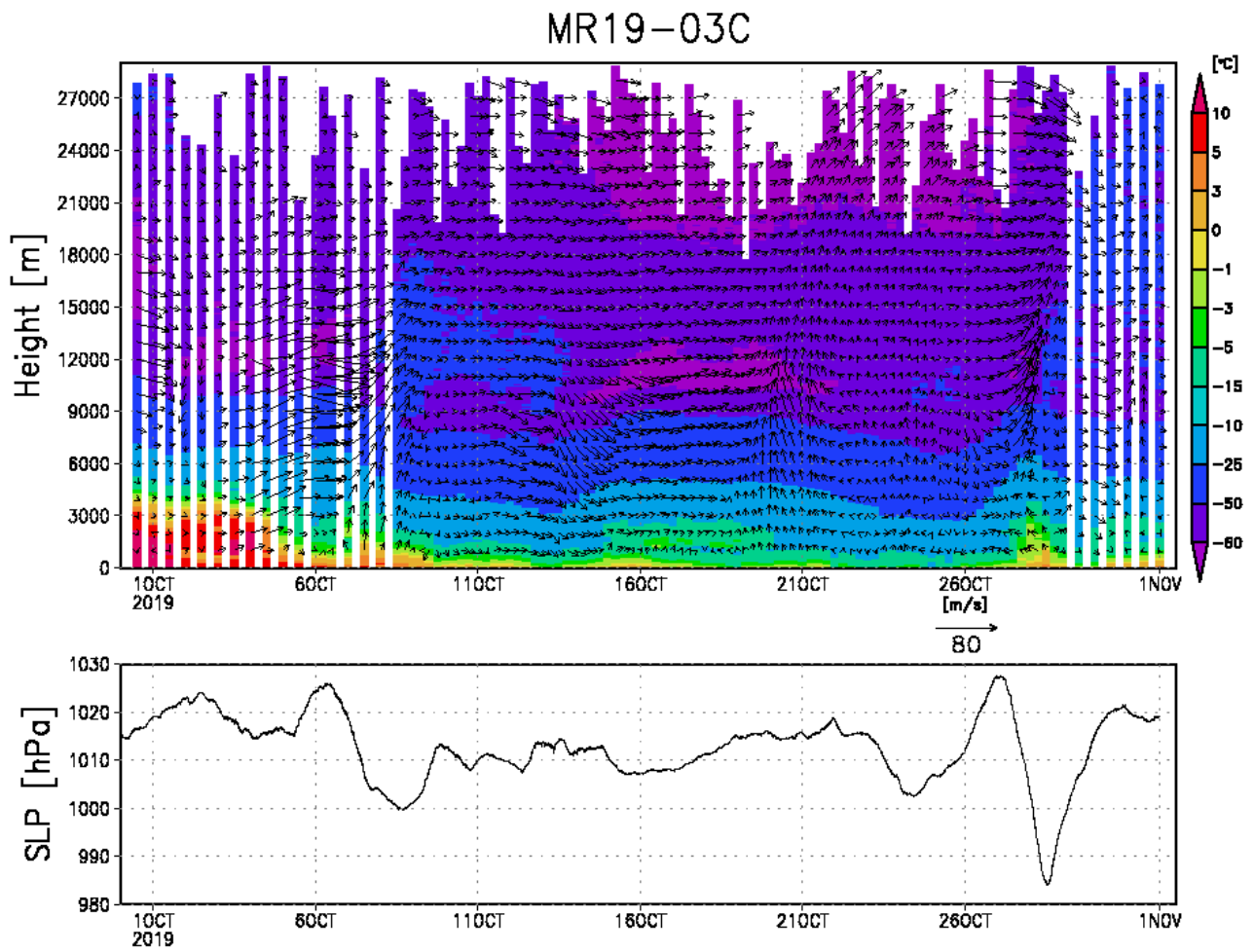Figure 2.1-1: Sounding stations during the cruise.

Figure 2.1-2: (a) Time-height cross section of air temperature (shading) and wind (vectors), and (b) time series of sea level pressure.

Table 2.1: Launch log

ID	Date YYYYMM DDHH	Latitude degN	Longitude degE	Psfc hPa	Tsfc degC	RHsfc %	WD deg	Wsp m/s	SST degC	Max height hPa	Max height m	Max height Duration	Cloud Amount	Cloud Type	remarks
RS001	2019093012	40.405	149.586	1014.3	19.5	84	335	8.6	21.77	16.4	27906	6694	-	-	
RS002	2019100100	41.910	152.235	1016.5	19.1	74	63	6.9	19.58	15.2	28388	6475	9	Cu,Sc	
RS003	2019100112	43.744	155.215	1018.7	12.5	98	56	7.0	13.53	15.1	28406	6656	-	-	
RS004	2019100200	45.558	158.235	1020.6	9.7	83	44	5.5	11.29	26.1	24827	5456	10	St	
RS005	2019100212	46.937	160.596	1021.7	7.9	69	245	2.9	9.57	28.2	24334	5637	-	-	
RS006	2019100300	48.803	163.926	1019.1	8.3	78	241	11.1	9.43	18.1	27178	5600	10	Sc	
RS007	2019100312	49.991	166.129	1016.0	9.4	85	232	14.6	9.33	30.8	23760	5326	-	-	
RS008	2019100400	51.359	168.484	1013.2	9.9	96	234	14.5	9.87	14.9	28411	6206	10	St	
RS009	2019100412	53.579	171.543	1013.3	9.9	90	244	10.0	9.77	13.8	28862	7109	-	-	
RS010	2019100500	55.281	174.007	1014.2	8.4	85	171	6.1	9.94	15	28318	6233	10	Cu,Sc	
RS011	2019100512	56.916	176.484	1015.3	7.5	77	325	9.5	9.82	45.6	21206	4974	-	-	
RS012	2019100600	58.118	178.431	1022.0	6.1	55	338	1.6	9.52	30.7	23743	5146	1	As	
RS013	2019100602	58.081	178.454	1022.3	6.3	54	115	0.7	9.58	16.7	27675	6256	9	Sc,As	
RS014	2019100612	59.435	-179.475	1023.2	5.1	61	153	2.7	9.06	21.6	26005	6124	-	-	
RS015	2019100700	61.255	-176.396	1017.3	5.5	72	144	13.5	7.39	17.9	27201	6127	10	Cu,As	
RS016	2019100712	62.898	-173.539	1005.6	5.8	96	140	15.0	5.71	34.3	22987	5066	-	-	
RS017	2019100800	64.580	-170.164	1001.5	4.1	100	185	8.8	2.55	15.2	28198	6188	10	St	
RS018	2019100812	66.187	-168.743	998.3	5.6	90	206	12.6	5.60	48.9	20648	5233	-	-	
RS019	2019100818	67.013	-168.708	997.5	4.8	90	187	11.3	7.07	30.4	23702	5468.3	8	St, Sc	
RS020	2019100901	68.166	-168.756	998.8	3.7	96	185	4.5	3.62	16.6	27553	6179	10	-	
RS021	2019100906	68.994	-168.753	1000.7	4.4	90	15	4.6	5.92	17	27398	6243.56	-	-	
RS022	2019100912	69.634	-168.754	1005.3	3.2	81	24	13.4	5.06	19.3	26523	6318	-	-	
RS023	2019100918	70.497	-168.754	1010.2	0.0	83	348	9.0	5.35	54.3	19860	5087.37	9	Sc, St	
RS024	2019101000	71.074	-166.732	1010.4	1.5	60	337	10.5	5.28	21.8	25728	6079	10	-	
RS025	2019101006	71.664	-164.684	1009.0	1.8	66	288	13.2	6.14	39.2	21927	5524.86	-	Cu	
RS026	2019101012	72.157	-162.945	1008.0	0.7	84	272	10.6	4.01	27.2	24231	5574	-	-	
RS027	2019101018	72.778	-160.780	1005.7	1.8	79	299	8.6	3.27	15.2	27904	6230.57	6	As, Sc	
RS028	2019101100	72.811	-158.599	1007.5	0.4	90	324	6.4	1.94	17.1	27145	6237	4	Cu,As,Ac,Ci	
RS029	2019101106	72.499	-156.270	1008.8	0.2	77	301	5.5	1.82	14.2	28319	7517.73	-	-	
RS030	2019101112	72.333	-155.005	1008.4	0.6	88	275	6.7	1.86	50.2	20276	5342	-	-	
RS031	2019101118	72.158	-153.783	1007.6	1.5	78	251	8.5	5.89	58.3	19298	4500.94	6	Sc, As, St	

17

RS032	2019101200	72.000	-151.546	1007.2	1.5	81	260	7.3	1.88	14.4	28222	6199	6	St,Sc,Ac	
RS033	2019101206	72.002	-148.341	1005.8	0.3	95	226	11.7	1.10	26.8	24284	5597.04	-	-	
RS034	2019101212	72.000	-147.088	1006.3	-0.1	90	287	13.4	0.59	31.3	23269	5843	-	-	
RS035	2019101218	71.998	-145.002	1010.0	-2.0	75	313	11.9	0.67	15	27874	6653.2	7	Sc, As	
RS036	2019101300	72.892	-144.994	1011.2	-2.2	76	288	10.0	0.24	14.8	27937	6587	5	Sc, Cu	CPS-exp.
RS037	2019101306	73.685	-145.042	1010.9	-2.7	61	299	12.0	0.20	23	25143	6900.15	-	-	
RS038	2019101312	73.758	-145.191	1011.7	-2.2	67	313	9.6	0.20	16.3	27194	6256	-	-	
RS039	2019101318	73.960	-144.721	1010.3	-1.1	78	264	13.2	0.10	20.9	25685	5611.89	10	St	
RS040	2019101400	74.360	-143.413	1009.6	-1.2	92	270	11.5	-1.40	20	25922	5350	10	-	
RS041	2019101406	74.078	-145.100	1010.0	-1.0	82	263	10.9	-0.11	33.5	22721	4493.43	-	-	CPS-exp.
RS042	2019101412	74.481	-148.232	1010.2	-0.1	68	280	8.8	0.67	15.5	27474	6543	-	-	
RS043	2019101418	74.769	-150.502	1010.6	0.5	59	222	5.2	1.05	18	26552	6079.73	8	St	
RS044	2019101500	74.954	-151.953	1008.8	0.0	95	185	10.1	-0.09	22.4	25192	5606	10	St	
RS045	2019101506	75.411	-155.051	1006.5	0.8	85	229	8.0	-0.19	12.3	28875	7513.46	6	Sc	
RS046	2019101512	76.157	-159.610	1005.1	1.3	93	227	5.0	0.99	13.9	28101	6997	-	-	
RS047	2019101518	76.467	-161.639	1004.8	1.0	97	192	3.7	0.67	15.7	27308	6165.91	10	St	
RS048	2019101600	76.930	-164.525	1005.0	0.6	97	206	4.3	0.56	16.2	27079	5680	10	St	
RS049	2019101606	77.000	-164.997	1005.4	0.6	88	197	5.5	0.30	33	22734	4884.39	-	-	CPS-exp.
RS050	2019101612	77.240	-165.001	1005.5	0.1	93	147	4.6	0.34	14.2	27891	6803	-	-	
RS051	2019101618	77.229	-164.972	1005.7	-0.2	74	167	4.5	0.37	22.5	25046	6221.91	10	-	
RS052	2019101700	78.082	-164.932	1005.5	-1.1	86	167	5.9	-1.49	19.6	25876	5802	10	St	
RS053	2019101706	77.368	-164.998	1005.9	-0.1	73	169	4.0	0.39	48.3	20338	5553.63	-	-	CPS-exp.
RS054	2019101712	77.500	-165.001	1006.9	-0.6	75	165	3.4	-0.77	14.2	27846	6868	-	-	
RS055	2019101718	77.753	-164.965	1007.8	-1.5	83	138	6.3	-1.28	18.8	26135	6259.31	10	-	
RS056	2019101800	78.006	-164.982	1009.0	-1.8	76	130	3.7	-1.49	27.8	23716	5861	10	St	
RS057	2019101806	77.250	-165.000	1009.3	-2.0	80	142	3.6	0.32	38.7	21700	5024.45	-	-	CPS-exp.
RS058	2019101812	77.573	-164.987	1010.1	-2.6	77	162	3.4	-1.40	34.3	22424	5195	-	-	
RS059	2019101818	77.758	-164.992	1011.3	-3.8	85	104	5.6	-1.06	49.4	20183	4702.94	8	St	
RS060	2019101900	78.067	-165.170	1012.6	-4.3	89	92	7.3	-1.51	16.5	26917	6555	7	Sc,As	
RS061	2019101906	77.301	-165.011	1012.4	-1.3	80	162	7.0	0.23	73.1	17737	4219.53	-	-	CPS-exp.
RS062	2019101912	77.254	-164.994	1013.1	-1.6	80	132	10.2	0.31	29.8	23310	5838	-	-	
RS063	2019101918	77.456	-164.789	1013.0	-2.0	84	124	8.3	0.24	46.3	20583	4635.84	10	-	CPS-exp.
RS064	2019102000	78.050	-165.001	1013.3	-2.1	85	162	9.0	-1.53	24.5	24500	6308	10	Sc	CPS-exp.
RS065	2019102006	77.398	-165.002	1012.3	-0.9	73	152	8.4	0.24	29.2	23430	5509.77	-	-	CPS-exp.
RS066	2019102012	77.199	-165.001	1012.2	-1.0	88	130	9.8	0.28	27.2	23863	5439	-	-	
RS067	2019102018	77.454	-164.799	1012.4	-1.1	75	133	9.3	0.27	44.1	20891	4467.14	4	Sc, St	

RS068	2019102100	78.017	-164.969	1013.4	-1.9	92	111	8.1	-1.53	35.9	22154	5159	8	Sc	
RS069	2019102106	77.253	-166.002	1012.4	-0.9	92	118	8.7	0.35	27	23922	6369.82	-	-	CPS-exp.
RS070	2019102112	77.005	-164.997	1013.4	-0.3	72	149	7.6	0.65	24.8	24459	5330	-	-	
RS071	2019102118	77.502	-165.002	1014.4	-0.9	76	121	12.3	0.26	15.1	27469	5730.25	-	-	
RS072	2019102200	78.025	-164.964	1016.4	-4.4	84	86	7.1	-1.51	16.4	26955	5763	10	Sc	
RS073	2019102206	77.074	-165.942	1013.0	-2.2	75	107	5.7	0.65	22.7	24999	6325.03	-	-	
RS074	2019102212	77.001	-164.996	1012.8	-3.1	79	117	9.5	0.74	12.7	28576	6569	-	-	
RS075	2019102218	77.502	-164.991	1013.0	-4.8	71	141	4.7	0.13	30.5	23145	4742.23	8	St	
RS076	2019102221	77.749	-164.512	1013.2	-5.5	79	121	6.7	-1.19	30.1	23236	5443	-	-	
RS077	2019102300	77.764	-164.250	1013.0	-5.6	76	107	6.5	-1.51	13.3	28228	6099	10	Sc	
RS078	2019102306	77.003	-164.011	1011.6	-4.9	70	170	3.8	0.47	45.1	20732	4091.92	2	Sc	
RS079	2019102312	77.002	-164.994	1008.5	-3.0	84	127	8.6	0.58	16.3	26992	6137	-	-	
RS080	2019102318	77.507	-164.969	1005.0	-4.1	86	118	11.6	-0.13	14	27873	5526.95	-	-	
RS081	2019102400	77.787	-163.587	1003.3	-3.4	81	114	6.8	-1.49	23.3	24744	5436	10	Sc	
RS082	2019102406	77.247	-164.015	1000.4	-3.1	81	139	10.1	-0.10	56.8	19208	4349.79	-	-	CPS-exp.
RS083	2019102412	77.004	-165.001	1000.2	-2.8	84	92	7.1	0.68	36.1	22018	5434	-	-	
RS084	2019102418	77.512	-165.006	1001.9	-4.2	75	81	9.5	-0.17	19.7	25709	5488.08	7	-	
RS085	2019102500	77.809	-163.516	1004.3	-8.9	94	61	6.8	-1.48	18.5	26087	5418	10	Sc	
RS086	2019102506	77.351	-166.490	1004.3	-5.9	89	52	8.9	0.04	14	27794	6162.29	-	-	
RS087	2019102512	77.002	-168.761	1006.4	-6.8	85	32	6.7	0.65	26.4	23878	5676	-	-	
RS088	2019102518	75.900	-168.744	1007.3	-3.6	80	30	9.9	1.11	31.1	22906	4760.96	8	-	
RS089	2019102600	74.733	-168.759	1009.2	-1.6	74	27	6.6	1.58	23.7	24612	5329	7	Sc	
RS090	2019102606	74.000	-168.742	1013.6	-2.7	79	303	10.3	1.99	19.6	25839	6176.74	-	-	
RS091	2019102612	73.272	-168.752	1018.3	-1.6	58	253	7.9	1.65	33.4	22573	5438	2	Cu,Sc	
RS092	2019102618	72.501	-168.741	1021.8	-1.2	60	244	7.3	1.350	12.7	28626	6323.34	8	-	
RS093	2019102700	71.569	-168.744	1025.1	-0.9	64	252	5.3	3.880	38.6	21809	4871	10	Sc	
RS094	2019102706	70.573	-168.745	1024.3	-0.6	54	93	3.9	3.500	46.7	20705	4848.26	-	-	
RS095	2019102712	69.773	-168.756	1018.5	0.1	65	55	13.0	2.090	15.7	27541	6069	-	-	
RS096	2019102718	69.003	-168.755	1010.3	0.3	88	69	9.6	3.120	12.8	28895	5877.23	10	-	
RS097	2019102800	68.309	-167.540	1002.0	2.4	91	66	9.3	3.590	13.1	28790	6094	-	-	
RS098	2019102806	68.014	-167.867	991.0	2.6	93	44	14.5	2.650	20.2	26166	7203.35	-	-	
RS099	2019102812	67.502	-168.751	982.5	3.7	100	354	1.3	2.640	16.6	27443	6230	-	-	
RS100	2019102818	66.502	-168.748	987.2	1.5	97	271	10.8	4.570	14.5	28372	5947.98	10	-	
RS101	2019102900	65.688	-168.517	994.2	1.4	93	316	10.5	3.880	16.9	27404	6121	10	St	
RS102	2019102912	63.969	-171.970	1004.2	-1.5	79	24	7.3	3.710	35.1	22849	5519	-	-	
RS103	2019103000	62.112	-175.382	1012.8	-1.2	72	302	7.4	4.570	22	25984	5573	10	Sc	

RS104	2019103012	60.288	-178.476	1017.6	2.5	60	251	6.7	4.580	14.3	28832	6458	-	-	
RS105	2019103100	58.474	178.617	1018.4	2.7	62	138	5.0	5.390	17.4	27586	6944	10	Cu,Sc	
RS106	2019103112	56.615	175.787	1016.6	3.6	73	82	4.9	4.730	15.1	28486	6274	-	-	
RS107	2019110100	54.747	173.080	1016.7	3.6	75	24	1.1	6.470	16.8	27781	6688	8	Cu,Sc	

2.2 CPS sonde

(1) Personnel

Jun Inoue	NIPR	- PI
Kazutoshi Sato	KIT	
Taro Maruo	Kobe University	
Jumpei Yamamoto	Tokyo University of Marine Science and Technology	
Taketani Fumikazu	JAMSTEC	
Ryo Oyama	NME	
Soichiro Sueyoshi	NME	
Shinya Okumura	NME	
Kazuho Yoshida	NME	
Yutaro Murakami	NME	
Hattori Takehito	MIRAI Crew	

(2) Objectives

To understand the vertical profiles of Arctic cloud, we conducted CPS sonde observations over the Arctic Ocean and the Bering Sea. The CPS sonde, developed by the Japanese Meisei Electric Co., Ltd. (Meisei), measures vertical distributions of cloud particles (number density, size and phase (i.e., water cloud or ice cloud)) in addition to meteorological elements (i.e., temperature, relative humidity, height, wind direction and wind speed). This was the inaugural trial of cloud particle observations over the Arctic Ocean in October during the R/V Mirai cruise.

(3) Parameters

Cloud particles (number of density, Particle size and Output signal voltage)
Wind speed and direction
Pressure
Temperature
Relative Humidity

(4) Instruments and methods

Overall, 12 CPS sondes were launched during 13–24 October 2019. The CPS sonde comprises a CPS sonde and a GPS radiosonde transmitter (RS-11G, Meisei). The CPS sonde was connected to a 350 g balloon (Totex TA-350), parachute and Vaisala radiosonde. We used the Meisei standard GPS sonde ground system (RD-08AC), software (MGPS-R) and 400 MHz antenna.

(5) Station list or Observation log

See Table 2.2 "CPS sonde launch log with surface observation and maximum sounding height".

(6) Preliminary results

Figure 2.2-1 shows the track of the R/V Mirai during MR19-03C and the locations of the CPS sonde launches over the Arctic Ocean. Figures 2.2-2–2.2-13 show vertical profiles of temperature and relative humidity obtained by the RS-11G GPS radiosondes and the number of particles, degree of polarization and P output obtained by the CPS sondes. We successfully observed 18 clouds including low, middle and high clouds.

(7) Data archive

The data obtained during the cruise will be submitted to the Data Management Group of JAMSTEC, and they will be made available to the public via the "Data Research System for Whole Cruise Information in JAMSTEC (DARWIN)" on the JAMSTEC website (http://www.godac.jamstec.go.jp/darwin/e)

(8) Remarks

To reduce the amount of helium used for balloon launches, we performed joint launches of the Meisei CPS sondes and Vaisala GPS radiosondes (RS41-SPG) during the MR19-03C cruise (identified as "CPS.exp" in Table 2.1). No relative humidity data were recorded for No.2 launch (14 October) because of difficulties receiving data.

Table 2.2: CPS sonde launch log with surface observations and maximum sounding height.

No.	Date (YYYYMMDD) Time (HH:MM) UTC	Lat (degN) Lon (degW)	Psfc (hPa)	Tsfc (°C)	RHsfc (%)	WDsfc (deg) WSsfc (m/s)	Max Alt (m)
01	20191013 06:00	73.75 145.07	1010.9	-2.7	61	299 12.0	25121
02	20191014 06:00	74.07 145.23	1009.9	-1.0	82	263 10.9	22677
03	20191016 06:00	77.00 164.99	1004.5	0.6	88	197 5.5	22724
04	20191017 06:00	77.27 165.02	1005.9	-0.1	73	169 4.0	20307
05	20191018 06:00	72.25 164.99	1009.3	-2.0	80	142 3.6	21680
06	20191019 06:00	77.21 164.94	1012.4	-1.3	80	162 7.0	17737
07	20191019 18:00	77.46 165.01	1012.9	-2.0	84	124 8.3	20576
08	20191020 00:00	78.05 164.99	1013.3	-2.1	85	162 9.0	24522
09	20191020 06:00	77.31 164.93	1012.3	-0.9	73	152 8.4	23427
10	20191021 06:00	77.25 166.00	1012.4	-0.9	92	118 8.7	23902
11	20191022 06:00	77.00 166.00	1012.9	-2.2	75	107 5.7	24969
12	20191024 06:00	77.24 163.99	1000.4	-3.1	81	139 10.1	19183
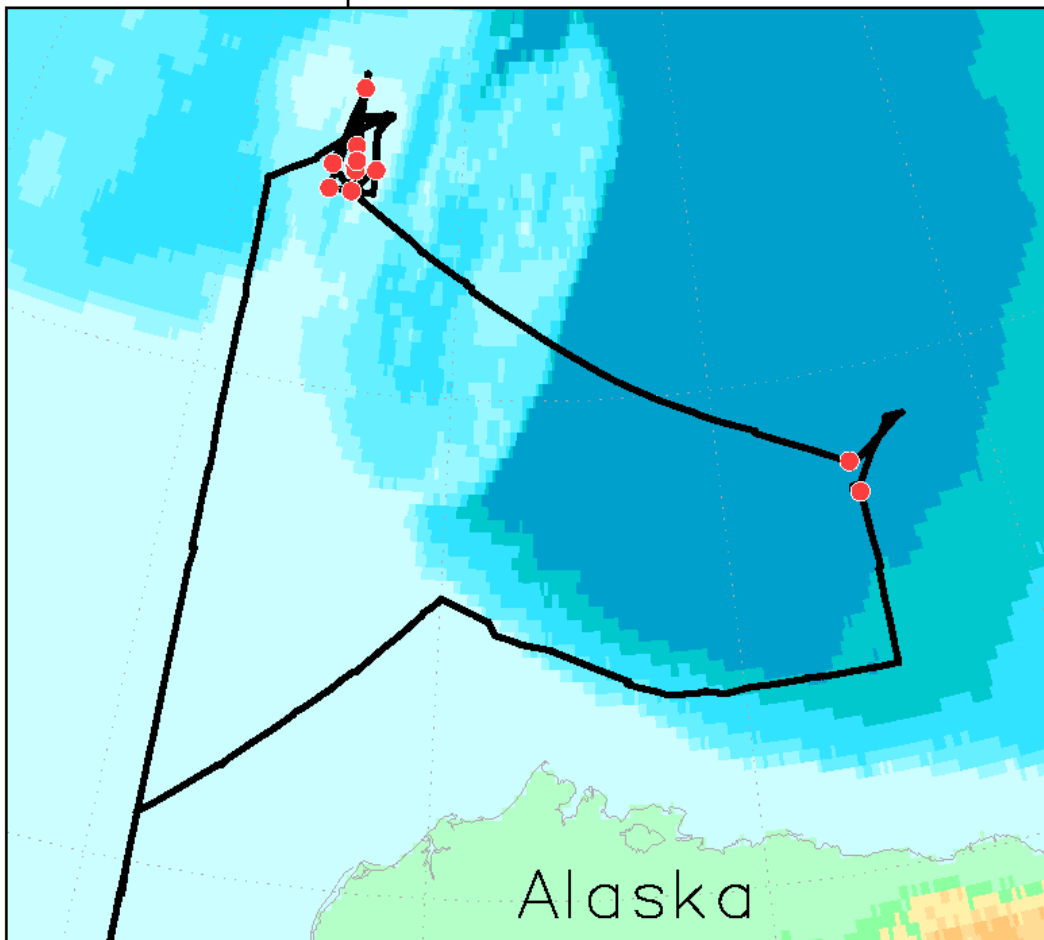
Figure 2.2-1: R/V Mirai track (black line) and CPS sonde launch points (red dots) over the Arctic Ocean.
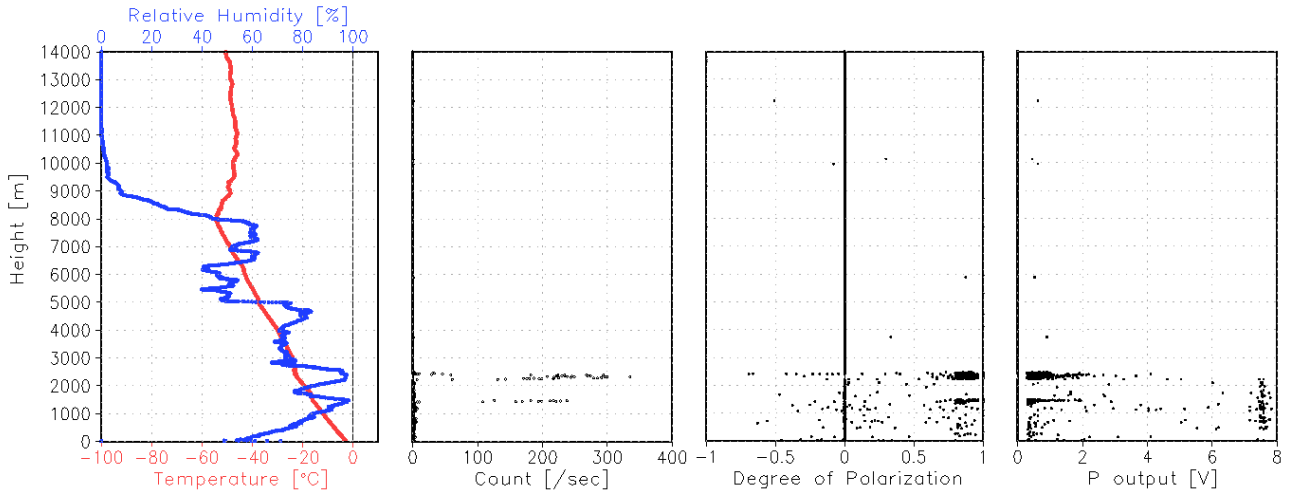
Figure 2.2-2: Vertical profiles of temperature (red) and humidity (blue) obtained by RS-11G radiosonde, and number of particles, degree of polarization and P output obtained by CPS sonde for No.1 launch (13 October).
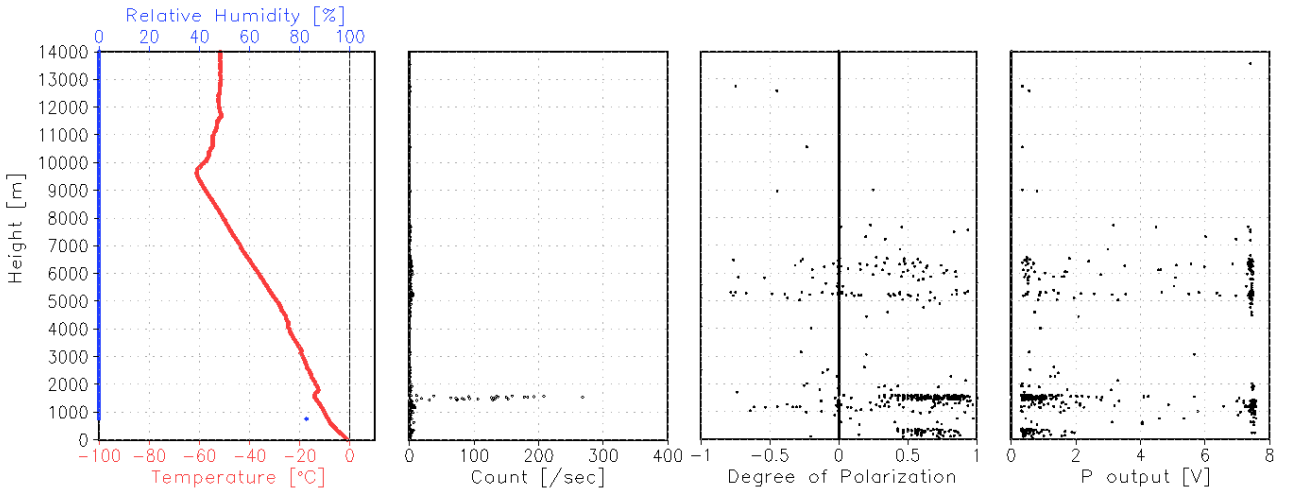
Figure 2.2-4: Same as in Figure 2.2-2, but for No.2 launch (14 October).
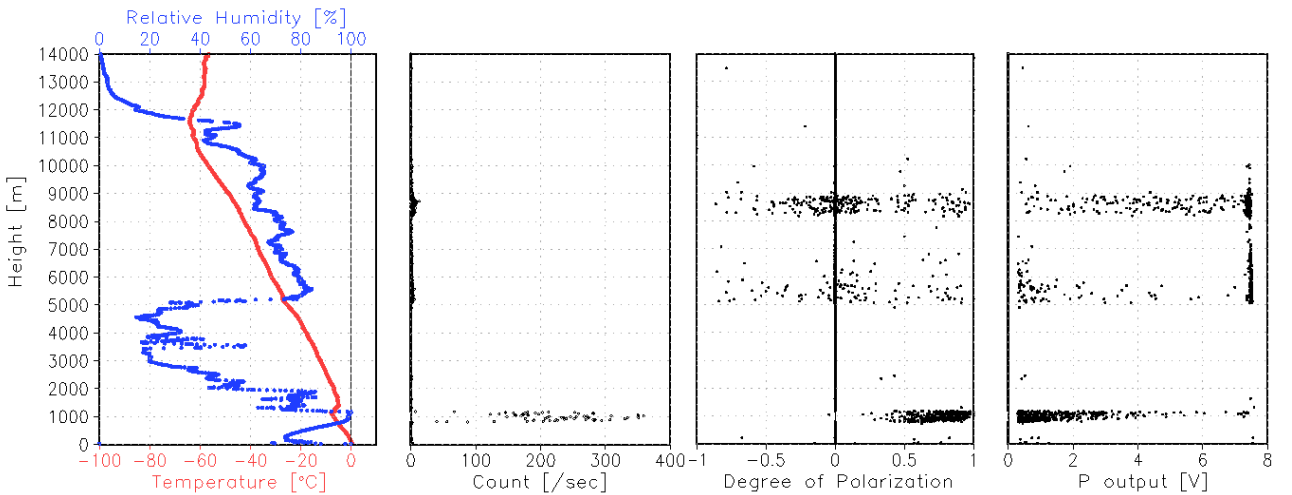
Figure 2.2-5: Same as in Figure 2.2-2, but for No.3 launch (16 October).
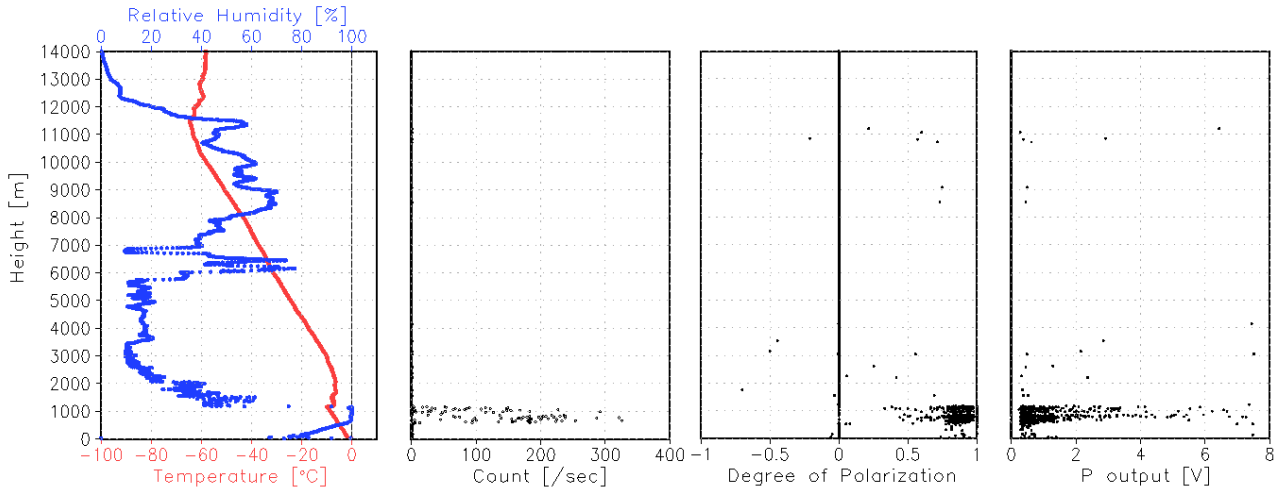
Figure 2.2-6: Same as in Figure 2.2-2, but for No.4 launch (17 October).
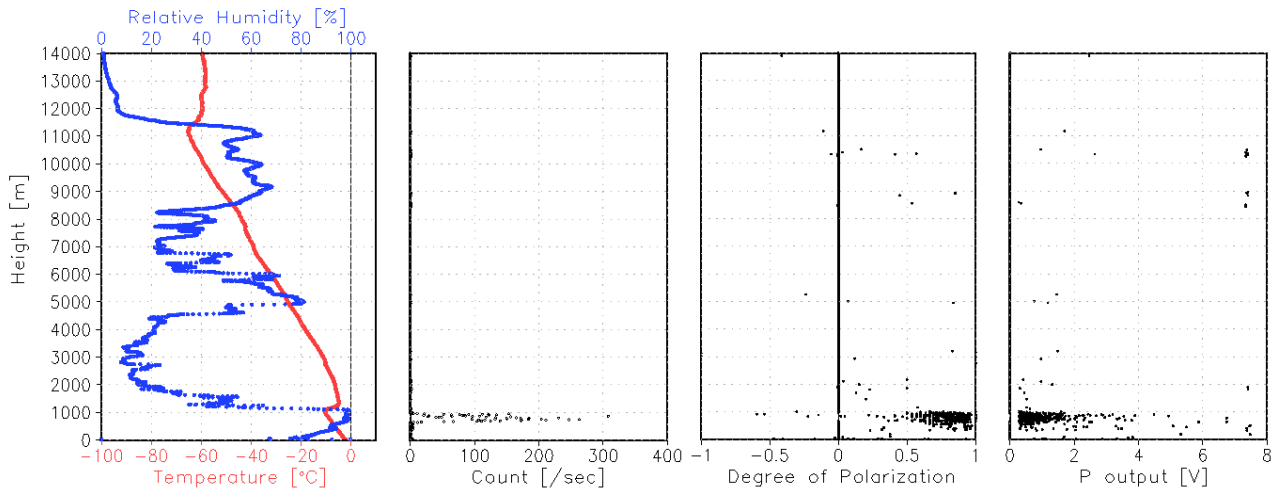
Figure 2.2-7: Same as in Figure 2.2-2, but for No.5 launch (18 October).
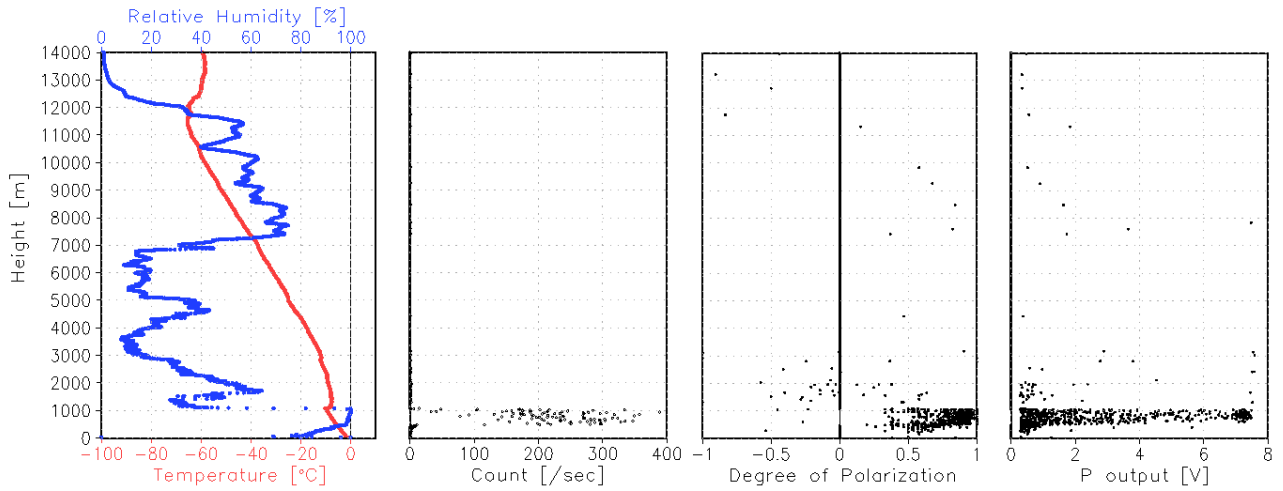
Figure 2.2-8: Same as in Figure 2.2-2, but for No.6 launch (06UTC on 19 October).
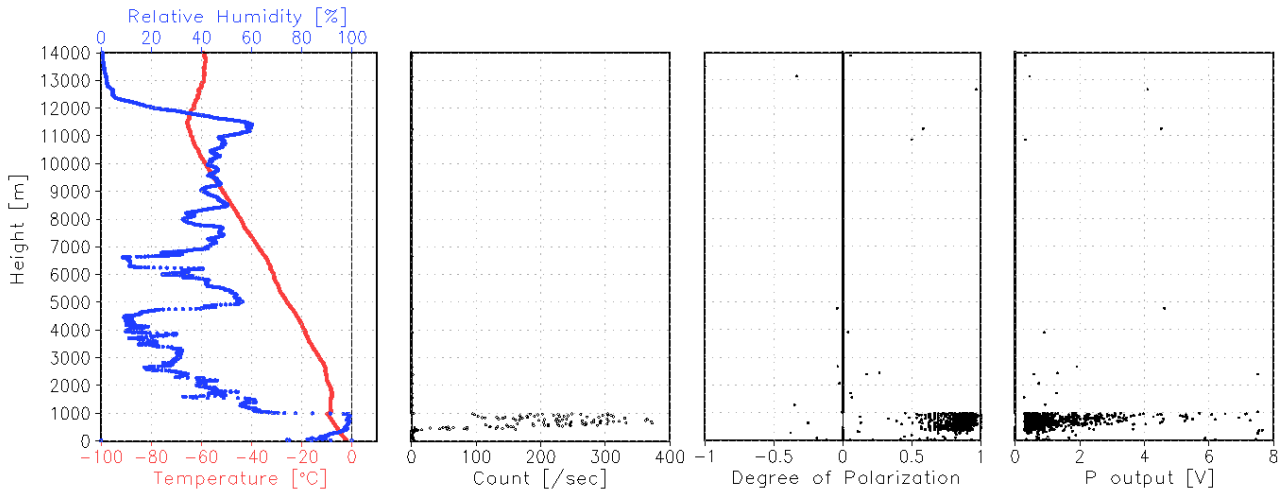
Figure 2.2-9: Same as in Figure 2.2-2, but for No.7 launch (18UTC 19 October).
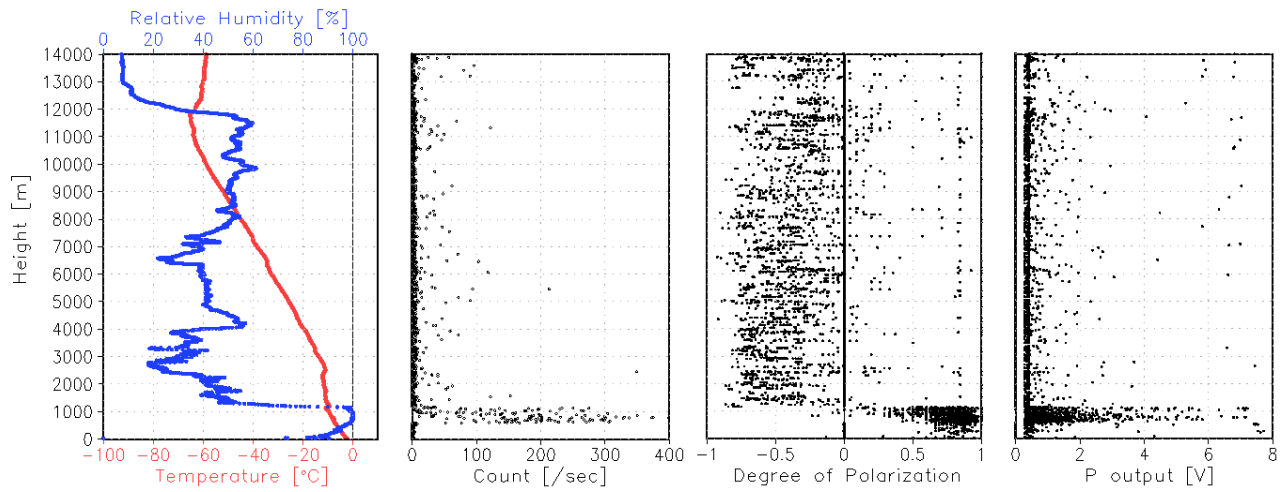
Figure 2.2-10: Same as in Figure 2.2-2, but for No.8 launch (00UTC on 20 October).

Figure 2.2-11: Same as in Figure 2.2-2, but for No.9 launch (06UTC on 20 October).
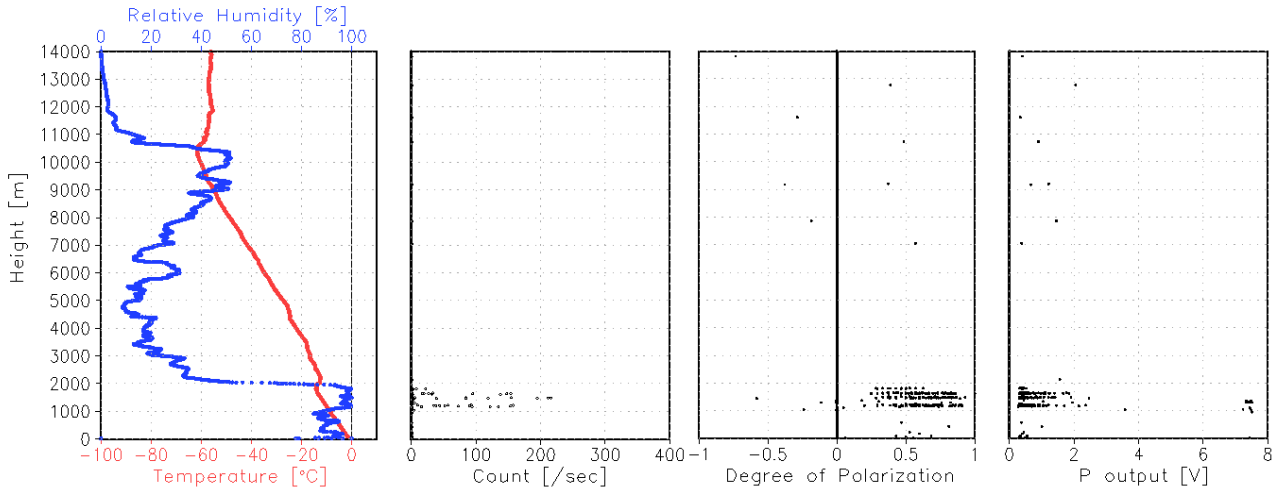
Figure 2.2-12: Same as in Figure 2.2-2, but for No.10 launch (21 October).
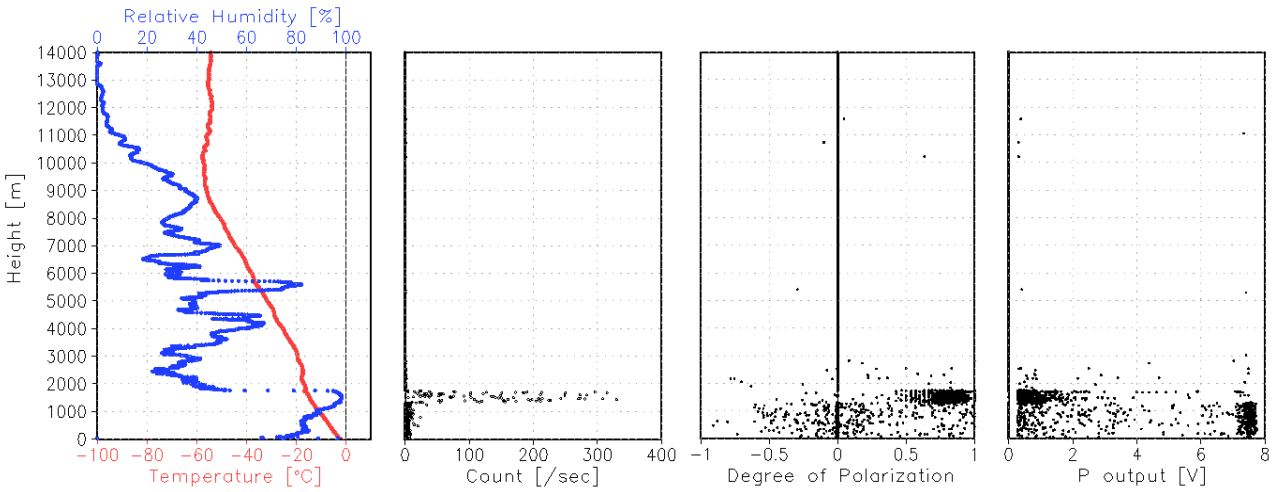
Figure 2.2-13: Same as in Figure 2.2-2, but for No.11 launch (22 October).
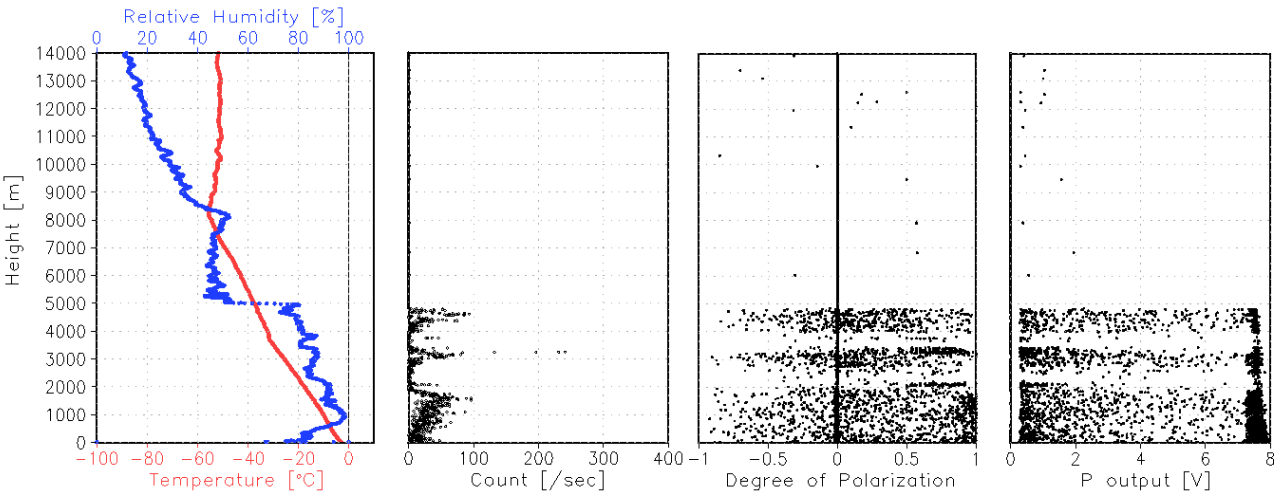
Figure 2.2-13: Same as in Figure 2.2-2, but for No.12 launch (24 October).

2.3 C-band Weather Radar

(1) Personnel

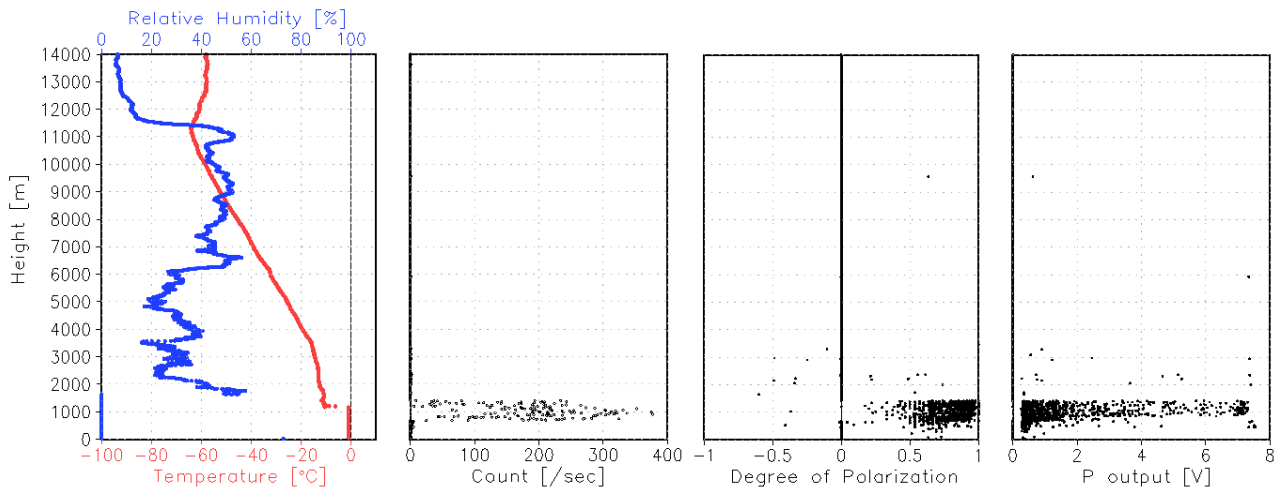|		
Kazutoshi Sato	KIT	- PI
Ryo Oyama	NME	
Souichiro Sueyoshi	NME	
Shinya Okumura	NME	
Kazuho Yoshida	NME	
Yutaro Murakami	NME	
Takehito Hattori	MIRAI Crew	

(2) Objectives

Low-level clouds over the Arctic Ocean, which usually dominate during early winter, have a key role in the sea/ice surface heat budget. In addition, cyclones that modify the sea-ice distribution are also very important with regard to comprehension of air–ice–sea interaction. To capture the broad-scale characteristics of cloud–precipitation systems and their temporal and spatial evolutions over the Arctic Ocean, the three-dimensional radar echo structure and wind field of rain/snow clouds were derived based on C-band Doppler radar observations.

(3) Parameters

The C-band Doppler weather radar observed the three-dimensional radar echo structure and wind field of rain/snow clouds.

The following lists the radar variables that are converted from the power and the phase of the backscattered signal of vertically and horizontally polarized channels:

Radar reflectivity:	Z
Doppler velocity:	Vr
Spectrum width of Doppler velocity:	SW
Differential reflectivity:	ZDR
Differential propagation phase:	ΦDP
Specific differential phase:	KDP
Co-polar correlation coefficients:	ρHV

(4) Instruments and methods

The basic specifications of the C-band Doppler weather radar installed onboard the R/V Mirai are as follows:

Frequency:	5370 MHz (C-band)
Polarimetry:	Horizontal and vertical
	(simultaneously transmitted and received)
Transmitter:	Solid-state transmitter
Pulse Configuration:	Using pulse-compression
Output Power:	6 kW (H) + 6 kW (V)
Antenna Diameter:	4 meter
Beam Width:	1.0 degrees
INU (Inertial Navigation Unit):	PHINS (IXBLUE S.A.S.)

The antenna is controlled to point in the commanded ground-relative direction by controlling the azimuth and elevation to cancel the ship attitude (i.e., roll, pitch and yaw) detected by the INU. The Doppler velocity is

also corrected by subtracting the ship motion in the beam direction.

As part of routine maintenance, the internal parameters of the radar were checked and calibrated at the beginning and end of the cruise, whereas the following parameters were checked on a daily basis: (1) frequency, (2) peak output power and (3) pulse width.

During the cruise, the radar was operated in two modes, as shown in Tables 2.3-1 and 2.3-2. The radar was operated typically by repeating a volume scan with 17 plan position indicators (PPIs) at 6-min intervals. A dual pulse repetition frequency (PRF) mode with typical maximum range of 100 km was used for the volume scan. A surveillance PPI scan was performed every 30 min in a single PRF mode with maximum range of 300 km. Range height indicator (RHI) scans were operated whenever necessary to determine vertical structures in certain azimuth directions. On the return leg from the Arctic Ocean, vertical point scans were added and performed to collect data for ZDR calibration.

(5) Station list or Observation log

The radar was operated continuously from 03:06 UTC on 30 September to 08:00 UTC on 7 November.

(6) Preliminary results

The radar operated continuously from 30 September to 7 November. During the MR19-03C cruise, several precipitation systems that passed near the track of the R/V Mirai were captured by the C-band weather radar. Figure 2.3 (lower panel) shows the temporal variation of the PPI areal coverage of the radar echo within the range of 100 km for precipitating events north of 66°N. The strong precipitation echoes shown in the upper panels of Figure 2.3 were captured when the low pressure systems approached the R/V Mirai (e.g., 09, 23 and 28 October 2019) and when heavy snowfall was observed near the ice edge (e.g., 12 and 22 October 2019).
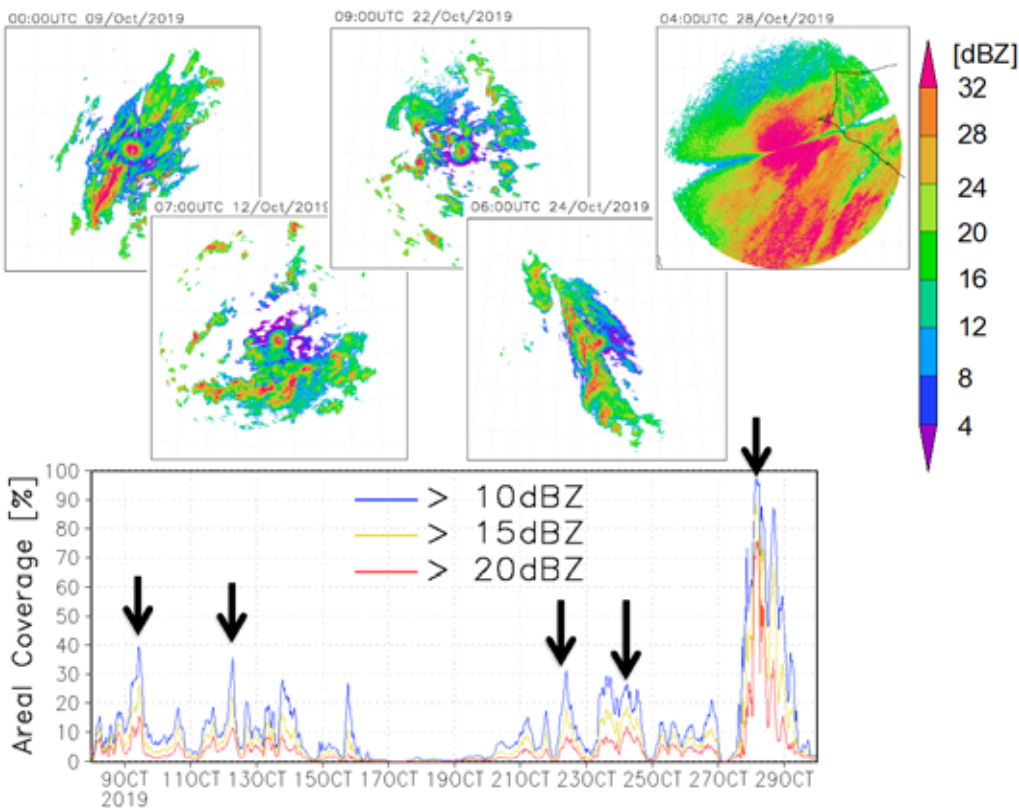
Figure 2.3: (Lower) Temporal variations of areal coverage of echoes exceeding threshold of 10 dBZ (blue), 15 dBZ (yellow) and 20 dBZ (red) within range of 100 km on the PPI scans. (Upper) Five PPI images of representative precipitation events obtained by the first PPI in the volume scan (elevation angle: 0.5°).

(7) Data archive

 The data obtained during the cruise will be submitted to the Data Management Group of JAMSTEC, and they will be made available to the public via the "Data Research System for Whole Cruise Information in JAMSTEC (DARWIN)" on the JAMSTEC website (http://www.godac.jamstec.go.jp/darwin/e)

(8) Remarks (Times in UTC)

   i)   Observation mode.
      [Auto-1] (Scan parameters are shown in Table 2.3-1)
          03:06 on 30 September 2019 to 10:30 on 31 October 2019.
      [Auto-3] (Scan parameters are shown in Table 2.3-2)
        10:36 on 31 October 2019 to 8 November 2019.

   ii)   During the following periods, data acquisition was suspended because of maintenance.
     03:18 on 30 September 2019 to 03:29 on 30 September 2019
     10:30 on 31 October 2019 to 10:36 on 31 October 2019.

   iii)   Re-unfolding correction of Doppler velocity was not used during this cruise.

Table 2.3-1: Parameters for scan strategy in Auto-1

	Surveillance PPI Scan	Volume Scan						RHI Scan
Repeated Cycle (min.)	30	6						6
Times in One Cycle	1	1						3
Pulse Width (long / short, in microsec)	200 / 2	64 / 1		32 / 1		32 / 1		32 / 1
Scan Speed (deg/sec)	18	18		24		36		9 (in el.)
PRF(s) (Hz)	400	dual PRF (ray alternative)						1250
		667	833	938	1250	1333	2000	
Pulses / Ray	16	26	33	27	34	37	55	32
Ray Spacing (deg.)	0.7	0.7		0.7		1.0		0.23
Azimuth	Full Circle							Optional
Bin Spacing (m)	150							
Max. Range (km)	300	150		100		60		100
Elevation Angle(s) (deg.)	0.5	0.5		1.0, 1.8, 2.6, 3.4, 4.2, 5.1, 6.2, 7.6, 9.7, 12.2, 15.2		18.7, 23.0, 27.9, 33.5, 40.0		-0.2 to 60.0

Table 2.3-2: Parameters for scan strategy in Auto-3

	Surveillance PPI Scan	Volume Scan						RHI Scan	Vertical Point Scan
Repeated Cycle (min.)	30	6						12	
Times in One Cycle	1	1						3	3
Pulse Width (long / short, in microsec)	200 / 2	64 / 1		32 / 1		32 / 1		32 / 1	32/1
Scan Speed (deg/sec)	18	18		24		36		9 (in el.)	36
PRF(s) (Hz)	400	dual PRF (ray alternative)						1250	2000
		667	833	938	1250	1333	2000		
Pulses / Ray	16	26	33	27	34	37	55	32	64
Ray Spacing (deg.)	0.7	0.7		0.7		1.0		0.23	1.0
Azimuth	Full Circle							Optional	Full Circle
Bin Spacing (m)	150								
Max. Range (km)	300	150		100		60		100	60
Elevation Angle(s) (deg.)	0.5	0.5		1.0, 1.8, 2.6, 3.4, 4.2, 5.1, 6.2, 7.6, 9.7, 12.2 15.2		18.7, 23.0, 27.9, 33.5, 40.0		-0.2 to 60.0	90

2.4 Surface Meteorological Observations

(1) Personnel

Kazutoshi Sato	KIT	-PI
Ryo Oyama	NME	
Souichiro Sueyoshi	NME	
Shinya Okumura	NME	
Kazuho Yoshida	NME	
Yutaro Murakami	NME	
Takehito Hattori	MIRAI Crew	

(2) Objectives

Surface meteorological parameters were observed as a basic dataset of the meteorology. These parameters provided information on the temporal variation of the meteorological conditions surrounding the ship.

(3) Instruments and methods

Two systems were used to observe surface meteorological parameters during this cruise.

i. *Mirai Surface Meteorological observation (SMet) system*

The instruments of the SMet system are listed in Table 2.4-1 and details of the parameters measured are listed in Table 2.4-2. The KOAC-7800 weather data processor (Koshin-Denki, Japan) was used to collect and process the data. The data included in this set consist of 6-s averages.

ii. *Shipboard Oceanographic and Atmospheric Radiation (SOAR) measurement system*

The SOAR system, designed by BNL (Brookhaven National Laboratory, USA), consists of the following six major parts.

a) Portable Radiation Package (PRP) designed by BNL – shortwave and longwave downward radiation.

b) Additional shortwave and longwave radiometers with ventilation units manufactured by Hukseflux, Netherlands – shortwave and longwave downward radiation measurements adapted to cold areas to complement the PRP measurement.

c) Analog meteorological data sampling with a CR1000 logger manufactured by Campbell Scientific Inc. Canada – wind, pressure and rainfall (via capacitive rain gauge) measurements.

d) Digital meteorological data sampling from individual sensors – air temperature, relative humidity and rainfall (via optical rain gauge (ORG)) measurements.

e) A photosynthetically available radiation (PAR) sensor manufactured by Biospherical Instruments Inc. (USA) – PAR and ultraviolet radiation (UV) measurements.

f) Scientific computer system (SCS) developed by NOAA (National Oceanic and Atmospheric Administration, USA) – centralized data acquisition and logging of all datasets.

The SCS recorded the PRP, air temperature, relative humidity, CR1000, ORG and PAR data. The SCS composed event data (JamMet) from these meteorological observations and ship navigational data at 6-s intervals. Information regarding the instruments and their locations is presented in Table 2.4-3 and details of the parameters measured are listed in Table 2.4-4.

For quality control, we performed the following checks of the sensors both before and after the cruise.

i.   Young rain gauge (SMet and SOAR)

      Inspection of the linearity of the output value from the rain gauge sensor associated with a change of input value (i.e., addition of a fixed quantity of test water).

ii.   Barometer (SMet and SOAR)

      Comparison with readings from a portable barometer (PTB220, Vaisala).

iii.   Thermometer (air temperature and relative humidity) (SMet and SOAR)

      Comparison with readings from a portable thermometer (HM70, Vaisala).

(4) Observation log

    27 Sep. 2019 to 10 Nov. 2019

(5) Preliminary results

    Figure. 2.4-1 shows the time series of the following parameters;

          Wind (SOAR)

          Air temperature (SMet)

          Relative humidity (SMet)

          Precipitation (SMet, ORG)

          Short wave radiation (SOAR)

          Long wave radiation (SMet)

          Pressure (SMet)

          Sea surface temperature (SMet)

          Significant wave height (SMet; stern)

    Figures 2.4-2 and 2.4-3 show time series of shortwave and longwave radiation, respectively, for comparison of the SOAR (PRP) with additional radiometers.

(6) Data archive

    The data obtained during the cruise will be submitted to the Data Management Group of JAMSTEC, and they will be made available to the public via the "Data Research System for Whole Cruise Information in JAMSTEC (DARWIN)" on the JAMSTEC website (http://www.godac.jamstec.go.jp/darwin/e)

(7) Remarks (times in UTC)

    i)   During the following period, the SMet SST data were available.

          05:31 on 29 September 2019 to 23:55 on 7 November 2019.

    ii)   At the following time, SMet capacitive rain gauge data were invalid because of test transmissions of the MF/HF radio.

          19:39 on 29 October 2019.

    iii)   During the following period, significant wave height and period data were invalid because of difficulty with PC logging.

          04:55 on 7 October 2019 to 05:55 on 7 October 2019.

    iv)   During the following periods, bow significant wave height and period data were invalid because of system trouble.

          09:35 on 1 November 2019 to 23:34 on 1 November. 2019

04:35 on 2 November 2019 to the end of the cruise.

v)   During the following periods, SMet wind speed/direction data were invalid because of sensor failure.

         20:47 on 10 October 2019 to 20:56 on 10 October 2019

         22:37 on 10 October 2019 to 22:50 on 10 October 2019

         00:57 on 19 October 2019 to 02:49 on 19 October 2019.

vi)   During the following periods, SMet wind speed/direction data were measured by the ultrasonic anemometer on the aftermast.

         20:56 on 10 October 2019 to 22:37 on 10 October 2019

         22:50 on 10 October 2019 to 06:06 on 12 October 2019.

vii)   During the following period, the SMet wind speed/direction data were measured by the KE-500 wind vane anemometer on the foremast.

         04:35 on 19 October 2019 to 00:00 on 10 November 2019.

viii)   During the following days, the SMet shortwave radiation data contained invalid nighttime values (more than 0.01 kW/m^2).

         27 September 2019 to 1 October 2019

         3 October 2019 to 6 October 2019.

ix)   During the following period, SOAR data acquisition was suspended for system maintenance.

         06:33 on 21 October 2019 to 06:44 on 21 October 2019.

x)   During the following period, the ORG rain intensity of the SOAR was invalid because of sensor failure.

         00:23 on 14 October 2019 to the end of the cruise.

xi)   The SOAR longwave radiation amount (PIR) must be corrected using appropriate calibration coefficients. This correction was performed after the cruise because the PIR sensor was replaced before the beginning of this cruise.

xii)   During the following periods, SOAR longwave radiation amount (PIR) contained bias because the output of the PIR case and/or the dome thermistor for radiation correction fell below the temperature measurement limit (-5.6 °C).

         20:11 on 22 October 2019 to 03:27 on 23 October 2019

         18:44 on 24 October 2019 to 07:17 on 24 October 2019

         08:27 on 25 October 2019 to 14:10 on 25 October 2019.

xiii)   During this cruise, FRSR data were not acquired.

Table 2.4-1: Instruments and installation locations of the SMet system

Sensors	Type	Manufacturer	Location(altitude from surface)
Anemometer(ultrasonic)	KS-5900	Koshin Denki, Japan	foremast (25 m)
			aftermast (37 m)

Anemometer(wind vane)	KE-500	Koshin Denki, Japan	foremast (24 m)
Tair/RH	HMP155	Vaisala, Finland	compass deck (21 m)
with 43408 Gill aspirated radiation shield R.M. Young, USA			starboard and port side
Thermometer: SST	RFN2-0	Koshin Denki, Japan	4th deck (-1m, inlet -5m)
Barometer	Model-370	Setra System, USA	captain deck (13 m)
			weather obs. room
Rain gauge	50202	R. M. Young, USA	compass deck (19 m)
Optical rain gauge	ORG-815DR	Osi, USA	compass deck (19 m)
Radiometer (short wave)	MS-802	Eko Seiki, Japan	radar mast (28 m)
Radiometer (long wave)	MS-202	Eko Seiki, Japan	radar mast (28 m)
Wave height meter	WM-2	Tsurumi-seiki, Japan	bow (10 m)
			stern(8m)

Table 2.4-2: Parameters of the SMet observation system

Parameter	Units	Remarks
1 Latitude	degree	
2 Longitude	degree	
3 Ship's speed	knot	Mirai log, DS-30 Furuno
4 Ship's heading	degree	Mirai Gyro, TOKYO-KEIKI,
	TG-8000	
5 Relative wind speed	m/s	6sec./10min. averaged
6 Relative wind direction	degree	6sec./10min. averaged
7 True wind speed	m/s	6sec./10min. averaged
8 True wind direction	degree	6sec./10min. averaged
9 Barometric pressure	hPa	adjusted to sea surface level
		6sec. averaged
10 Air temperature (starboard)	degC	6sec. averaged
11 Air temperature (port side)	degC	6sec. averaged
12 Dewpoint temperature (starboard)	degC	6sec. averaged
13 Dewpoint temperature (port side)	degC	6sec. averaged
14 Relative humidity (starboard)	%	6sec. averaged
15 Relative humidity (port side)	%	6sec. averaged
16 Sea surface temperature	degC	6sec. averaged
17 Rain rate (optical rain gauge)	mm/hr	hourly accumulation
18 Rain rate (capacitive rain gauge)	mm/hr	hourly accumulation
19 Down welling shortwave radiation	W/m^2	6sec. averaged
20 Down welling infra-red radiation	W/m^2	6sec. averaged
21 Significant wave height (bow)	m	hourly
22 Significant wave height (stern)	m	hourly
23 Significant wave period (bow)	second	hourly
24 Significant wave period (stern)	second	hourly

Table 2.4-3: Instruments and installation locations of the SOAR system

Sensors (Meteorological)	Type	Manufacturer	Location (altitude from surface)
Anemometer	05106	R.M. Young, USA	foremast (25 m)
Barometer	PTB210	Vaisala, Finland	foremast (23 m)

with 61002 Gill pressure port, R.M.   Young, USA

Rain gauge	50202	R.M. Young, USA	foremast (24 m)
Tair/RH	HMP155	Vaisala, Finland	foremast (23 m)
with 43408 Gill aspirated radiation shield R.M. Young, USA			
Optical rain gauge	ORG-815DR	Osi, USA	foremast (24 m)

Sensors (PRP)	Type	Manufacturer	Location (altitude from surface)
Radiometer (short wave)	PSP	Epply Labs, USA	foremast (25 m)
Radiometer (long wave)	PIR	Epply Labs, USA	foremast (25 m)
Fast rotating shadowband radiometer		Yankee, USA	foremast (25 m)

Sensors (PAR)	Type	Manufacturer	Location (altitude from surface)
PAR sensor	PUV-510	Biospherical Instruments Inc., USA	Navigation deck (18m)

Sensors (Additional Radiation)	Type	Manufacturer	Location (altitude from surface)
Radiometer (short wave)	SR-20	HukseFlux, Netherland	Compassdeck(20m)
with VU-01 Ventilation Unit HukseFlux, Netherland			
Radiometer (long wave)	IR-20	HukseFlux, Netherland	Compassdeck(20m)
with VU-01 Ventilation Unit HukseFlux, Netherland			

Table 2.4-4: Parameters of the SOAR system

Parameter	Units	Remarks
1 Latitude	degree	
2 Longitude	degree	
3 SOG	knot	
4 COG	degree	
5 Relative wind speed	m/s	
6 Relative wind direction	degree	
7 Barometric pressure	hPa	
8 Air temperature	degC	
9 Relative humidity	%	
10 Rain rate (optical rain gauge)	mm/hr	
11 Precipitation (capacitive rain gauge)	mm	reset at 50 mm
12 Down welling shortwave radiation(PSP)	W/m^2	
13 Down welling infra-red radiation(PIR)	W/m^2	
14 Defuse irradiance	W/m^2	Not observed
15 PAR	microE/cm2/sec	
16 UV	microW/cm2/nm	
17 Additional Down welling shortwave radiation(SR20)	W/m^2	
18 Additional Down welling longwave radiation(IR20)	W/m^2	
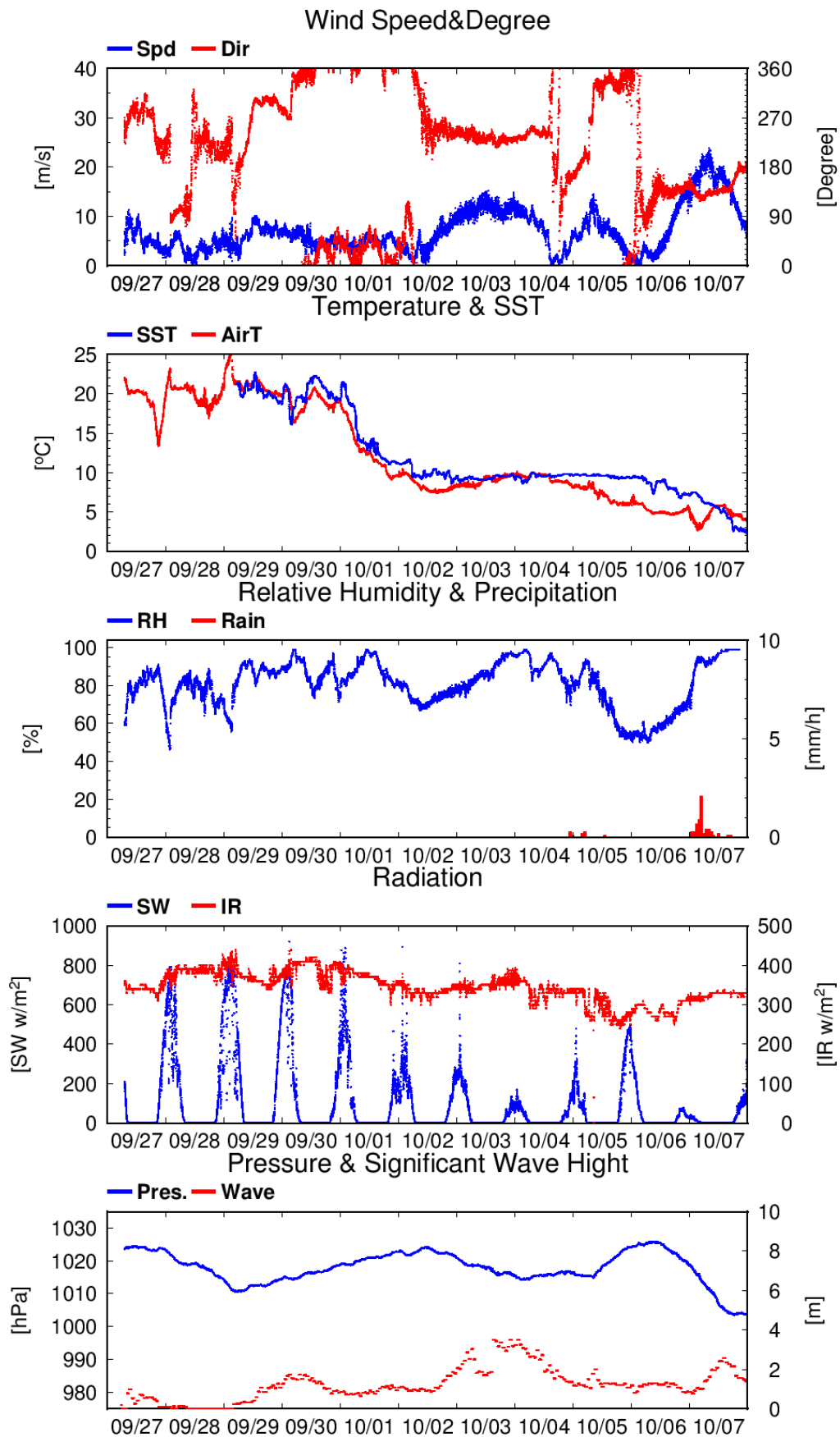
Figure 2.4-1: Time series of surface meteorological parameters monitored during this cruise

Figure 2.4-1: (continued)

Wind Speed&Degree

Temperature & SST

Relative Humidity & Precipitation

Radiation

Pressure & Significant Wave Hight

Figure 2.4-1: (continued)

Wind Speed&Degree

Temperature & SST

Relative Humidity & Precipitation

Radiation

Pressure & Significant Wave Hight

Figure 2.4-1: (continued)

42
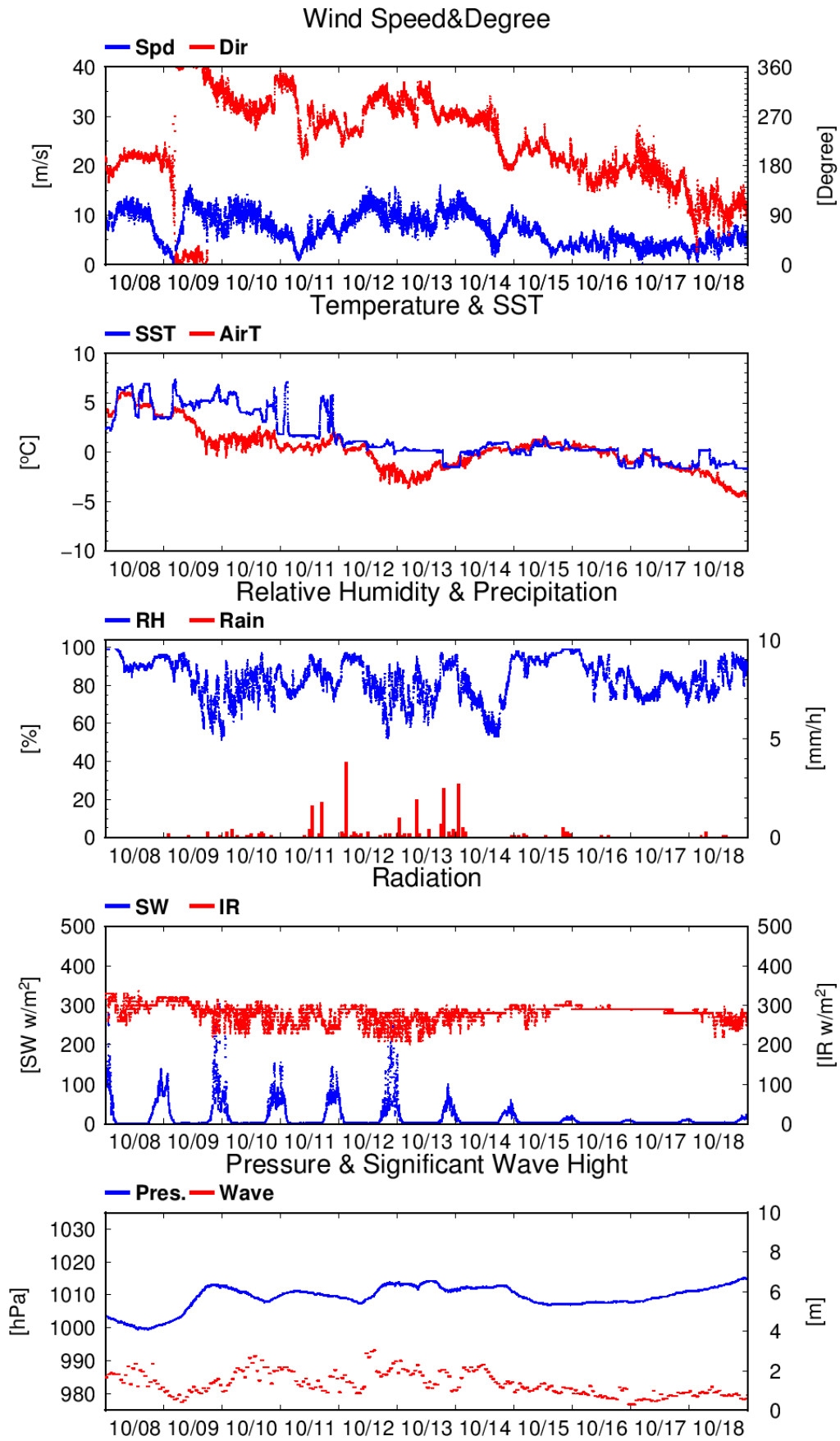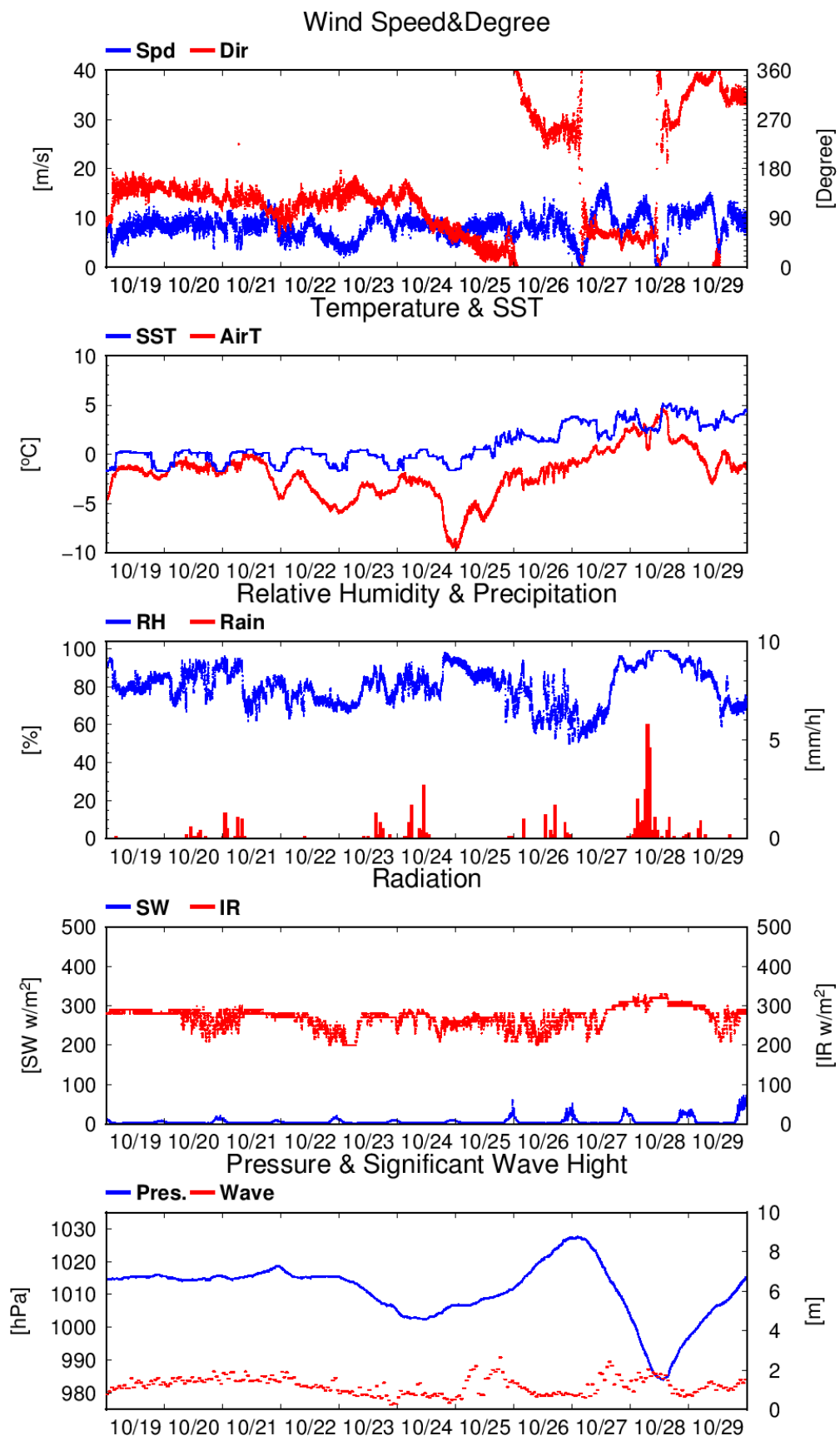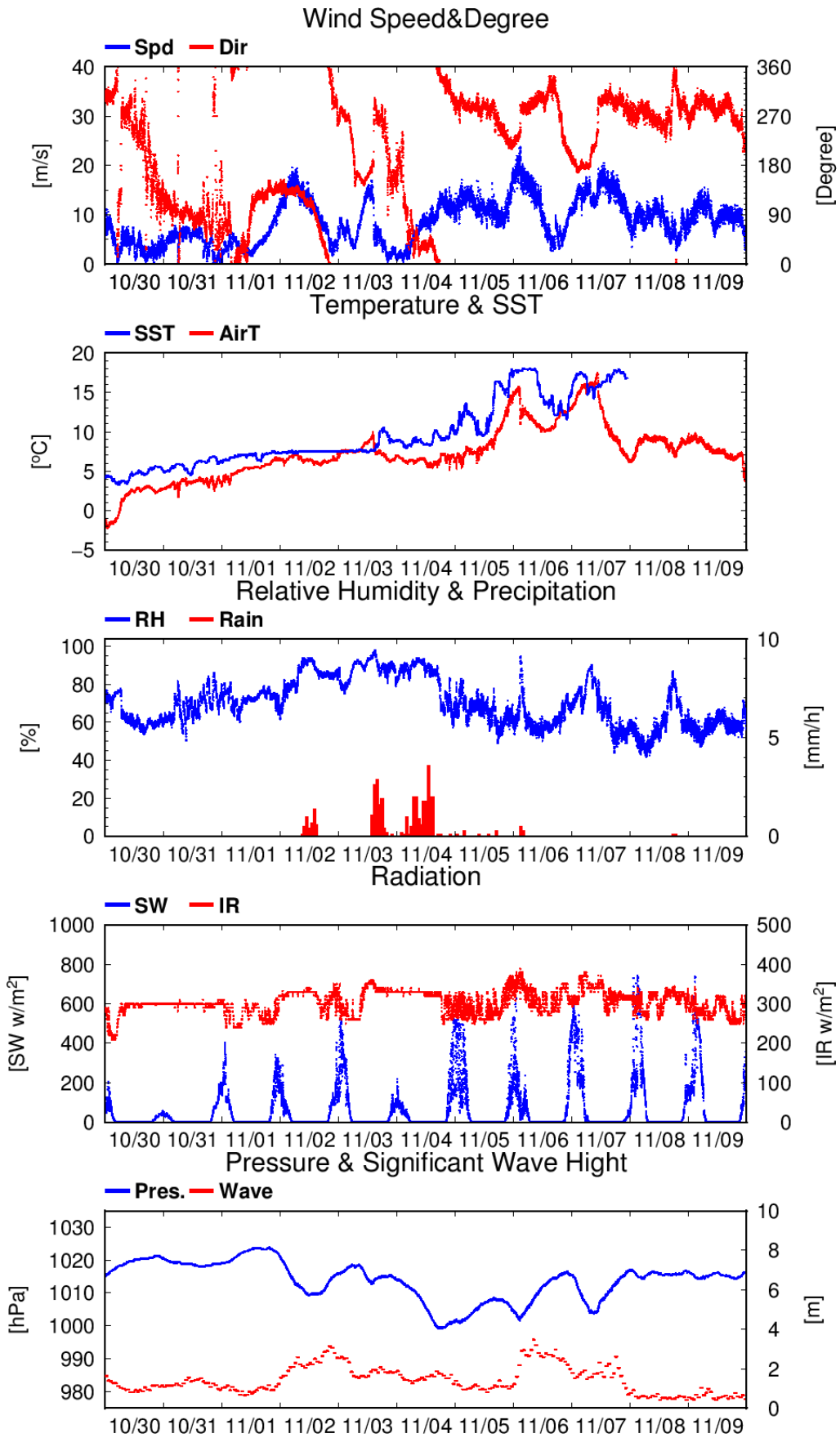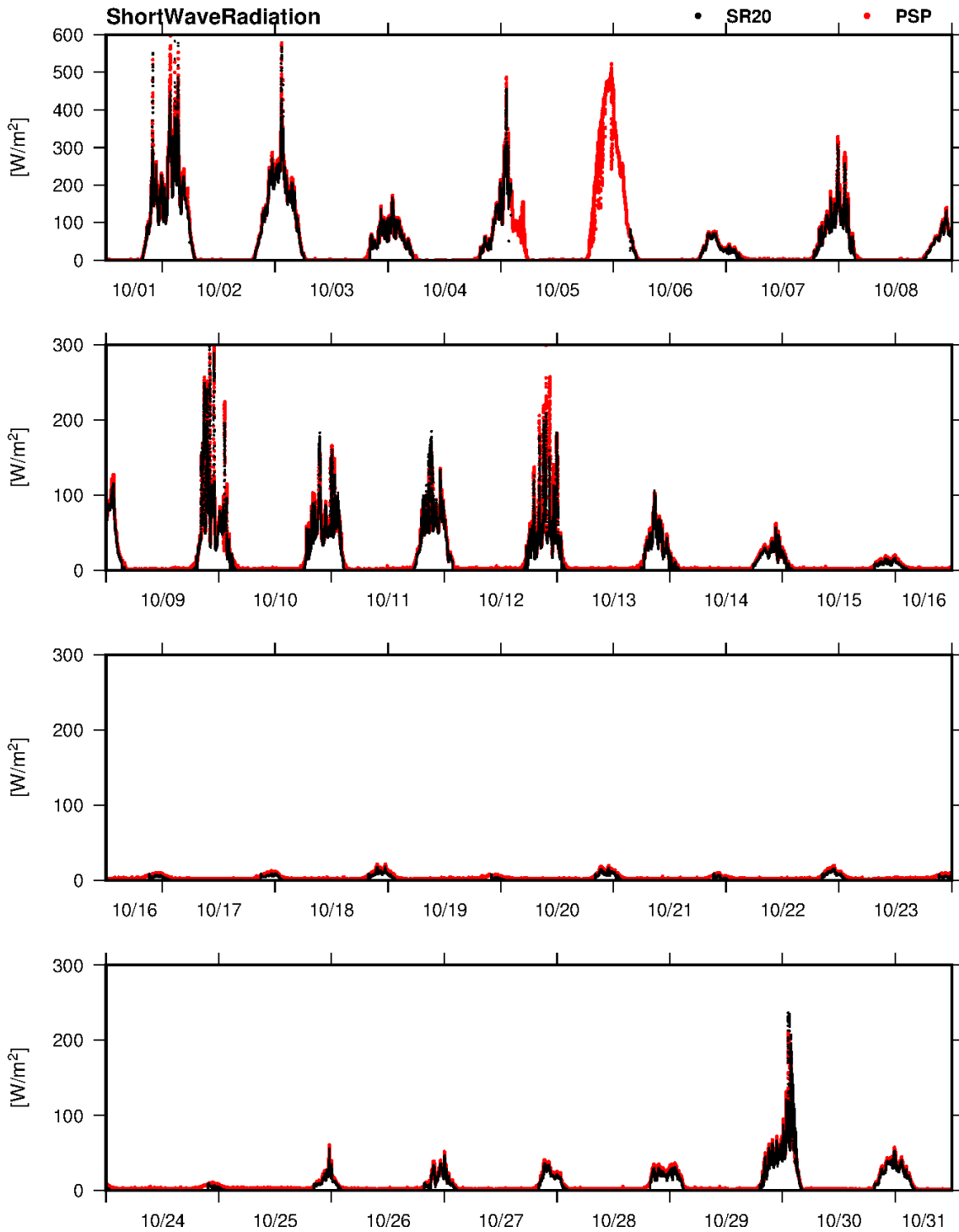
Figure 2.4-2: Time series of shortwave radiation amount measured by the SR20 (additional radiometer) and PSP in October 2019
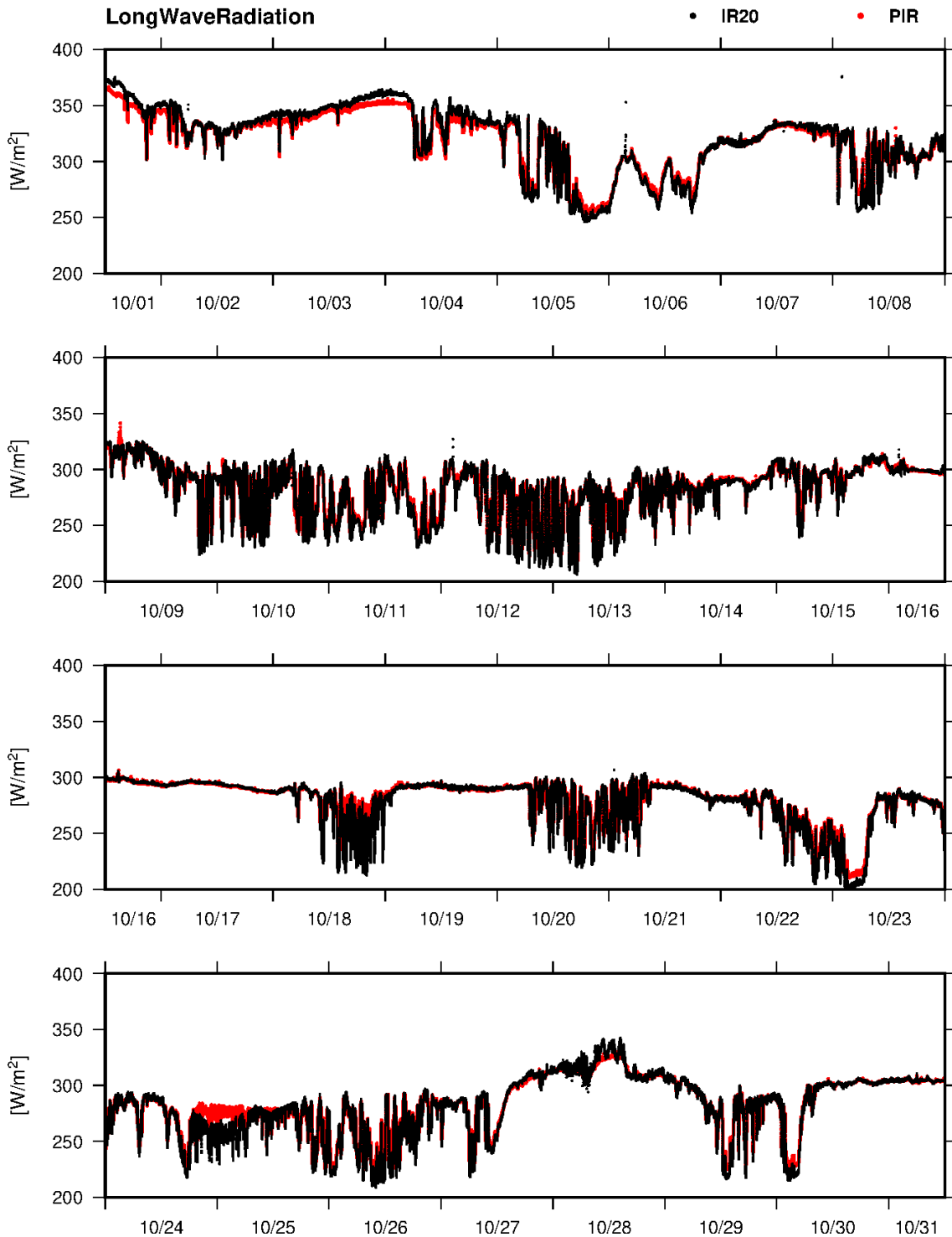
Figure 2.4-3: Time series of longwave radiation amount measured by the IR20 (additional radiometer) and PIR in October 2019

2.5 Ceilometer

(1) Personnel

Kazutoshi Sato	KIT	-PI
Ryo Oyama	NME	
Souichiro Sueyoshi	NME	
Shinya Okumura	NME	
Kazuho Yoshida	NME	
Yutaro Murakami	NME	
Takehito Hattori	MIRAI Crew	

(2) Objectives

Information on cloud base height and liquid water amount around cloud base is important for comprehension of the process of cloud formation. During this cruise, cloud base height was measured using a ceilometer.

(3) Parameters
1. Cloud base height (unit: m).
2. Backscatter profile, sensitivity and range normalized at 10-m resolution.
3. Estimated cloud amount (unit: oktas) and height (unit: m); Sky Condition Algorithm.

(4) Instruments and methods

We measured cloud base height and the backscatter profile using a ceilometer (CL51, Vaisala, Finland) throughout this cruise.

Major parameters for the measurement configuration are as follows;

Laser source:	Indium Gallium Arsenide (InGaAs) Diode Laser
Transmitting center wavelength:	910±10 nm at 25 degC
Transmitting average power:	19.5 mW
Repetition rate:	6.5 kHz
Detector:	Silicon avalanche photodiode (APD)
Measurement range:	0 ~ 15 km
	0 ~ 13 km (Cloud detection)
Resolution:	10 meter in full range
Sampling rate:	36 sec
Sky Condition	0, 1, 3, 5, 7, 8 oktas (9: Vertical Visibility)
	(0: Sky Clear, 1: Few, 3: Scattered, 5-7: Broken, 8: Overcast)

Cloud base height and the backscatter profile in the archive dataset were recorded with resolution of 10 m.

(5) Observation log
27 Sep. 2019 - 10 Nov. 2019

(6) Preliminary results

Figure 2.5 shows the time series of cloud base height measured by the ceilometer during this cruise.

(7) Data archives

The data obtained during the cruise will be submitted to the Data Management Group of JAMSTEC, and they will be made available to the public via the "Data Research System for Whole Cruise Information in

JAMSTEC (DARWIN)" on the JAMSTEC website (http://www.godac.jamstec.go.jp/darwin/e)

(8) Remarks (times in UTC)
    1. Window cleaning
        01:07UTC 29 Sep. 2019
        05:43UTC 02 Oct. 2019
        01:52UTC 08 Oct. 2019
        02:40UTC 12 Oct. 2019
        23:52UTC 12 Oct. 2019
        19:25UTC 13 Oct. 2019
        02:16UTC 16 Oct. 2019
        00:10UTC 21 Oct. 2019
        01:05UTC 21 Oct. 2019
        01:03UTC 23 Oct. 2019
        00:47UTC 24 Oct. 2019
        19:29UTC 29 Oct. 2019
        04:44UTC 07 Nov. 2019

    2. Use of the heated blower was stopped during this cruise because of its poor insulation.

Figure 2.5: Time series of cloud base height during this cruise.

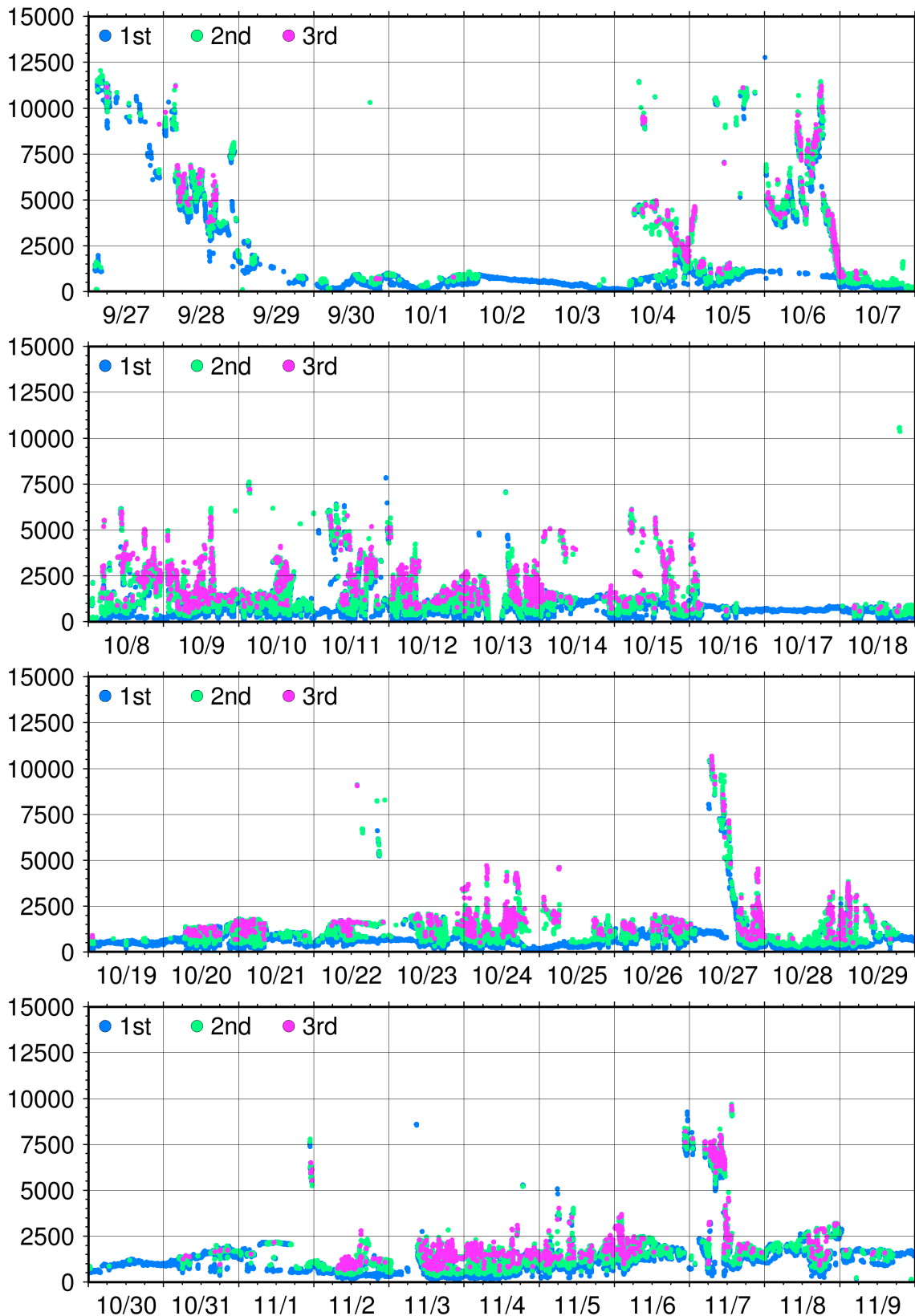## 2.6 Drones

(1) Personnel

Jun INOUE	NIPR	- PI
Kazutoshi SATO	KIT	
Tsubasa KODAIRA	The University of Tokyo	

(2) Objectives

The objectives of this observation approach were to monitor the surface conditions of the sea and the sea ice.

(3) Instruments and methods

Three types of DJI drones were used (i.e., Mavic Air, Mavic2 Enterprise Dual and Phantom4 Pro+). The specifications of each type of drone are shown in Table 2.6-1. All flights were made during daytime under calm wind conditions. One or two assistants took flight field notes (e.g., drawing the flight track and checking the status of the drone) and maintained visual contact with the flying drone (Figure 2.6-1).

Table 2.6-1

DJI Drones	Mavic Air	Mavic2 Enterprise Dual	Phantom4 Pro+
Weight (g)	430	899	1388
Endurance (min)	21	31	30
Communication system	Wifi	OcuSync2.0	Lightbridge
Frequency	2.4GHz	2.4GHz	2.4GHz
Remarks	Intelligent flight mode	Self-heating batteries, a top-mount beacon, an infrared camera	

Figure 2.6-1: Preflight check with flight assistants on the deck.

Table 2.6-2: Flight summary

No.	mm/dd	Takeoff (SMT)	Landing (SMT)	Time (min)	Lat (°N)	Lon (°W)	Type of Drone	Purpose of flight / Remarks (errors & other issues)
001	10/08	13:12	13:22	10	68.17	168.76	Mavic2	Test flight (GPS, gyrocompass, radio wave)
002	10/08	13:28	13:39	11	68.17	168.75	Mavic Air	Test flight (GPS, gyrocompass, radio wave, intelligent flight)
003	10/08	13:45	13:49	4	68.16	168.75	Phantom	Test flight (GPS, gyrocompass, radio wave)
		13:54	13:56	2				Errors (gyrocompass, GPS lost, gimbal)
004	10/15	14:52	15:12	20	77.10	164.62	Mavic2	Test flight (high altitude, RTH command, low battery)
005	10/16	11:54	12:09	15	78.08	164.93	Mavic2	Sea monitoring (sea ice distribution)
								Shipboard LIDAR beamed to the visible camera
006	10/17	10:01	10:02	1	78.01	165.02	Phantom	
		10:09	10:11	2				Errors (gyrocompass)
007	10/17	10:21	10:30	9	78.00	165.02	Mavic Air	Sea monitoring (sea ice distribution)
008	10/17	10:34	10:46	12	78.00	165.02	Mavic2	Sea monitoring (sea ice distribution)
009	10/18	11:25	11:42	17	78.07	165.17	Mavic2	Sea monitoring (surface temperature)
010	10/18	11:47	11:57	10	78.05	165.17	Phantom	Sea monitoring (sea ice distribution, waves)
								Errors (gyrocompass, unexpected flight App termination)
011	10/18	12:02	12:07	5	78/05	165.17	Mavic Air	Sea monitoring
								Errors (motor electric error), unexpected landing
012	10/24	10:52	11:09	17	77.81	163.52	Mavic2	Sea monitoring (surface temperature, waves)
								Errors (gyrocompass)
013	10/24	11:31	11:32	1	77.81	163.51	Phantom	Errors (gyrocompass, gimbal)
014	10/24	11:45	12:00	15	77.81	163.52	Mavic2	Sea monitoring (sea ice distribution, waves)
								Icing on propellers

(4) Preliminary results

Table 2.6-2 presents the flight summary. The total number of flights was 14 (1.5 h). Flights #001–004 were test flights conducted to check operation on the ship. Specific conditions related to onboard operation at low temperatures with heavy winter gear at high latitudes were assessed carefully from the perspective of safety. In particular, the status of the Global Navigation Satellite System (GPS & GLONASS), radio waves (2.4 GHz) and gyrocompass were fundamental for stable and safe drone operations. Subsequent flights focused on monitoring sea ice (i.e., horizontal distribution, surface temperature and related wave attenuation). During flight #005, large numbers of small pancake ice floes were observed near the ship (Figure 2.6-2). The surface temperature of the sea ice was monitored using an infrared camera (Figure 2.6-3) and compared with data acquired using a shipboard infrared radiometer.

(5) Data archive

The drone data comprised photographs, movies and additional information. All data obtained during this cruise will be submitted to the JAMSTEC Data Management Group (DMG).
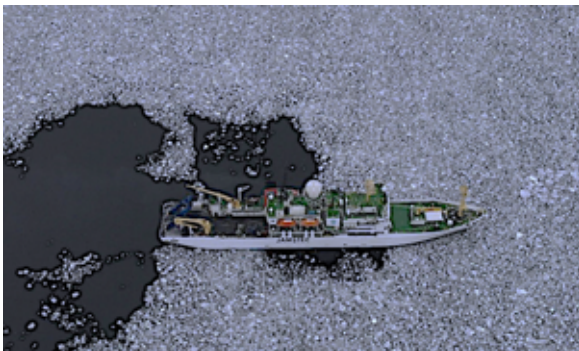
Figure 2.6-2: Sea-ice distribution around the ship (from flight #005).
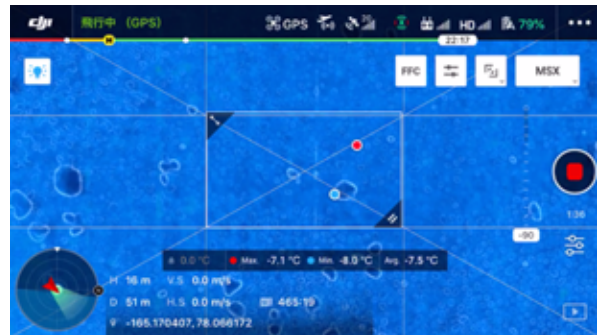
Figure 2.6-3: Screenshot of sea-ice surface temperature monitored by an infrared camera (from flight #009).

(6) Remarks

Flights by the Phantom4 Pro+ drone (#003 & #013) did not provide data because the drone did not fly correctly owing to several mechanical errors. The time stamps of flights by the Mavic Air drone (#002, #007 & #011) were incorrect for some reason. The flights by the Mavic2 drone (#001, #004, #005, #008, #009, #012 & #014) provided visible and infrared images, although the digital values in the infrared images were not available originally. However, RPReplay*.MP4 provided the values shown in the flight app on the flight monitor (iPad mini).

2.7 Infrared radiometer

(1) Personnel

Jun INOUE   NIPR   - PI

(2) Objectives

Surface temperature is a very important parameter in the surface heat budget. The parameter is often used to calculate surface turbulent heat fluxes by bulk methods, upward longwave radiation, and conductive heat flux of sea ice. The objectives of this observation approach were to monitor the skin temperature of the sea and ice surfaces and to develop a method of quality control.

(3) Parameters

Surface temperature of water or sea-ice.

(4) Instruments and methods

The SI-431 model (Apogee Instruments, Inc.) infrared radiometer has a spectral range of 8–14 µm with a 14° half-angle field of view. The detectable range is from -40 to +70 °C with accuracy of 0.179 °C. The sensor was mounted on the starboard side of the compass deck (approximately 20 m above the sea surface) with a 60° mounting angle (Figure 2.7-1). Thus, the distance to the target (sea/ice surface) and the target area were approximately 40 m and 852 m^2, respectively, in the along-ship direction ~20 m from the starboard of the ship (i.e., beyond the ship's wake). The data were collected at 10-min intervals and recorded in a data logger (C-CR300). The raw dataset consists of time (yyyy-mm-dd hh:mm:ss), record number, target temperature, detector temperature, data logger temperature and battery voltage.
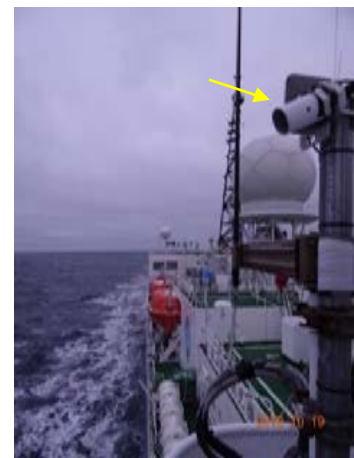
Figure 2.7-1: IR sensor on the compass deck (yellow arrow).

Daily maintenance was usually performed after 08:30 SMT (19:30 UTC) using a cotton swab dipped in alcohol to remove frost, snow, dew and sea spray (Table 2.7-1). It was desirable to exclude periods when rain and/or snowfall was observed. An optical rain gauge (see section 2.11 Precipitation) that can also detect sea sprays was found very useful for maintaining the data quality of the observed infrared temperature. Fog is a condition that is inappropriate for acquiring surface measurements. In cases of icing and snow accretion on the sensor, the temperature of the material on the sensor is observed rather than that of the target sea/ice surface. To reduce these uncertainties in the dataset, the following quality control (QC) procedures were considered effective.

1. Exclude periods when the relative humidity exceeds 99% to remove fog situations.
2. Exclude periods when the 10-min averaged intensity of precipitation (and/or sea spray) exceeds 0.01 mm/h, as determined using the Laser Precipitation Monitor (LPM2) (Adolf Thies GmbH & Co) (see Section 2.11. Precipitation).
3. Exclude periods when the 1-h mean difference in temperature between a target and the detector was <0.2 °C to remove situations of icing and snow accretion.

In the QC-ed dataset "ir_data_lev01.txt," suspect values have been replaced by the "-999.9" identifier.

In addition to this QC process, the data should be also corrected for atmospheric effects and emissivity. The radiation (E_o) observed by the instrument contains two components: radiation emitted directly by the specific atmospheric layer (E_a) with emissivity ε_a, and radiation from the surface (E_s). Furthermore, E_s can be divided into two components: direct radiation from the target surface (E_t) with emissivity ε_t, and reflected radiation of the background (E_b) with emissivity ε_b. Thus, E_o can be

expressed as in the following equation using the emissivity (ε) and reflectivity (1 − ε) of the target surface:

$$E_o = \varepsilon_a E_a + (1 - \varepsilon_a)E_s = \varepsilon_a E_a + (1 - \varepsilon_a)[\varepsilon_t E_t + (1 - \varepsilon_t)\varepsilon_b E_b] \qquad (1)$$

Equation (1) can be written in terms of temperature using the Stefan–Boltzmann law by the fourth power of its absolute temperature:

$$\sigma T_o^4 = \varepsilon_a \sigma T_a^4 + (1 - \varepsilon_a)\sigma[\varepsilon_t T_t^4 + (1 - \varepsilon_t)\,\varepsilon_b T_b^4] \qquad (2)$$

where σ is the Stefan–Boltzmann constant (5.67×10^{-8} Wm^{-2} K^{-4}). The actual surface temperature (T_t) can be calculated by rearrangement of Eq. (2):

$$T_t = \sqrt[4]{\frac{T_o^4 - \varepsilon_a T_a^4 - (1 - \varepsilon_a)(1 - \varepsilon_t)\,\varepsilon_b T_b^4}{(1 - \varepsilon_a)\varepsilon_t}} \qquad (3)$$

Here, T_a is the air temperature observed by the ship, and its emissivity ε_a is estimated empirically using the effective water vapor (w*: mm) in the specific layer:

$$\varepsilon_a = 0.33 \ln[1 + 3(w^*)^{0.45}] \qquad (4)$$

$$w^* = 0.2167\frac{e}{T_a}\Delta z \qquad (5)$$

where e is the water vapor pressure (hPa), and Δz (m) is the distance between the surface and the sensor. The corrected data (level 2 data: "ir_data_lev02.txt") are for the simple case of $\varepsilon_t = 1.00$ (i.e., without the reflection of background radiation).

In the case of $\varepsilon_t < 1.00$ (i.e., reflection at the surface is considered), $\varepsilon_b T_b$ might be approximated by the downward longwave radiation ($LWD = \varepsilon_b \sigma T_b^4$) observed by the onboard infrared pyrgeometer with spectral range of 4–50 µm (PIR Eppley Labs, USA) at 31-m height. The corrected data are archived as "ir_data_lev03.txt."

Figure 2.7-2: Preliminary result of surface temperature observed by the infrared radiometer: raw data (yellow), quality-controlled surface temperature (red) and detector temperature (green). Precipitation intensity is indicated by black bars.

(4) Preliminary results

Figure 2.7-2 shows the time series of raw infrared temperature (yellow), QC-ed temperature (red) and detector temperature (green) obtained by the instrument. As a reference, 10-min averages of air temperature (blue: JamMet) and precipitation intensity (black bars: LPM2) data are also shown. During 10:00–12:00 UTC on 23 October, the value of the raw infrared temperature dropped from 0 to -3.5 °C and then followed the values of the detector and the 10-min air temperatures. It suggests that the instrument was observing snow temperature or the temperature of accreted snow on the sensor (heavy snowfall was observed on this day, as shown in Figure 2.7-3). At the time of daily maintenance at 19:30 UTC on 23 October, snow accretion was found and cleared. Although the raw temperature data seem reasonable, the continuous snowfall on 24 October meant the requirement for QC-ed data was not satisfied (yellow line on 24 Oct). After daily maintenance at 19:30 UTC on 24 October, the temperature became normal. At this time, snow accretion and frost were found on the sensor, Figure 2.7-4. After the routine maintenance, the surface temperature over the area covered with grease ice was monitored well under the conditions of the cold environment (i.e., below -7 °C) on 24–25 October (Figure 2.7-5).

Figure 2.7-3: Photo of snowfall at 16:56 UTC on 23 October. The yellow arrow indicates the position of the IR sensor.

Figure 2.7-4: Photo of icing and snow accretion at 19:33 UTC on 24 October.
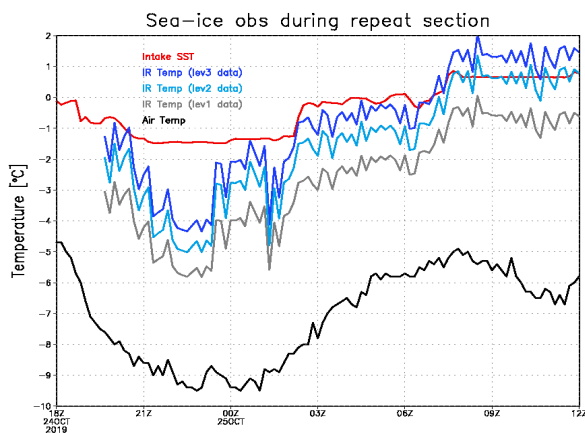
Figure 2.7-5: Comparison of surface temperature among the QC-ed datasets during the repeat section on 25 October.
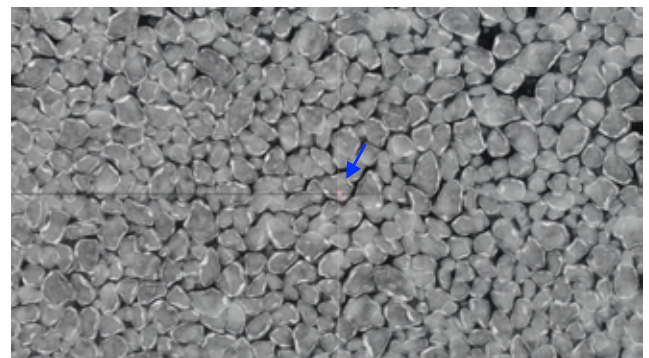
Figure 2.7-6: Photo of sea-ice condition at 22:00 UTC on 24 October taken by a drone. The area overlaps the target surface of the IR sensor. Blue arrow in Figure 2.7-5 indicates the time of image acquisition.

On 24 October, the ship entered the MIZ at 20:31 UTC (based on the ice navigator's log). The intake SST remained at -1.5 °C for a few hours, but the actual sea surface was covered by sea ice (Figure 2.7-6). The ice surface temperatures of the three QC-ed datasets are compared here. The temperature was -5.5 °C (level 1), -4.6 °C (level 2) and -4.0 °C (level 3). Considering the SST at 09:00 UTC on 25 October, the level 1 dataset clearly underestimated the surface temperature, whereas the level 2 and 3 datasets were better approximations.

Figure 2.7-7: Example of hard icing just before daily maintenance at 19:36 UTC on 29 October.

(5) Data Archive

The data obtained during the cruise will be submitted to the Data Management Group of JAMSTEC, and they will be made available to the public via the "Data Research System for Whole Cruise Information in JAMSTEC (DARWIN)" on the JAMSTEC website (http://www.godac.jamstec.go.jp/darwin/e)

(6) Remarks

Note that the period of suspect data was 05:00–19:30 UTC on 24 October, as shown in Figure 2.7-2. However, the data acquired during 00:00–19:30 UTC on 29 October were influenced by hard icing (Figure

As the trace of these suspect periods remained after the QC process, the raw values during these periods were replaced with a value of "-999.9" in the QC-ed files.

All QC-ed data could be subject to further modification because the data sources utilized in the QC processes (e.g., relative humidity and precipitation) might also be changed after their own QC checks.

Table 2.7-1: Daily maintenance times

mm/dd	9/29	9/30	10/1	10/2	10/2	10/3	10/4	10/5	10/6	10/7	10/8
hh:mm (UTC)	03:00	23:31	0:05 22:22	21:23	21:23	21:31	23:37	20:27	19:31	19:36	1:31 19:34
remark	Start recording					fog				Sea spray	fog
mm/dd	10/9	10/10	10/11	10/12	10/13	10/14	10/15	10/16	10/17	10/18	10/19
hh:mm	19:35	19:32	19:34	19:32	19:34	19:35	19:34	19:41	21:52	19:32	19:36
remark				frost			drizzle			Sea spray	
mm/dd	10/20	10/21	10/22	10/23	10/24	10/25	10/26	10/27	10/28	10/26	10/27
hh:mm	19:33	19:35		0:13 19:34	19:32	19:33	19:32	19:35	19:42	19:32	19:35
remark		Sea spray		Snow accretion	Frost, snow accretion				Rain or sea spray		
mm/dd	10/28	10/29	10/30	10/31	11/1	11/2	11/3	11/4	11/5	11/6	11/7
hh:mm	19:42	19:36 19:42	19:35	20:32	20:32	20:32	21:31	21:31	22:31	22:31	22:30
remark	Heavy rain	Hard icing			Sea spray	Sea spray	Rain	Rain		Sea spray	End of recording

2.8 Sea spray

(1) Personal

Jun Inoue	NIPR	- PI
Toshihiro Ozeki	Hokkaido Univ. of Education	- not on board
Hajime Yamaguchi	University of Tokyo	- not on board
Ryo Kusakawa	University of Tokyo	

(2) Objectives

Marine disasters caused by ship icing occur frequently in cold regions. The typical growth mechanism of sea spray icing is as follows. First, sea spray is generated from the bow of the ship. Next, the spray drifts and impinges upon the superstructure, after which there is a wet growth of ice from the brine water flow. To address the issue of ship icing, we focused on the impinging seawater spray, investigating the drop size of this spray on the R/V Mirai.

(3) Parameters

Number of sea spray particles
Spray particle size distribution
Liquid water contents
The amount of spray impinging on ships

(4) Instruments and methods

The amount of seawater spray and the size distribution of the seawater particles were measured using a spray particle counter (SPC) and a marine rain gauge type spray gauge (MRS).

(4-1) Spray particle counter (SPC)

The SPC, which was developed originally for measurements of drifting snow, was improved for use as a seawater SPC. The flux distribution and the transport rate can be calculated as a function of particle size. The SPC (SPC-S7; Niigata Denki) consists of a sensor, data processor and personal computer, and the measurement range covers particles with diameter of 100–1000 μm. The sensing area is 25-mm wide, 3-mm high and 0.5-mm deep and superluminescent diode light is used as a parallel ray. The sensor measures light attenuation caused by particles that pass through the sensing area. The processor divides the particles into 32 classes depending on their diameter. The particles in each class are counted every second. The volume flux of the spray was calculated as $4\pi r_c^3/3$, where r_c is the class value of particle radius. The unit of the volume flux is millimeters [mm] per unit time, which is also the unit of precipitation.

(4-2) Marine rain gauge type spray gauge (MRS)

The MRS consists of a marine rain gauge (C–YG-50202, R M Young) and a cylindrical spray trap. The marine rain gauge was developed to measure rainfall on ships. It collects seawater spray or precipitation in a catchment funnel that has a cross-sectional area of 100 cm^2. The inside diameter of the funnel is 112 mm. The cylindrical spray trap is attached above the marine rain gauge to capture seawater spray from the horizontal direction rather than precipitation falling vertically. The impinging spray particles are drained into the catchment funnel. The spray trap has diameter of 76.3 mm, height of 120 mm and the projected area is 92 cm^2. The amount of seawater spray is measured every minute. The smallest measurable unit is 0.1 mm.

To reveal the positional relationship of the amount of seawater spray, observations were conducted from three different points on the deck. An SPC was installed in the center of the compass deck, and an MRS was installed on the port side and another on the starboard side of the bridge deck, set on the bulwark 42 m from the bow.

(5) Station list or Observation log

Data were acquired continually from the SPC and MRSs throughout the cruise from 27 September 2019 to 7 November 2019. Experimental cruises for generating sea spray were conducted during 06:20–08:20 UTC on 13 November 2019, 15:45–17:45 UTC on 19 November 2019 and 16:50–18:50 UTC on 20 November 2019.

(6) Preliminary results
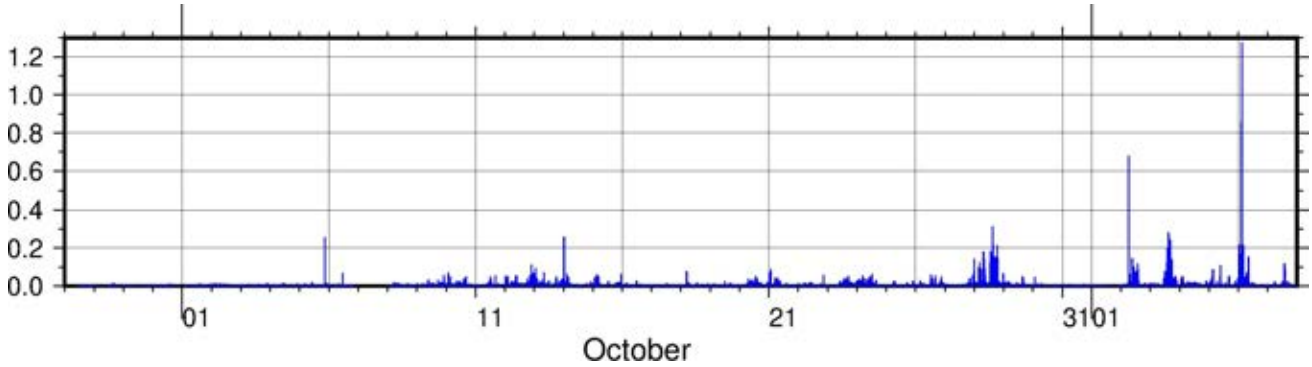
Figure 2.8-1: Spray and rainfall flux observed by the SPC.
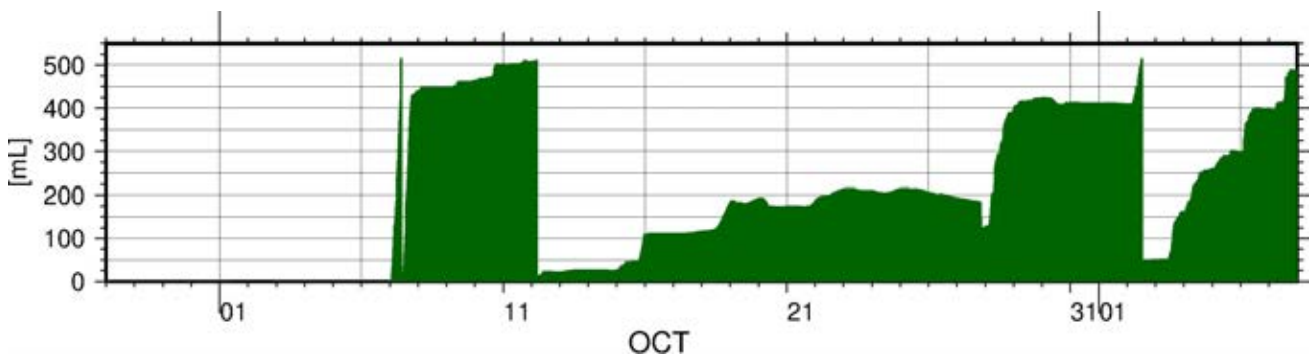
Figure 2.8-2: Spray and rainfall amount observed by the starboard side MRS.
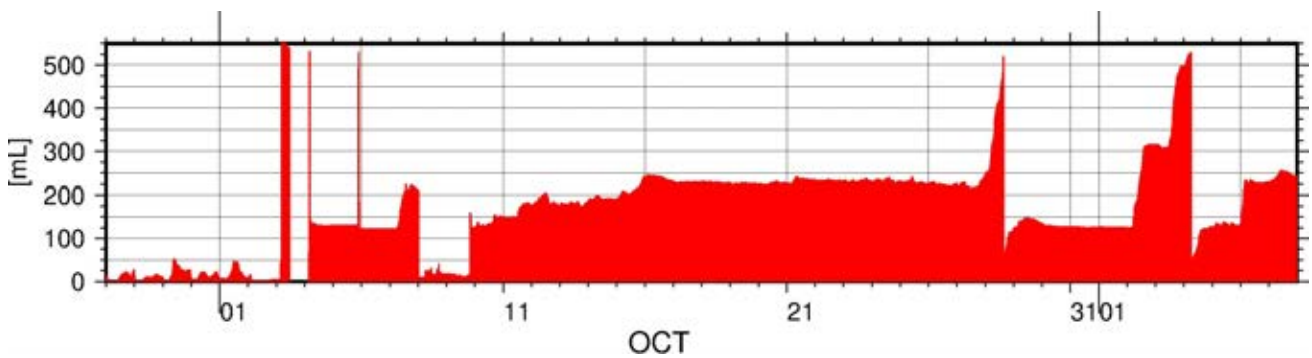
Figure 2.8-3: Spray and rainfall amount observed by the port side MRS.

(6) Data archive

The data obtained during the cruise will be submitted to the Data Management Group of JAMSTEC, and they will be made available to the public via the "Data Research System for Whole Cruise Information in JAMSTEC (DARWIN)" on the JAMSTEC website (http://www.godac.jamstec.go.jp/darwin/e)

2.9. Water vapor

2.9.1 Isotope observation

(1) Personnel

Hotaek Park   JAMSTEC   PI

(2) Background and objective

The decline of Arctic sea ice linked to global warming is progressing at a rate beyond the range of modeling projection. This enhanced decline is identified as the result of increased cyclonic activity and cloud coverage, further warming by ice–albedo feedbacks (especially significant in autumn and winter) and increased pan-Arctic precipitation. The ocean warming caused by rising air temperature enhances energy exchange with the atmosphere, particularly in autumn when the recovery of sea ice is initiated. The resultant moisture of the lower-atmosphere boundary is likely transported into adjacent regions through atmospheric circulation. Indeed, the increased snow depth in autumn and early winter in northern Arctic terrestrial regions is evidence of such transport, although debate continues regarding the correlation between the increase in snow depth and the decline of sea ice. Snow is an import component of the hydrological cycle, climate and permafrost. The snow accumulated during the winter season is nowadays melting rapidly in spring, adding to the levels of soil moisture and river discharge. The observed levels of discharge indicate significant increases in melting in spring, with advancement of the time of onset of melting due to the rising temperatures. Snow insulates the permafrost during winter, enhancing the warming and thus meaning that some of the water discharged into rivers likely derives from melted permafrost. The linkage between terrestrial hydrology and Arctic sea ice suggests that the decline in sea ice could affect the hydrological processes of terrestrial regions.

The application of numerical models is useful for identifying the linkage between the declining sea ice and terrestrial hydrology; however, such modeling requires validation of the simulated results against observations. Isotopic characterization allows backward tracing to the source area of precipitated water. The combination of model simulations and isotope observations makes it possible to explore the relationship between the declining sea ice and the terrestrial water cycle. Therefore, consecutive observations of the isotopes of atmospheric water vapor were conducted during the MR19-03C Arctic cruise. The preliminary results of those observations are documented here.

(3) Parameters

Isotope ratios of oxygen and hydrogen and water vapor concentration

(4) Instrument and method

The isotopes of atmospheric water vapor were monitored using a cavity ringdown spectrometer (L2130-i, Isotopic H_2O, Picarro, Figure 2.9.1-1), which simultaneously observes the isotope ratios of oxygen and hydrogen (frequency: 1–2 Hz), including water vapor concentration. The observed data were archived within the storage space of the spectrometer that is operated by the Windows system. Two standard liquids with isotope values of -0.262 and -30.873 per mil in oxygen were injected individually for 15 min at 12-h intervals, and the derived linear regression equation was used to calibrate the values monitored by the spectrometer.

Figure 2.9.1-1: Isotope observing spectrometer system.

(5) Preliminary results

The observed isotope ratio data, averaged into hourly time steps (Figure 2.9.1-2), showed diurnal and interdaily variability consistent with the raw data. Figure 2.9.1-2 displays the observations acquired in the Arctic Ocean during 10–27 October. The isotope ratios generally decreased with time, representing the influence of the decrease in air temperature. Overall, the isotope of oxygen showed significant correlation with air temperature (Figure 2.9.1-3), as addressed by other observations. However, the isotopes showed large diurnal and daily variability (Figure 2.9.1-2). Here, we discuss three days (i.e., 13, 15 and 25 October) that recorded the lowest and highest isotope ratios. The isotope of oxygen indicated minimum values of -29.0 per mil on 13 October and -28.5 per mil on 25 October (when the recorded air temperature was -9 °C). The oxygen isotope has high correlation with air temperature, as mentioned above. The air temperature on 13 October was higher than on 25

Figure 2.9.1-2: Variability of air temperature, sea surface temperature, and isotopes of oxygen and hydrogen during 10-27 October.

October, which suggests variables other than air temperature had an effect on the isotope. One such variable is the transport of warmer/colder water vapor by wind. There was strong wind from the north on 13 October, whereas strong southerly wind transported warmer air with higher levels of water vapor across the area on 25 October. Investigation of the quantification of the impact of wind on isotopic changes will be explored using the methods of model simulation and backward trajectory.

Both oxygen and hydrogen indicated significantly high correlation. Their relationship yielded a slope of 6.1, which is within the range of 5–7 generally obtained in Arctic regions.

(6) Data archive

The data obtained during the cruise will be submitted to the Data Management Group of JAMSTEC, and they will be made available to the public via the "Data Research System for Whole Cruise Information in JAMSTEC (DARWIN)" on the JAMSTEC website (http://www.godac.jamstec.go.jp/darwin/e)

Figure 2.9.1-3: Relationship between d-excess and difference in temperature between sea surface and air.

2.9.2 GNSS precipitable water

(1) Personnel

Fumikazu TAKETANI   JAMSTEC   - PI
Masaki KATSUMATA   JAMSTEC   - not on board
Mikiko FUJITA   JAMSTEC   - not on board
Kyoko TANIGUCHI   JAMSTEC   - not on board

(2) Objective

To obtain GNSS satellite data for estimation of the total column integrated water vapor content of the atmosphere.

(3) Method

The GNSS satellite data were archived to the receiver (Trimble NetR9) at 5-s intervals. The GNSS antenna (Margrin) was set on the roof of aft wheelhouse. The observations were performed throughout the entire cruise.

(4) Results

We will calculate the total column integrated water from the observed GNSS satellite data after completion of the cruise.

(5) Data archive

The data obtained during the cruise will be submitted to the Data Management Group of JAMSTEC, and they will be made available to the public via the "Data Research System for Whole Cruise Information in JAMSTEC (DARWIN)" on the JAMSTEC website (http://www.godac.jamstec.go.jp/darwin/e)
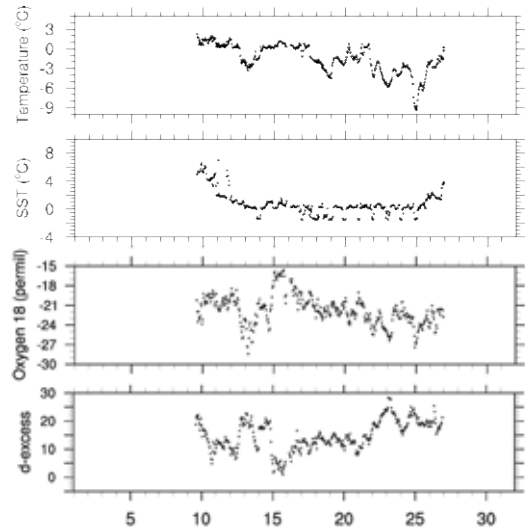
2.10 Tropospheric gas and particles observation in the Arctic Marine Atmosphere
2.10.1 Surface measurement
(1) Personnel

Fumikazu Taketani	JAMSTEC	- PI
Taro Maruo	JAMSTEC/Kobe Univ.	
Yugo Kanaya	JAMSTEC	- not on board
Takuma Miyakawa	JAMSTEC	- not on board
Kaori Kawana	JAMSTEC	- not on board
Hisahiro Takashima	JAMSTEC/Fukuoka Univ.	- not on board
Yutaka Tobo	NIPR	- not on board
Yoko Iwamoto	Hiroshima Univ.	- not on board
Masayuki Takigawa	JAMSTEC	- not on board
Masahiro Yamaguchi	JAMSTEC	- not on board
Zhu Chunmao	JAMSTEC	- not on board
Kazuyuki Miyazaki	JAMSTEC	- not on board
Kazuyo Yamaji	JAMSTEC/Kobe Univ.	- not on board

(2) Objectives
• To investigate the roles of aerosols in the marine atmosphere in relation to climate change
• To investigate the processes of biogeochemical cycles between the atmosphere and the ocean
• To investigate the contribution of suspended particles to rain and snow

(3) Parameters
• Black carbon(BC) and fluorescent particles
• Particle size distribution
• Particle number concentration
• Aerosol extinction coefficient (AEC)
• Composition of ambient particles
• Composition of snow and rain
• Surface ozone(O_3), and carbon monoxide(CO) mixing ratios

(4) Instruments and methods
(4-1) Online aerosol observations:
 (4-1-1) Particle number concentration and size distribution
   The number concentration of ament particles was measured using a mixing condensation particle counter (MCPC) (Model 1720, Brechtel). The size distribution of the particles was measured using a scanning mobility particle sizer (SMPS) (Nano Scan model 3910, TSI) and a handheld optical particle counter (OPC) (KR-12A, Rion). The number concentration of the cloud condensation nuclei (CCN) in the ambient air was measured using a CCN counter (CCNC) (CCN-100, Droplet Measurement Technologies). The CCNC detected activated particles using an OPC under supersaturated water vapor conditions in a 50-cm-high column.
 (4-1-2) Black carbon (BC)
   The number of particles and mass concentration of BC were measured using an instrument based on laser-induced incandescence, i.e., a single particle soot photometer (SP2) (model D, Droplet Measurement Technologies). The laser-induced incandescence technique based on an intracavity Nd:YVO4 laser operating at 1064 nm was used for detection of single BC particles.
 (4-1-3) Fluorescent property

Fluorescent properties of aerosol particles were measured using a single particle fluorescence sensor, i.e., a Waveband Integrated bioaerosol sensor (WIBS4) (WIBS-4A, Droplet Measurement Technologies). Two pulsed xenon lamps emitting UV light (280 and 370 nm) were used for excitation. Fluorescence emitted from a single particle within wavelength windows of 310–400 and 420–650 nm was recorded.

(4-1-4) Aerosol extinction coefficient (AEC)

Multi-Axis Differential Optical Absorption Spectroscopy (MAX-DOAS), a passive remote sensing technique measuring the spectra of scattered visible and UV solar radiation, was used for atmospheric aerosol and gas profile measurements. Our MAX-DOAS instrument consisted of two main components: an outdoor telescope unit and an indoor spectrometer (Acton SP-2358 with Princeton Instruments PIXIS-400B), connected to each other via a 14-m bundled optical fiber cable. The line of sight was in the direction of the portside of the vessel and the scanned elevation angles were 1.5, 3, 5, 10, 20, 30 and 90 degrees in a 30-min cycle. The roll motion of the ship was measured for automatic compensation of additional motion of the prism employed for scanning the elevation angle. For the selected spectra recorded with elevation angles with reasonable accuracy, DOAS spectral fitting was performed to quantify the slant column density (SCD) of NO_2 (and other gases) and O_4 (O_2–O_2, collision complex of oxygen) for each elevation angle. Then, the O_4 SCDs were converted to the aerosol optical depth (AOD) and the vertical profile of the aerosol extinction coefficient (AEC) using an optimal estimation inversion method with a radiative transfer model. Using derived aerosol information, retrievals of the tropospheric vertical column/profile of NO_2 and other gases were achieved.

For the SP2, MCPC, SMPS and CCNC instruments, ambient air was sampled from the compass deck via a 3-m-long conductive tube routed through a dryer to dry the particles, and then introduced to each instrument installed in the environmental research room. The WIBS4 and OPC instruments were installed on the compass deck and ambient air was introduced directly to the instruments. The MAX-DOAS instrument was installed on the deck above the ship's stabilizer.

(4-2) Ambient air sampling

Ambient air sampling was performed using air samplers installed on the compass deck. Ambient particles were collected on quartz filters ($\phi = 110$ and $\phi = 55$) and nuclepore polycarbonate membrane filters (half-moon of 37 mm and $\phi = 47$mm) along the cruise track. The particle composition and ice nucleation capability were analyzed using a high-volume air sampler (HV-525PM, SIBATA), NANO sampler (model 3182, Kanomax), custom-made air sampler and MOUDI sampler (MOUDI-10, MSP) operated at flow rates of 500, 40, 10 and 1.8 L/min, respectively. Ambient aerosol sampling for bioaerosol analysis: Coarse-mode aerosol particles (≥ 0.9 μm) were also sampled to a vial bottle using a cyclone (PM1, URG) with a flow rate of 20 L/min. For ambient bioaerosol analysis, Milli-Q water was added to the vial bottles and the solution was filtered through a membrane filter onto a gold-coated chip. Stained fluorescence measurements were also conducted with reagents of DAPI and Hoechst. Then, the abundance of bioaerosol particles (dead/alive) was counted using a Bioplorer (KB-VKH01, Koyo Sangyo Co., Ltd) based on fluorescence measurements with UV and green light excitation.

To avoid collecting particles emitted from the funnel of the vessel, the sampling period was controlled automatically using a "wind-direction selection system." The sampling logs are listed in Tables 2.10-1, 2.10-2, 2.10-3, 2.10-4 and 2.10-5. The collected samples will be analyzed in the laboratory after completion of the cruise.

(4-4) CO and O_3

Ambient air was sampled continuously on the compass deck and drawn through ~20-m-long Teflon tubes connected to a gas filter correlation CO analyzer (Model 48C, Thermo Fisher Scientific) and a UV

photometric ozone analyzer (2TB) located in the Research Information Center. The data will be used for characterizing air mass origins.

(5) Observation log

Table 2.10.1-1: Log of ambient particle sampling on the quartz filters by the HV sampler

On board ID	Date Collected					Latitude			Longitude		
	YYYY	MM	DD	hh:mm:ss	UTC/JST	Deg.	Min.	N/S	Deg.	Min.	E/W
MR1903C-HV-001	2019	9	29	07:11	UTC	40	22.65	N	142	28.29	E
MR1903C-HV-002	2019	10	1	01:19	UTC	42	13.80	N	152	47.16	E
MR1903C-HV-003	2019	10	2	22:31	UTC	48	43.12	N	163	46.54	E
MR1903C-HV-004	2019	10	4	21:14	UTC	55	01.43	N	173	38.17	E
MR1903C-HV-005	2019	10	6	20:59	UTC	60	56.43	N	176	56.95	W
MR1903C-HV-006	2019	10	8	20:23	UTC	67	33.49	N	168	45.04	W
MR1903C-HV-007	2019	10	10	20:09	UTC	72	59.92	N	160	01.04	W
MR1903C-HV-008	2019	10	12	20:04	UTC	72	20.40	N	144	59.75	W
MR1903C-HV-009	2019	10	14	20:48	UTC	74	46.45	N	150	30.51	W
MR1903C-HV-010	2019	10	16	20:13	UTC	77	39.86	N	165	00.08	W
MR1903C-HV-011	2019	10	18	20:13	UTC	78	02.11	N	164	58.68	W
MR1903C-HV-012	2019	10	20	20:18	UTC	77	45.00	N	165	00.11	W
MR1903C-HV-013	2019	10	23	00:44	UTC	77	46.78	N	164	03.13	W
MR1903C-HV-014	2019	10	24	20:04	UTC	77	46.15	N	164	32.57	W
MR1903C-HV-015	2019	10	26	20:34	UTC	72	00.01	N	168	45.01	W
MR1903C-HV-016	2019	10	28	20:08	UTC	66	02.61	N	168	44.96	W
MR1903C-HV-017	2019	10	30	19:58	UTC	58	56.86	N	179	21.09	E
MR1903C-HV-018	2019	11	1	21:20	UTC	51	18.65	N	168	19.35	E
MR1903C-HV-019	2019	11	3	22:20	UTC	47	49.53	N	162	11.19	E
MR1903C-HV-020	2019	11	5	23:10	UTC	41	36.35	N	151	44.69	E

Table 2.10.1-2: Log of ambient particle sampling on the quartz filters by the NANO sampler

On board ID	Date Collected					Latitude			Longitude		
	YYYY	MM	DD	hh:mm:ss	UTC/JST	Deg.	Min.	N/S	Deg.	Min.	E/W
MR1903C-NANO-001	2019	9	29	07:11	UTC	40	22.65	N	142	28.29	E
MR1903C-NANO-002	2019	10	1	01:19	UTC	42	13.80	N	152	47.16	E
MR1903C-NANO-003	2019	10	2	22:31	UTC	48	43.12	N	163	46.54	E
MR1903C-NANO-004	2019	10	5	20:52	UTC	58	06.54	N	168	23.17	W
MR1903C-NANO-005	2019	10	8	20:23	UTC	67	33.49	N	168	45.04	W
MR1903C-NANO-006	2019	10	11	20:08	UTC	72	05.53	N	153	21.91	W
MR1903C-NANO-007	2019	10	14	20:48	UTC	74	46.45	N	150	30.51	W
MR1903C-NANO-008	2019	10	18	02:24	UTC	77	42.91	N	165	00.29	W
MR1903C-NANO-009	2019	10	20	20:18	UTC	77	45.00	N	165	00.11	W
MR1903C-NANO-010	2019	10	23	20:29	UTC	77	45.36	N	163	53.40	W
MR1903C-NANO-011	2019	10	26	20:34	UTC	72	00.01	N	168	45.01	W
MR1903C-NANO-012	2019	10	29	20:30	UTC	62	29.98	N	174	41.13	W
MR1903C-NANO-013	2019	11	1	21:20	UTC	51	18.65	N	168	19.35	E
MR1903C-NANO-014	2019	11	3	22:20	UTC	47	49.53	N	162	11.19	E
MR1903C-NANO-015	2019	11	5	23:10	UTC	41	36.35	N	151	44.69	E

Table 2.10.1-3: Log of ambient particle sampling on the nuclepore filters

On board ID	Date Collected					Latitude			Longitude		
	YYYY	MM	DD	hh:mm:ss	UTC/JST	Deg.	Min.	N/S	Deg.	Min.	E/W
MR1903C-INP-001	2019	9	29	0.2993056	UTC	40	22.65	N	142	28.29	E
MR1903C-INP-002	2019	10	1	0.0548611	UTC	42	13.80	N	152	47.16	E
MR1903C-INP-003	2019	10	2	0.9381944	UTC	48	43.12	N	163	46.54	E
MR1903C-INP-004	2019	10	4	0.8847222	UTC	55	01.43	N	173	38.17	E
MR1903C-INP-005	2019	10	6	0.8743056	UTC	60	56.43	N	176	56.95	W
MR1903C-INP-006	2019	10	8	0.8493056	UTC	67	33.49	N	168	45.04	W
MR1903C-INP-007	2019	10	10	0.8395833	UTC	72	59.92	N	160	01.04	W
MR1903C-INP-008	2019	10	12	0.8361111	UTC	72	20.40	N	144	59.75	W
MR1903C-INP-009	2019	10	14	0.8666667	UTC	74	46.45	N	150	30.51	W
MR1903C-INP-010	2019	10	16	0.8423611	UTC	77	39.86	N	165	00.08	W
MR1903C-INP-011	2019	10	18	0.8423611	UTC	78	02.11	N	164	58.68	W
MR1903C-INP-012	2019	10	20	0.8458333	UTC	77	45.00	N	165	00.11	W
MR1903C-INP-013	2019	10	23	0.0305556	UTC	77	46.78	N	164	03.13	W
MR1903C-INP-014	2019	10	24	0.8361111	UTC	77	46.15	N	164	32.57	W
MR1903C-INP-015	2019	10	26	0.8569444	UTC	72	00.01	N	168	45.01	W
MR1903C-INP-016	2019	10	28	0.8388889	UTC	66	02.61	N	168	44.96	W
MR1903C-INP-017	2019	10	30	0.8319444	UTC	58	56.86	N	179	21.09	E
MR1903C-INP-018	2019	11	1	0.8888889	UTC	51	18.65	N	168	19.35	E
MR1903C-INP-019	2019	11	3	0.9305556	UTC	47	49.53	N	162	11.19	E
MR1903C-INP-020	2019	11	5	0.9652778	UTC	41	36.35	N	151	44.69	E

Table 2.10.1-4: Log of ambient particle sampling on the polycarbonate filters by the MOUDI sampler

On board ID	Date Collected					Latitude			Longitude		
	YYYY	MM	DD	hh:mm:ss	UTC/JST	Deg.	Min.	N/S	Deg.	Min.	E/W
MR1903C-MOUDI-001	2019	9	29	07:11	UTC	40	22.65	N	142	28.29	E
MR1903C-MOUDI-002	2019	10	6	20:59	UTC	60	56.43	N	176	56.95	W
MR1903C-MOUDI-003	2019	10	14	20:48	UTC	74	46.45	N	150	30.51	W
MR1903C-MOUDI-004	2019	10	21	22:53	UTC	78	01.36	N	164	58.01	W
MR1903C-MOUDI-005	2019	10	29	20:30	UTC	62	29.98	N	174	41.13	W

Table 2.10.1-5: Log of ambient particle sampling by the PM1 cyclone

On board ID	Date Collected					Latitude			Longitude		
	YYYY	MM	DD	hh:mm:ss	UTC/JST	Deg.	Min.	N/S	Deg.	Min.	E/W
MR1903C-Cyclone-001	2019	10	8	01:36	UTC	64	50.60	N	169	30.20	W
MR1903C-Cyclone-002	2019	10	9	19:37	UTC	70	38.46	N	168	15.51	W
MR1903C-Cyclone-003	2019	10	11	20:08	UTC	72	05.12	N	153	12.82	W
MR1903C-Cyclone-004	2019	10	13	19:46	UTC	74	23.03	N	143	36.95	W
MR1903C-Cyclone-005	2019	10	15	19:38	UTC	76	34.41	N	162	15.18	W
MR1903C-Cyclone-006	2019	10	18	02:24	UTC	77	42.91	N	165	00.29	W
MR1903C-Cyclone-007	2019	10	19	19:55	UTC	77	47.07	N	164	59.84	W
MR1903C-Cyclone-008	2019	10	21	22:54	UTC	78	01.38	N	164	59.98	W
MR1903C-Cyclone-009	2019	10	24	01:37	UTC	77	29.01	N	164	08.35	W
MR1903C-Cyclone-010	2019	10	25	19:38	UTC	75	21.58	N	168	45.00	W
MR1903C-Cyclone-011	2019	10	27	19:43	UTC	68	30.05	N	168	45.10	W
MR1903C-Cyclone-012	2019	10	29	19:38	UTC	62	26.30	N	174	48.00	W
MR1903C-Cyclone-013	2019	10	31	20:30	UTC	55	08.37	N	173	38.31	E
MR1903C-Cyclone-014	2019	11	2	20:40	UTC	49	59.99	N	166	06.92	E
MR1903C-Cyclone-015	2019	11	4	21:32	UTC	44	47.12	N	156	57.12	E

(6) Data archives

The data obtained during the cruise will be submitted to the Data Management Group of JAMSTEC, and they will be made available to the public via the "Data Research System for Whole Cruise Information in JAMSTEC (DARWIN)" on the JAMSTEC website (http://www.godac.jamstec.go.jp/darwin/e)

2.10.2 Tethered balloon observation

(1) Personnel

Fumikazu Taketani	JAMSTEC	- PI
Taro Maruo	JAMSTEC/Kobe Univ.	
Yugo Kanaya	JAMSTEC	- not on board
Takuma Miyakawa	JAMSTEC	- not on board
Yoko Iwamoto	Hiroshima Univ.	- not on board
Masayuki Takigawa	JAMSTEC	- not on board
Kazuyo Yamaji	JAMSTEC/Kobe Univ.	- not on board
Ryo Oyama	NME	

(2) Objectives
• To investigate vertical profiles of aerosol number concentration and size distribution in the marine atmosphere

(3) Parameters
• Particle size distribution
• Particle number concentration
• Black carbon(BC) mass concentration
• Composition of ambient particles

(4) Instruments and methods

Tethered-balloon observations were performed using an airship-shaped balloon (15 m^3, Kikyu-Seisakujo) connected by cable to a portable winch installed on the upper deck (Figure 2.10.2-1). The bag of installed instruments and the GPS sonde were connected 5 and 10 m below the balloon, respectively (Figure 2.10.2-2). Vertical profiles of particle number concentration, BC mass concentration and particle size distribution were measured using a condensation particle counter (CPC) (Model 3007, TSI), BC monitor (AE51, Magii) and OPC (HHPC6+, Beckman coulter), respectively. Aerosol particles were also sampled using a custom-made sampler placed at the highest position during each observation session. These samples will be analyzed in the laboratory after completion of the cruise. We undertook seven sessions of tethered-balloon observations during the cruise, the dates and locations of which are listed in Table 2.10.2

(5) Preliminary results

Figure 2.10.2-3 presents the results of vertical profiles of the number concentration, size-selected number concentration and relative humidity measured by the CPC, OPC and GPS sonde.

(6) Data archives

The data obtained during the cruise will be submitted to the Data Management Group of JAMSTEC, and they will be made available to the public via the "Data Research System for Whole Cruise Information in JAMSTEC (DARWIN)" on the JAMSTEC website (http://www.godac.jamstec.go.jp/darwin/e)

Figure 2.10.2-1: Tethered-balloon observation.

Figure 2.10.2-2: Instruments employed in the tethered-balloon observations.

Table 2.10.2 Logs of tethered-balloon observations

	date(UTC)	Lat(N)	Long(E)	Attained height(m)	location
1st	10/2 0:23	45.61	158.36	850	North Western Pacific
2nd	10/6 0:12	58.13	178.45	1200	Bering Sea
3rd	10/11 1:01	72.73	201.68	500	Arctic Ocean
4th	10/16 0:40	76.98	195.25	950	Arctic Ocean
5th	10/17 19:06	77.75	195.02	700	Arctic Ocean
6th	10/17 23:45	78.01	195.02	660	Arctic Ocean(MIZ)
7th	10/22 21:00	77.76	195.31	1050	Arctic Ocean
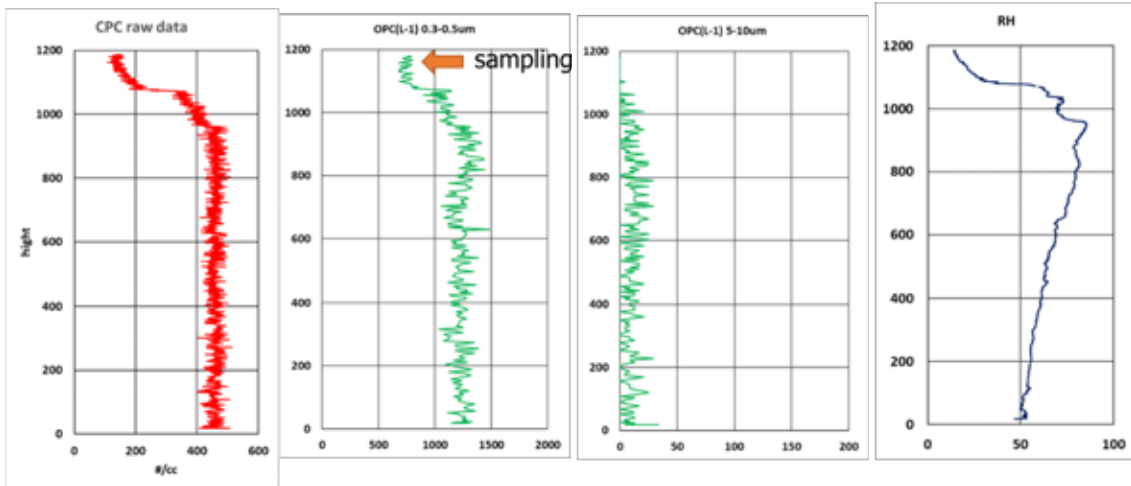
Figure 2.10.2-3: Vertical profiles of number concentration, size-selected number concentration and relative humidity.

2.11 Precipitation

2.11.1 Disdrometer

(1) Personnel

Fumikazu TAKETANI	JAMSTEC	- PI
Masaki KATSUMATA	JAMSTEC	- not on board
Biao GENG	JAMSTEC	- not on board
Kyoko TANIGUCHI	JAMSTEC	- not on board

(2) Objectives

A disdrometer can continuously obtain the size distribution of raindrops. The objectives of this observation program were as follows: (a) to reveal the microphysical characteristics of rainfall depending on the type and temporal stage of the precipitating clouds; (b) to retrieve a coefficient to convert radar reflectivity (especially from the C-band radar mentioned in Section 2.3) to rainfall amount; and (c) to validate the algorithms and products of satellite-borne precipitation radars, i.e., TRMM/PR and GPM/DPR.

(3) Instrumentations and Methods

Two laser precipitation monitors (LPMs) (Adolf Thies GmbH & Co) were utilized in this program. The LPMs were installed on the starboard bow corner on top of the antiroll system, as shown in Figure 2.11.1-1. One (located aft of the other) was equipped with a wind protection "element" to reduce the effect of wind on the measurements, and analysis of the effectiveness of the "element" was performed through comparison of the data acquired by the two sensors. The LPM adopted for this purpose was an optical disdrometer that consists of a transmitter unit that houses the infrared laser and a receiver unit that detects the intensity of the laser light after its passage over a certain distance in air. When a precipitating particle falls through the laser beam, the received intensity of the laser light is reduced. The receiver unit detects the magnitude and duration of the reduction and converts that information into particle size and fall speed. The sampling volume, i.e., the size of the laser beam "sheet" is 20 mm (W) x 228 mm (D) x 0.75 mm (H). The numbers of particles were categorized based on the detected size and fall speed and counted in 1-min intervals. The categories are shown in Table 2.11.1.

(4) Preliminary Results

The data were obtained throughout the entire cruise, except when in nonpermissive territorial waters and EEZs. An example of the obtained data is shown in Figure 2.11.1-2. Further analyses of the rainfall amount and drop-size-distribution parameters will be performed after the cruise is completed.

(5) Data Archive

The data obtained during the cruise will be submitted to the Data Management Group of JAMSTEC, and they will be made available to the public via the "Data Research System for Whole Cruise Information in JAMSTEC (DARWIN)" on the JAMSTEC website (http://www.godac.jamstec.go.jp/darwin/e)

(6) Acknowledgment

The operations are supported by the Japan Aerospace Exploration Agency (JAXA) Precipitation Measurement Mission (PMM).

Figure 2.11.1-1: Onboard LPM sensors. (Left) Sensor location indicated by the red broken circle. (Right) Photo of the sensors showing the wind protection "element" mounted on the right-hand (aft) unit.
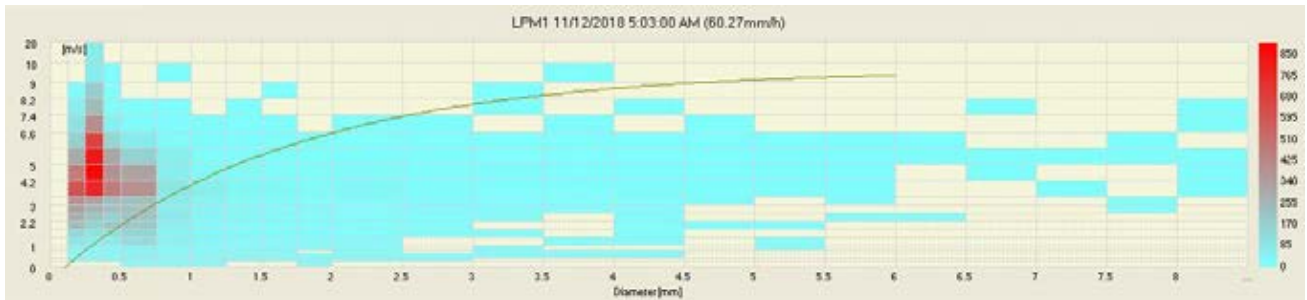
Figure 2.11.1-2: Example of 1-min raw data obtained by LPM at 05:03 UTC on 12 November 2018. Data are shown as two-dimensional histogram to display the numbers of observed raindrops categorized by diameter (x-axis) and fall speed (y-axis).

Table 2.11.1: Categories of particle size and fall speed

Particle Size			Fall Speed			
Class	Diameter [mm]	Class width [mm]	Class	Speed [m/s]	Class	width [m/s]
1	≥ 0.125	0.125	1	≥ 0.000		0.200
2	≥ 0.250	0.125	2	≥ 0.200		0.200
3	≥ 0.375	0.125	3	≥ 0.400		0.200
4	≥ 0.500	0.250	4	≥ 0.600		0.200
5	≥ 0.750	0.250	5	≥ 0.800		0.200
6	≥ 1.000	0.250	6	≥ 1.000		0.400
7	≥ 1.250	0.250	7	≥ 1.400		0.400
8	≥ 1.500	0.250	8	≥ 1.800		0.400
9	≥ 1.750	0.250	9	≥ 2.200		0.400
10	≥ 2.000	0.500	10	≥ 2.600		0.400
11	≥ 2.500	0.500	11	≥ 3.000		0.800
12	≥ 3.000	0.500	12	≥ 3.400		0.800
13	≥ 3.500	0.500	13	≥ 4.200		0.800
14	≥ 4.000	0.500	14	≥ 5.000		0.800
15	≥ 4.500	0.500	15	≥ 5.800		0.800
16	≥ 5.000	0.500	16	≥ 6.600		0.800
17	≥ 5.500	0.500	17	≥ 7.400		0.800
18	≥ 6.000	0.500	18	≥ 8.200		0.800
19	≥ 6.500	0.500	19	≥ 9.000		1.000
20	≥ 7.000	0.500	20	≥ 10.000		10.000
21	≥ 7.500	0.500				
22	≥ 8.000	unlimited				

2.11.2 Micro Rain Radar

(1) Personnel

Fumikazu TAKETANI	JAMSTEC	- PI
Masaki KATSUMATA	JAMSTEC	- not on board
Biao GENG	JAMSTEC	- not on board
Kyoko TANIGUCHI	JAMSTEC	- not on board

(2) Objectives

The micro rain radar (MRR) is a compact vertically pointing Doppler radar used to detect vertical profiles of raindrop size distribution. The objective of this observation program was to elucidate the detailed vertical structure of precipitating systems.

(3) Instruments and Methods

The MRR-2 (METEK GmbH) was utilized for this program, the specifications of which are listed in Table 2.11.2. The antenna unit was installed on the starboard side of the antiroll system (see Figure 2.11.2-1) and wired to a junction box and laptop PC inside the vessel.

The data were averaged and stored at 1-min intervals. The vertical profile of each parameter was obtained for 100-m bins over a range (i.e., height) of up to 3100 m. The parameters recorded were drop size distribution, radar reflectivity, path-integrated attenuation, rain rate, liquid water content and fall velocity.

Figure 2.11.2-1: Photo of the antenna unit of the
MRR

Table 2.11.2: Specifications of the MRR-2

Transmitter power	50 mW
Operating mode	FM-CW
Frequency	24.230 GHz
	(modulation 1.5 to 15 MHz)
3dB beam width	1.5 degrees
Spurious emission	< -80 dBm / MHz
Antenna Diameter	600 mm
Gain	40.1 dBi

(4) Preliminary Results

The data were obtained throughout the entire cruise, except when in nonpermissive territorial waters and EEZs. Figure 2.11.2-2 displays an example of the time–height cross section for a single day. The temporal variation corresponds reasonably with the rainfall measured by the Mirai SMet sensors (see Section 2.4) and C-band radar (see Section 2.3). Further analyses will be conducted after the cruise is completed.
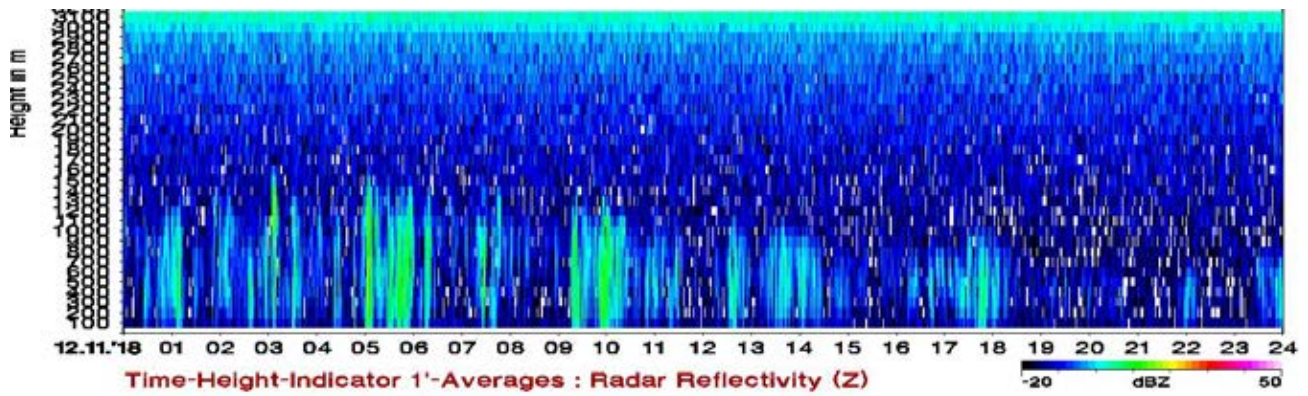
Figure 2.11.2-2: Example of the time-height cross section of the radar reflectivity for the 24-h period from 00:00UTC on 12 November.

(5) Data Archive

The data obtained during the cruise will be submitted to the Data Management Group of JAMSTEC, and they will be made available to the public via the "Data Research System for Whole Cruise Information in JAMSTEC (DARWIN)" on the JAMSTEC website (http://www.godac.jamstec.go.jp/darwin/e)

(6) Acknowledgment

The operations are supported by the Japan Aerospace Exploration Agency (JAXA) Precipitation Measurement Mission (PMM).

2.11.3 Precipitation sampling

(1) Personnel

Hotaek Park	JAMSTEC
Fumikazu Taketani	JAMSTEC

(2) Objectives

• To investigate the contribution of suspended particles to rain and snow

• To investigate the ratio of hydrogen and oxygen isotopes in rain and snow

(3) Parameters

• Chemical composition of snow and rain

• Isotopic ratio of oxygen in rain and snow

(4) Instruments and methods

Snow and rain samples were corrected using a custom-made rain/snow sampler. The sampling log is presented in Table 2.11.3. To investigate both the isotopic ratio in rain/snow and the interaction with aerosols of rain/snow, the samples will be analyzed in the laboratory after completion of the cruise.

(5) Observation log

Table 2.11.3: Log of precipitation sampling

No.	Date (UTC)	latitude	longitude	type
1	10/4	56-12N	175-24E	rain
2	10/7	64-08N	171-28W	rain
3	10/9	71-18N	165-55W	rain
4	10/10	72-59N	160-00W	mixed
5	10/11	72-07N	153-38W	snow
6	10/11	72-00N	148-29W	snow
7	10/13	74-21N	143-38W	snow
8	10/14	74-46N	150-31W	mixed
9	10/15	76-34N	162-07W	mixed
10	10/15	76-46N	163-27W	mixed
11	10/16	77-30N	164-59W	snow
12	10/20	77-39N	164-59W	snow
13	10/21	77-39N	164-59W	snow
14	10/23	77-45N	164-49W	snow
15	10/24	77-46N	165-00W	snow
16	10/28	66-01N	168-45W	rain
17	10/29	62-38N	174-24W	rain
18	11/3	49-59N	166-06E	rain

19	11/4	47-54N	162-19E	rain
20	11/4	46-54N	160-33E	rain
21	11/5	44-45N	156-54E	rain
22	11/6	41-40N	151-52E	rain

(6) Data archives

The data obtained during the cruise will be submitted to the Data Management Group of JAMSTEC, and they will be made available to the public via the "Data Research System for Whole Cruise Information in JAMSTEC (DARWIN)" on the JAMSTEC website (http://www.godac.jamstec.go.jp/darwin/e)

2.12 Lidar Observations

(1) Personnel

Fumikazu TAKETANI	JAMSTEC	- PI
Masaki KATSUMATA	JAMSTEC	- not on board
Kyoko TANIGUCHI	JAMSTEC	- not on board
Ryo OYAMA	NME	
Souichiro SUEYOSHI	NME	
Shinya OKUMURA	NME	
Kazuho YOSHIDA	NME	
Yutaro MURAKAMI	NME	

(1) Objective

The objective of this observation program was to capture the vertical distribution of clouds, aerosols, and water vapor with high spatiotemporal resolution.

(2) Instruments and methods

The Mirai lidar system transmits a 10-Hz pulse laser in three wavelengths: 1064, 532 and 355 nm. For cloud and aerosol observations, the system detects Mie scattering at these wavelengths. The separate detections of polarization components at 532 and 355 nm provide additional characterizations of the targets. The system also detects Raman water vapor signals at 660 and 408 nm and Raman nitrogen signals at 607 and 387 nm at nighttime. Based on the signal ratio of Raman water vapor to Raman nitrogen, the system can produce water vapor mixing ratio profiles.

(3) Preliminary results

The lidar system observed the lower atmosphere throughout the entire cruise, except when in EEZs and nonpermissive territorial waters. All data will be reviewed after completion of the cruise to maintain data quality.

(4) Data Archive

The data obtained during the cruise will be submitted to the Data Management Group of JAMSTEC, and they will be made available to the public via the "Data Research System for Whole Cruise Information in JAMSTEC (DARWIN)" on the JAMSTEC website (http://www.godac.jamstec.go.jp/darwin/e)

2.13 Greenhouse gasses observation

(1) Personnel

Yasunori Tohjima	NIES	-PI, not on board
Shigeyuki Ishidoya	AIST	-not on board
Fumikazu Taketani	JAMSTEC	
Taro Maruo	JAMSTEC	
Shinji Morimoto	Tohoku Univ.	-not on board
Shuji Aoki	Tohoku Univ.	-not on board
Ryo Fujita	Tohoku Univ.	-not on board
Hideki Nara	NIES	-not on board
Daisuke Goto	NIPR	-not on board
Prabir Patra	JAMSTEC	-not on board
Hiroshi Uchida	JAMSTEC	-not on board
Shohei Murayama	AIST	-not on board

(2) Objective

(2-1) Continuous observations of CO_2, CH_4 and CO mixing ratios

The Arctic region is considered vulnerable to the effects of global warming, which could potentially enhance emissions of greenhouse gases (including CO_2 and CH_4) into the atmosphere from carbon pools in the Arctic region. The objective of this study was to detect the early stages of increases in atmospheric greenhouse gas levels associated with ongoing global warming in the Arctic region. The continuous observations of atmospheric CO_2 and CH_4 mixing ratios during the MR19-03C cruise should allow us to both detect the enhancement of the mixing ratios associated with regional emissions and estimate the distribution of the regional emission sources. The atmospheric CO mixing ratios, which were observed concurrently, could be used as an indicator of the level of anthropogenic emissions associated with combustion processes.

(2-2) Discrete flask sampling

To clarify the spatial variations and air–sea exchanges of greenhouse gases at northern high latitudes, whole air samples were collected in 40 stainless-steel flasks onboard the R/V Mirai (MR19-03C). The collected air samples will be analyzed for the mixing ratios of CO_2, O_2, Ar, CH_4, CO, N_2O and SF_6 and the stable isotope ratios of CO_2 and CH_4.

(3) Parameters

(3-1) Continuous observations of CO_2, CH_4 and CO mixing ratios

Mixing ratios of atmospheric CO_2, CH_4, and CO.

(3-2) Discrete flask sampling

Mixing ratios of atmospheric CO_2, O_2 (O_2/N_2 ratio), Ar (Ar/N_2 ratio), CH_4, CO, N_2O and SF_6, $\delta^{13}C$ and $\delta^{18}O$ of

CO_2, $\delta^{13}C$ and δD of CH_4.

(4) Instruments and methods

(4-1) Continuous observations of CO_2, CH_4 and CO mixing ratios

Atmospheric CO_2, CH_4 and CO mixing ratios were measured using a wavelength-scanned cavity ringdown spectrometer (WS-CRDS, Picarro, G2401). An air intake, capped with an inverted stainless-steel beaker covered with stainless-steel mesh, was placed on the starboard side of the upper deck. A diaphragm pump (GAST, MOA-P108) was used to draw in outside air at a flow rate of ~8 L min^{-1}. Water vapor in the sampled air was removed to a dew point of approximately 2 °C and approximately -35 °C by passing it through a thermoelectric dehumidifier (KELK, DH-109) and a Nafion drier (PERMA PURE, PD-50T-24), respectively. Then, the dried sample air was introduced into the WS-CRDS at a flow rate of 100 ml min^{-1}. The WS-CRDS was calibrated automatically at 50–h intervals by introducing three standard airs with known CO_2, CH_4 and CO mixing ratios. The analytical precision for the CO_2, CH_4 and CO mixing ratios was approximately 0.02 ppm, 0.3 ppb and 3 ppb, respectively.

(4-2) Discrete flask sampling

The air sampling equipment consisted of an air intake, a piston pump (GAST LOA), a water trap, solenoid valves (CKD), an ethanol bath as refrigerant, a flow meter and an immersion cooler (EYELA ECS-80). Ambient air was pumped from an air intake using a piston pump, dried cryogenically and collected in a 1-L stainless-steel flask at a pressure of 0.55 MPa.

(5) Station list or Observation log

Continuous observations of CO_2, CH_4 and CO mixing ratios were conducted during the entire cruise. The log of the discrete flask sampling is presented in Table 2.13.

Table 2.13: Log of the discrete flask sampling

On board ID	Date Collected					Latitude			Longitude		
	YYYY	MM	DD	hh:mm:ss	UTC/JST	Deg.	Min.	N/S	Deg.	Min.	E/W
MR1903C-F001	2019	9	29	06:50	UTC	40	23.4	N	142	19.9	E
MR1903C-F002	2019	9	30	07:26	UTC	40	09.84	N	148	38.36	E
MR1903C-F003	2019	10	1	01:42	UTC	42	16.1	N	152	50.57	E
MR1903C-F004	2019	10	2	07:05	UTC	46	17.66	N	159	29.52	E
MR1903C-F005	2019	10	3	07:23	UTC	49	59.93	N	166	7.1	E
MR1903C-F006	2019	10	4	07:08	UTC	52	50.29	N	170	31.14	E
MR1903C-F007	2019	10	4	22:54	UTC	55	29.4	N	173	45.1	E
MR1903C-F008	2019	10	6	05:53	UTC	58	38.81	N	179	13.81	E
MR1903C-F009	2019	10	7	02:41	UTC	61	47.49	N	175	77.29	W
MR1903C-F010	2019	10	8	00:53	UTC	64	42.55	N	169	48.93	W
MR1903C-F011	2019	10	9	01:48	UTC	68	17.49	N	168	45.17	W
MR1903C-F012	2019	10	10	00:21	UTC	71	6.75	N	166	31.24	W
MR1903C-F013	2019	10	10	21:01	UTC	72	58.52	N	159	49.5	W
MR1903C-F014	2019	10	12	00:21	UTC	72	0.39	N	151	17.67	W
MR1903C-F015	2019	10	13	01:16	UTC	73	1.334	N	144	55.28	W
MR1903C-F016	2019	10	13	21:59	UTC	74	25.31	N	143	2.82	W
MR1903C-F017	2019	10	14	23:58	UTC	74	59.7	N	152	16.4	W
MR1903C-F018	2019	10	15	22:09	UTC	76	49.02	N	163	46.3	W
MR1903C-F019	2019	10	17	01:57	UTC	77	54.59	N	164	59.49	W
MR1903C-F020	2019	10	18	06:26	UTC	77	15.03	N	164	59.94	W
MR1903C-F021	2019	10	19	00:38	UTC	78	3.23	N	165	10.28	W
MR1903C-F022	2019	10	20	00:26	UTC	78	3.37	N	164	57.79	W
MR1903C-F023	2019	10	20	22:33	UTC	78	0.57	N	164	59.28	W
MR1903C-F024	2019	10	22	00:25	UTC	77	56.86	N	165	02.00	W
MR1903C-F025	2019	10	23	02:10	UTC	77	46.26	N	164	3.98	W
MR1903C-F026	2019	10	23	22:01	UTC	77	46.69	N	163	36.97	W
MR1903C-F027	2019	10	24	20:56	UTC	77	47.58	N	163	54.96	W
MR1903C-F028	2019	10	25	23:57	UTC	74	41.48	N	168	46.03	W
MR1903C-F029	2019	10	26	21:19	UTC	71	56.4	N	168	44.77	W
MR1903C-F030	2019	10	28	00:29	UTC	68	18.11	N	167	11.07	W
MR1903C-F031	2019	10	28	20:49	UTC	65	59.99	N	168	44.97	W
MR1903C-F032	2019	10	30	00:46	UTC	65	52.39	N	175	45.97	W
MR1903C-F033	2019	10	30	03:24	UTC	58	8.51	N	178	6.1	E
MR1903C-F034	2019	11	1	01:55	UTC	54	22.35	N	172	25.97	E
MR1903C-F035	2019	11	2	21:47	UTC	51	16.17	N	168	16.67	E
MR1903C-F036	2019	11	3	00:51	UTC	50	0.06	N	166	7.26	E
MR1903C-F037	2019	11	4	02:39	UTC	47	19.05	N	161	17.75	E
MR1903C-F038	2019	11	5	02:04	UTC	44	12.76	N	155	58.83	E
MR1903C-F039	2019	11	6	07:02	UTC	41	8.05	N	150	41.12	E
MR1903C-F040	2019	11	7	03:04	UTC	40	17.07	N	146	18.88	E

(6) Data archives

The data obtained during the cruise will be submitted to the Data Management Group of JAMSTEC, and they will be made available to the public via the "Data Research System for Whole Cruise Information in JAMSTEC (DARWIN)" on the JAMSTEC website (http://www.godac.jamstec.go.jp/darwin/e)

2.14 Sea ice radar

(1) Personnel

Kazutoshi Sato	KIT	-PI
Ryo Oyama	NME	
Souichiro Sueyoshi	NME	
Shinya Okumura	NME	
Kazuho Yoshida	NME	
Yutaro Murakami	NME	
Takehito Hattori	MIRAI Crew	

(2) Objectives

In sea-ice areas, marine radar is important for the detection of sea ice and icebergs. It is important to monitor sea ice on a daily basis and to produce ice forecasts to assist ship traffic and other marine operations. Therefore, the objective was to develop techniques for the prediction of ice condition and to use image information from the sea-ice radar to construct an algorithm for optimal route selection.

(3) Parameters

Capture format: JPEG

Capture interval: 60 seconds

Resolution: 1,280×1,024 pixel

Color tone: 256 gradation

(4) Instruments and methods

The R/V MIRAI is equipped with an ice navigation radar (Sigma S6 Ice Navigator, Rutter Inc.). The analog signal of the X-band ice navigation radar is converted by a modular radar interface and displayed as a digital video image (Figure 2.14). The sea-ice radar is equipped with a screen capture function and it saves data at arbitrary time intervals.

(5) Observation Period

6 Oct. 2019 - 29 Oct. 2019

(6) Data archives

The data obtained during the cruise will be submitted to the Data Management Group of JAMSTEC, and they will be made available to the public via the "Data Research System for Whole Cruise Information in JAMSTEC (DARWIN)" on the JAMSTEC website (http://www.godac.jamstec.go.jp/darwin/e)
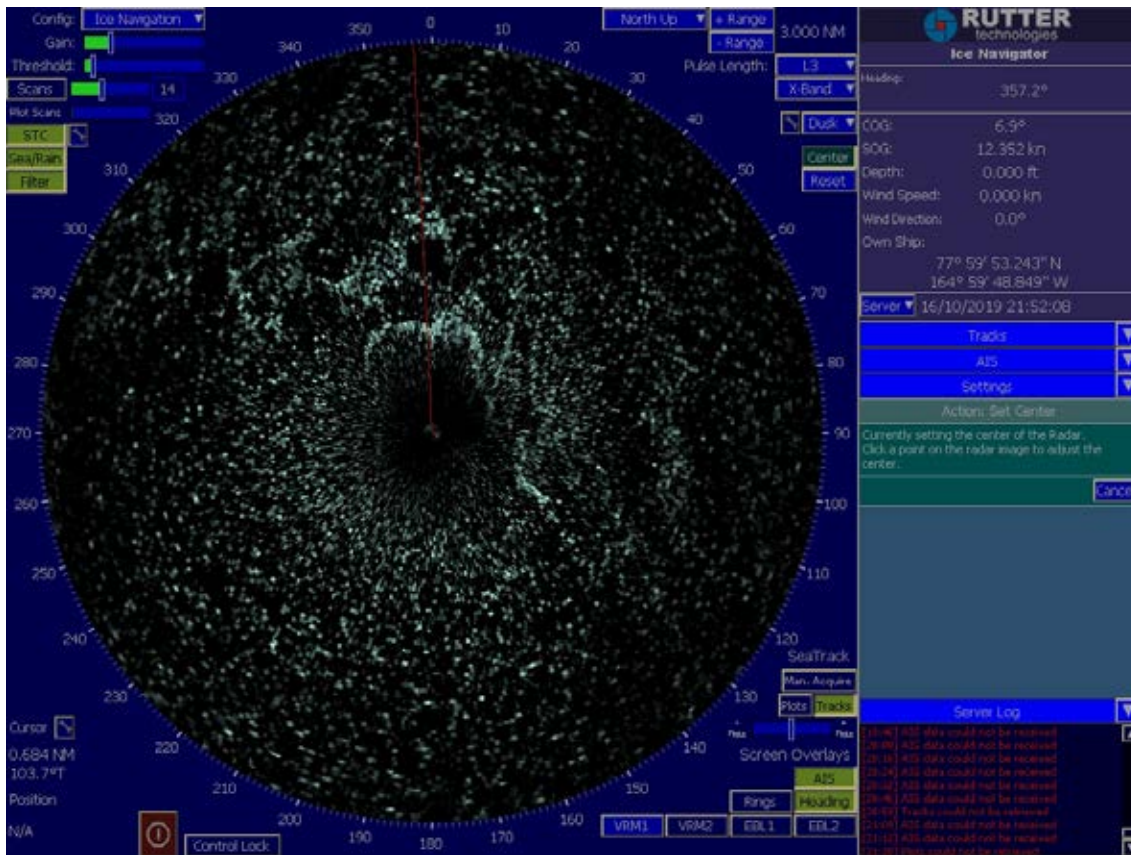
Figure 2.14: Image of sea ice from the sea-ice radar.

3. Physical Oceanography

3.1 CTD cast and water sampling

(1) Personnel

Yusuke KAWAGUCHI	The University of Tokyo	- not on board, PI
Shigeto NISHINO	JAMSTEC	- not on board, PI
Akihiko Murata	JAMSTEC	
Shinsuke TOYODA	MWJ	- Operation leader
Rio KOBAYASHI	MWJ	
Shungo OSHITANI	MWJ	
Tun Htet Aung	MWJ	

(2) Objective

Investigation of oceanic structure and water sampling.

(3) Parameters

Temperature (primary and secondary)

Salinity (primary and secondary)

Pressure

Dissolved oxygen (primary "RINKO III" and secondary "SBE43")

Fluorescence (primary and secondary)

Beam transmission

Turbidity

Nitrate

Altimeter

Deep Ocean Standards Thermometer

(4) Instruments and Methods

A CTD/carousel water sampling system, which included a 36-position carousel water sampler (CWS; Sea-Bird Electronics, Inc.) with 12-L sample bottles, was used for sampling seawater. The instruments used to measure temperature (primary and secondary), conductivity (primary and secondary), pressure, dissolved oxygen (primary: RINKO III, secondary: SBE43), fluorescence (primary and secondary), beam transmission, turbidity, and nitrate were deployed on the CTD sensor together with an altimeter and a Deep Ocean Standards Thermometer. Salinity was computed based on the measured values of pressure, conductivity and temperature. The CTD/CWS was deployed from the starboard side of the working deck.

Specifications of the sensors are listed below.

CTD: SBE911plus CTD system

Under water unit:

SBE9plus (S/N: 09P21746-0575, Sea-Bird Electronics, Inc.)

Pressure sensor: Digiquartz pressure sensor (S/N: 79492)

Calibrated Date: 18 Apr. 2019

Carousel water sampler:

SBE32 (S/N: 3254451-0826, Sea-Bird Electronics, Inc.)

Temperature sensors:

Primary: SBE03-04/F (S/N: 031525, Sea-Bird Electronics, Inc.)

Calibrated Date: 01 Jun. 2019

Secondary: SBE03-04/F (S/N: 031464, Sea-Bird Electronics, Inc.)
Calibrated Date: 01 Jun. 2019

Conductivity sensors:
Primary: SBE04C (S/N: 042435, Sea-Bird Electronics, Inc.)
Calibrated Date: 25 Jun. 2019
Secondary: SBE04C (S/N: 043036, Sea-Bird Electronics, Inc.)
Calibrated Date: 25 Jun. 2019

Dissolved Oxygen sensor:
Primary: RINKOIII (S/N: 0287_163011BA, JFE Advantech Co., Ltd.)
Calibrated Date: 29 May. 2019

Secondary: SBE43 (S/N: 430575 Sea-Bird Electronics, Inc.)
Calibrated Date: 02 Jul. 2019

Fluorescence:
Primary:
Chlorophyll Fluorometer (S/N: 3618, Seapoint Sensors, Inc.)
Gain setting: 30X, 0-5 ug/l
Calibrated Date: None
Offset: 0.000
Secondary:
Chlorophyll Fluorometer (S/N: 3700, Seapoint Sensors, Inc.)
Gain setting: 3X, 0-50 ug/l
Calibrated Date: None
Offset: 0.000

Transmission meter:
C-Star (S/N CST-1726DR, WET Labs, Inc.)
Calibrated Date: 13 Jun. 2019
Casts used: 000M001-021M005

C-Star (S/N CST-1727DR, WET Labs, Inc.)
Calibrated Date: 03 Jun. 2015
Casts used:025M001-00M004

Nitrate:
Deep SUNA (S/N 895, Satlantic, Inc.)
Calibration Date: 19 Sep. 2019
Casts used: 000M001, 000M002, 001M001-014M001, 018M001

Turbidity:
Turbidity Meter (S/N: 14953)
Gain setting: 100X
Scale factor: 1.000
Calibrated Date: None

Altimeter:

Benthos PSA-916T (S/N: 1157, Teledyne Benthos, Inc.)

Submersible Pump:

Primary: SBE5T (S/N: 055816, Sea-Bird Electronics, Inc.)

Secondary: SBE5T (S/N: 054598, Sea-Bird Electronics, Inc.)

Bottom contact switch: (Sea-Bird Electronics, Inc.)

Deck unit: SBE11plus (S/N 11P54451-0872, Sea-Bird Electronics, Inc.)

Configuration file: MR1903C_A.xmlcon
000M001, 001M001 - 014M001, 018M001
MR1903C_B.xmlcon
000M002, 015M001 - 017M001, 019M001 - 021M004
MR1903C_C.xmlcon
024M001, 019M004, 020M006, 021M005
MR1903C_D.xmlcon
025M001 – 000M004,

The CTD raw data were acquired in real time using Seasave-Win32 (ver. 7.23.2; provided by Sea-Bird Electronics, Inc.) and stored on the hard disk of a PC. Seawater was sampled during the upcast by sending fire commands from the control PC.

At depths where the vertical gradients of the exchanged water properties were expected to be large, water sampling was triggered after a 60-s pause at the sampling depth to enhance the exchange of water between the inside and the outside of the bottle. Below the thermocline, a 30-s pause was adopted for stabilization prior to firing. Overall, eight casts of CTD measurements were conducted (Table 3.1).

The data processing procedures and used utilities of the SBE Data Processing-Win32 (ver. 7.26.7.114) and SEASOFT were as follows.

(The processing sequence)

DATCNV: Converts the binary raw data to engineering unit data. DATCNV also extracts bottle information where scans were marked with the bottle confirm bit during acquisition. The duration was set to 4.4 s and the offset was set to 0.0 s.

TCORP (original module): Corrects the pressure sensitivity of the temperature (SBE3) sensor.
S/N 031525: -1.714e-008 (degC/dbar)
S/N 031464: + 7.75293156e-009 (degC/dbar)

RINKOCOR (original module): Corrects the time-dependent pressure-induced effect (hysteresis) of the RINKO III profile data.

RINKOCORROS (original module): Corrects the time-dependent pressure-induced effect (hysteresis) of the RINKO III bottle information data using the hysteresis-corrected profile data.

BOTTLESUM: Creates a summary of the bottle data. The data were averaged over 4.4 s.

ALIGNCTD: Converts the time sequence of sensor outputs into a pressure sequence to ensure that all calculations were made using measurements from the same parcel of water. Dissolved oxygen data were systematically delayed with respect to depth mainly because of the long time constant of the dissolved oxygen sensor and an additional delay from the transit time of water in the pumped plumbing line. This delay was compensated by advancing the dissolved oxygen sensor (SBE43) output (dissolved oxygen voltage) by 5 s relative to the temperature data. The RINKO III voltage (user polynomial 0) was advanced by 1 s and the transmission data were advanced by 2 s.

WILDEDIT: Marks extreme outliers in the data files. The first pass of WILDEDIT obtained accurate estimates of the true standard deviation of the data. The data were read in blocks of 1000 scans. Data with values greater than 10 standard deviations were flagged. The second pass computed a standard deviation over the same 1000 scans excluding the flagged values. Values greater than 20 standard deviations were marked as bad data. This process was applied to pressure, depth, temperature (primary and secondary), conductivity (primary and secondary), and dissolved oxygen voltage (SBE43).

CELLTM: Removes conductivity cell thermal mass effects from the measured conductivity. Typical values used were thermal anomaly amplitude, alpha = 0.03 and a time constant, 1/beta = 7.0.

FILTER: Performs a low-pass filter on pressure and depth data with a time constant of 0.15 s. To produce a zero phase lag (i.e., no time shift), the filter is first run forward and then backward.

WFILTER: Performs a median filter to remove spikes in the fluorescence data (primary and secondary), transmission data, transmission beam attenuation, transmission voltage, turbidity and nitrate. A median value was determined by 49 scans of the window.

SECTIONU (original module of SECTION): Selects the time span of the data based on scan number to reduce file size. The minimum number was set to the starting time when the CTD package was beneath the sea surface after activation of the pump. The maximum number was set to the end time when the package broke the surface.

LOOPEDIT: Marks scans where the CTD was moving less than the minimum velocity of 0.0 m/s (traveling backward due to ship roll).

DESPIKE (original module): Removes spikes in the data. A median and mean absolute deviation was calculated in 1-dbar pressure bins for both the downcast and the upcast, excluding flagged values. Values greater than 4 mean absolute deviations from the median were marked as bad data for each bin. This process was performed twice for temperature, conductivity and dissolved oxygen (RINKO

III and SBE43) voltage.

DERIVE: Computes dissolved oxygen (SBE43).

BINAVG: Averages the data into 1-dbar bins.

BOTTOMCUT (original module): Deletes discontinuous scan bottom data when created by BINAVG.

DERIVE: Computes salinity, potential temperature and sigma-theta data.

SPLIT: Separates the data from the input ".cnv" file into downcast and upcast files.

(5) Station list

During this cruise, 67 casts of CTD observations were performed. The dates, times and locations of the CTD casts are listed in Table 3.1. In the case of bottom attack on shallow casts, a bottom contact switch was also used.

(6) Preliminary Results

During this cruise, we judged noise, spike or shift in the data of some casts. These were as follows.

000M001:   Secondary Salinity
            down 30 dbar : spike

            Nitrate
            down 55 dbar - down 501 dbar, up 500 dbar - up 37 dbar: overrange

000M002:   Beam Transmission
            down 2060 dbar - down 2266 dbar: noise

005M001:   Secondary Salinity
            down 45 dbar: spike

014M001:   Nitrate
            down 2 dbar - down 1644 dbar, up 1643 dbar - up 1 dbar: bad data

018M001   Primary Dissolved Oxygen (RINKO III)
            down 1363 dbar - down 1368 dbar, down 1403 dbar - down 1409 dbar: spike, down 1702 dbar - down 1754 dbar: noise

            Nitrate
            down 3 dbar - down 1761 dbar, up 1760 dbar - up 1 dbar: bad data

021M001   Primary Salinity
            down 10 dbar: spike

020M005   Secondary Temperature,   Secondary Salinity

down 28 dbar: spike

024M001 Secondary Temperature, Secondary Salinity
down 96 dbar: spike

019M004 Primary Temperature, Primary Salinity
down 205 dbar – down 208 dbar: spike

Secondary Temperature, Secondary Salinity
down 179 dbar, down 205 dbar – down 208 dbar: spike

026M001 Primary Temperature, Primary Salinity, Secondary Temperature, Secondary Salinity
down 203 dbar: spike

Beam Transmission
down 353 dbar – down 357 dbar: spike

019M006 Primary Temperature, Primary Salinity, Secondary Temperature, Secondary Salinity
down 204 dbar: spike

027M001 Primary Temperature, Primary Salinity, Secondary Temperature, Secondary Salinity
down 207 dbar: spike

019M007 Primary Temperature, Primary Salinity, Secondary Temperature, Secondary Salinity
down 204 dbar – down 208 dbar: spike

021M008 Beam Transmission
down 231 dbar - down 232 dbar: spike

035M001 Secondary Temperature, Secondary Salinity
down 32 dbar: spike

037M001 Primary Temperature
down 24 dbar, down 39 dbar: spike

Primary Salinity
down 24 dbar, down 28 dbar, down 39 dbar: spike

Secondary Dissolved Oxygen (SBE43)
down 39 dbar: spike

038M001 Primary Salinity
down 36 dbar: spike

015M001   sample bottle #13 was not closed

             bottle flag 4

000M004   sample bottle #26 was not closed

             bottle flag 4

(7) Data archive

    The data obtained during the cruise will be submitted to the Data Management Group of JAMSTEC, and they will be made available to the public via the "Data Research System for Whole Cruise Information in JAMSTEC (DARWIN)" on the JAMSTEC website (http://www.godac.jamstec.go.jp/darwin/e)

Table 3.1: Log of MR19-03C CTD casts

Stnnbr	Castno	Date(UTC) (mmddyy)	Time(UTC) Start	End	Bottom Position Latitude	Longitude	Depth (m)	Wire Out (m)	HT Above Bottom (m)	Max Depth	Max Pressure	CTD Filename	Remark
000	1	100319	07:06	07:58	49-59.92N	166-07.07E	5396.0	495.4	-	496.1	501.0	000M001	
000	2	100319	10:06	14:02	49-59.29N	166-07.87E	5395.0	5399.3	8.7	5374.2	5490.0	000M002	
001	1	100819	06:34	07:00	65-39.18N	168-27.77W	53.1	41.9	7.3	45.5	46.0	001M001	
002	1	100819	09:34	09:56	66-00.17N	168-44.72W	52.5	43.0	6.5	45.5	46.0	002M001	
003	1	100819	12:48	13:05	66-30.32N	168-45.09W	54.3	43.2	7.5	46.5	47.0	003M001	
004	1	100819	16:06	16:28	67-00.13N	168-44.26W	44.6	33.8	6.5	37.6	38.0	004M001	
005	1	100919	05:16	05:35	69-00.19N	168-45.18W	52.5	42.8	6.2	45.5	46.0	005M001	
006	1	100919	09:25	09:48	69-30.16N	168-45.21W	51.0	43.0	5.0	45.5	46.0	006M001	
007	1	100919	13:36	13:53	69-59.96N	168-45.03W	40.5	30.5	5.2	34.6	35.0	007M001	
008	1	100919	17:06	17:24	70-29.86N	168-45.38W	39.4	26.3	8.2	29.7	30.0	008M001	
009	1	101019	07:59	08:15	71-59.76N	163-29.99W	38.4	29.6	5.4	32.7	33.0	009M001	
010	1	101019	14:09	14:25	72-29.84N	161-44.78W	44.1	34.2	5.8	37.6	38.0	010M001	
011	1	101019	18:57	19:35	72-60.00N	160-00.20W	192.0	182.1	8.9	184.0	186.0	011M001	
012	1	101119	05:42	07:24	72-30.13N	156-16.69W	1607.0	1595.9	8.7	1589.3	1612.0	012M001	
013	1	101119	10:55	12:50	72-19.98N	155-00.52W	1957.0	1959.6	8.2	1956.3	1986.0	013M001	
014	1	101119	16:47	18:33	72-09.43N	153-47.41W	1637.0	1635.6	8.7	1620.8	1644.0	014M001	
015	1	101219	06:34	09:13	71-59.99N	147-29.98W	3515.0	3507.4	9.9	3500.0	3566.0	015M001	
016	1	101219	14:40	17:18	72-00.00N	145-00.05W	3316.0	3309.4	9.7	3303.3	3364.0	016M001	
017	1	101419	15:08	18:11	74-46.09N	150-30.13W	3834.0	3824.7	9.1	3819.5	3895.0	017M001	
018	1	101519	16:58	18:48	76-27.95N	161-38.51W	1750.0	1738.7	10.0	1735.3	1761.0	018M001	
019	1	101619	05:11	06:19	76-59.96N	164-59.94W	680.0	675.9	5.2	675.7	684.0	019M001	
020	1	101619	08:33	09:26	77-15.04N	164-59.71W	367.0	359.4	4.3	359.9	364.0	020M001	
020	2	101719	07:04	07:56	77-15.00N	164-59.93W	370.0	360.2	6.1	361.8	366.0	020M002	
021	1	101719	10:17	11:06	77-30.01N	165-00.01W	308.0	301.5	5.2	301.6	305.0	021M001	
022	1	101719	12:58	13:56	77-45.00N	165-00.01W	445.0	438.4	5.3	437.9	443.0	022M001	
020	3	101819	06:36	07:28	77-15.01N	164-59.99W	372.0	358.1	4.6	359.9	364.0	020M003	
021	2	101819	09:45	10:33	77-30.07N	165-00.19W	310.0	300.4	4.7	302.6	306.0	021M002	
022	2	101819	12:55	13:52	77-45.05N	165-00.19W	446.0	439.5	4.4	439.9	445.0	022M002	
023	1	101819	20:09	21:06	78-02.13N	164-58.49W	453.0	443.6	8.2	442.8	448.0	023M001	
019	2	101919	08:07	09:01	77-00.01N	164-59.96W	685.0	496.3	-	496.1	502.0	019M002	
020	4	101919	11:15	12:06	77-15.14N	164-59.89W	366.0	358.5	3.8	360.9	365.0	020M004	
021	3	101919	13:41	14:33	77-30.06N	164-59.93W	309.0	301.4	4.4	303.6	307.0	021M003	
019	3	102019	08:59	09:55	77-00.06N	164-59.94W	690.0	495.0	-	496.1	502.0	019M003	
020	5	102019	12:18	13:12	77-15.14N	164-59.65W	367.0	358.3	5.1	361.8	366.0	020M005	
021	4	102019	14:48	15:42	77-30.05N	164-59.99W	310.0	299.2	5.5	301.6	305.0	021M004	
024	1	102119	06:37	07:52	77-15.00N	165-59.97W	851.0	847.7	5.8	846.3	857.0	024M001	
019	4	102119	10:43	11:42	77-00.28N	164-59.75W	687.0	494.9	-	496.1	502.0	019M004	
020	6	102119	13:54	14:53	77-15.01N	165-00.05W	370.0	358.0	4.4	359.9	364.0	020M006	
021	5	102119	17:40	18:33	77-30.50N	164-59.67W	308.0	231.2	-	238.3	241.0	021M005	no sampling water
025	1	102219	07:04	08:15	77-00.37N	165-59.88W	711.0	708.7	5.7	708.3	717.0	025M001	
019	5	102219	10:27	11:28	77-00.10N	164-59.57W	685.0	495.0	-	496.1	502.0	019M005	
020	7	102219	13:43	14:43	77-15.00N	165-00.06W	371.0	359.8	3.7	360.9	365.0	020M007	
021	6	102219	17:32	17:48	77-30.30N	164-58.80W	306.0	299.5	3.9	301.6	305.0	021M006	no sampling water
026	1	102319	06:30	07:24	77-00.01N	164-00.01W	437.0	431.8	4.7	431.0	436.0	026M001	
019	6	102319	09:32	10:34	77-00.07N	164-59.32W	678.0	495.6	-	495.2	501.0	019M006	
020	8	102319	13:25	14:18	77-15.17N	164-59.94W	365.0	357.6	5.4	358.9	363.0	020M008	
021	7	102319	16:29	17:17	77-30.31N	164-58.79W	304.0	299.2	5.3	300.6	304.0	021M007	
027	1	102419	06:36	07:25	77-15.00N	164-00.01W	366.0	356.3	5.7	358.9	363.0	027M001	
019	7	102419	10:09	11:08	77-00.23N	165-00.16W	697.0	494.5	-	495.2	501.0	019M007	
020	9	102419	13:15	14:06	77-15.04N	165-00.14W	366.0	356.3	4.9	357.9	362.0	020M009	
021	8	102419	16:59	17:47	77-30.74N	165-00.21W	311.0	301.5	6.4	302.6	306.0	021M008	
028	1	102519	08:59	10:46	77-00.22N	168-46.13W	1896.0	1884.6	8.9	1882.4	1911.0	028M001	
029	1	102619	05:39	06:14	74-00.01N	168-44.83W	185.0	172.4	5.2	175.1	177.0	029M001	
030	1	102619	09:11	09:41	73-30.00N	168-45.00W	115.0	106.0	5.6	108.8	110.0	030M001	
031	1	102619	13:08	13:30	73-00.03N	168-45.04W	61.4	48.0	5.0	55.4	56.0	031M001	
032	1	102619	16:51	17:11	72-30.03N	168-44.61W	58.5	48.0	4.7	52.4	53.0	032M001	
033	1	102719	05:42	05:57	70-30.00N	168-44.92W	38.2	28.5	5.2	32.7	33.0	033M001	
034	1	102719	08:46	09:05	70-00.00N	168-45.04W	40.5	31.4	5.2	34.6	35.0	034M001	
035	1	102719	13:00	13:18	69-30.19N	168-45.23W	51.3	39.7	5.1	45.5	46.0	035M001	
036	1	102719	16:19	16:37	68-59.99N	168-45.29W	52.5	42.4	5.4	46.5	47.0	036M001	
037	1	102819	05:05	05:23	68-00.88N	167-52.05W	52.5	41.0	6.5	45.5	46.0	037M001	
038	1	102819	07:36	07:56	67-46.99N	168-36.29W	50.5	39.5	6.0	43.6	44.0	038M001	
039	1	102819	10:42	10:59	67-30.07N	168-45.11W	49.4	40.1	5.2	43.6	44.0	039M001	
040	1	102819	13:59	14:15	67-00.06N	168-44.71W	44.9	35.5	5.9	38.6	39.0	040M001	
041	1	102819	17:22	17:40	66-29.99N	168-45.02W	54.0	45.8	5.1	48.5	49.0	041M001	
000	3	110219	22:07	22:57	50-00.11N	166-07.40E	5397.0	494.1	-	497.1	502.0	000M003	
000	4	110319	00:06	04:04	49-59.95N	166-07.13E	5396.0	5389.4	7.9	5376.1	5492.0	000M004	

3.2 Salinity measurements

(1) Personnel

Shigeto NISHINO	JAMSTEC	- PI
Akihiko MURATA	JAMSTEC	
Shungo OSHITANI	MWJ	-Operation leader
Shinsuke TOYODA	MWJ	

(2) Objective

    To measure salinity of bottle samples obtained by CTD casts, bucket sampling and the continuous sea surface water monitoring system (TSG).

(3) Method

 a. Salinity sample collection

    Seawater samples were collected in 12-L water sampling bottles and by the TSG. We used 250-mL brown glass salinity sample bottles with screw caps for storing the sampled water. Each bottle was rinsed three times in sample water and then filled with sample water to the bottle shoulder. The salinity sample bottles for the TSG were sealed with a plastic cone and a screw cap because we took into consideration the possibility that the samples might be stored for approximately one month. The caps were rinsed three times in sample seawater before use. Each bottle was stored for more than 24 h in the laboratory before the salinity measurements were performed. The types and numbers of samples taken are listed in Table 3.2.

Table 3.2: Types and numbers of samples

Kind of Samples	Number of Samples
Samples for CTD and Bucket	586
Samples for TSG	34
Total	620

 b. Instruments and method

    The salinity analysis was undertaken onboard the R/V Mirai during the MR19-03C cruise using a Model 8400B "AUTOSAL" salinometer (Guildline Instruments Ltd.: S/N 72874) with an additional peristaltic-type intake pump (Ocean Scientific International, Ltd.). A pair of precision digital thermometers (1502A; FLUKE: S/N B78466 and B81550) were used for monitoring the ambient temperature and the bath temperature of the salinometer. The specifications of the AUTOSAL salinometer and thermometer were as follows.

Salinometer (Model 8400B "AUTOSAL" ;　Guildline Instruments Ltd.)

Measurement Range	:	0.005 to 42 (PSU)
Accuracy	:	Better than ±0.002 (PSU) over 24 hours
		without re-standardization
Maximum Resolution	:	Better than ±0.0002 (PSU) at 35 (PSU)

Thermometer (1502A: FLUKE)

Measurement Range	:	16 to 30 deg C (Full accuracy)
Resolution	:	0.001 deg C
Accuracy	:	0.006 deg C (@ 0 deg C)

The measurement system was almost the same as used by Aoyama *et al.* (2002). The salinometer was operated in the ship's air-conditioned laboratory. The ambient temperature varied in the range of approximately 21–23 °C, whereas the bath temperature of 24 °C was very stable and varied only within ±0.002 °C on rare occasions. The measurement for each sample was done with a double conductivity ratio and defined as the median of 31 readings of the salinometer. Data collection started 5 s after the cell was filled with the sample and it took approximately 10 s to collect the 31 readings using a PC. Data were taken for the sixth and seventh fillings of the cell. In cases where the difference between the double conductivity ratio of these two fillings was <0.00002, the average value of the double conductivity ratio was used to calculate the bottle salinity using the algorithm for the practical salinity scale, 1978 (UNESCO, 1981). If the difference was ≥0.00003, an eighth filling of the cell was performed. In cases where the difference between the double conductivity ratio of these two fillings was <0.00002, the average value of the double conductivity ratio was used to calculate the bottle salinity. The measurements were conducted over an ~8-h period and the cell was cleaned with soap after the final measurement of the day.

(4) Results

a. Standard seawater

Standardization control of the salinometer was set to 549 and all measurements were performed at this setting. The value of STANDBY was 24 + 5996 − 6004 and that of ZERO was 0.0 ± 0000 − 0004. The conductivity ratio of the IAPSO Standard Seawater batch P162 was 0.99983 (double conductivity ratio was 1.99966) and it was used as the standard for salinity. Overall, 33 bottles of P162 were measured.

Figure 3.2.-1 shows the time series of the double conductivity ratio of the Standard Seawater batch P162. The average of the double conductivity ratio was 1.99966 and the standard deviation was 0.00005, which is equivalent to 0.0009 in salinity.

Figure 3.2.-2 shows the time series of the double conductivity ratio of the Standard Seawater batch P162 after correction. The average of the double conductivity ratio after correction was 1.99966 and the standard deviation was 0.00001, which is equivalent to 0.0002 in salinity.

The specifications of the Standard Seawater used on this cruise are as follows.

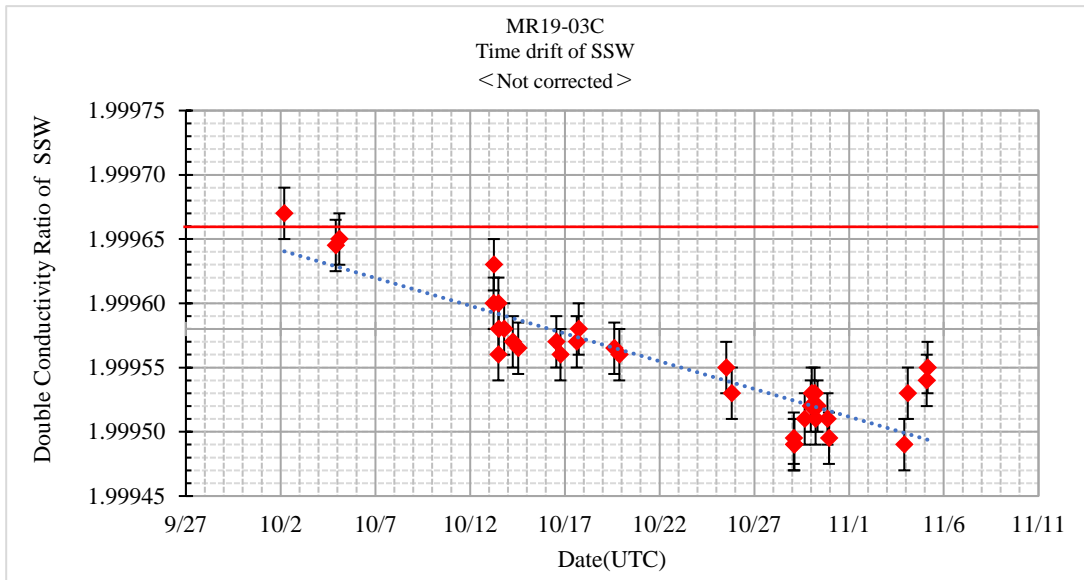|		
Batch	:	P162
Conductivity ratio	:	0.99983
Salinity	:	34.993
Use by	:	16th April. 2021

Figure 3.2-1: Time series of double conductivity ratio for the Standard Seawater batch P162
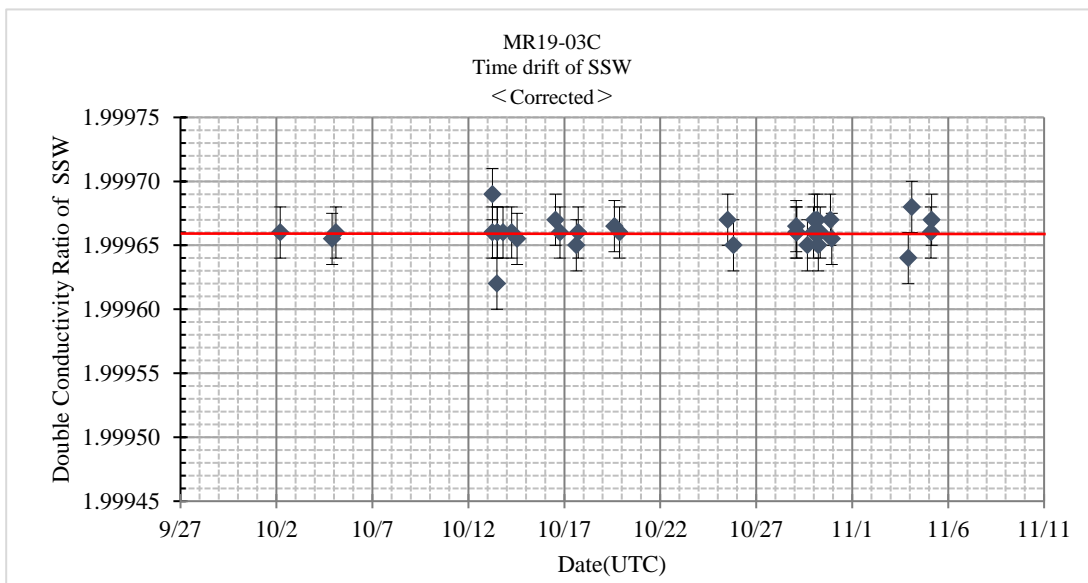(before correction).

Figure 3.2-2: Time series of double conductivity ratio for the Standard Seawater batch P162
(after correction).

b. Substandard seawater

Substandard seawater was made from surface seawater passed through a filter with 0.2-μm pore size and then stored in a 20-L container made of polyethylene. The water was stirred for at least 24 h before performing the measurements, and measurements were conducted on approximately every sixth sample to check for possible sudden drifts of the salinometer.

c. Replicate samples

We estimated the precision of this method using 108 pairs of replicate water samples taken from the same sampling bottle. Figure 3.2-3 shows the histogram of the absolute difference between each pair of replicate samples. The average and the standard deviation of the absolute difference among the 108 pairs of replicate samples were 0.0006 and 0.0006 in salinity, respectively.
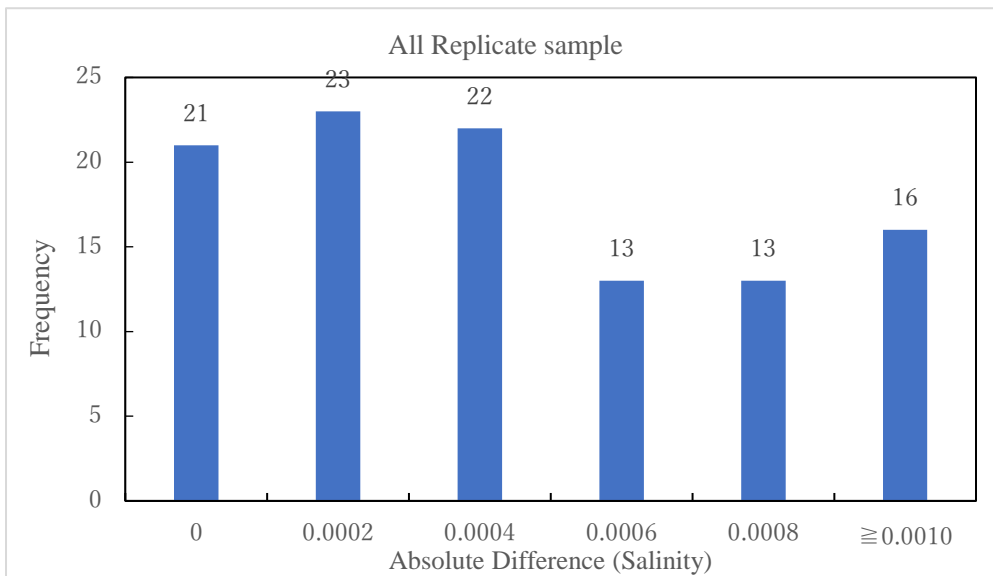
91

Figure 3.2-3: Histogram of the double conductivity ratio for the absolute difference of all replicate samples.

We used 33 pairs of replicate samples to estimate the precision of shallow (<200 dbar) samples. Figure 3.2-4 shows the histogram of the absolute difference between each pair of shallow (<200 dbar) replicate samples. The average and the standard deviation of the absolute difference among the 33 pairs were 0.0006 and 0.0007 in salinity, respectively.

Figure 3.2-4: Histogram of the absolute difference between shallow (< 200dbar) replicate samples.

We used 75 pairs of replicate samples to estimate the precision of deep (≥200 dbar) samples. Figure 3.2-5 shows the histogram of the absolute difference between each pair of deep (≥200 dbar) replicate samples. The average and the standard deviation of the absolute difference among the 75 pairs were 0.0006 and 0.0005 in salinity, respectively.
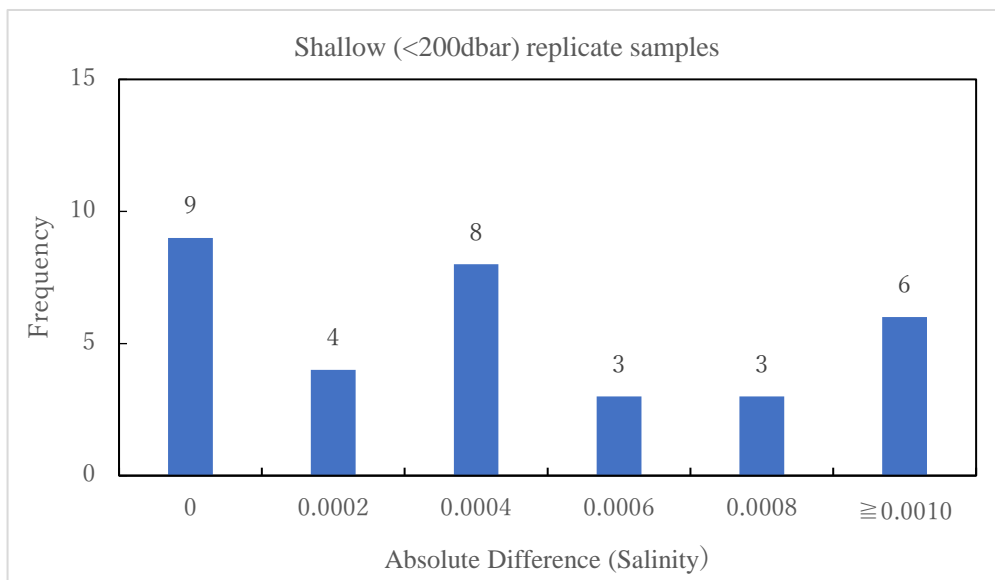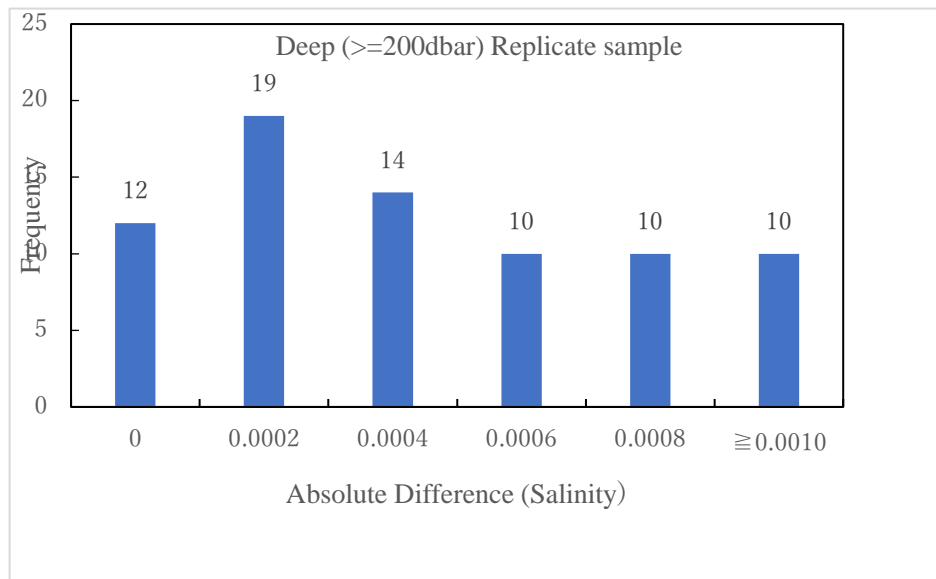
Figure 3.2-5: Histogram of the absolute difference between deep (>200 dbar) replicate samples.

(5) Data archive

　　　　The data obtained during the cruise will be submitted to the Data Management Group of JAMSTEC, and they will be made available to the public via the "Data Research System for Whole Cruise Information in JAMSTEC (DARWIN)" on the JAMSTEC website (http://www.godac.jamstec.go.jp/darwin/e)

(6) Reference

　　　・Aoyama, M., T. Joyce, T. Kawano and Y. Takatsuki : Standard seawater comparison up to
　　　　P129. Deep-Sea Research, I, Vol. 49, 1103～1114, 2002
　　　・ UNESCO : Tenth report of the Joint Panel on Oceanographic Tables and Standards.
　　　　UNESCO Tech. Papers in Mar. Sci., 36, 25 pp., 1981

3.3 XCTD

(1) Personnel

Jun Inoue	NIPR	-PI
Takuji Waseda	The University of Tokyo	- not on board
Tsubasa Kodaira	The University of Tokyo	
Yusuke Kawaguchi	The University of Tokyo	- not on board
Eun Yae Son	The University of Tokyo	
Ryo Oyama	NME	
Shinya Okumura	NME	
Kazuho Yoshida	NME	
Yutaro Murakami	NME	
Soichiro Sueyoshi	NME	

(2) Objective

To obtain vertical profiles of seawater temperature and salinity (calculated based on the function of temperature, pressure (depth), and conductivity).

(3) Parameters

The range and accuracy of parameters measured by the XCTD (eXpendable Conductivity, Temperature & Depth profiler) are as follows;

Parameter	Range	Accuracy
Conductivity	0 ~ 60 [mS/cm]	+/- 0.03 [mS/cm]
Temperature	-2 ~ 35 [deg-C]	+/- 0.02 [deg-C]
Depth	0 ~ 1000 [m]	5 [m] or 2 [%] (either of them is major)

(4) Instruments and Methods

We observed the vertical profiles of the seawater temperature and conductivity measured using an XCTD-1 manufactured by the Tsurumi-Seiki Co. (TSK). The signal was converted using MK-150N (TSK) and recorded using AL-12B software (Ver. 1.1.4, TSK). We launched 26 probes via an automatic launcher. The summary of the XCTD observation log is shown in Table 3.3.

Table 3.3: XCTD observation log

No.	Date [YYYY/MM/DD]	Time [hh:mm]	Latitude [degN]	Longitude [degW]	Depth [m]	SST [deg-C]	SSS [PSU]	Probe S/N	Probe Type
1	2019/10/08	20:06	67-29.9969	168-44.9535	48	3.503	32.195	17110515	XCTD-1
2	2019/10/08	22:32	68-00.0631	168-45.1056	58	3.610	31.971	17110517	XCTD-1
3	2019/10/09	02:38	68-30.0533	168-45.0005	53	3.583	32.311	17110516	XCTD-1
4	2019/10/09	22:29	71-00.0009	166-59.9931	45	6.831	31.605	17110518	XCTD-1
5	2019/10/10	03:41	71-29.9875	165-15.0715	43	6.099	30.987	17110519	XCTD-1
6	2019/10/12	06:47	71-59.9908	147-29.9095	3512	1.255	26.497	17110520	XCTD-1
7	2019/10/13	05:36	73-45.3341	145-06.3694	3710	0.200	26.647	19040333	XCTD-1
8	2019/10/13	19:13	74-18.0722	143-49.5586	3711	−1.378	26.333	19040334	XCTD-1
9	2019/10/13	21:40	74-25.4099	143-00.2768	3705	−1.391	26.323	19040335	XCTD-1
10	2019/10/14	00:00	74-17.1291	143-31.0744	3710	−1.399	26.374	19040337	XCTD-1
11	2019/10/14	01:04	74-17.1291	143-46.4098	3709	−1.392	26.272	17110522	XCTD-1
12	2019/10/14	01:28	74-15.0270	144-00.0245	3710	−1.366	26.313	17110523	XCTD-1
13	2019/10/14	01:44	74-13.4356	144-08.2456	3711	−0.963	26.452	17110524	XCTD-1
14	2019/10/14	01:50	74-12.8899	144-11.0899	3711	−0.274	26.591	17110525	XCTD-1
15	2019/10/14	02:27	74-11.9213	144-14.0936	3709	0.154	26.723	17110526	XCTD-1
16	2019/10/14	03:24	74-09.2035	144-28.7344	3712	0.121	26.714	19040399	XCTD-1
17	2019/10/14	03:55	74-06.7290	144-43.5529	3723	−0.026	26.724	19040338	XCTD-1
18	2019/10/14	04:42	74-03.9046	144-58.0717	3719	−0.055	26.719	19040332	XCTD-1
19	2019/10/16	22:36	78-05.0731	164-55.3744	488	−1.496	28.479	19040340	XCTD-1
20	2019/10/20	19:32	77-38.0633	165-00.0179	316	−0.806	28.851	19040342	XCTD-1
21	2019/10/20	20:52	77-49.9459	164-59.8765	405	−0.935	28.812	19040344	XCTD-1
22	2019/10/20	21:17	77-55.0005	164-59.9874	391	−1.254	28.722	19040343	XCTD-1
23	2019/10/21	01:49	77-40.0096	165-27.7923	497	−0.739	28.883	19040341	XCTD-1
24	2019/10/21	02:57	77-27.8973	165-43.1546	731	−0.104	29.060	19040345	XCTD-1
25	2019/10/25	16:34	75-59.9980	168-45.1069	601	1.598	29.738	18086022	XCTD-1
26	2019/11/03	00:18	50-00.0733	166-07.3278	5400	7.707	32.788	18086.23	XCTD-1

SST: Sea Surface Temperature [deg-C] measured by TSG (Thermo Salino Graph).

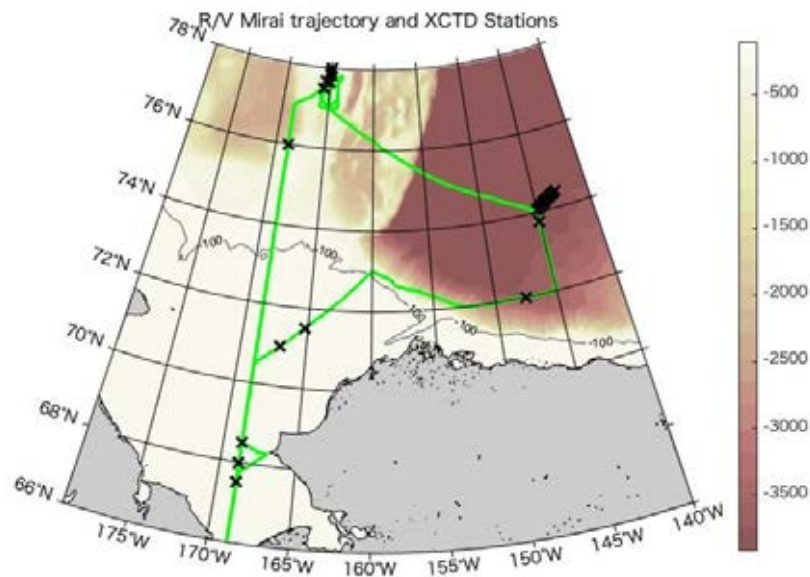SSS: Sea Surface Salinity [PSU] measured by TSG.

Figure 3.3-1: Trajectory of the R/V Mirai (green line) and XCTD measurement locations (×). The colored shading represents bathymetry.

(5) Preliminary results

An intensive program of XCTD measurements was conducted during 13–14 October 2019 near the MIZ (Figure 3.3-1). The measurements were linked to the ocean turbulence measurements and deployments of surface drifting buoys, some of which measured surface waves, while others measured upper-ocean currents and temperature. The XCTD data revealed the hydrographic conditions within the zone of sea-ice formation and a subsurface oceanic eddy under the sea-ice area (see Figure 3.3-2). Most other probes were used to map the hydrographic conditions near the ridge and the Chukchi Shelf.
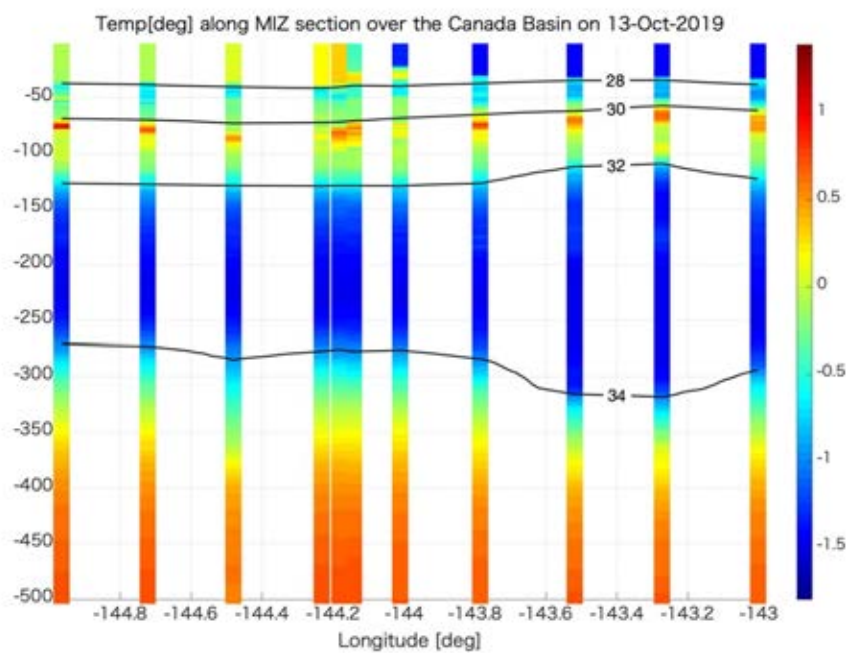
Figure 3.3-2: XCTD measurement results along the section between the open ocean and the ice-covered area. Colored shading represents temperature (°C) and the black lines indicate salinity (psu).

(6) Data archives

The data obtained during the cruise will be submitted to the Data Management Group of JAMSTEC, and they will be made available to the public via the "Data Research System for Whole Cruise Information in JAMSTEC (DARWIN)" on the JAMSTEC website (http://www.godac.jamstec.go.jp/darwin/e)

3.4 Shipboard ADCP

(1) Personnel

Kazutoshi Sato	KIT	-PI
Ryo Oyama	NME	
Sueyoshi Souichiro	NME	
Shinya Okumura	NME	
Kazuho Yoshida	NME	
Yutaro Murakami	NME	
Takehito Hattori	MIRAI Crew	

(2) Objectives

To obtain continuous measurement data of the current profile along the ship's track.

(3) Parameters

Major parameters for the measurement, Direct Command, are shown in Table 3.4.

Table 3.4: Major parameters

_____

Bottom-Track Commands

    BP = 001   Pings per Ensemble (almost less than 1,200m depth)

Environmental Sensor Commands

    EA = 04500   Heading Alignment (1/100 deg)

    ED = 00065   Transducer Depth (0 - 65535 dm)

    EF = +001   Pitch/Roll Divisor/Multiplier (pos/neg) [1/99 - 99]

    EH = 00000   Heading (1/100 deg)

    ES = 35   Salinity (0-40 pp thousand)

    EX = 00000   Coordinate Transform (Xform:Type; Tilts; 3Bm; Map)

    EZ = 10200010   Sensor Source (C; D; H; P; R; S; T; U)

        C (1): Sound velocity calculates using ED, ES, ET (temp.)

        D (0): Manual ED

        H (2): External synchro

        P (0), R (0): Manual EP, ER (0 degree)

        S (0): Manual ES

        T (1): Internal transducer sensor

        U (0): Manual EU

    EV = 0   Heading Bias (1/100 deg)

Timing Commands

    TE = 00:00:02.00   Time per Ensemble (hrs:min:sec.sec/100)

    TP = 00:02.00   Time per Ping (min:sec.sec/100)

Water-Track Commands

    WA = 255   False Target Threshold (Max) (0-255 count)

WC = 120	Low Correlation Threshold (0-255)
WD = 111 100 000	Data Out (V; C; A; PG; St; Vsum; Vsum^2; #G; P0)
WE = 1000	Error Velocity Threshold (0-5000 mm/s)
WF = 0800	Blank After Transmit (cm)
WN = 100	Number of depth cells (1-128)
WP = 00001	Pings per Ensemble (0-16384)
WS = 800	Depth Cell Size (cm)
WV = 0390	Radial Ambiguity Velocity (cm/s)

(4) Instruments and methods

Upper-ocean current measurements were made during this cruise using a hull-mounted acoustic Doppler current profiler (ADCP) system. For most of its operation, the instrument was configured for water-tracking mode. The bottom-tracking mode, which interleaved bottom-ping with water-ping functionality, was adopted to obtain calibration data for evaluating the transducer misalignment angle in shallow water. The features of the operation of the ADCP system onboard the R/V Mirai are as follows.

1. An Ocean Surveyor for vessel-mount ADCP (frequency 76.8 kHz; Teledyne RD Instruments, USA) is installed on the R/V Mirai. The instrument has a phased-array transducer with a single ceramic assembly that creates four acoustic beams electronically. We mounted the transducer head rotated to a ship-relative angle of 45° azimuth from the keel.

2. The ship's gyrocompass (Tokyo Keiki, Japan) is used to provide a continuous heading to the ADCP system directory. Additionally, we have an Inertial Navigation Unit (Phins, Ixblue, France) that provides high-precision heading, attitude, pitch and roll information. All data are stored in ".N2R" data files with a time stamp.

3. A differential GNSS system (Star Pack-D, Fugro, Netherlands) provides precise information regarding the ship's position.

4. We use VmDas software version 1.49 (TRDI) for data acquisition.

5. To synchronize the time stamp of pings with the computer time, the clock of the logging computer is adjusted to GPS time server every 10 min.

6. Fresh water is charged in the sea chest to prevent biofouling at the transducer face.

7. The sound speed at the transducer, which does affect the vertical bin mapping and vertical velocity measurements, is calculated based on temperature, salinity (constant value; 35.0 PSU) and depth (6.5 m; transducer depth) using the equation in Medwin (1975).

Data were recorded every ping as raw ensemble (.ENR) data. Additionally, 15-s and 300-s averages were recorded as short-term average (.STA) and long-term average (.LTA) data, respectively. The blanking distance (command: WF) was set at 8 m. However, in shallow water (depth < 100 m) and in the Arctic Ocean, the blanking distance was changed to 2 m; thus, the center depth of the first layer was changed from approximately 23 to 17 m below the sea surface.

(5) Preliminary results

Figure 3.4 shows the time series plot of the current velocity during the stay in the repeat section (round-trip from Sta.039 to the MIZ).

(6) Observation Log

27 Sep. 2019 to 10 Nov. 2019

(7) Data archives

The data obtained during the cruise will be submitted to the Data Management Group of JAMSTEC, and they will be made available to the public via the "Data Research System for Whole Cruise Information in JAMSTEC (DARWIN)" on the JAMSTEC website (http://www.godac.jamstec.go.jp/darwin/e)
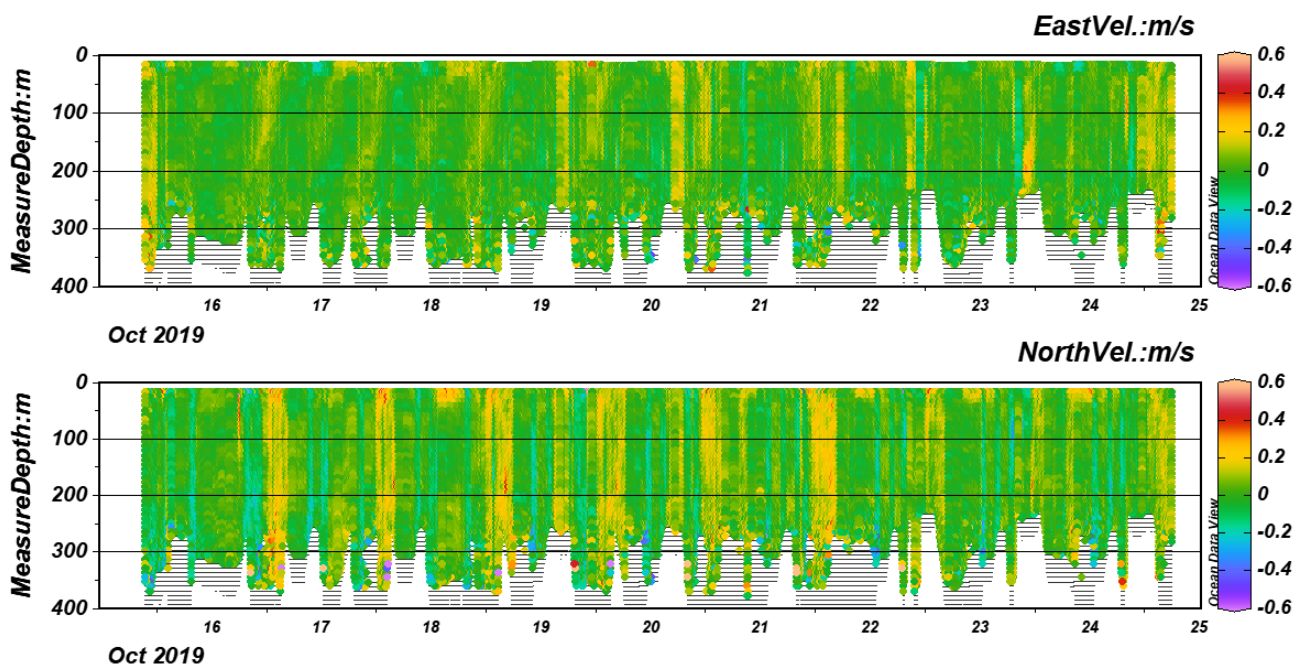
Figure 3.4: Time series plot of the current velocity

3. 5 RINKO Profiler

(1) Personnel

Jun Inoue	NIPR	-PI
Koji Shimada	Tokyo University of Marine Science and Technology	-not on board
Junpei Yamamoto	Tokyo University of Marine Science and Technology	
Rio Maya	Tokyo University of Marine Science and Technology	
Eri Yoshizawa	Korea Polar Research Institute	
Tsubasa Kodaira	University of Tokyo	

(2) Objectives

Knowledge of the thermohaline of the oceanic surface mixed layer is fundamental for forecasting the timing of freeze-up in the Arctic Ocean. To investigate its variation in the freeze-up season, vertical profiles of temperature and salinity were observed using a hand-operated CTD profiler. Daily observations were conducted just after the launch of the GPS radiosondes during 7–28 October 2019. In addition to these routine observations, some casts were performed at other hydrographic observation stations to complement the mapping of hydrography. The obtained data will be used to assess oceanic impacts on freeze-up and to validate forecasts.

(3) Parameters

Temperature, conductivity, depth, turbidity, chlorophyll and dissolved oxygen.

(4) Instruments and methods

A RINKO-Profiler (model: ASTD102, S/N: 0563) manufactured by the JFE Advantech Co. was used for all casts. The profiler incorporates multiple sensors for the measurement of physical and bio-optical parameters. The manufacture's nominal specifications regarding the type, range and accuracy of the parameters measured are listed below.

Parameter	Type	Range	Accuracy
Temperature	Platinum wire thermistor	-3-45 deg-C	±0.01 deg-C
Conductivity	Inductive cell	0.5-70 mS/cm	±0.01 mS/cm
Depth	Semiconductor stain gauge	0-600 m	±0.3 %
Turbidity	Backscatter	0-1000 FTU	±0.3 FTU
Chlorophyll	Fluorescence	0-400 ppb	±1 %
Dissolved Oxygen	Phosphorescence	0-200% or 0-20 mg/l	±2 %

We deployed the profiler by hand from the starboard side of the working deck and collected data at 0.1-s intervals. After recovery of the profiler, the raw data recorded in binary format were converted to CSV format using the

RINKO-Profiler software (ver. 1. 09).

To test the performance of the temperature and conductivity measurements, comparisons with SBE9plus data were conducted. The RINKO-Profiler was deployed together with the SBE9plus sensor in test casts at 50-00 N, 166-07 E conducted on 3 October and 2 November 2019. During the upcasts, data for the comparison were collected at the following depths: 170, 250, 300, 400 and 500 m. The standard deviations of the differences between the two datasets were negligibly small at each depth for both temperature and salinity.

(5) Station list

Observations were performed at the stations listed in Table 3.5.

Table 3.5: Station list of RINKO-Profiler observation.

St. No	Cast. No	Date (UTC) [yyyy/mm/dd]	Time (UTC) [hh:mm]	Lat. [deg-min]	Lon. [deg-min]	Observation depth [m]	Bottom depth [m]
0	1	2019/10/3	7:03	50-00.001 N	166-07.143 E	497	5398
1	1	2019/10/7	23:51	64-40.137 N	169-55.153 W	32	47
2	1	2019/10/8	23:32	68-09.910 N	168-45.382 W	31	58
3	1	2019/10/9	23:32	71-06.540 N	166-30.656 W	30	45
4	1	2019/10/10	23:37	72-46.903 N	158-22.495 W	33	299
5	1	2019/10/11	23:32	72-00.620 N	151-17.739 W	35	2588
6	1	2019/10/12	23:35	72-58.535 N	144-55.523 W	36	3547
7	1	2019/10/13	23:29	74-20.085 N	143-30.897 W	37	3712
8	1	2019/10/14	23:33	74-59.965 N	152-16.159 W	39	3844
9	1	2019/10/15	23:31	76-57.802 N	164-45.190 W	36	396
10	1	2019/10/16	18:00	77-15.108 N	164-59.484 W	39	367
11	1	2019/10/16	23:33	78-03.941 N	164-56.893 W	37	490
12	1	2019/10/17	2:00	77-53.380 N	164-59.984 W	40	411
13	1	2019/10/17	23:23	78-00.287 N	164-59.055 W	35	461
14	1	2019/10/18	2:00	77-45.129 N	165-00.094 W	36	445
15	1	2019/10/18	23:34	78-03.878 N	165-10.126 W	36	478
16	1	2019/10/19	2:17	77-45.217 N	164-59.798 W	41	443
17	1	2019/10/19	23:33	78-03.066 N	164-59.602 W	40	457
18	1	2019/10/20	2:40	77-45.168 N	165-00.328 W	50	443
19	1	2019/10/20	20:11	77-44.981 N	164-59.959 W	55	442
20	1	2019/10/20	23:33	78-00.916 N	164-58.441 W	42	452
21	1	2019/10/21	19:59	77-44.872 N	164-59.985 W	40	446

22	1	2019/10/21	23:33	78-01.559 N	164-57.640 W	38	475
23	1	2019/10/22	19:13	77-44.961 N	165-00.199 W	41	456
24	1	2019/10/22	23:33	77-46.149 N	164-05.429 W	38	276
25	1	2019/10/23	18:45	77-44.985 N	165-00.319 W	41	444
26	1	2019/10/23	23:24	77-47.021 N	163-35.816 W	41	284
27	1	2019/10/24	19:08	77-44.999 N	165-00.324 W	41	444
28	1	2019/10/24	23:33	77-47.621 N	163-40.605 W	44	282
29	1	2019/10/25	23:33	74-41.305 N	168-45.668 W	41	183
30	1	2019/10/26	20:12	72-00.073 N	168-45.013 W	44	50
30	2	2019/10/26	20:35	72-00.073 N	168-45.013 W	50	50
31	1	2019/10/26	23:29	71-30.190 N	168-44.615 W	48	48
32	1	2019/10/27	2:30	71-00.027 N	168-44.826 W	44	44
33	1	2019/10/27	19:46	68-30.125 N	168-45.190 W	51	53
34	1	2019/10/27	23:49	68-18.125 N	167-23.016 W	44	46
35	1	2019/10/28	20:28	66-00.033 N	168-44.923 W	53	54
36	1	2019/10/28	23:33	65-36.852 N	168-28.797 W	53	52
37	1	2019/11/02	21:57	50-00.020 N	166-07.300 E	497	5396

(6) Preliminary results

During the repeat observations of the north–south section along 168-00 W, temporal variations of the surface mixed layer were monitored at 77-45 N during 19–24 October 2019. This site was located in an open-water area near the MIZ. An evident surface mixed layer was captured throughout the observational period. The surface mixed layer depth defined by the buoyancy frequency maximum was almost unchanged (~30.5 m) with vertically homogeneous salinity (~29.0), as shown in Figure 3.5a. In this layer, temperature was highly variable in the vertical direction and it reached local maxima of up to 0.5 °C at the base of the layer (Figure 3.5b). The temperature was 0.5–2.0 °C higher than the local freezing temperature throughout the entire surface mixed layer, suggesting that oceanic conditions were responsible for slowing the freeze-up timing.
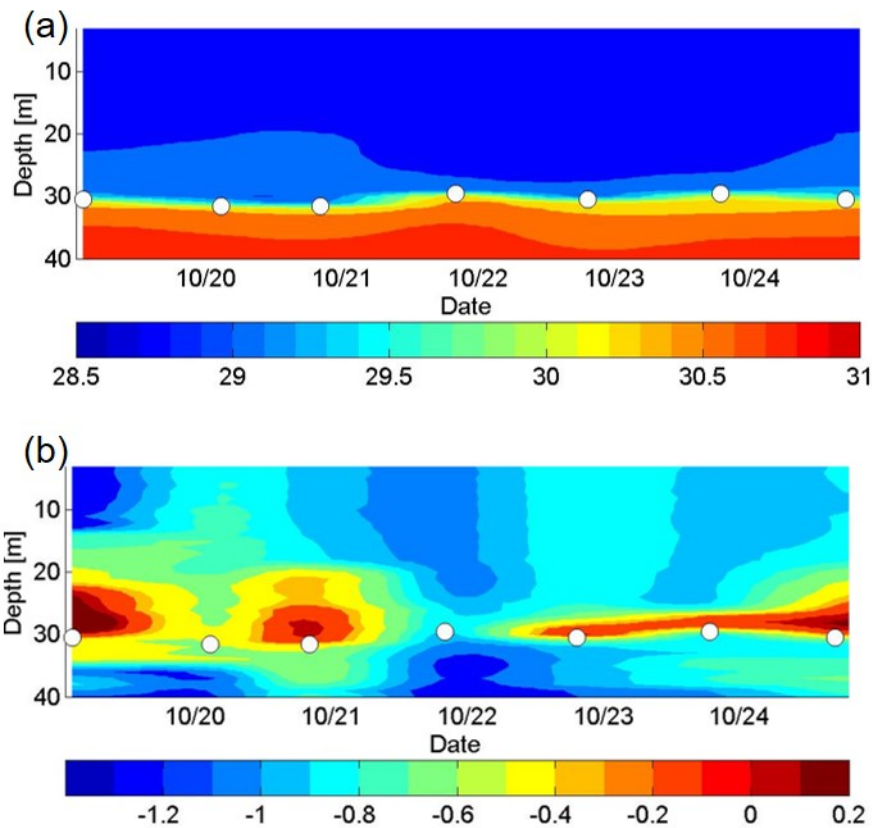
Figure 3.5: Time–depth cross section of (a) salinity and (b) in situ temperature at the site of 77-45 N, 168-00 W during 18–24 October 2019. The surface mixed layer depth defined by the buoyancy frequency maximum is denoted by white dots.

(7) Data archive

The data obtained during the cruise will be submitted to the Data Management Group of JAMSTEC, and they will be made available to the public via the "Data Research System for Whole Cruise Information in JAMSTEC (DARWIN)" on the JAMSTEC website (http://www.godac.jamstec.go.jp/darwin/e)

(8) Remarks

Station 0: Test cast was performed. Conductivity data collected at depths deeper than 400 m in down cast was bad, because of contaminations of inductive cell.

Station 30: Cast 2 was performed to obtain near bottom data that was not collected in cast 1.
Station 37: Test cast was performed.

3.6 Microstructure measurement

(1) Personnel

Yusuke Kawaguchi	University of Tokyo	- not on board, PI
ShigetoNishino	JAMSTEC	-not on board
Eun Yae Son	University of Tokyo	
Tsubasa Kodaira	University of Tokyo	
Yoshizawa Eri	KOPRI	
Ryo Oyama	NME	-Operation leader
Shinya Okumura	NME	
Kazuho Yoshida	NME	
Yutaro Murakami	NME	
Soichiro Sueyoshi	NME	
Takehito Hattori	NME	

(2) Objectives

1. Investigate turbulent mixing at the surface front in the MIZ and under newly formed sea ice during MR19-03C.

2. Collect examples for verification of proper fine-scale parameterization in the Arctic Basin.

(3) Parameter

The manufacture's nominal specifications of the range, accuracy and sampling rates of the parameters measured are shown in Table 3.6-1.

Table 3.6-1:

Parameter	Sensor type	Measurable range	Accuracy	Sampling rate
$\partial u/\partial z$ (primary)	Shear probe	0~10 /s	5%	512Hz
$T+\partial T/\partial z$	FPO-7 thermistor	±0.01°C	±0.01°C	512Hz
T	Platinum wire	−5~45°C	±0.01°C	64 Hz
Conductivity	Inductive Cell	0~70 mS	±0.01 mS	64 Hz
Depth	Semiconductor strain	0~1000 m	±0.2%	64Hz
x- acceleration	Solid-state fixed mass	±2 G	±1%	256 Hz
y- acceleration	Solid-state fixed mass	±2 G	±1%	256 Hz
z- acceleration	Solid-state fixed mass	±2 G	±1%	64Hz
Chlorophyll	Solid-state fixed mass	0~100 μg/Lm	0.5 μg/L or ±1%	256 Hz
Turbidity	Backscatter	0~100 ppm	1ppm or ±2%	256 Hz
$\partial u/\partial z$ (Secondary)	$\partial u/\partial z$ Shear	0~10 s^{-1}	5%	512 Hz

(4) Instruments and method

A Turbulence Ocean Microstructure Acquisition Profiler (TurboMAP-L, manufactured by JFE Alec Co Ltd.) was used to measure turbulence-scale temperature and shear. TurboMAP is a quasi-free-falling instrument that obtains turbulent mixing parameters ($\partial u/\partial z$ and $\partial T/\partial z$), bio-optical parameters (in vivo fluorescence and backscatter) and hydrographic parameters (conductivity, temperature and pressure). TurboMAP is a loosely tethered free-fall profiler that carries two airfoil shear probes, a fast-response thermistor (FP07), a light-emitting diode fluorescence/turbidity probe and a CTD package (Wolk et al. 2002). TurboMAP collects vertical profiles of microscale velocity shear, high- and low-resolution temperature, conductivity and pressure as the underwater device descends from the surface to its maximum depth. The free-falling speed of the instrument is approximately 0.5–0.6 m s^{-1}. Operation of the ship's side thrusters is halted during TurboMAP deployment to avoid creating any artificial noise corruption or disturbance in the microscale data. Use of microscale data obtained at depths of <5 m is not recommended in analysis because they might include noise attributable to the instrument's initial adjustment to free-fall. The TurboMAP observation log is shown in Table 3.6-2.

Table 3.6-2: Station lists

Stn.	Date [Y/M/D]	Lat. [deg-min]	Lon. [deg-min]	Time (UTC) Start	Time (UTC) End	Dep. [m]	Obs. Dep. [m]	Sensor S/N FP07	Sensor S/N Sh1	Sensor S/N Sh2
01	2019/10/03	49-59.8521N	166-06.9197E	8:06	8:25	5398	567	144	1232	1233
02	2019/10/03	49-59.7338N	166-07.0970E	8:59	9:17	5401	596	144	1232	1234
03	2019/10/08	65-39.8021N	168-27.6861W	7:23	7:28	52	48	144	1232	1234
04	2019/10/08	65-39.9191N	168-27.6569W	7:29	7:30	52	45	144	1232	1234
05	2019/10/08	65-40.0093N	168-27.6242W	7:31	7:33	52	42	144	1232	1234
06	2019/10/08	66-30.6988N	168-45.261W	13:19	13:21	54	44	144	1232	1234
07	2019/10/08	66-30.7587N	168-45.2213W	13:22	13:23	54	45	144	1232	1234
08	2019/10/08	66-30.8066N	168-45.1858W	13:24	13:25	54	43	144	1232	1234
09	2019/10/08	67-00.4760N	168-43.2958W	16:40	16:43	45	41	144	1232	1234
10	2019/10/08	67-00.5035N	168-43.1616W	16:44	16:45	45	42	144	1232	1234
11	2019/10/08	67-00.5306N	168-43.0656W	16:46	16:47	45	39	144	1232	1234
12	2019/10/08	68-09.9216N	168-45.3434W	23:41	23:43	58	50	144	1232	1234
13	2019/10/08	68-09.9351N	168-45.3301W	23:44	23:47	58	52	144	1232	1234
14	2019/10/08	68-09.9532N	168-45.3045W	23:47	23:49	58	50	144	1232	1234

15	2019/10/09	69-00.4770N	168-45.3655W	5:45	5:47	52	49	144	1232	1234
16	2019/10/09	69-00.5034N	168-45.4092W	5:49	5:49	52	48	144	1232	1234
17	2019/10/09	69-00.5374N	168-45.4578W	5:52	5:52	52	45	144	1232	1234
18	2019/10/09	69-30.3513N	168-45.9433W	9:59	10:02	51	44	144	1233	1234
19	2019/10/09	69-30.3581N	168-45.0331W	10:03	10:05	51	44	144	1233	1234
20	2019/10/09	69-30.3597N	168-45.1039W	10:05	10:07	51	43	144	1233	1234
21	2019/10/09	70-29.8375N	168-45.7190W	17:38	17:39	38	28	144	1233	1234
22	2019/10/09	70-29.8366N	168-45.7784W	17:40	17:41	38	32	144	1233	1234
23	2019/10/09	70-29.8357N	168-45.8826W	17:42	17:43	38	33	144	1233	1234
24	2019/10/10	71-09.2483N	166-25.1891W	0:44	0:46	44	30	144	1233	1234
25	2019/10/10	71-09.2483N	166-25.1891W	0:47	0:49	44	32	144	1233	1234
26	2019/10/10	71-09.2483N	166-25.1891W	0:49	0:51	44	37	144	1233	1234
27	2019/10/10	71-59.3997N	163-30.7643W	8:33	8:35	38	33	144	1233	1234
28	2019/10/10	71-59.3748N	163-30.8411W	8:37	8:37	38	35	144	1233	1234
29	2019/10/10	71-59.3461N	163-30.9131W	8:38	8:38	38	33	144	1233	1234
30	2019/10/10	71-29.7207N	161-44.9374W	14:37	14:38	44	42	144	1233	1234
31	2019/10/10	71-29.7002N	161-44.9267W	14:40	14:41	44	39	144	1233	1234
32	2019/10/10	71-29.6716N	161-44.8961W	14:43	14:43	44	36	144	1233	1234
33	2019/10/10	72-59.9234N	160-01.0259W	20:06	20:11	189	172	144	1233	1234
34	2019/10/10	72-59.9244N	160-01.1010W	20;14	20:19	189	150	144	1233	1234
35	2019/10/10	72-46.9092N	158-22.9159W	23:45	23:54	300	265	144	1233	1234
36	2019/10/10	72-46.9417N	158-23.7892W	23:58	0:07	305	278	144	1233	1234
37	2019/10/11	72-30.1502N	156-18.7587W	7:35	7:51	1619	579	144	1233	1234
38	2019/10/11	72-19.9306N	155-00.7130W	13:20	13:38	1955	680	144	1233	1234
39	2019/10/11	72-08.8840N	153-48.3499W	18:40	-	1705	565	144	1233	1234
40	2019/10/11	72-00.6442N	151-18.0845	23:42	23:59	2669	580	144	1233	1234
41	2019/10/12	71-59.9922N	147-29.9673W	9:41	9:43	3514	600	144	1233	1234
42	2019/10/12	71-59.7477N	144-59.9952W	17:32	17:58	3321	600	144	1233	1234
43	2019/10/12	72-58.5125N	144-55.5249W	23:46	0:00	3555	570	144	1233	1234
44	2019/10/13	72-58.3191N	144-55.8316W	0:11	0:26	3554	566	144	1233	1234
45	2019/10/13	74-25.6864N	142-58.3406W	21:13	21:18	3702	115	144	1233	1234
46	2019/10/13	74-25.5952N	142-58.5283W	21:20	21:24	3707	117	144	1233	1234
47	2019/10/13	74-23.1989N	143-16.1473W	22:26	22:30	3709	117	144	1233	1234
48	2019/10/13	74-23.1594N	143-16.1506W	22:33	22:36	3710	117	144	1233	1234

49	2019/10/13	74-20.3644N	143-30.8557W	23:39	23:44	3712	120	144	1233	1234
50	2019/10/13	74-20.3193N	143-30.8302W	23:47:00	23:51	3710	127	144	1233	1234
51	2019/10/14	74-17.7599N	143-45.1738W	0:35	0:40	3709	-	144	1233	1234
52	2019/10/14	74-17.6544N	143-44.8224W	0:44	0:52	3711	132	144	1233	1234
53	2019/10/14	74-12.2673N	144-13.7462W	2:01	2:06	3710	112	144	1233	1234
54	2019/10/14	74-12.2052N	144-13.7180W	2:08	2:11	3711	122	144	1233	1234
55	2019/10/14	74-09.4681N	144-28.5057W	3:03	3:07	3712	108	144	1233	1234
56	2019/10/14	74-09.3755N	144-28.4901W	3:10	3:14	3712	115	144	1233	1234
57	2019/10/14	74-03.9934N	144-57.8202W	4:27	4:31	3719	116	144	1233	1234
58	2019/10/14	74-46.4150N	150-31.1201W	20:23	20:40	3835	563	144	1233	1234
59	2019/10/14	74-59.7055N	152-16.4074W	23:46	0:04	3848	587	144	1233	1234
60	2019/10/15	74-59.6590N	152-16.1599W	0:14	0:30	3846	572	144	1233	1234
61	2019/10/16	76-57.7674N	164-45.3915W	23:51	23:55	396	392	144	1233	1234
62	2019/10/16	76-57.7642N	166-44.9311W	0:00	0:08	396	392	144	1233	1234
63	2019/10/16	77-15.0015N	164-59.8112W	7:54	8:02	370	230	144	1233	1234
64	2019/10/16	77-15.0454N	164-59.5942W	8:06	8:13	370	233	144	1233	1234
65	2019/10/16	77-03.9297N	164-56.3229W	23:42	23:49	471	219	144	1233	1234
66	2019/10/16	77-03.9478N	164-55.5717W	23:54	23:59	471	320	144	1233	1234
67	2019/10/17	77-14.9617N	164-59.9329W	5:47	5:55	367	235	144	1233	1234
68	2019/10/17	77-14.9679N	164-59.7267W	6:00	6:07	371	239	144	1233	1234
69	2019/10/17	77-30.0435N	165-00.1776W	9:36	9:43	308	232	144	1233	1234
70	2019/10/17	77-30.0675N	165-00.0837W	9:47	9:54	310	240	144	1233	1234
71	2019/10/17	78-00.2441N	165-00.7489W	21:59	21:07	454	244	144	1233	505
72	2019/10/17	78-00.2612N	165-00.1502W	22:12	22:19	454	229	144	1233	505
73	2019/10/18	77-15.0006N	164-59.9585W	4:56	5:04	370	227	144	1233	505
74	2019/10/18	77-15.0571N	164-59.8944W	5:07	5:14	366	230	144	1233	505
75	2019/10/18	77-30.0269N	165-00.2550W	9:03	9:11	308	245	144	1233	505
76	2019/10/18	77-30.0603N	165-00.2145W	9:16	9:23	309	234	144	1233	505
77	2019/10/18	77-45.0392N	164-59.8296W	14:31	14:38	348	215	144	1233	505
78	2019/10/18	77-45.1693N	164-59.9306W	14:42	14:49	348	238	144	1233	505
79	2019/10/18	77-45.5226N	164-59.4505W	17:59	18:07	439	222	144	1233	505
80	2019/10/18	77-45.6783N	164-59.0496W	18:11	18:17	439	219	144	1233	505
81	2019/10/19	78-04.0251N	165-10.3834W	23:48	23:55	473	222	144	1233	505

82	2019/10/19	78-04.1496N	165-10.3560W	23:59	0:05	473	216	144	1233	505
83	2019/10/19	77-00.0231N	164-59.8730W	6:47	6:54	669	230	144	1233	505
84	2019/10/19	77-00.0550N	164-59.7756W	6:59	7:05	671	236	144	1233	505
85	2019/10/19	77-15.1084N	165-00.1615W	10:35	10:42	362	236	144	1233	505
86	2019/10/19	77-15.1605N	165-00.0141W	10:46	10:53	364	226	144	1233	505
87	2019/10/19	77-30.0184N	164-59.9647W	15:01	15:07	309	188	144	1233	505
88	2019/10/19	77-30.0613N	164-59.7102W	15:16	15:18	309	198	144	1233	505
89	2019/10/19	77-30.1162N	164-59.5181W	15:21	15:26	309	177	144	1233	505
90	2019/10/19	78-03.1133N	164-59.1429W	23:45	23:50	460	173	144	1233	505
91	2019/10/19	78-03.1731N	164-58.6471W	23:54	23:59	460	168	144	1233	505
92	2019/10/20	78-03.2298N	164-58.2186W	0:02	0:06	460	163	144	1233	505
93	2019/10/20	77-00.0290N	164-59.8200W	7:27	7:33	672	171	144	1233	505
94	2019/10/20	77-00.0676N	164-59.7295W	7:35	7:40	663	170	144	1233	505
95	2019/10/20	77-00.1151N	164-59.6577W	7:43	7:48	662	167	144	1233	505
96	2019/10/20	77-15.0168N	164-59.9991W	11:35	11:41	365	167	144	1233	505
97	2019/10/20	77-15.0742N	164-59.7690W	11:44	11:49	365	167	144	1233	505
98	2019/10/20	77-15.1499N	164-59.5407W	11:52	11:57	362	165	144	1233	505
99	2019/10/20	77-30.1018N	164-59.1995W	16:09	16:15	308	165	144	1233	505
100	2019/10/20	77-30.1588N	164-58.8220W	16:18	16:22	308	164	144	1233	505
101	2019/10/20	77-30.2305N	164-58.4328W	16:26	16:30	308	163	144	1233	505
102	2019/10/20	78-00.3450N	165-00.4578W	21:57	22:03	455	172	144	1233	505
103	2019/10/20	78-00.4221N	165-00.1065W	22:06	22:11	455	163	144	1233	505
104	2019/10/20	78-00.4893N	164-59.6686W	22:14	22:18	455	167	144	1233	505
105	2019/10/21	77-15.0072N	165-59.9773W	4:17	4:23	852	178	144	1233	505
106	2019/10/21	77-15.0470N	165-59.9454W	4:27	4:32	852	180	144	1233	505
107	2019/10/21	77-15.0948N	165-59.8892W	4:35	4:36	852	20	144	1233	505
108	2019/10/21	77-15.1001N	165-59.8671W	4:36	4:41	852	168	144	1233	505
109	2019/10/21	77-00.0690N	164-59.9934W	10:02	10:08	708	168	144	1233	505
110	2019/10/21	77-00.1433N	164-59.8591W	10:12	10:17	708	178	144	1233	505
111	2019/10/21	77-00.1973N	164-59.7176W	10:20	10:25	708	176	144	1233	505
112	2019/10/21	77-15.0228N	164-59.9817W	15:02	15:08	372	180	144	1233	505
113	2019/10/21	77-15.0846N	164-59.8435W	15:11	15:16	372	178	144	1233	505
114	2019/10/21	77-15.1262N	164-59.7434W	15:19	15:24	372	173	144	1233	505
115	2019/10/21	77-30.0902N	165-00.0872W	16:58	17:04	306	172	144	1233	505

116	2019/10/21	77-30.1491N	164-59.9966W	17:07	17:11	306	167	144	1233	505
117	2019/10/21	77-30.1932N	164-59.7542W	17:15	17:20	306	171	144	1233	505
118	2019/10/21	78-00.5449N	164-59.9344W	21:57	22:03	463	157	144	1233	505
119	2019/10/21	78-00.7032N	164-59.6497W	22:07	22:12	463	158	144	1233	505
120	2019/10/21	78-00.8762N	164-59.3135W	22:16	22:21	463	164	144	1233	505
121	2019/10/22	77-00.1451N	166-00.1091W	5:35	5:41	603	169	144	1233	505
122	2019/10/22	77-00.2049N	166-00.0938W	5:44	4:49	603	186	144	1233	505
123	2019/10/22	77-00.2541N	166-00.0728W	5:53	5:58	603	173	144	1233	505
124	2019/10/22	76-59.9157N	165-00.0425W	9:40	9:45	737	164	144	1233	505
125	2019/10/22	76-59.9833N	164-59.8779W	9:49	9:54	737	184	144	1233	505
126	2019/10/22	77-00.0394N	164-59.7181W	9:57	10:02	737	164	144	1233	505
127	2019/10/22	77-15.0187N	164-59.9712W	14:54	15:00	371	174	144	1233	505
128	2019/10/22	77-15.0650N	164-59.8826W	15:02	15:07	371	173	144	1233	505
129	2019/10/22	77-15.1104N	169-59.8076W	15:10	15:14	371	175	144	1233	505
130	2019/10/22	77-30.0320N	164-59.6690W	16:47	16:52	309	178	144	1233	505
131	2019/10/22	77-30.1032N	164-59.4797W	16:55	16:59	309	169	144	1233	505
132	2019/10/22	77-30.1599N	164-59.2379W	17:02	17:07	309	164	144	1233	505
133	2019/10/22	77-46.2299N	164-04.7955W	23:52	23:53	275	180	144	1233	505
134	2019/10/22	77-46.2981N	164-04.5649W	23:56	0:01	275	171	144	1233	505
135	2019/10/23	77-46.3559N	164-04.3546W	0:04	0:09	275	168	144	1233	505
136	2019/10/23	76-59.9702N	163-59.7083W	5:06	5:12	437	171	144	1233	505
137	2019/10/23	77-00.0281N	163-59.8135W	5:15	5:20	437	168	144	1233	505
138	2019/10/23	77-00.0839N	164-00.0240W	5:23	5:28	437	166	144	1233	505
139	2019/10/23	76-59.9250N	164-59.7254W	8:49	8:55	670	167	144	1233	505
140	2019/10/23	77-00.0136N	164-59.5948W	8:58	9:03	670	173	144	1233	505
141	2019/10/23	77-00.0548N	164-59.3884W	9:07	9:12	670	175	144	1233	505
142	2019/10/23	77-14.9759N	165-00.3586W	12:43	12:49	365	165	144	1233	505
143	2019/10/23	77-15.0343N	165-00.1760W	12:52	12:59	365	163	144	1233	505
144	2019/10/23	77-15.1011N	164-59.9652W	13:00	13:04	365	168	144	1233	505
145	2019/10/23	77-29.9561N	165-00.2722W	15:47	15:52	309	161	144	1233	505
146	2019/10/23	77-30.0408N	165-00.0219W	15:50	16:01	309	163	144	1233	505
147	2019/10/23	77-30.1203N	164-59.6431W	16:04	16:09	309	171	144	1233	505
148	2019/10/23	77-46.7549N	163-36.4233W	22:00	22:06	289	172	144	1233	505
149	2019/10/23	77-46.8118N	163-36.2003W	22:09	22:14	289	174	144	1233	505

150	2019/10/23	77-46.8951N	163-35.9086W	22:18	22:23	289	167	144	1233	505
151	2019/10/24	77-15.0406N	164-00.2612W	2:53	2:58	365	174	144	1233	505
152	2019/10/24	77-15.0632N	164-00.0346W	3:01	3:06	365	182	144	1233	505
153	2019/10/24	77-15.0751N	163-59.7522W	3:10	3:15	365	173	144	1233	505
154	2019/10/24	77-00.0379N	165-00.3718W	9:24	9:29	682	180	144	1233	505
155	2019/10/24	77-00.0882N	165-00.3285W	9:33	9:38	682	167	144	1233	505
156	2019/10/24	77-00.1615N	165-00.1762W	9:42	9:47	682	171	144	1233	505
157	2019/10/24	77-15.0317N	164-59.9736W	14:28	14:33	370	164	144	1233	505
158	2019/10/24	77-15.1114N	165-00.0154W	14:36	14:41	370	160	144	1233	505
159	2019/10/24	77-15.2027N	165-00.2230W	14:44	14:48	370	160	144	1233	505
160	2019/10/24	77-30.0955N	164-59.9872W	16:19	16:25	307	162	144	1233	505
161	2019/10/24	77-30.2165N	164-59.9896W	16:28	16:33	307	153	144	1233	505
162	2019/10/24	77-30.3441N	165-00.1151W	16:35	16:40	307	160	144	1233	505
163	2019/10/25	77-48.1967N	163-46.2576W	0:03	0:08	237	163	144	1233	505
164	2019/10/25	77-48.3194N	163-46.7506W	0:13	0:17	237	169	144	1233	505
165	2019/10/25	77-48.4510N	163-47.2585W	0:21	0:26	237	165	144	1233	505
166	2019/10/25	76-59.9434N	168-44.6127W	8:10	8:14	1885	102	144	1233	505
167	2019/10/25	76-59.9892N	168-45.0471W	8:17	8:29	1885	439	144	1233	505
168	2019/10/25	74-41.5100N	168-46.0646W	23:45	23:51	184	167	144	1233	505
169	2019/10/25	74-41.5528N	168-46.1547W	23:53	23:58	184	164	144	1233	505
170	2019/10/25	74-41.6773N	168-46.4730W	0:01	0:05	184	170	144	1233	505
171	2019/10/26	74-00.1065N	168-44.2929W	4:21	4:26	186	166	144	1233	505
172	2019/10/26	74-00.0775N	168-44.3735W	4:29	4:34	186	166	144	1233	505
173	2019/10/26	74-00.0730N	168-44.3841W	4:37	4:41	186	166	144	1233	505
174	2019/10/26	73-00.0892N	168-45.2488W	12:45	12:46	61	46	144	1233	505
175	2019/10/26	73-00.0795N	168-45.2376W	12:48	12:49	61	41	144	1233	505
176	2019/10/26	73-00.0705N	168-45.2071W	12:51	12:50	61	46	144	1233	505
177	2019/11/02	50-00.2626N	166-07.3557E	23:08	23:24	5398	536	144	1233	1234

(5) Remarks

TurboMAP is designed for stand-alone operation without additional CTD observations. However, it is recommended that the quality of the incoming CTD data be checked by comparison with SBE9plus (Sea-Bird Electronics) data. We conducted several joint TurboMAP and CTD observations at depths down to 500 m in the Canada Basin. However, as it is not possible to attach TurboMAP to the CTD frame, the TurboMAP cast was performed immediately after or before the CTD cast. The validity of the sensor readings was judged based on the temperature, salinity and pressure below the pycnocline where there is no significant variation within short periods (Figure 3.6-1).

As the observations were conducted under cold air temperatures (<0 °C), the slow temperature sensor showed a delayed response to the real upper-ocean temperature. Therefore, it is recommended that data acquired from the second or third cast be used for the CTD, shear and FP07 data. In areas where the bottom depth was 200–300 m, regular noise with 4-2 frequency was detected by both shear sensors. This noise was associated with the multibeam sonar that measures bottom depth using an acoustic signal. The multibeam sonar was turned off after cast No. 79.

TurboMAP has two shear probes for checking the validity of the shear data. Although TurboMAP can be used with just one shear probe, use of the pair of shear sensors is recommended. Figure 3.6-2 shows the turbulence dissipation rate obtained by each shear sensor. During MR19-03C, we changed the shear probe twice (St.18: shear1 to S/N 1233; St.71: shear2 to S/N 505). After leaving the Arctic Ocean, we performed another test cast to check the CTD and shear probe (S/N 1234) status. Shear probe S/N 1234 was found affected by repeated noise that was again revealed attributable to the acoustic signal of the multibeam sonar (Figure 3.6-3).
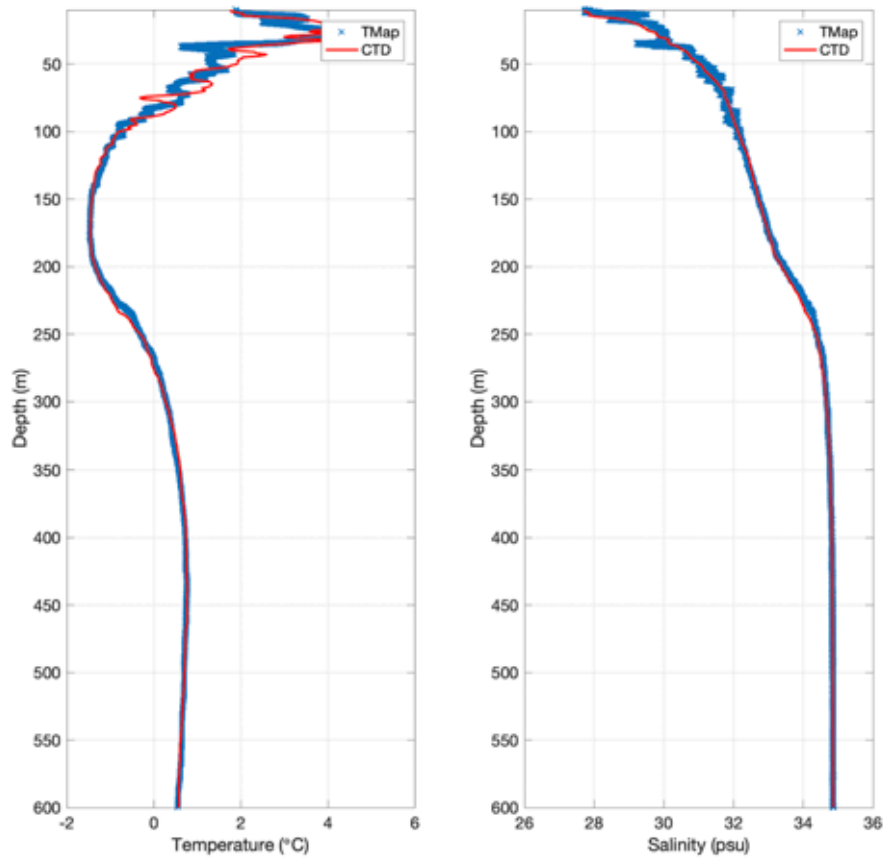
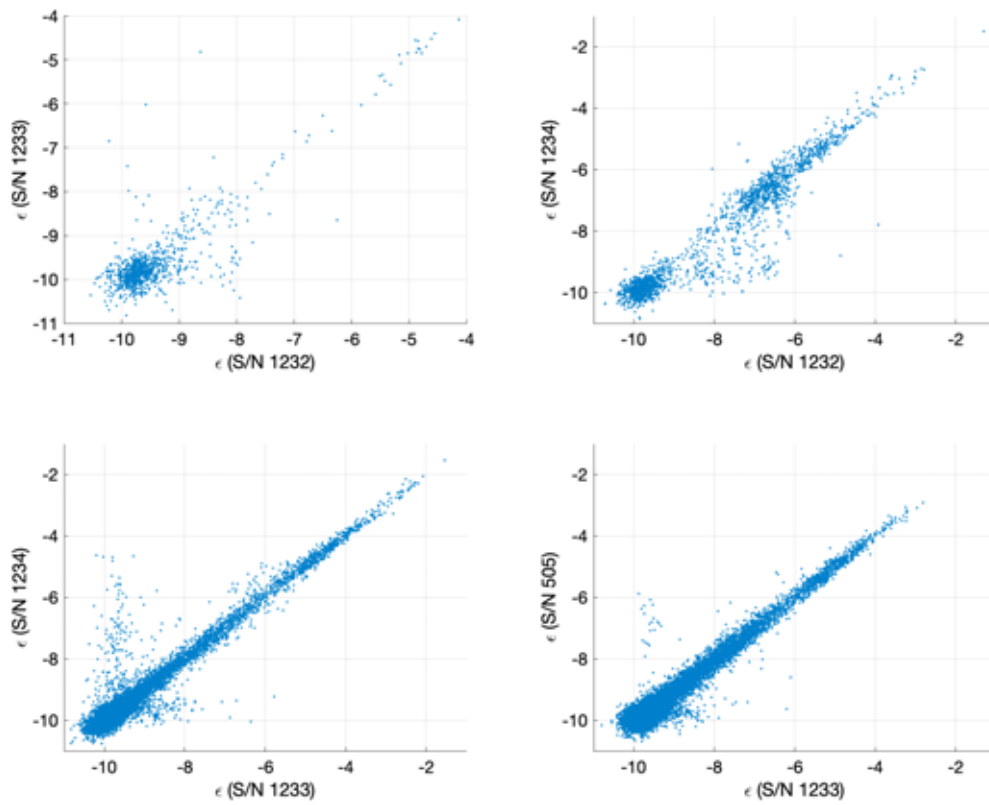Figure 3.6-1: Comparison of temperature and salinity acquired by SBE9plus and TurboMAP.

Figure 3.6-2: Correlation between the two shear sensors used during MR19-03C.
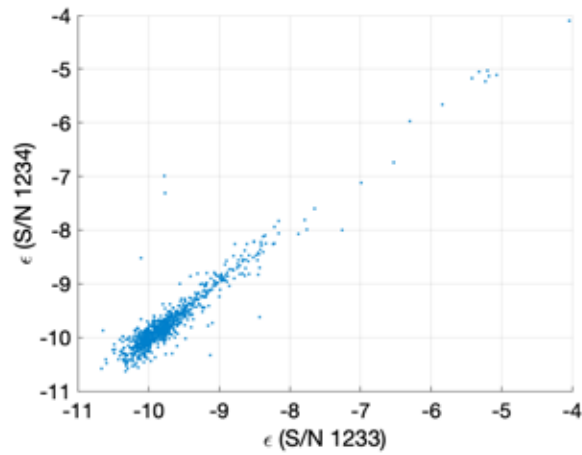
Figure 3.6-3: Correlation between shear probes of S/N 1234 and 1233 from the test cast

(6) Data archive

The data obtained during the cruise will be submitted to the Data Management Group of JAMSTEC, and they will be made available to the public via the "Data Research System for Whole Cruise Information in JAMSTEC (DARWIN)" on the JAMSTEC website (http://www.godac.jamstec.go.jp/darwin/e)

3.7 Subsurface ocean current and heat observation with drifting buoy

(1) Personnel

Yusuke Kawaguchi	University of Tokyo	- not on board, PI
Shigeto Nishino	JAMSTEC	- not on board
Eun Yae Son	University of Tokyo	

(2) Objectives

To examine the upper-ocean bulk heat variation in the western Arctic Ocean during the season of sea-ice formation, and to explore the upper-ocean currents at the surface front between dense warm water and fresh cold water in the MIZ.

(3) Parameter

Surface Velocity Profiler (SVP)

GPS positions of drifting buoy

IceBTC60/40

GPS positions and air pressure of drifting buoy

Water temperature and hydrostatic pressure at certain depth

(4) Instruments and methodology

We deployed two types of drifting buoy for the investigation of the upper-ocean currents and heat variability in the MIZ. We deployed two SVP buoys with a drogue at depths of 40 and 15 m in the area of the surface front where surface temperature changes rapidly (MIZ5). The IceBTC60/40 buoy, which is designed for use in the areas covered by sea ice, has a 60-m-long thermistor chain with pressure sensors. It measures upper-ocean temperature with accuracy of ±0.1 °C (resolution: 0.04 °C) and air pressure with accuracy of ±1 hPa (resolution: 0.1 hPa). The IceBTC40/60 buoy has thermistors at depths of 0, 2.5, 5, 7.5, 10, 12.5, 15, 17.5, 20, 25, 30, 35, 40, 45, 50, 55 and 60 m and hydrostatic pressure sensors at depths of 20, 40, and 60 m. We deployed the IceBTC40/60 buoy in the MIZ, which was covered with grease ice (MIZ2), to explore the upper-ocean bulk heat flux during the season of sea-ice formation.

Table 3.7: Deployment information

Type	S/N	Deploy time (UTC)	Deploy location [deg-min]	Data interval	Drogue depth	denotes
SVP	35924	02:20 Oct 14, 2019	74-12.2052N, 144-13.718W	hourly	40 m	Deployed in surface front
SVP	145580	02:26 Oct 14, 2019	74-12.2052N, 144-13.718W	hourly	15 m	Deployed in surface front
IceBTC40/60	11800	23:43 Oct 13, 2019	74-23.15N, 143-16.151W	hourly	-	Deployed in the grease ice zone

(5) Data archive

The raw data obtained in this cruise will be submitted to the Data Management Group (DMG) of JAMSTEC.

3.8 Surface wave measurement

(1) Personnel

Jun Inoue	NIPR	-PI
Takuji Waseda	The University of Tokyo	- not on board
Tsubasa Kodaira	The University of Tokyo	
Takehiko Nose	The University of Tokyo	- not on board

(2) Objective

Recent research has identified surface ocean waves as one of the key physical processes in the freeze-up/break-up of sea ice. We aimed to study the generation, propagation and attenuation of surface ocean waves under sea ice based on in situ observations over the western Arctic Ocean. Drifting-type wave buoys and an onboard stereo camera system were used to measure surface wave characteristics.

(3) Parameters

Drifting wave buoys: significant wave height (Hm0), peak period (Tp), peak direction, peak directional spread, mean period (Tm01), mean direction, mean directional spread, power spectral density (PSD), time and GPS coordinates.

Stereo camera system: monochrome images (4064 × 4064 pixels), acceleration (3-axis), gyro (3-axis) and geomagnetism (3-axis).

(4) Instruments and methods

Drifting wave buoys. The type of drifting wave buoy used was a Spotter device manufactured by Sofar Ocean Technologies (Figure 3.8-1). The device is fully solar powered and has a two-way communication function via Iridium satellite communication. One of the three wave buoys was deployed at the north of Pt. Barrow to measure the waves for a reasonably long time. The two other wave buoys were deployed near the sea-ice zone: one in an area covered with pancake ice and the other in an open-ocean area, separated by a distance of approximately 40 km.

Stereo camera system. The two cameras, mounted in separate housing on the portside of the R/V Mirai, were synchronized to allow stereo reconstruction of the captured images of surface ocean waves. Both cameras were connected via USB cables to a laptop computer placed in a watertight black plastic box (Figure 3.8-1). A 5-bay HDD storage device and wireless rooter were also installed in the box. A 9-axis inertial moment unit (ZMP-IMUZ) was also placed in the box to measure the motion of the cameras.
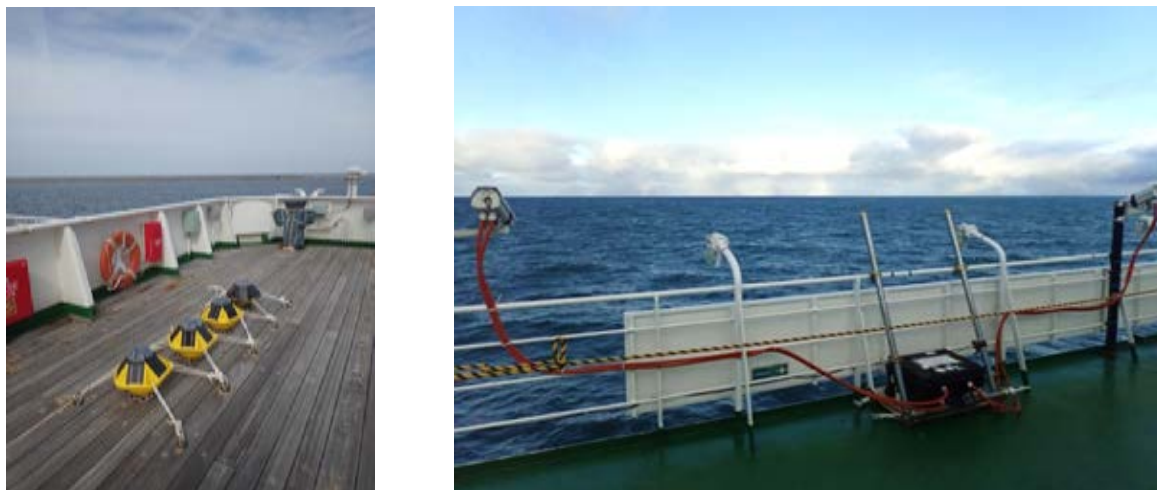

Figure 3.8-1: Drifting wave buoys (left) and the onboard stereo camera system on board (right).

(5) Observation log

Drifting wave buoys. One of the wave buoys (SPOT-0339) was deployed in open water at 10:35 UTC on 11 October 2019 at 72.3407°N, 155.0548°W (Figure 3.8-2). The wave buoy stopped sending data at 20:50 UTC on 21 October 2019 because the battery was not charged sufficiently because of the limited solar radiation at high latitudes in October.

The two other wave buoys (SPOT-0257 and SPOT-0258) were deployed near the sea-ice edge to compare the characteristics of waves under the sea ice and in the open ocean. The deployment of SPOT-0257, in water covered with pancake ice, was at 21:40 UTC on 13 October 2019 at 74.4235°N, 143.0032°W. Subsequently, SPOT-0258 was deployed in an open-ocean area at the thermal front at 02:20 UTC on 14 October 2019 at 74.2012°N, 144.2273°W (Figure 3.8-2). The transmissions from SPOT-0257 and SPOT-0258 stopped at 05:01 UTC on 21 October 2019 and 17:01 UTC on 19 October 2019, respectively.
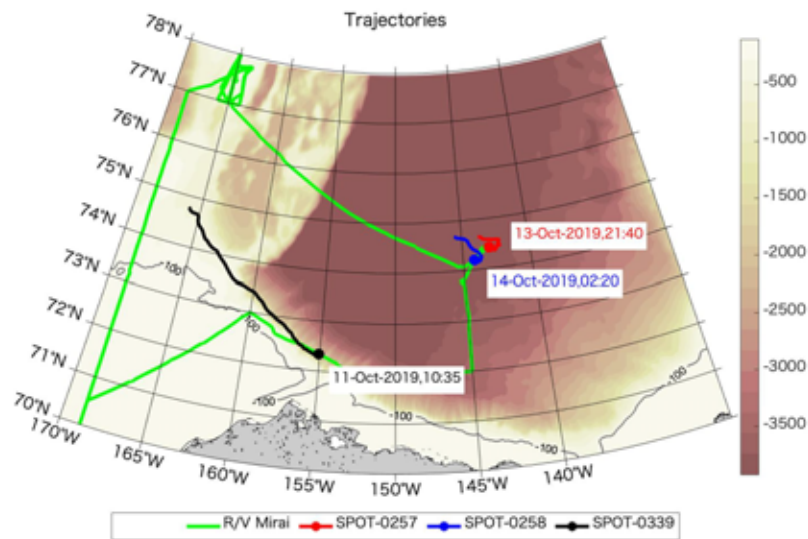
Figure 3.8-2: Trajectories of the R/V Mirai and the drifting wave buoys. Circles indicate deployment locations of the buoys. Text near each circle indicates the date and time (UTC) of buoy deployment. Colored shading represents bathymetry.

Stereo camera system. The stereo camera system was used hourly and sometimes half-hourly when the track of the R/V Mirai cruise approached the area covered with sea ice.

(6) Preliminary Results

Drifting wave buoys. Figure 3.8-3 shows the wave statistics recorded by the drifting wave buoys. SPOT-0339 measured a maximum significant wave height of 3.38 m with peak period of 9.31 s at 06:50 UTC on 12 October 2019. The wave height changed with time as the wind speed changed. Concurrent measurements of surface waves under the sea ice by SPOT-0257 and those in the open ocean by SPOT-0258 revealed the transformation of surface waves by the sea ice. Initially, the waves under the sea ice were of height similar to those in the open ocean, but they gradually became smaller. The results indicate that the waves were attenuated or scattered as they propagated over the sea-ice region. In addition, the mean period of the waves under the sea ice was consistently smaller than in the open ocean, while the peak period was similar in both areas. The results imply that shorter waves are attenuated more easily than longer waves.
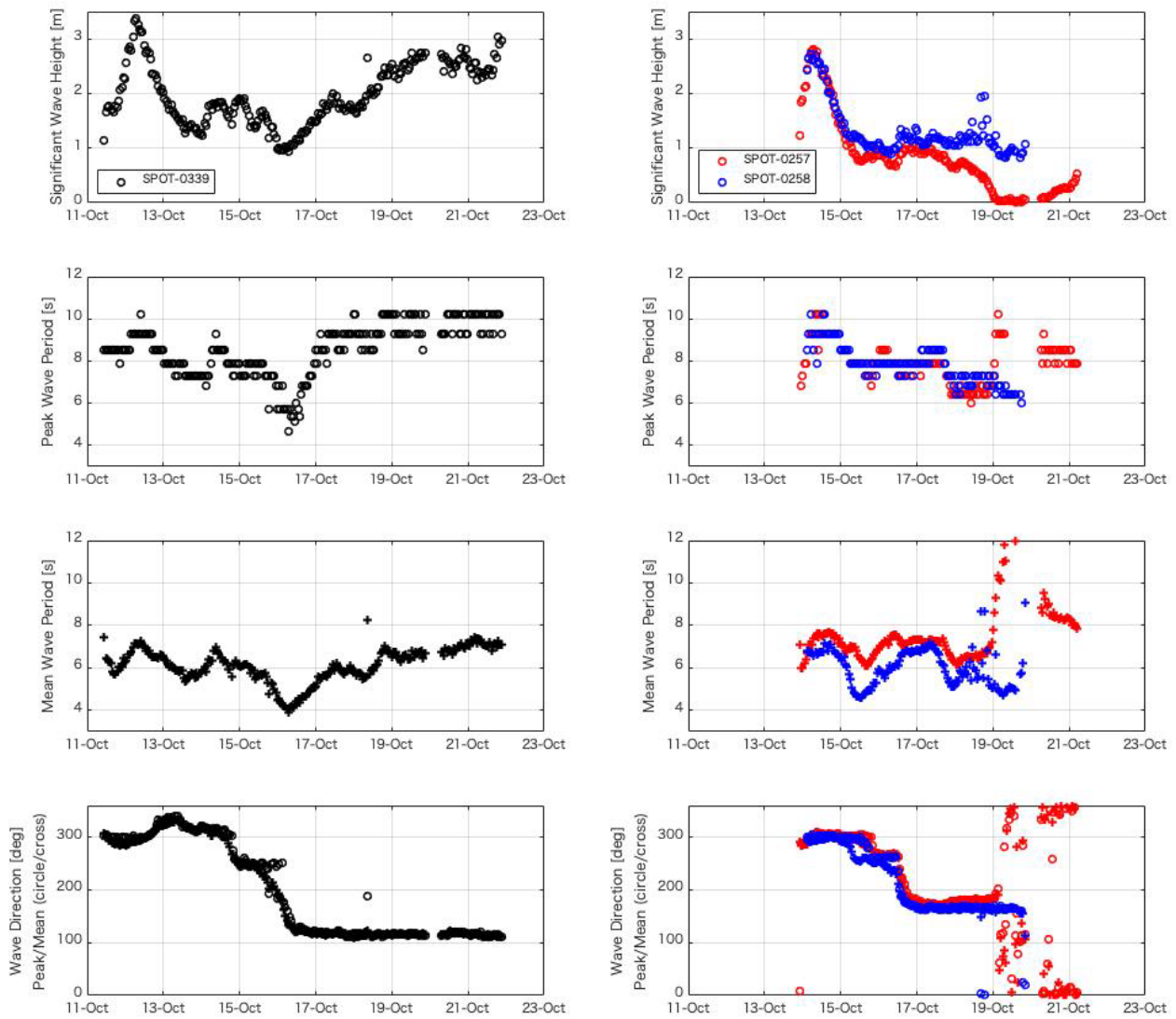
Figure 3.8-3: Significant wave height (top), peak and mean wave periods (middle) and wave direction (bottom).

Left column shows SPOT-339 data and the right column shows SPOT-0257 and SPOT-0258 data.

Figure 3.8-4: Sample images obtained by the stereo camera system.

(7) Data archives

The data obtained during the cruise will be submitted to the Data Management Group of JAMSTEC, and they will be made available to the public via the "Data Research System for Whole Cruise Information in JAMSTEC (DARWIN)" on the JAMSTEC website (http://www.godac.jamstec.go.jp/darwin/e)

3.9 LADCP

(1) Personnel

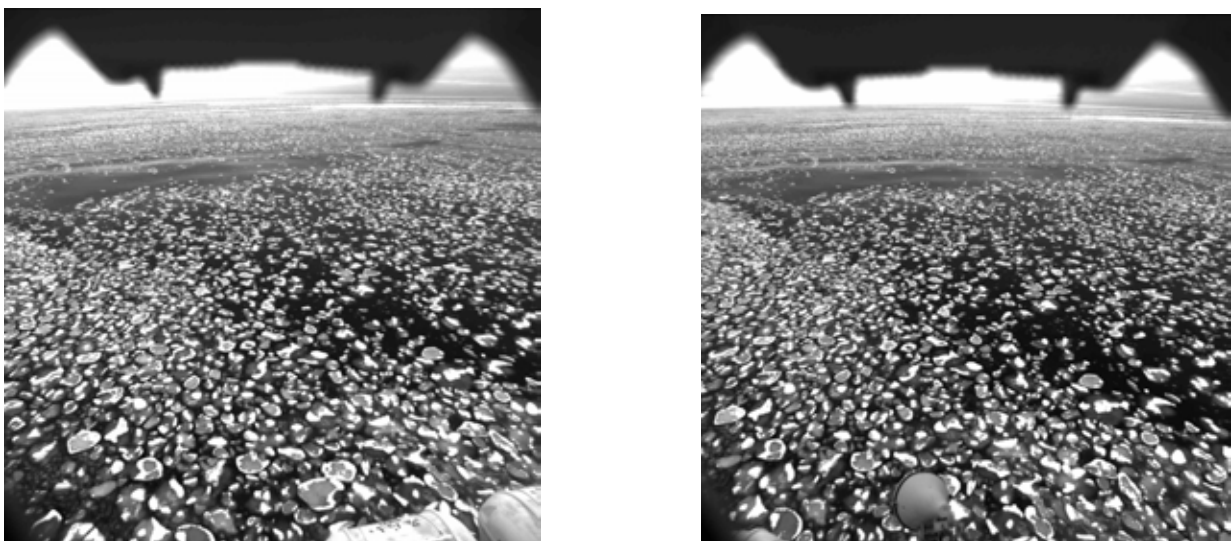|		
Yusuke Kawaguchi	University of Tokyo	- not on board, PI
Shigeto Nishino	JAMSTEC	- not on board
Eun Yae Son	University of Tokyo	
Shinsuke Toyoda	MWJ	- Operation leader
Rio Kobayashi	MWJ	
Tun Htet Aung	MWJ	

(2) Objectives and methodology

The Workhorse Monitor WHM300 (Teledyne RD Instrument, San Diego, California, USA) lowered ADCP (LADCP) was deployed at every CTD point on the MR19-03C cruise to obtain concurrent shear data. The LADCP system consists of two ADCP (upward and downward looking) transducers and a 45V battery package. The LADCP system was set for recording before the CTD cast and its data were recovered immediately after completion of the CTD cast. Velocity conversion from the two transducers was performed using LDEO LADCP software (version 10; Visbeck 2002). For the data conversion, navigational data and CTD data were applied to improve the data quality.

The LADCP data were separated into independent folders that were given the same name as the CTD station. Details of the configuration are listed below.

Bin size: 8.0 m

Number of bins: 25

Pings per ensemble: 1

Ping interval: 1.0 sec

(3) Data archive

The raw data obtained in this cruise will be submitted to the Data Management Group (DMG) of JAMSTEC.

Reference

Visbeck, M. (2002): Deep velocity profiling using Acoustic Doppler Current Profilers: Bottom track and inverse solutions, J. Atmos. Oceanic Technol., 19, 794–807.

4. Chemical and Biological Oceanography

4.1 Dissolved Oxygen

(1) Personnel

Akihiko Murata	JAMSTEC	- PI
Erii Irie	MWJ	- Operation Leader
Yuko Miyoshi	MWJ	
Kanako Yoshida	MWJ	

(2) Objective

Determination of dissolved oxygen in seawater using Winkler titration.

(3) Parameters

Dissolved Oxygen

(4) Instruments and methods

The following procedure is based on the Winkler method.

a. Instruments

Burette for sodium thiosulfate and potassium iodate;

Automatic piston burette (APB-510 / APB-610 / APB-620) manufactured by Kyoto Electronics

Manufacturing Co., Ltd. / 10 cm^3 of titration vessel

Detector;

Automatic photometric titrator (DOT-15X) manufactured by Kimoto Electric Co., Ltd.

Software;

DOT_Terminal Ver. 1.3.1

b. Reagents

Pickling Reagent I: Manganese(II) chloride solution (3 mol dm^{-3})

Pickling Reagent II:

Sodium hydroxide (8 mol dm^{-3}) / Sodium iodide solution (4 mol dm^{-3})

Sulfuric acid solution (5 mol dm^{-3})

Sodium thiosulfate (0.025 mol dm^{-3})

Potassium iodate (0.001667 mol dm^{-3})

c. Sampling

Seawater samples were collected with a Niskin bottle attached to the CTD/CWS system (CTD system). Seawater for oxygen measurement was transferred from the bottle to a volume-calibrated flask (ca. 100 cm^3) and the flask was allowed to overflow by three times its volume while filling. Temperature was measured simultaneously using a digital thermometer during the overflowing. After transferring the sample, two reagent solutions (Reagent I and II; vol.: 1 cm^3 of each) were added immediately and the stopper was inserted carefully into the flask. The sample flask was then shaken vigorously to mix the contents and to disperse the precipitate

throughout. After the precipitate had settled at least halfway down the flask, the flask was again shaken vigorously to disperse the precipitate. The sample flasks containing pickled samples were then stored in a laboratory until required for titration.

d. Sample measurement

The pickled samples were measured onboard the R/V Mirai following a period of at least 2 h after the re-shaking. Sulfuric acid solution (vol.: 1 cm^3) and a magnetic stirrer bar were placed into the sample flask and the sample was stirred. The samples were titrated using sodium thiosulfate solution whose morality was determined by potassium iodate solution. The temperature of the sodium thiosulfate during titration was recorded using a digital thermometer. Dissolved oxygen concentration (µmol kg^{-1}) was calculated based on the sample temperature during seawater sampling, salinity of the sensor on the CTD system, flask volume and titrated volume of sodium thiosulfate solution without the blank. During this cruise, two sets of titration apparatus were used.

e. Standardization and determination of the blank

The concentration of the sodium thiosulfate titrant was determined using potassium iodate solution. Pure potassium iodate was dried in an oven at 130 ℃, and a 1.7835 g sample was dissolved in deionized water in a flask and diluted to a final weight of 5 kg. After 10 cm^3 of the standard potassium iodate solution was added to another flask using a volume-calibrated dispenser, 90 cm^3 of deionized water, 1 cm^3 of sulfuric acid solution and 1 cm^3 of pickling reagent solution II and I were added in order. The amount of titrated volume of sodium thiosulfate for this diluted standard potassium iodate solution (usually the average of five measurements) gave the morality of the sodium thiosulfate titrant.

The oxygen in pickling reagents I (1 cm^3) and II (1 cm^3) was assumed to be 7.6×10^{-8} mol (Murray et al., 1968). The blank due to other than oxygen was determined as follows. First, 1 and 2 cm^3 of the standard potassium iodate solution were added to each flask using a calibrated dispenser. Then, 100 cm^3 of deionized water, 1 cm^3 of sulfuric acid solution, 1 cm^3 of pickling reagent solution II and the same volume of pickling reagent solution I were added into the flask in order. The blank was determined based on the difference between the first (1 cm^3 of potassium iodate) and second (2 cm^3 of potassium iodate) titrated volume of the sodium thiosulfate. The titrations were conducted three times and their average was used as the blank value.

(5) Observation log

a. Standardization and determination of the blank

Table 4.1-1 shows the results of the standardization and the blank determination during this cruise.

Table 4.1-1: Results of the standardization and the blank determinations during the cruise

Date (yyyy/mm/dd)	Potassium iodate ID	Sodium thiosulfate ID	DOT-01X (No.9)		DOT-01X (No.10)		Instrumental Error (%)	Stations
			E.P. (cm³)	Blank (cm³)	E.P. (cm³)	Blank (cm³)		
2019/10/2	K19C04	T-19G	3.954	0.001	3.964	0.001	-0.21	Stn.000 Cast001, Stn.000 Cast002
2019/10/5	K19C06	T-19G	3.955	-0.002	3.965	0.001	-0.18	Stn.001 Cast001, Stn.004 Cast001, Stn.006 Cast001, Stn.008 Cast001, Stn.009 Cast001
			3.959	0.000	3.966	0.002	-0.12	Stn.002 Cast001, Stn.003 Cast001, Stn.005 Cast001, Stn.007 Cast001 Stn.008 Cast001, Stn.009 Cast001
2019/10/10	K19C05	T-19I	3.955	0.002	3.965	0.006	-0.16	Stn.010 Cast001, Stn.011 Cast001, Stn.012 Cast001, Stn.013 Cast001, Stn.014 Cast001, Stn.015 Cast001,

								Stn.016 Cast001
2019/10/14	K19C08	T-19I	3.956	0.000	3.965	0.004	-0.14	Stn.017 Cast001, Stn.018 Cast001, Stn.019 Cast001, Stn.020 Cast001
2019/10/16	K19C10	T-19K	3.965	-0.001	3.967	0.003	0.07	Stn.019 Cast002, Stn.020 Cast002- 004, Stn.021 Cast001-003, Stn.022 Cast001-002, Stn.023 Cast001
2019/10/20	K19D01	T-19K	3.963	-0.003	3.966	0.001	0.03	Stn.019 Cast003-004, Stn.020 Cast005- 006, Stn.021 Cast004-005, Stn.024 Cast001

2019/10/22	K19D02	T-19J	3.965	-0.004	3.966	0.000	0.08	Stn.019 Cast005-007, Stn.020 Cast007- 009, Stn.021 Cast007-008, Stn.025 Cast001, Stn.026 Cast001, Stn.027 Cast001, Stn.028 Cast001
2019/10/26	K19D03	T-19J	3.967	-0.001	3.969	0.001	0.02	Stn.029 Cast001, Stn.030 Cast001 Stn.031 Cast001, Stn.032 Cast001, Stn.033 Cast001, Stn.034 Cast001, Stn.035 Cast001, Stn.036 Cast001 Stn.037 Cast001, Stn.038 Cast001, Stn.039 Cast001, Stn.040 Cast001, Stn.041 Cast001,

2019/11/4	K19D05	T-19M	3.972	0.005	3.970	0.006	0.09	Stn.000 Cast003 - 004

b. Repeatability of sample measurement

Replicate samples were taken at every CTD cast. The standard deviation of the replicate measurement (Dickson et al., 2007) was 0.13 µmol kg^{-1} (n = 174). Results of the replicate sample measurements based on preliminary data are shown in Table 4.1-2 and illustrated in Figure 4.1. The standard deviation (s) is given by the following expression:

$$s = \sqrt{\frac{\sum_{i=1} d_i^2}{2k}}$$

where d and k represent the difference of the replicate measurements and the number of replicate samples, respectively.

Table 4.1-2: Results of the replicate sample measurements

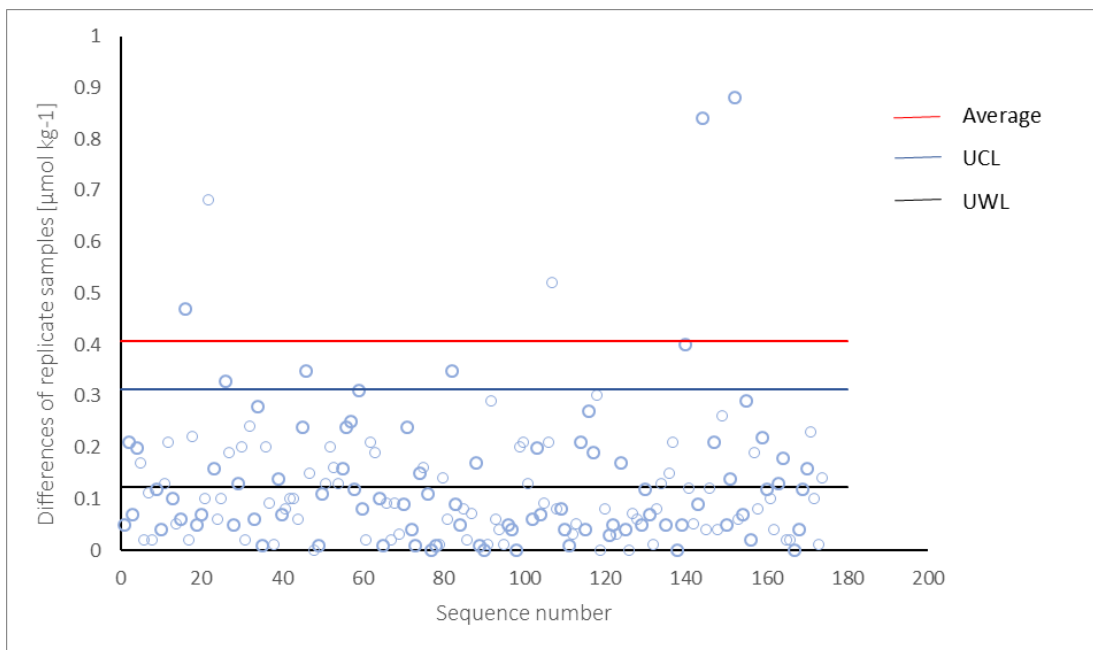| Layer	Number of replicate sample pairs	Oxygen concentration (µmol kg^{-1}) Standard Deviation
200m>	86	0.14
>=200m	88	0.11
All	174	0.13

Figure 4.1: Difference of replicate samples against sequence number

127

(6) Data archives

The data obtained during the cruise will be submitted to the Data Management Group of JAMSTEC, and they will be made available to the public via the "Data Research System for Whole Cruise Information in JAMSTEC (DARWIN)" on the JAMSTEC website (http://www.godac.jamstec.go.jp/darwin/e)

(7) References

Culberson, C. H. (1991). *Dissolved Oxygen.* WHPO Publication 91-1.

Dickson, A. G. (1996). Determination of dissolved oxygen in sea water by Winkler titration. In *WOCE Operations Manual*, Part 3.1.3 Operations & Methods, WHP Office Report WHPO 91-1.

Dickson, A. G., Sabine, C. L., & Christian, J. R.(Eds.), (2007). *Guide to best practices for ocean CO_2 measurements, PICES Special Publication 3*: North Pacific Marine Science Organization.

Murray, C. N., Riley, J. P., & Wilson, T. R. S. (1968). The solubility of oxygen in Winklerreagents used for the determination of dissolved oxygen. *Deep Sea Res.*, 15, 237-238.

4.2. Nutrients

(1) Personnel

Michio AOYAMA	JAMSTEC/Tsukuba Univ.	-PI
Akihiko MURATA	JAMSTEC	
Mikio KITADA	MWJ	- Operation Leader
Shinichiro YOKOGAWA	MWJ	
Keitaro MATSUMOTO	MWJ	
Tomomi SONE	MWJ	

(2) Objectives

The objective of the nutrient analyses during the R/V Mirai MR19-03C cruise in the Arctic Ocean (EXPOCODE: 49NZ20190927) was to describe the present status of nutrient concentrations with excellent comparability using certified reference material of nutrients in seawater.

(3) Parameters

The determinants are nitrate, nitrite, silicate, phosphate and ammonia in the Arctic Ocean.

(4) Instruments and methods

(4.1) Analytical detail using QuAAtro 2-HR systems (BL TEC K.K.)

We analyzed nitrate + nitrite and nitrite following a modification of the method of Grasshoff (1976). The sample nitrate was reduced to nitrite in a cadmium tube, the inside of which was coated with metallic copper. The sample stream after reduction was treated with an acidic sulfanilamide reagent to produce a diazonium ion. N-1-Naphthylethylenediamine dihydrochloride was added to the sample stream to produce a red azo dye. With reduction of the nitrate to nitrite, both nitrate and nitrite react and can be measured; without reduction, only nitrite reacts. Thus, for the nitrite analysis, no reduction was performed and use of the alkaline buffer was not necessary; nitrate was computed by the difference.

The method used for silicate was analogous to that described for phosphate. The method used was essentially that of Grasshoff et al. (1999). Silicomolybdic acid was first formed from the silicate in the sample and molybdic acid. The silicomolybdic acid was reduced to silicomolybdous acid or molybdenum blue using ascorbic acid.

The method used for the phosphate analysis was a modification of the procedure of Murphy and Riley (1962). Molybdic acid was added to the seawater sample to form phosphomolybdic acid that was in turn reduced to phosphomolybdous acid using L-Ascorbic acid as the reductant.

The ammonia in seawater was mixed with an alkaline containing EDTA, which allowed ammonia in the gas state to form from the seawater. The ammonia (gas) was absorbed in sulfuric acid through a membrane filter (ADVANTEC PTFE; pore size: 0.5 μm) at the dialyzer attached to the analytical system. The ammonia absorbed in sulfuric acid was determined by coupling with phenol and hypochlorite to form indophenols blue. The wavelength used in the ammonia analysis was 630 nm, i.e., the absorbance of indophenols blue.

The details of the modifications of the analytical methods used for the four parameters (nitrate, nitrite, silicate and phosphate) on this cruise are compatible with the methods described in the nutrients section of the new GO-SHIP repeat hydrography nutrients manual (Becker et al., 2019), which is revised version of the previous manual (Hydes et al., 2019). The analytical method used for ammonia is compatible with the approach to determine

ammonia in seawater using a vaporization membrane permeability method (Kimura, 2000). Flow diagrams and the reagents for each parameter are shown in Figures 4.2-1 to 4.2-5.

(4.2) Nitrate + nitrite reagents

50% Triton solution

A volume of 50 mL Triton™ X-100 provided by Sigma-Aldrich Japan G.K. (CAS No. 9002-93-1) was mixed with 50 mL ethanol (99.5%).

Imidazole (buffer), 0.06 M (0.4% w/v)

A sample of 4 g imidazole (CAS No. 288-32-4) was dissolved in 1000 mL ultrapure water, following which 2 mL hydrogen chloride (CAS No. 7647-01-0) was added. After mixing, 1 mL 50% Triton solution was added.

Sulfanilamide, 0.06 M (1% w/v) in 1.2 M HCl

A sample of 10 g 4-Aminobenzenesulfonamide (CAS No. 63-74-1) was dissolved in 900 mL of ultrapure water, following which 100 mL hydrogen chloride (CAS No. 7647-01-0) was added. After mixing, 2 mL 50% Triton solution was added.

NED, 0.004 M (0.1% w/v)

A sample of 1 g N-(1-Naphthalenyl)-1,2-ethanediamine dihydrochloride (CAS No. 1465-25-4) was dissolved in 1000 mL of ultrapure water and 10 mL hydrogen chloride (CAS No. 7647-01-0) was added. After mixing, 1 mL 50% Triton solution was added. This reagent was stored in a dark bottle.

Figure 4.2-1: NO$_3$ + NO$_2$ (1ch.) flow diagram.

(4.3) Nitrite reagents

50% Triton solution

A volume of 50 mL Triton™ X-100 provided by Sigma-Aldrich Japan G.K. (CAS No. 9002-93-1) was mixed with 50 mL ethanol (99.5%).

Sulfanilamide, 0.06 M (1% w/v) in 1.2 M HCl

A sample of 10 g 4-Aminobenzenesulfonamide (CAS No. 63-74-1) was dissolved in 900 mL of ultrapure water, following which 100 mL hydrogen chloride (CAS No. 7647-01-0) was added. After mixing, 2 mL 50% Triton solution was added.

NED, 0.004 M (0.1% w/v)

A sample of 1 g N-(1-Naphthalenyl)-1,2-ethanediamine dihydrochloride (CAS No. 1465-25-4) was dissolved in 1000 mL of ultrapure water and 10 mL hydrogen chloride (CAS No. 7647-01-0) was added. After mixing, 1 mL 50% Triton solution was added. This reagent was stored in a dark bottle.
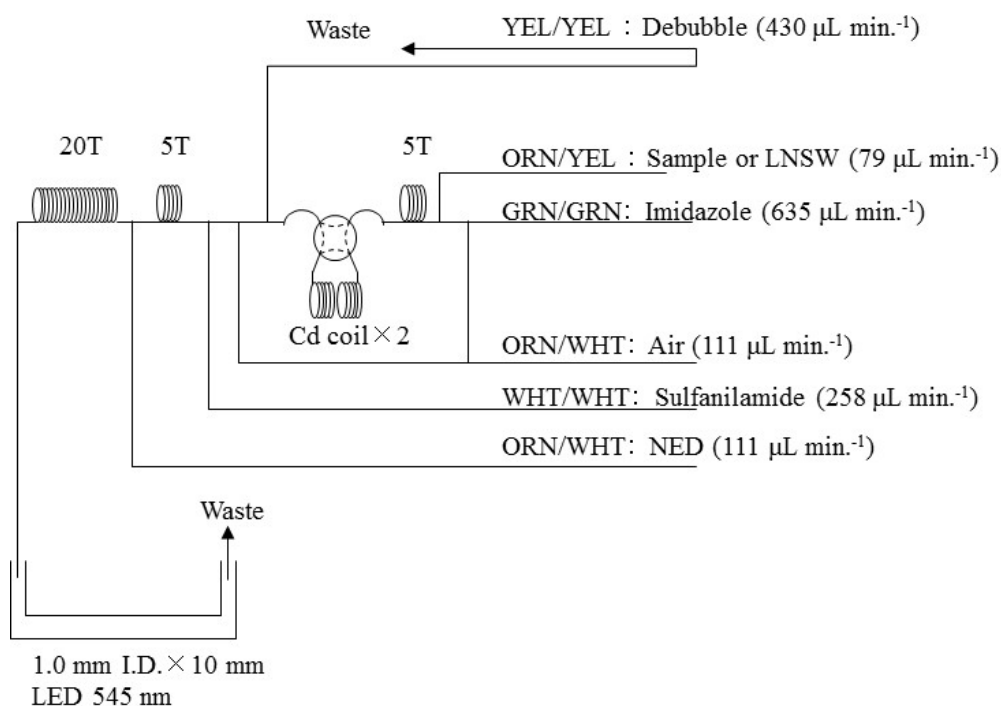

Figure 4.2-2: NO_2 (2ch.) flow diagram.

(4.4) Silicate reagents

15% Sodium dodecyl sulfate solution

A sample of 75 g sodium dodecyl sulfate (CAS No. 151-21-3) was mixed with 425 mL of ultrapure water.

Molybdic acid, 0.03 M (1% w/v)

A sample of 7.5 g sodium molybdate dihydrate (CAS No. 10102-40-6) was dissolved in 980 mL of ultrapure water, following which 12 mL 4.5M sulfuric acid was added. After mixing, 20 mL 15% sodium dodecyl sulfate solution

was added. Note: the amount of sulfuric acid used was reduced from that mentioned in a previous report because we readjusted the method to Grasshoff et al. (1999).

Oxalic acid, 0.6 M (5% w/v)

A sample of 50 g oxalic acid (CAS No. 144-62-7) was dissolved in 950 mL of ultrapure water.

Ascorbic acid, 0.01 M (3% w/v)

A sample of 2.5 g L-Ascorbic acid (CAS No. 50-81-7) was dissolved in 100 mL of ultrapure water. This reagent was prepared fresh every day.
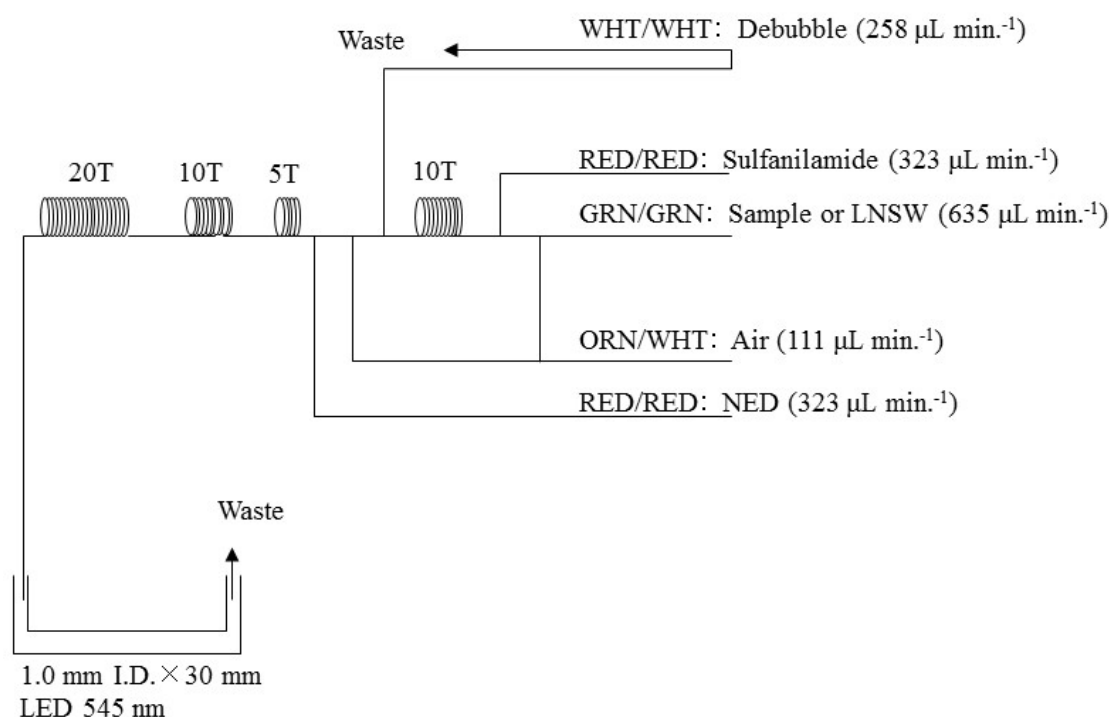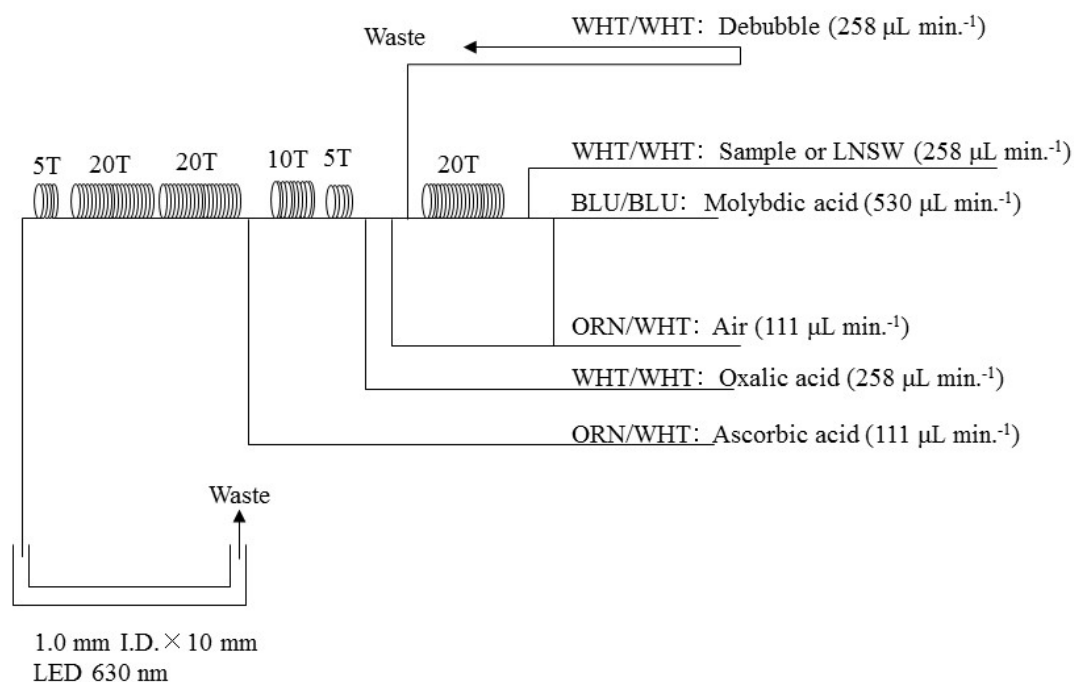

Figure 4.2-3: SiO_2 (3ch.) flow diagram.

(4.5) Phosphate reagents

15% sodium dodecyl sulfate solution

A sample of 75 g sodium dodecyl sulfate (CAS No. 151-21-3) was mixed with 425 mL of ultrapure water.

Stock molybdate solution, 0.03 M (0.8% w/v)

Samples of 8 g sodium molybdate dihydrate (CAS No. 10102-40-6) and 0.17 g antimony potassium tartrate trihydrate (CAS No. 28300-74-5) were dissolved in 950 mL of ultrapure water, following which 50 mL sulfuric acid (CAS No. 7664-93-9) was added.

PO_4 color reagent

A sample of 1.2 g L-Ascorbic acid (CAS No. 50-81-7) was dissolved in 150 mL of stock molybdate solution. After mixing, 3 mL 15% sodium dodecyl sulfate solution was added. This reagent was prepared fresh before every measurement.
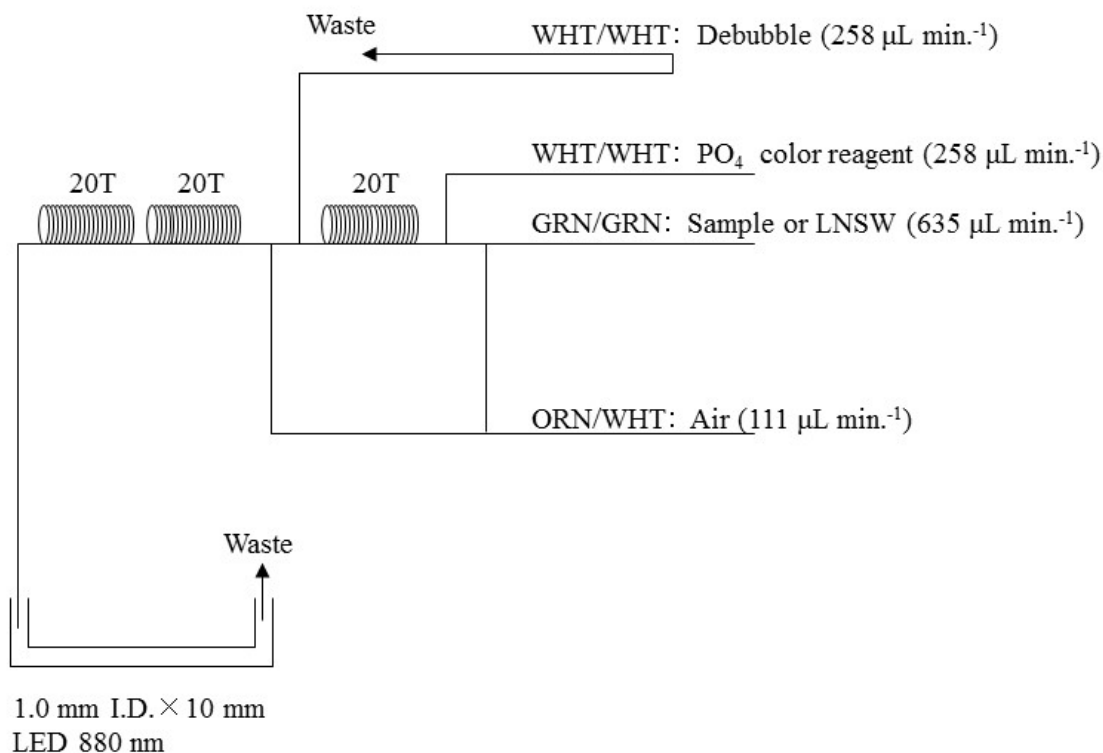
Figure 4.2-4: PO_4 (4ch.) flow diagram.

(4.6) Ammonia Reagents

30% Triton solution

A volume of 30 mL Triton™ X-100 provided by Sigma-Aldrich Japan G.K. (CAS No. 9002-93-1) was mixed with 70 mL of ultrapure water.

EDTA

Samples of 41 g tetrasodium;2-[2-[bis(carboxylatomethyl)amino]ethyl-(carboxylateme-thyl)amino]acetate;tetrahydrate (CAS No. 13235-36-4) and 2 g boric acid (CAS No. 10043-35-3) were dissolved in 200 mL of ultrapure water. After mixing, 1 mL 30% Triton solution was added. This reagent was prepared approximately one week in advance of use.

NaOH liquid

Samples of 1.5 g sodium hydroxide (CAS No. 1310-73-2) and 16 g tetrasodium;2-[2-[bis(carboxylatomethyl)amino]ethyl-(carboxylatomethyl)amino]acetate;tetrahydrate (CAS No. 13235-36-4) were dissolved in 100 mL of ultrapure water. This reagent was prepared approximately one week in advance of use. Note: we reduced the amount of sodium hydroxide from 5 to 1.5 g because the pH of C standard solutions was lowered to 1 because of a change in the recipe of B standard solutions.

Stock nitroprusside

A sample of 0.25 g sodium nitroferricyanide dihydrate (CAS No. 13755-38-9) was dissolved in 100 mL of ultrapure water and 0.2 mL 1M sulfuric acid was added. This reagent was stored in a dark bottle and prepared approximately one month in advance of use.

Nitroprusside solution

Samples of 4 mL stock nitroprusside and 5 mL 1M sulfuric acid were mixed in 500 mL of ultrapure water. After mixing, 2 mL 30% Triton solution was added. This reagent was stored in a dark bottle and prepared every two or three days.

Alkaline phenol

Samples of 10 g phenol (CAS No. 108-95-2), 5 g sodium hydroxide (CAS No. 1310-73-2) and 2 g sodium citrate dihydrate (CAS No. 6132-04-3) were dissolved in 200 mL ultrapure water. This reagent was stored in a dark bottle and prepared approximately one week in advance of use.

NaClO solution

A sample of 5 mL sodium hypochlorite (CAS No. 7681-52-9) was mixed in 45 mL of ultrapure water. This reagent was stored in a dark bottle and prepared fresh before every measurement. This reagent is prepared with 0.3% available chlorine.

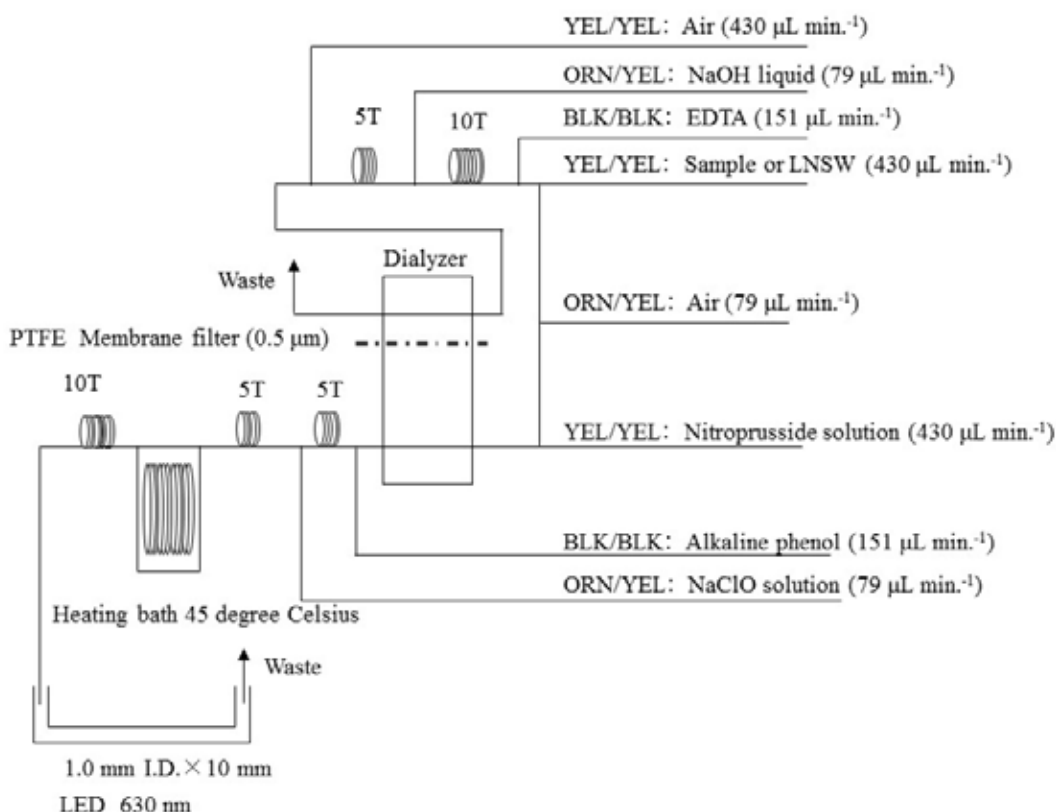Figure 4.2-5: NH_4 (5ch.) flow diagram.

(4.7) Sampling procedures

Sampling of nutrients followed that of oxygen, salinity and trace gases. Samples were drawn into virgin 10 mL polyacrylate vials without sample drawing tubes. These were rinsed three times before filling and the vials were capped immediately after the drawing. The vials were placed into a water bath adjusted to ambient temperature

(21.1 ± 1.0 °C) and the samples allowed to stabilize for approximately 30 min. When we found the value of Xmiss of the sample was <95%, or doubtful for the particles in the sample, we centrifuged the samples using a CN-820 (Hsiang Tai) centrifuge for 2.5 min at approximately 3400 rpm. We also put coolant in the centrifuge to suppress the temperature increase of the samples during centrifugation.

No transfer was made and the vials were set directly in an auto sampler tray. Samples were analyzed within 24 h after collection.

(4.8) Data processing

Raw data from QuAAtro 2-HR were treated as follows:

- Check baseline shift.
- Check the shape of each peak and the positions of the peak values taken, and then change the positions of the peak values taken if necessary.
- Apply carry-over correction and baseline drift correction to peak heights of each samples followed by sensitivity correction.
- Perform baseline correction and sensitivity correction using linear regression.
- Load pressure and salinity information from uncalibrated CTD data to provide tentative calculation of the density of seawater. To calculate the final nutrient concentrations we used salinity obtained from bottle samples for 62 samples and salinity derived from uncalibrated CTD data for 896 samples.
- Derive calibration curves to obtain nutrient concentrations assuming second-order equations.

(4.9) Summary of nutrients analysis

During MR19-03C, we performed 34 QuAAtro runs for the water column samples collected by 62 casts at 41 stations, as shown in Table 4.2-1. The total amount of layers of the seawater sample reached 958. We also measured five samples from a test cast conducted before commencing the observation program. We performed duplicate measurements. The station locations of the nutrient measurements are shown in Figure 4.2-6.
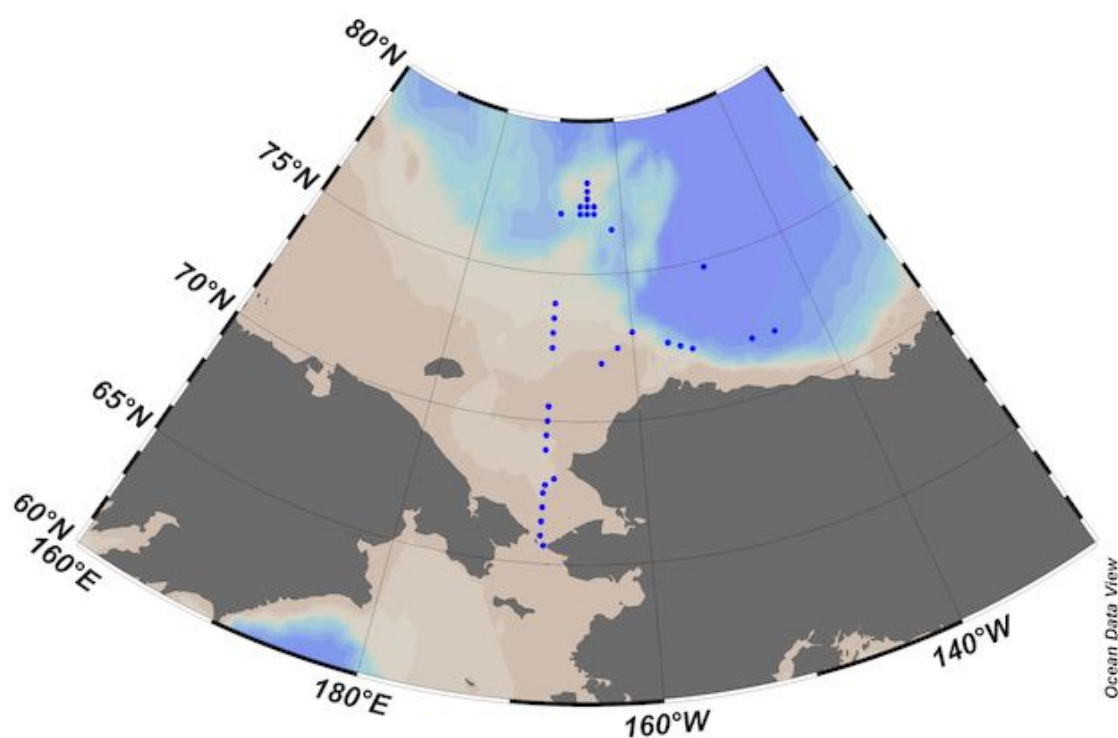
Figure 4.2-6: Positions of nutrient sampling.

(5) Station list

The list of sampling stations for nutrients is shown in Table 4.2-1.

Table 4.2-1: List of sampling stations

Station	Cast	Date (UTC) (mmddyy)	Position* Latitude	Longitude	Depth (m)
001	1	100819	65-39.18N	169-32.23W	53
002	1	100819	66-00.17N	169-15.28W	53
003	1	100819	66-30.32N	169-14.90W	54
004	1	100819	67-00.13N	169-15.74W	45
005	1	100919	69-00.19N	169-14.82W	53
006	1	100919	69-30.16N	169-14.79W	51
007	1	100919	69-59.96N	169-14.97W	41
008	1	100919	70-29.86N	169-14.62W	39
009	1	101019	71-59.77N	164-30.01W	38
010	1	101019	72-29.84N	162-15.22W	44
011	1	101019	72-59.99N	161-59.80W	192
012	1	101119	72-30.13N	157-43.31W	1607
013	1	101119	72-19.98N	156-59.48W	1957
014	1	101119	72-09.43N	154-12.59W	1637
015	1	101219	71-59.99N	148-30.02W	3515
016	1	101219	72-00.01N	146-59.95W	3316
017	1	101419	74-46.10N	151-29.87W	3834
018	1	101519	76-27.95N	162-21.49W	1750
019	1	101619	76-59.96N	165-00.06W	680
020	1	101619	77-15.04N	165-00.29W	367
020	2	101719	77-14.99N	165-00.07W	370
021	1	101719	77-30.01N	166-59.99W	308
022	1	101719	77-45.00N	166-59.99W	445
020	3	101819	77-15.01N	165-00.01W	372
021	2	101819	77-30.07N	166-59.81W	310
022	2	101819	77-45.05N	166-59.81W	446
023	1	101819	78-02.13N	165-01.52W	453
019	2	101919	77-00.01N	165-00.04W	685
020	4	101919	77-15.14N	165-00.11W	366
021	3	101919	77-30.06N	165-00.07W	309
019	3	102019	77-00.06N	165-00.06W	690

020	5	102019	77-15.14N	165-00.35W	367
021	4	102019	77-30.05N	165-00.01W	310
024	1	102119	77-15.00N	166-00.04W	851
019	4	102119	77-00.28N	165-00.25W	687
020	6	102119	77-15.01N	166-59.95W	370
021	5	102119	77-30.50N	165-00.34W	308
025	1	102219	77-00.37N	166-00.12W	711
019	5	102219	77-00.10N	165-00.43W	685
020	7	102219	77-15.01N	166-59.94W	371
026	1	102319	77-00.01N	165-59.99W	437
019	6	102319	77-00.07N	165-00.68W	678
020	8	102319	77-15.17N	165-00.07W	365
021	7	102319	77-30.31N	165-01.21W	304
027	1	102419	77-15.00N	165-59.99W	366
019	7	102419	77-00.23N	166-59.84W	697
020	9	102419	77-15.04N	166-59.86W	366
021	8	102419	77-30.74N	166-59.79W	311
028	1	102519	77-00.22N	169-13.87W	1896
029	1	102619	74-00.01N	169-15.17W	185
030	1	102619	73-30.00N	169-15.00W	115
031	1	102619	73-00.03N	169-14.96W	61
032	1	102619	72-30.03N	169-15.39W	59
033	1	102719	70-30.01N	169-15.08W	38
034	1	102719	70-00.01N	169-14.96W	41
035	1	102719	69-30.19N	169-14.77W	51
036	1	102719	68-59.99N	169-14.71W	53
037	1	102819	68-00.88N	168-07.96W	53
038	1	102819	67-46.99N	169-23.71W	51
039	1	102819	67-30.07N	169-14.89W	49
040	1	102819	67-00.06N	169-15.29W	45
041	1	102819	66-29.99N	169-14.98W	54

*: Position indicates latitude and longitude at which the CTD cast reached its maximum depth

(6) Certified reference material of nutrients in seawater

KANSO certified reference materials (CRMs; Lots: CE, CJ and CG) were used to ensure the comparability and traceability of the nutrient measurements during this cruise. The details of the CRMs are described below.

Production

The CRMs used for inorganic nutrients in seawater were produced by KANSO Co., Ltd. These CRMs were

produced using autoclaved natural seawater following the quality control system of ISO Guide 34 (JIS Q 0034). KANSO Co., Ltd. has been accredited under the Accreditation System of the National Institute of Technology and Evaluation (ASNITE) as a CRM producer since 2011 (Accreditation No.: ASNITE 0052 R).

Property value assignment

The certified values are arithmetic means of the results of 30 bottles from each batch (measured in duplicates) analyzed by KANSO Co., Ltd. and the Japan Agency for Marine-Earth Science and Technology (JAMSTEC) using the colorimetric method (continuous flow analysis method). The salinity of the calibration solutions was adjusted to the salinity of this CRM (± 0.5).

Metrological Traceability

Each certified value of nitrate, nitrite and phosphate of the KANSO CRMs was calibrated versus one of the Japan Calibration Service System (JCSS) standard solutions for nitrate ions, nitrite ions and phosphate ions. JCSS standard solutions are calibrated versus JCSS secondary solutions for each of these ions. The JCSS secondary solutions are calibrated versus the specified primary solutions produced by the Chemicals Evaluation and Research Institute (CERI), Japan. CERI specified primary solutions are calibrated versus the National Metrology Institute of Japan (NMIJ) primary standard solutions of nitrate ions, nitrite ions and phosphate ions.

The certified value of silicate of the KANSO CRM was determined based on the Merck KGaA silicon standard solution 1000 mg L^{-1} Si traceable to the National Institute of Standards and Technology (NIST) SRM of silicon standard solution (SRM 3150).

The certified values of nitrate, nitrite and phosphate of the KASNO CRMs are thus traceable to the International System of Units (SI) through the unbroken chain of calibrations of JCSS, CERI and NMIJ solutions, each having stated uncertainties. The certified value of silicate of the KANSO CRM is traceable to the International System of Units (SI) through the unbroken chain of calibrations of Merck KGaA and NIST SRM 3150 solutions, each having stated uncertainties.

As stated in the certificate of the NMIJ CRMs, each certified value of dissolved silica, nitrate ions and nitrite ions was determined by more than one method using one of the NIST SRM of silicon standard solutions and NMIJ primary standard solutions of nitrate ions and nitrite ions. The concentration of phosphate ions, as a stated value in the certificate, was determined using the NMIJ primary standard solution of phosphate ions. The values in the certificates of the NMIJ CRMs are traceable to the International System of Units (SI).

One of the analytical methods used for certification of the NMIJ CRMs for nitrate ions, nitrite ions, phosphate ions and dissolved silica was the colorimetric method (continuous mode and batch mode). The colorimetric method is the same as the analytical method (continuous mode only) used for certification of the KANSO CRMs. For certification of dissolved silica, exclusion chromatography/isotope dilution–inductively coupled plasma mass spectrometry and ion exclusion chromatography with post-column detection were used. For certification of nitrate ions, ion chromatography by direct analysis and ion chromatography after halogen-ion separation were used. For certification of nitrite ions, ion chromatography by direct analysis was used.

The NMIJ CRMs were analyzed at the time of the certification process for the CRMs and the results were confirmed within the expanded uncertainty stated in the certificate of NMIJ CRMs.

(6.1) CRMs for this cruise

CRM lots CE, CJ and CG, which broadly cover the range of nutrient concentrations in the Arctic Ocean, were prepared in 21 sets.

The CRM assignments were undertaken based on random numbers. The CRM bottles were stored in the biochemical laboratory onboard the ship, in which the temperature was maintained at 17.8–22.6 °C.

(6.2) CRM concentrations

The nutrient concentrations for CRM lots CE, CJ and CG used on the cruise are shown in Table 4.2-2.

Table 4.2-2 Certified concentration and uncertainty (k = 2) of the CRMs.

unit: μmol kg^{-1}

Lot	Nitrate	Nitrite	Silicate	Phosphate	Ammonia*
CE	0.01 ± 0.03	0.02 ± 0.01	0.06 ± 0.09	0.012 ± 0.006	0.69
CJ	16.20 ± 0.20	0.03 ± 0.01	38.50 ± 0.40	1.190 ± 0.020	0.77
CG	23.70 ± 0.20	0.06 ± 0.03	56.40 ± 0.50	1.700 ± 0.020	0.61

*For ammonia values are references

Note for Nitrite concentration: We observed systematic increase of nitrite concentration in the CRMs at a rate about 0.02 μmol kg^{-1} year^{-1}. Therefore, as shown in Figure 4.2-13, the observed concentration of nitrite for CRM lot CG were high compared with certified concentration.

(7) Nutrient standards

(7.1) Volumetric laboratory ware of in-house standards

All volumetric glassware and polymethylpentene (PMP)-ware used were calibrated gravimetrically. Plastic volumetric flasks were calibrated gravimetrically at the temperature of use (±4 K).

(7.1.1) Volumetric flasks

Volumetric flasks of Class quality (Class A) are used because their nominal tolerances are ≤0.05% over the size ranges likely to be used in this work. Class A flasks are made of borosilicate glass, and the standard solutions were transferred to plastic bottles as quickly as possible after they were made up to volume and well mixed to prevent excessive dissolution of silicate from the glass. PMP volumetric flasks were calibrated gravimetrically and used only within ±4 K of the calibration temperature.

The computation of volume contained by glass flasks at various temperatures other than the calibration temperatures was undertaken using the coefficient of linear expansion of borosilicate crown glass.

Owing to the larger temperature coefficients of cubical expansion and the lack of tables constructed for these materials, the plastic volumetric flasks were calibrated gravimetrically over the temperature range of intended use and used at the temperature of calibration within ±4 K. The weights obtained in the calibration were corrected for the density of water and air buoyancy.

(7.1.2) Pipettes

All pipettes had nominal calibration tolerances of 0.1% or better. These were calibrated gravimetrically to

verify and improve upon this nominal tolerance.

(7.2) Reagents; general considerations

(7.2.1) Specifications

For the nitrate standard, we used "potassium nitrate 99.995 suprapur®" provided by Merck, Batch B1452165, CAS No. 7757-79-1.

For the nitrite standard solution, we used the "nitrite ion standard solution (NO_2^- 1000) provided by Wako, Lot APJ6212, Code. No. 140-06451." This standard solution was certified by Wako using the ion chromatograph method. The calibration result was 1003 mg L^{-1} at 20 °C, and the expanded uncertainty of the calibration (k = 2) was 0.8% for the calibration result.

For the silicate standard, we changed from the "silicon standard solution SiO_2 in NaOH 0.5 M CertiPUR®" provided by Merck, to the JAMSTEC-KANSO in-house Si standard solution exp64, which was produced using the alkali fusion technique from 5N SiO_2 powder. The mass fraction of Si in the exp64 solution was calibrated based on the NMIJ CRM 3645-a02 Si standard solution.

For the phosphate standard, we used "potassium dihydrogen phosphate anhydrous 99.995 suprapur®" provided by Merck, Batch B1642608, CAS No.: 7778-77-0.

For the ammonia standard, we used "ammonium chloride" provided by NMIJ, CAS No. 12125-02-9. We used NMIJ CRM 3011-a. The purity of this standard was >99.9%, and the expanded uncertainty of calibration (k = 2) was 0.053%.

(7.2.2) Ultrapure water

Freshly drawn ultrapure water (Milli-Q water) was used for preparation of the reagents, standard solutions and for measurements of the reagent and system blanks.

(7.2.3) Low nutrient seawater (LNSW)

Surface water having low nutrient concentration was taken and filtered using a 0.20-µm pore capsule cartridge filter during the MR18-04 cruise in August 2018. This water was stored in a 20 L Cubitainer® in a cardboard box.

LNSW concentrations were assigned to February 2019.

(7.2.4) Concentrations of nutrients for A, D, B and C standards

Nominal concentrations of nutrients for A, D, B and C standards were set as shown in Table 4.2-3.

We changed from the Merck silicon standard solution to the JAMSTEC-KANSO in-house Si standard solution for the A standard of silicate. We also developed new recipe for the preparation of the B standard without requiring the addition of hydrochloric acid, which was previously added to neutralize alkali in the Merck silicon standard solution. Pure water was used to prepare the B standard, and to adjust the salinity and density, we added sodium chloride powder as appropriate.

The C standard was prepared according to the recipes shown in Table 4.2-4. All volumetric laboratory tools were calibrated prior to the cruise, as stated in paragraph (6.1). The actual concentrations of the nutrients in each fresh standard were calculated based on both the ambient and solution temperatures and the determined factors of the volumetric laboratory ware.

The calibration curves for each run were obtained using four levels: C-1, C-2, C-3 and C-4.

Table 4.2-3: Nominal concentrations of nutrients for A, D, B and C standards

(unit: $\mu mol\ kg^{-1}$)

	A	D	B	C-1	C-2	C-3	C-4
NO_3	22500	900	675	LNSW	13	27	40
NO_2	21800	870	26	LNSW	0.5	1.0	1.6
SiO_2	35600		1430	LNSW	29	58	86
PO_4	6000		60	LNSW	1.2	2.4	3.6
NH_4	4000		160	LNSW	3.2	6.4	9.6

Table 4.2-4: Working calibration standard recipes

C Std.	B Std.
C-2	10 mL
C-3	20 mL
C-4	30 mL

(7.2.5) Renewal of in-house standard solutions

As stated in paragraph (6.2), the in-house standard solutions were renewed according to the timings shown in Table 4.2-5(a)–(c).

Table 4.2-5(a): Timing of renewal of in-house standards

NO_3, NO_2, SiO_2, PO_4, NH_4	Renewal
A-1 Std. (NO_3)	maximum a month
A-2 Std. (NO_2)	commercial prepared solution
A-3 Std. (SiO_2)	JAMSTEC-KANSO in-house Si standard solution
A-4 Std. (PO_4)	maximum a month
A-5 Std. (NH_4)	maximum a month
D-1 Std.	maximum 8 days
D-2 Std.	maximum 8 days
B Std. (mixture of A-1, D-2, A-3, A-4 and A-5 std.)	maximum 8 days

Table 4.2-5(b): Timing of renewal of working calibration standards

Working standards	Renewal
C Std. (dilute B Std.)	every 24 hours

Table 4.2-5(c): Timing of renewal of in-house standards for reduction estimation

Reduction estimation	Renewal
36 μM NO_3 (dilute D-1 Std.)	when C Std. renewed

35 μM NO₂ (dilute D-2 Std.)   when C Std. renewed

_____

(8) Quality control

(8.1) Precision of nutrient analyses during the cruise

The precision of nutrient analyses during this cruise was evaluated based on 6–10 measurements performed on every 7 to 14 samples during a run at the concentration of the C-4 std. A summary of the precision of the analyses is shown in Table 4.2-6 and Figures 4.2-7 to 4.2-11. The precision for each parameter is reasonable considering the analytical precision during the cruises of the R/V Mirai conducted in 2009–2018. During this cruise, the analytical precisions were 0.15% for nitrate, 0.17% for nitrite, 0.12% for silicate, 0.11% for phosphate and 0.26% for ammonia (in terms of the median of precision), respectively. Thus, we can conclude that the analytical precision for nitrate, nitrite, silicate, phosphate and ammonia was maintained throughout this cruise.

Table 4.2-6: Summary of precision based on the replicate analyses

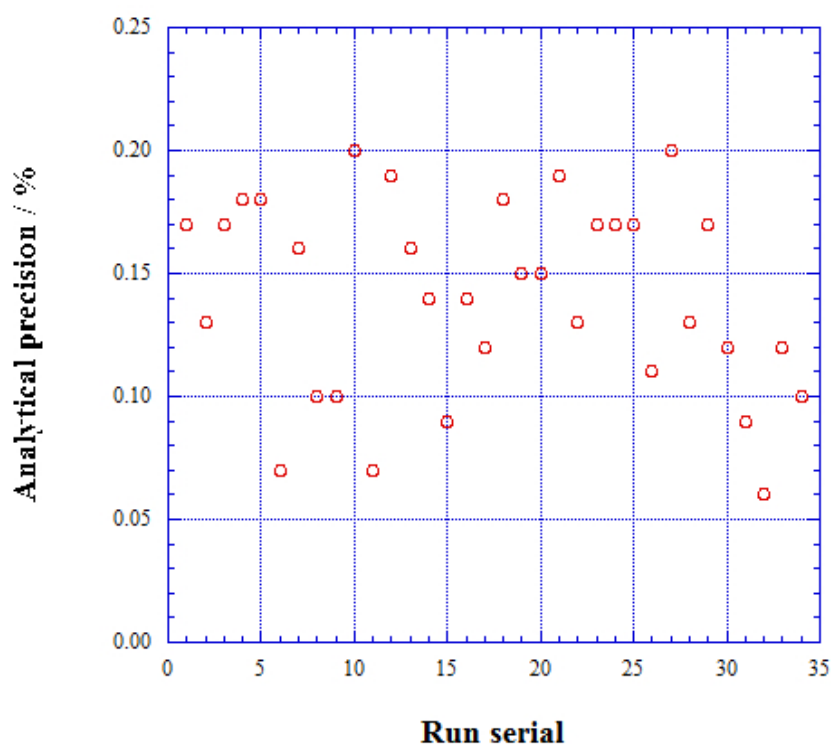|	Nitrate CV %	Nitrite CV %	Silicate CV %	Phosphate CV %	Ammonia CV %
Median	0.15	0.17	0.12	0.11	0.26
Mean	0.14	0.17	0.11	0.11	0.27
Maximum	0.20	0.41	0.18	0.18	0.54
Minimum	0.06	0.05	0.05	0.05	0.07
N	34	34	34	34	34

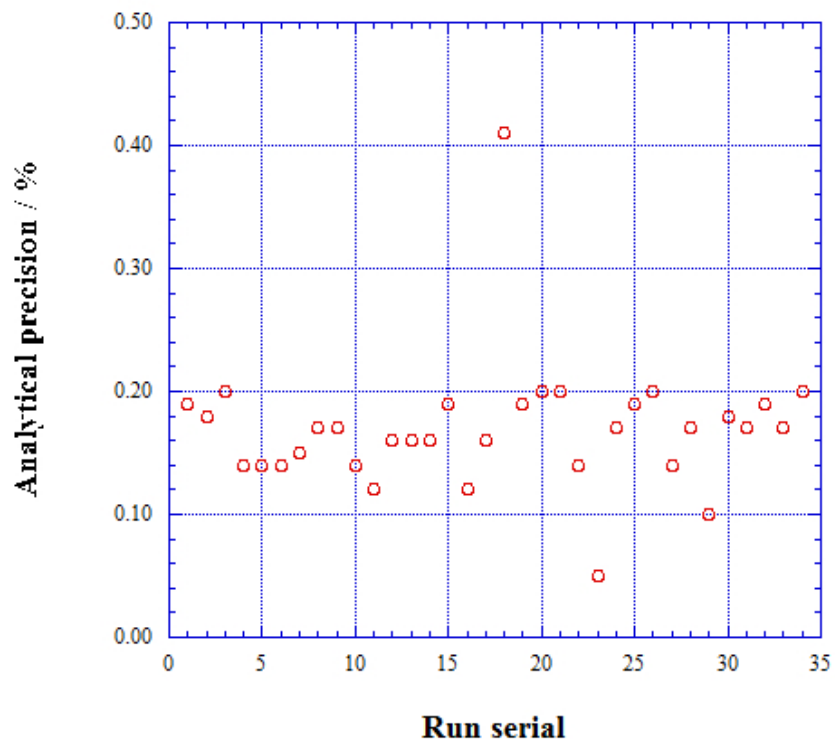Figure 4.2-7: Time series of precision of nitrate during MR19-03C

Figure 4.2-8: Time series of precision of nitrite during MR19-03C.
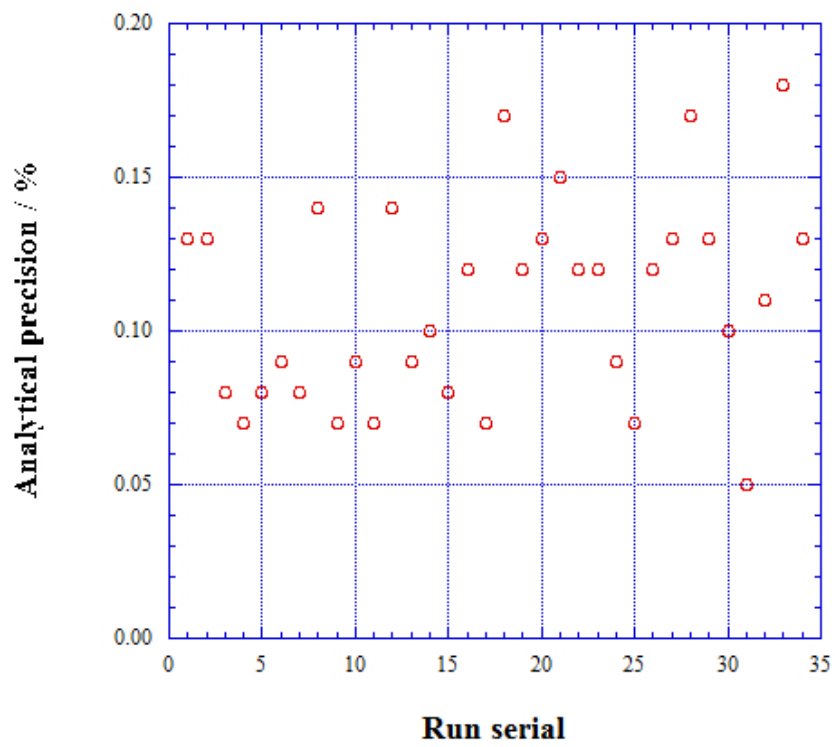

Figure 4.2-9: Time series of precision of silicate during MR19-03C.
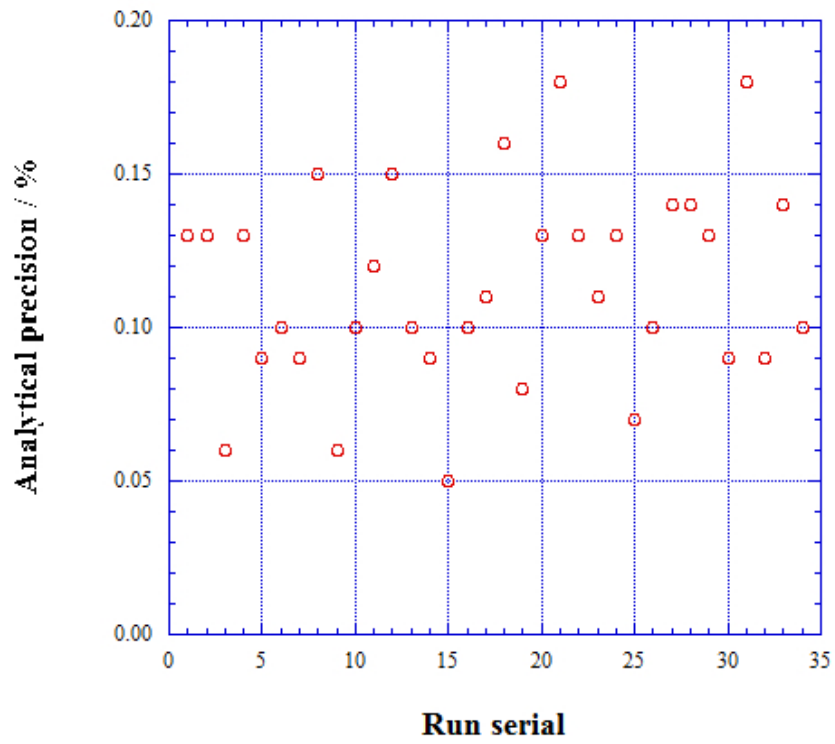
Figure 4.2-10: Time series of precision of phosphate during MR19-03C.
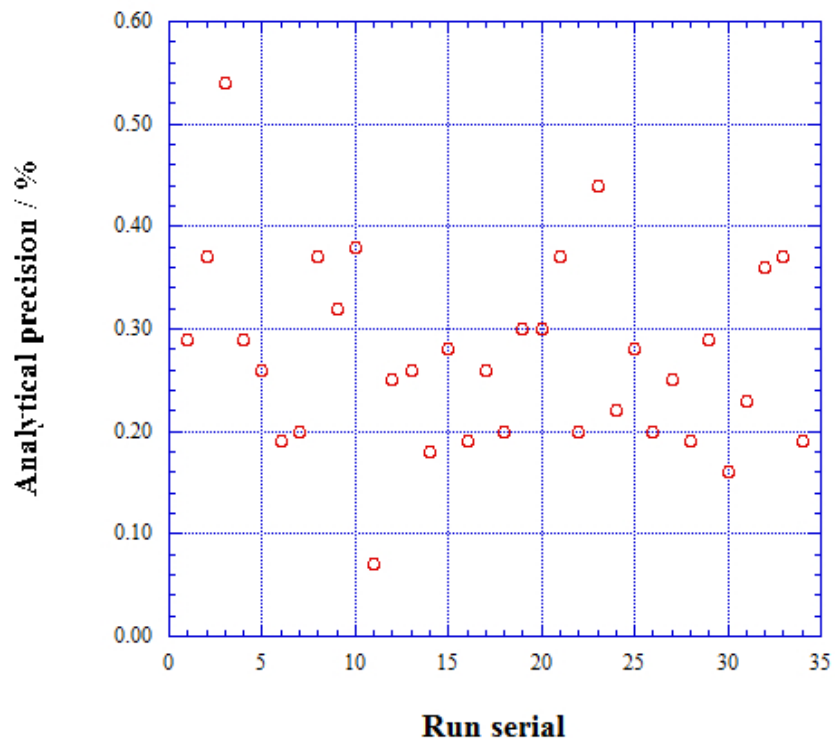
Figure 4.2-11: Time series of precision of ammonia during MR19-03C.

144

(8.2) CRM lot. CG measurement during this cruise

CRM lot. CG was measured every run to ensure comparability. The results of lot CG during this cruise are shown in Figures 4.2-12 to 4.2-16.

Figure 4.2-12: Time series of CRM-CG of nitrate during MR19-03C. Green line is the certified nitrate

concentration of the CRM.

Figure 4.2-13: Time series of CRM-CG of nitrite during MR19-03C. Green line is the certified nitrite concentration
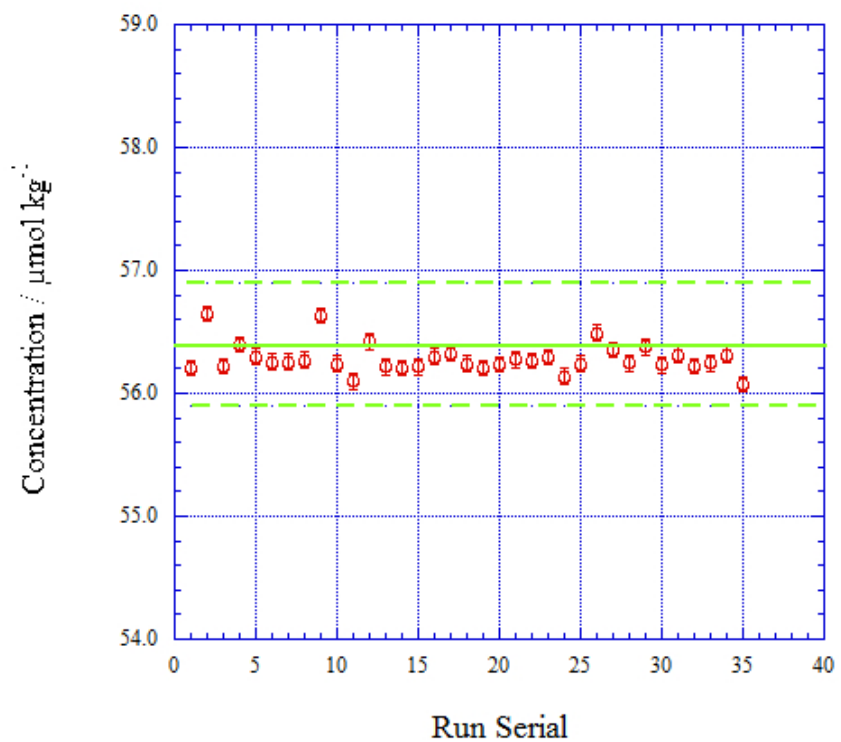
of the CRM.

Figure 4.2-14: Time series of CRM-CG of silicate during MR19-03C. Green line is the certified silicate

concentration of the CRM.

146

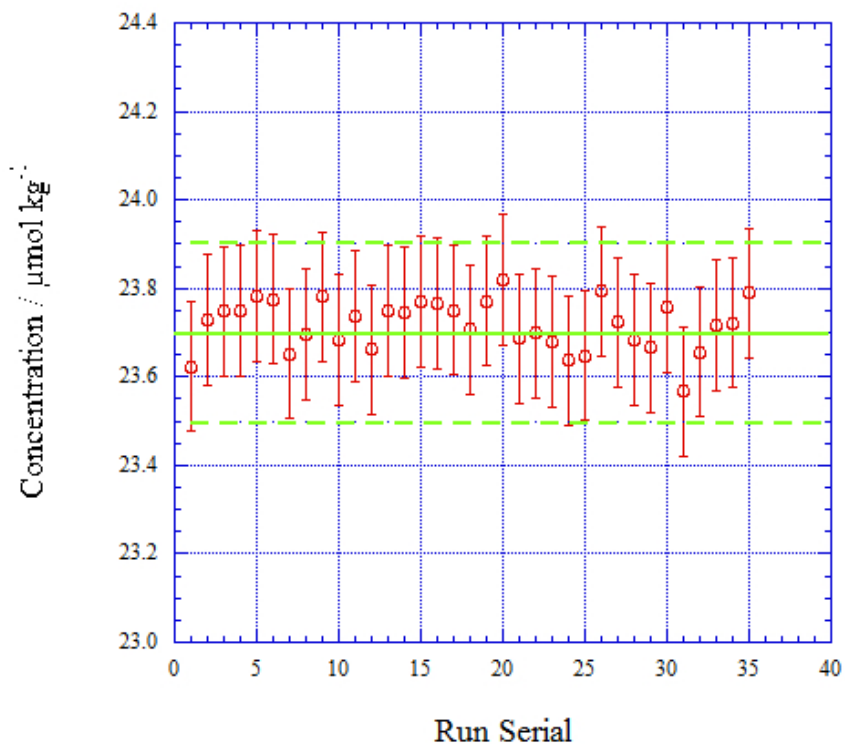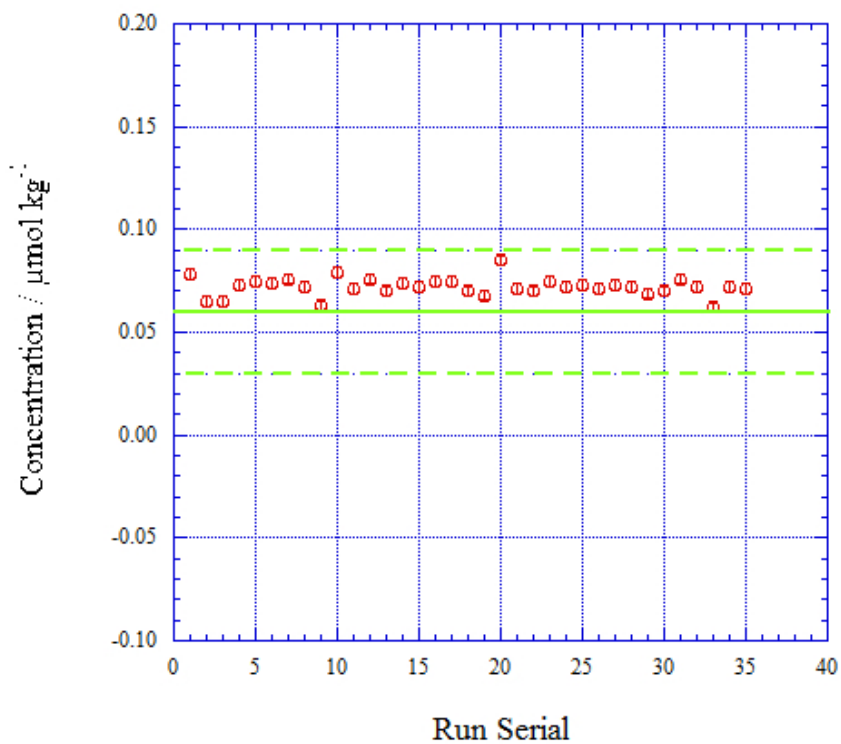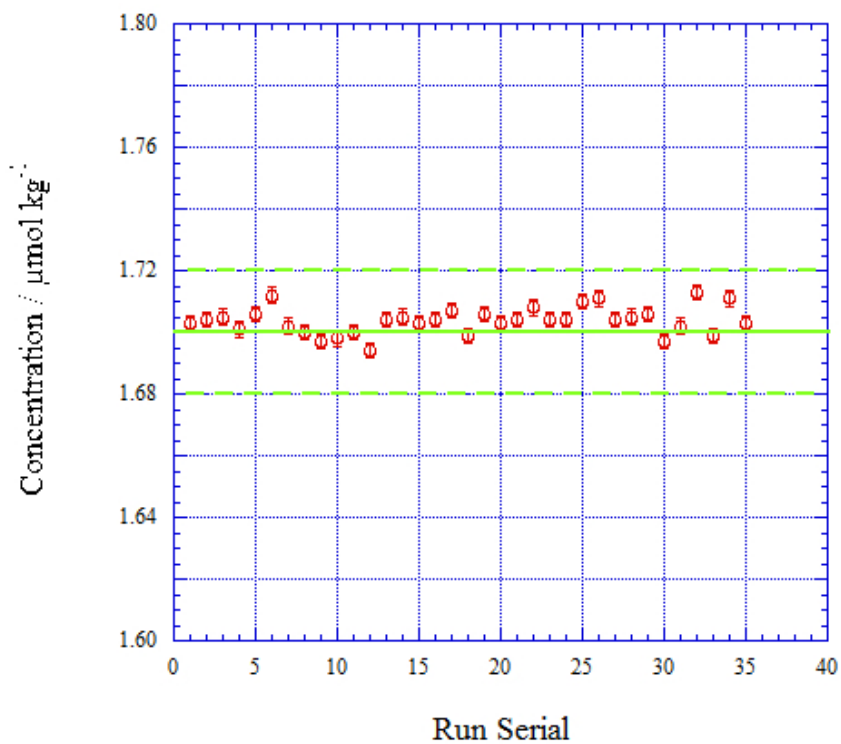Figure 4.2-15: Time series of CRM-CG of phosphate during MR19-03C. Green line is the certified phosphate

concentration of the CRM.
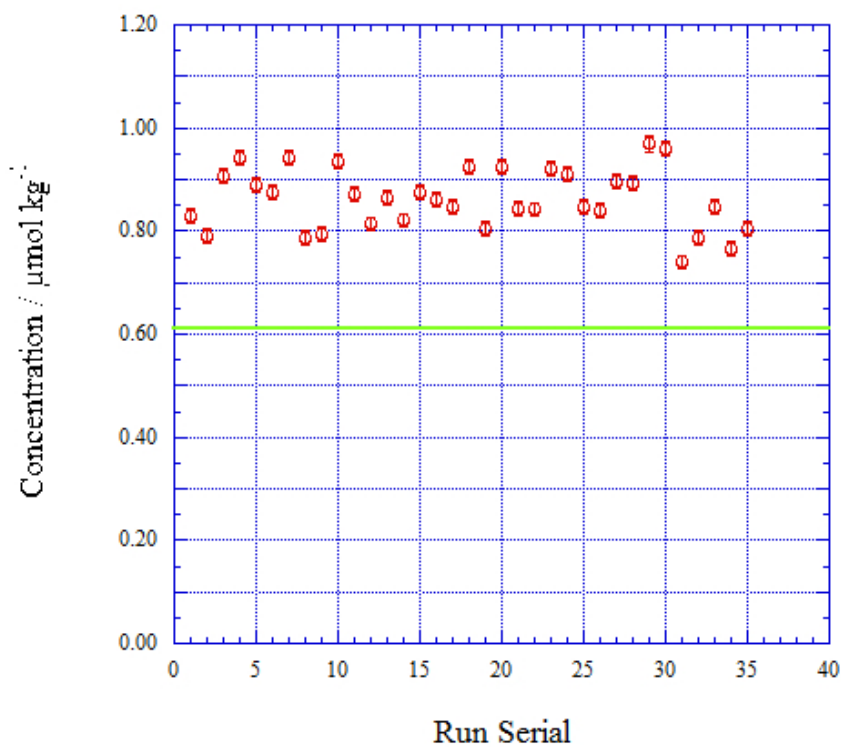
Figure 4.2-16: Time series of CRM-CG of ammonia during MR19-03C. Green line is the reference value of the

ammonia concentration of the CRM.

(8.3) Carry over

We can also summarize the magnitudes of the carry over throughout the cruise. These were sufficiently small and within acceptable levels, as shown in Table 4.2-7 and Figures 4.2-17 to 4.2-21.

Table 4.2-7: Summary of carry over throughout MR19-03C

	Nitrate	Nitrite	Silicate	Phosphate	Ammonia
	%	%	%	%	%
Median	0.18	0.04	0.09	0.10	0.37
Mean	0.18	0.05	0.10	0.10	0.38
Maximum	0.34	0.28	0.19	0.22	0.71
Minimum	0.04	0.00	0.03	0.00	0.21
N	34	34	34	34	34
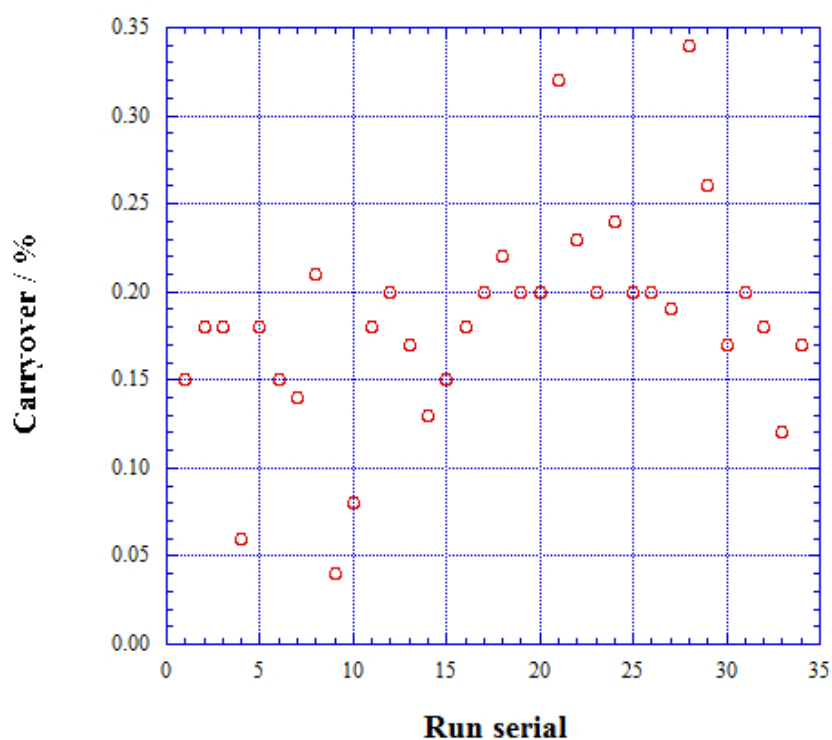
Figure 4.2-17: Time series of carry over of nitrate during MR19-03C.
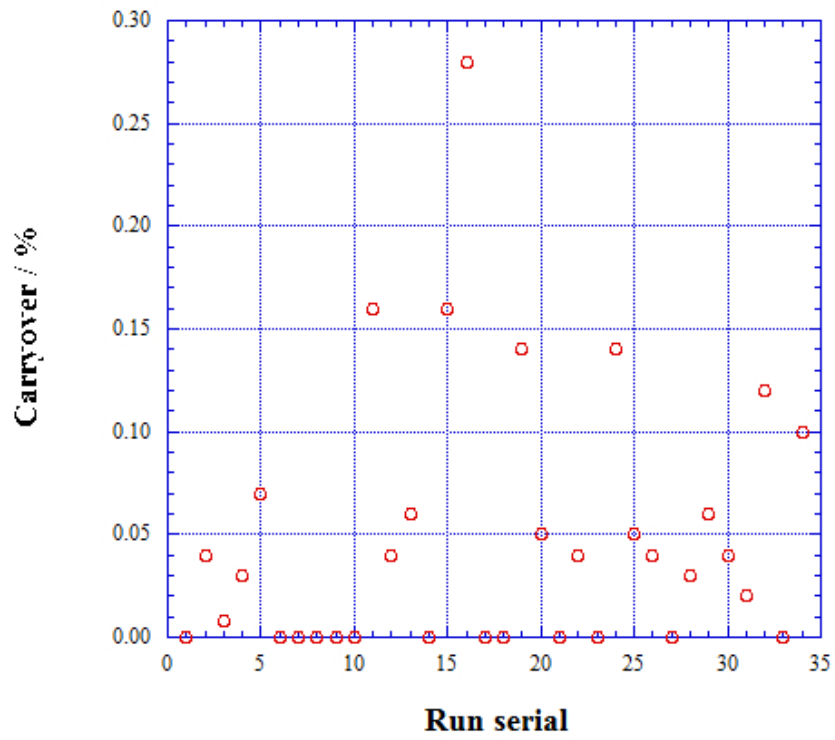
Figure 4.2-18: Time series of carry over of nitrite during MR19-03C.
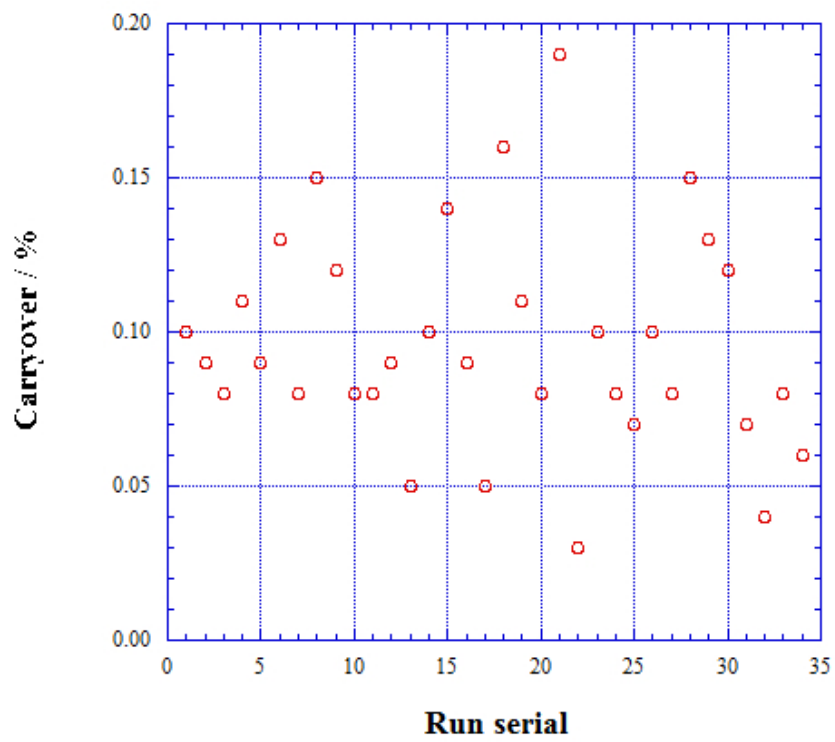
Figure 4.2-19: Time series of carry over of silicate during MR19-03C.

Figure 4.2-20: Time series of carry over of phosphate during MR19-03C.

Figure 4.2-21: Time series of carry over of ammonia during MR19-03C.

(8.4) Estimation of uncertainty of nitrate, silicate, phosphate, nitrite and ammonia concentrations

Empirical equations (Eqs. (1)–(5)) used to estimate the uncertainty of the measurements of nitrate, nitrite, silicate, phosphate and ammonia were based on the differences of 958 pairs of duplicate measurements and drift samples during each run. These empirical equations can be expressed as follows.
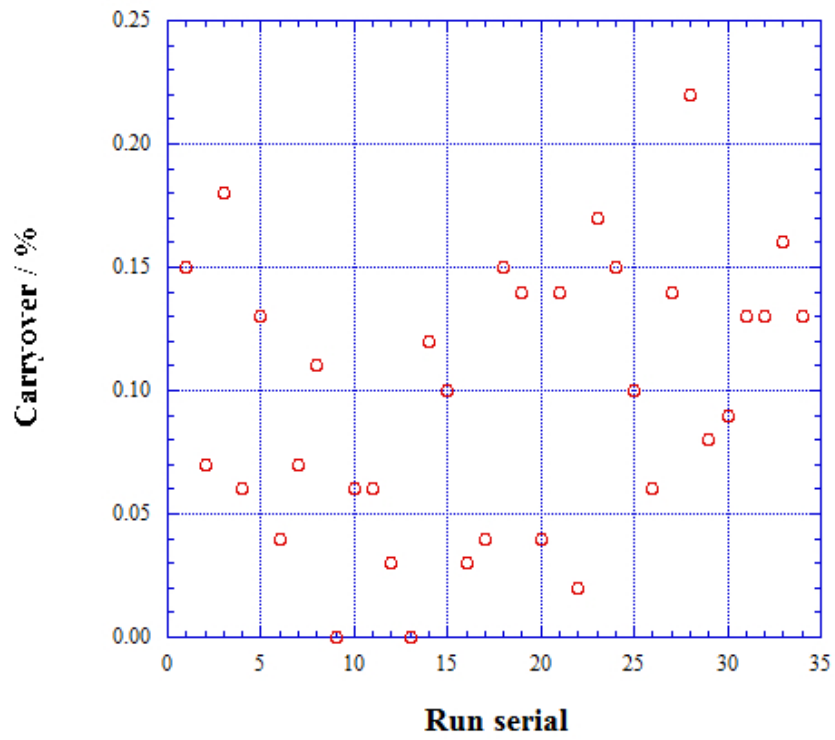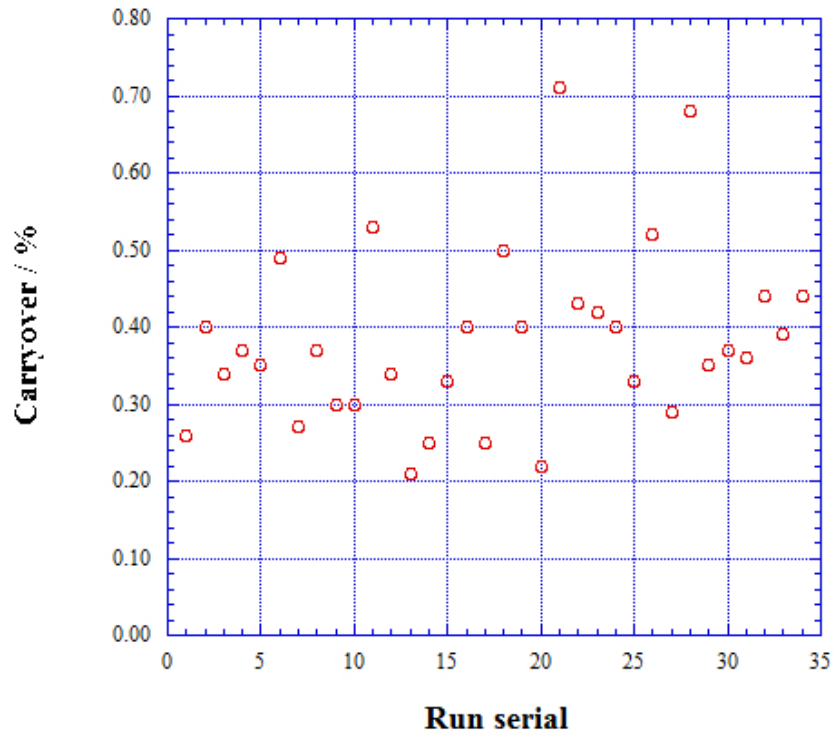
Nitrate concentration C_{NO3} in µmol kg^{-1}:

Uncertainty of measurement of nitrate (%) =

$0.51165 + 2.5869 * (1 / C_{NO3})$ --- (1)

where C_{NO3} is the nitrate concentration of the sample.

Nitrate concentration C_{NO2} in µmol kg^{-1}:

Uncertainty of measurement of nitrite (%) =

$0.51152 + 0.2095 * (1 / C_{NO2}) – 0.000048789 * (1 / C_{NO2}) * (1 / C_{NO2})$ --- (2)

where C_{NO2} is the nitrite concentration of the sample.

Silicate concentration C_{SiO2} in µmol kg^{-1}:

Uncertainty of measurement of silicate (%) =

$0.078148 + 1.9825 * (1/ C_{SiO2})$ --- (3)

where C_{SiO2} is the silicate concentration of the sample.

Phosphate concentration C_{PO4} in µmol kg^{-1}:

Uncertainty of measurement of phosphate (%) =

$0.11934 + -0.017782 * (1/ C_{PO4}) – 0.10545 * (1 / C_{PO4}) * (1 / C_{PO4})$ --- (4)

where C_{PO4} is the phosphate concentration of the sample.

Ammonia concentration C_{NH4} in µmol kg^{-1}:

Uncertainty of measurement of ammonia (%) =

$0.30581 + 1.1441 * (1 / C_{NH4}) – 0.01213 * (1 / C_{NH4}) * (1 / C_{NH4})$ --- (5)

where C_{NH4} is the ammonia concentration of the sample.

(9) Problems / improvements occurred and solutions.

When we changed the LNSW from box#62 to box#12 at RUN#20, we observed systematic decrease of phosphate concentration of CRM lot CE from 0.015 to 0.007 µmol kg^{-1}. We had assumed that the phosphate concentration of the LNSW in these two boxes was the same but it was not. We made direct comparison of the LNSW once, which revealed that the phosphate concentration of the LNSW in box#62 was 0.044 µmol kg^{-1} and that in box#12 was 0.053 µmol kg^{-1}. Therefore, we recalculated the phosphate concentration using the value of 0.053 µmol kg^{-1} as the LNSW concentration from box#12 after run#20. Consequently, the phosphate concentration of CRM lot CE returned to a value of around 0.015 µmol kg^{-1}. The impact of the recalculation on the samples was <0.005 µmol kg^{-1} for phosphate concentration in the range 0.5–1.8 µmol kg^{-1}.

(10) List of reagent

A list of the reagents used during the MR19-03C cruise is shown in Table 4.2-8.

Table 4.2-8: List of reagents used during MR19-03C

IUPAC name	CAS Number	Formula	Compound Name	Manufacture	Grade
4-Aminobenzenesulfonamide	63-74-1	C6H8N2O2S	Sulfanilamide	Wako Pure Chemical Industries, Ltd.	JIS Special Grade
Ammonium sulfate	7783-20-2	(NH4)2SO4	Ammonium Sulfate	National Metrology Institute of Japan	Certified Reference Material
Antimony potassium tartrate trihydrate	28300-74-5	K2(SbC4H2O6)2·3H2O	Bis[(+)-tartrato]diantimonate(III) Dipotassium Trihydrate	Wako Pure Chemical Industries, Ltd.	JIS Special Grade
Boric acid	10043-35-3	H3BO3	Boric Acid	Wako Pure Chemical Industries, Ltd.	JIS Special Grade
Hydrogen chloride	7647-01-0	HCl	Hydrochloric Acid	Wako Pure Chemical Industries, Ltd.	JIS Special Grade
Imidazole	288-32-4	C3H4N2	Imidazole	Wako Pure Chemical Industries, Ltd.	JIS Special Grade
L-Ascorbic acid	50-81-7	C6H8O6	L-Ascorbic Acid	Wako Pure Chemical Industries, Ltd.	JIS Special Grade
N-(1-Naphthalenyl)-1,2-ethanediamine, dihydrochloride	1465-25-4	C12H16Cl2N2	N-1-Naphthylethylenediamine Dihydrochloride	Wako Pure Chemical Industries, Ltd.	for Nitrogen Oxides Analysis
Oxalic acid	144-62-7	C2H2O4	Oxalic Acid	Wako Pure Chemical Industries, Ltd.	Wako Special Grade
Phenol	108-95-2	C6H6O	Phenol	Wako Pure Chemical Industries, Ltd.	JIS Special Grade
Potassium nitrate	7757-79-1	KNO3	Potassium Nitrate	Merck KGaA	Suprapur®
Potassium dihydrogen phosphate	7778-77-0	KH2PO4	Potassium dihydrogen phosphate anhydrous	Merck KGaA	Suprapur®
Sodium citrate dihydrate	6132-04-3	Na3C6H5O7·2H2O	Trisodium Citrate Dihydrate	Wako Pure Chemical Industries, Ltd.	JIS Special Grade
Sodium dodecyl sulfate	151-21-3	C12H25NaO4S	Sodium Dodecyl Sulfate	Wako Pure Chemical Industries, Ltd.	for Biochemistry
Sodium hydroxide	1310-73-2	NaOH	Sodium Hydroxide for Nitrogen Compounds Analysis	Wako Pure Chemical Industries, Ltd.	for Nitrogen Analysis
Sodium hypochlorite	7681-52-9	NaClO	Sodium Hypochlorite Solution	Kanto Chemical co., Inc.	Extra pure
Sodium molybdate dihydrate	10102-40-6	Na2MoO4·2H2O	Disodium Molybdate(VI) Dihydrate	Wako Pure Chemical Industries, Ltd.	JIS Special Grade
Sodium nitroferricyanide dihydrate	13755-38-9	Na2[Fe(CN)5NO]·2H2O	Sodium Pentacyanonitrosylferrate(III) Dihydrate	Wako Pure Chemical Industries, Ltd.	JIS Special Grade
Sulfuric acid	7664-93-9	H2SO4	Sulfuric Acid	Wako Pure Chemical Industries, Ltd.	JIS Special Grade
tetrasodium;2-[2-[bis(carboxylatomethyl)amino]ethyl-(carboxylatomethyl)amino]acetate;tetrahydrate	13235-36-4	C10H12N2Na4O8·4H2O	Ethylenediamine-N,N,N',N'-tetraacetic Acid Tetrasodium Salt Tetrahydrate (4NA)	Dojindo Molecular Technologies, Inc.	-
Synonyms: t-Octylphenoxypolyethoxyethanol 4-(1,1,3,3-Tetramethylbutyl)phenyl-polyethylene glycol Polyethylene glycol tert-octylphenyl ether	9002-93-1	(C2H4O)nC14H22O	Triton™ X-100	Sigma-Aldrich Japan G.K.	-

(11) Data archives

The data obtained during the cruise will be submitted to the Data Management Group of JAMSTEC, and they will be made available to the public via the "Data Research System for Whole Cruise Information in JAMSTEC (DARWIN)" on the JAMSTEC website (http://www.godac.jamstec.go.jp/darwin/e)

(12) References

Susan Becker, Michio Aoyama E. Malcolm S. Woodward, Karel Bakker, Stephen Coverly, Claire Mahaffey, Toste Tanhua, (2019) The precise and accurate determination of dissolved inorganic nutrients in seawater, using Continuous Flow Analysis methods, n: The GO-SHIP Repeat Hydrography Manual: A Collection of Expert Reports and Guidelines. Available online at: http://www.go-ship.org/HydroMan.html. DOI: http://dx.doi.org/10.25607/OBP-555

Grasshoff, K. 1976. Automated chemical analysis (Chapter 13) in Methods of Seawater Analysis. With contribution by Almgreen T., Dawson R., Ehrhardt M., Fonselius S. H., Josefsson B., Koroleff F., Kremling K. Weinheim, New York: Verlag Chemie.

Grasshoff, K., Kremling K., Ehrhardt, M. et al. 1999. Methods of Seawater Analysis. Third, Completely Revised and Extended Edition. WILEY-VCH Verlag GmbH, D-69469 Weinheim (Federal Republic of Germany).

Hydes, D.J., Aoyama, M., Aminot, A., Bakker, K., Becker, S., Coverly, S., Daniel, A., Dickson, A.G., Grosso, O., Kerouel, R., Ooijen, J. van, Sato, K., Tanhua, T., Woodward, E.M.S., Zhang, J.Z., 2010. Determination of Dissolved Nutrients (N, P, Si) in Seawater with High Precision and Inter-Comparability Using Gas-Segmented Continuous Flow Analysers, In: GO-SHIP Repeat Hydrography Manual: A Collection of Expert Reports and Guidelines. IOCCP Report No. 14, ICPO Publication Series No 134.

Kimura, 2000. Determination of ammonia in seawater using a vaporization membrane permeability method. 7th auto analyzer Study Group, 39-41.

Murphy, J., and Riley, J.P. 1962. Analytica chimica Acta 27, 31-36.

4.3 DIC and TA

(1) Personnel

Akihiko Murata	JAMSTEC	-PI
Minoru Hamana	JAMSTEC	
Masahiro Orui	MWJ	
Hiroshi Hoshino	MWJ	
Atsushi Ono	MWJ	

(2) Objectives

Concentrations of CO_2 in the atmosphere are now increasing at a rate of 1.9 ppmv y^{-1} owing to human activities such as burning of fossil fuels, deforestation and cement production. It is an urgent task to estimate as accurately as possible the absorption capacity of the oceans against the increased concentration of atmospheric CO_2, as well as to clarify the mechanism of CO_2 absorption. This is because the magnitude of the anticipated global warming depends on the level of CO_2 in the atmosphere, and because the ocean currently absorbs 1/3 of the 6 Gt of carbon emitted into the atmosphere annually by human activities.

During this cruise, our objective was to quantify how much anthropogenic CO_2 absorbed in the ocean is transported to and redistributed within the Arctic Ocean. For this purpose, we measured CO_2-system parameters such as dissolved inorganic carbon (DIC) and total alkalinity (TA).

(3) Apparatus

Measurements of DIC and TA were undertaken using a DIC–TA measuring system (Nippon ANS, Inc., Japan) that included separate units capable of analyzing DIC and TA simultaneously. The DIC unit includes a seawater dispensing system, CO_2 extraction system and coulometer. The seawater dispensing system has an autosampler (six ports) that takes seawater in a 250 mL borosilicate glass bottle ((DURAN® glass bottle, 250 mL) and dispenses the seawater into a pipette of nominal 15-mL volume under the control of a PC. The pipette is maintained at a temperature of 25 °C by a water jacket fed from a water bath set at 25 °C. The CO_2 dissolved in a seawater sample is extracted in the stripping chamber of the CO_2 extraction system by the addition of phosphoric acid (10% v/v). The stripping chamber is approximately 25-cm long and has a fine frit at the bottom. The acid is added to the stripping chamber from the bottom of the chamber by pressurizing an acid bottle for a given time that pushes out the correct amount of acid. The pressurizing is conducted using nitrogen gas (99.9999%). After the acid is transferred to the stripping chamber, the seawater sample in the pipette is introduced to the stripping chamber using the same method as for adding the acid. The seawater reacts with phosphoric acid and is stripped of its CO_2 by bubbling the nitrogen gas through the fine frit at the bottom of the stripping chamber. The CO_2 stripped in the chamber is carried by the nitrogen gas (flow rate: is 130 mL min^{-1}) to the coulometer through a dehydrating module.

The TA unit comprises a water dispensing system, autosyringe (Hamilton) for hydrochloric acid, spectrophotometer (TM-UV/VIS C10082CAH, Hamamatsu Photonics, Japan) and light source (Mikropack, Germany) that are controlled automatically by a PC. The water dispensing system has a water-jacketed pipette and a titration cell maintained at the temperature of 25 °C.

A seawater sample of approximately 42 mL is transferred from a sample bottle (DURAN® glass bottle, 250 mL) into a pipette by pressurizing the sample bottle (using nitrogen gas), following which it is introduced into the

titation cell. First, seawater is used to rinse the titration cell and then Milli-Q water is introduced into the titration cell for a further rinse. A seawater sample of approximately 42 mL is then weighed again in the pipette and transferred into the titration cell. For a seawater blank, the absorbance is measured at three wavelengths (730, 616 and 444 nm). After the measurement, an acid titrant, which is a mixture of approximately 0.05 M HCl at 25 °C in 0.65 M NaCl and 38 μM bromocresol green, is added into the titration cell. The volume of the acid titrant is changed between 1.780 and 2.100 mL according to the estimated values of the TA. The seawater + acid titrant solution is stirred for over 9 min with bubbling by nitrogen gas in the titration cell. Then, the absorbance at the three wavelengths is measured.

Calculation of TA is performed using the following equation:

$$TA \ = \ (-[H^+]_T V_{SA} + \ M_A V_A)/V_S,$$

where M_A is the molarity of the acid titrant added to the seawater sample, $[H^+]_T$ is the total excess hydrogen ion concentration in the seawater, and V_S, V_A and V_{SA} are the initial seawater volume, added acid titrant volume and combined seawater plus acid titrant volume, respectively. $[H^+]_T$ is calculated from the measured absorbance based on the following equation (Yao and Byrne, 1998):

$$pH_T = -\log[H^+]_T = 4.2699 + 0.002578(35 - S) + \log((R - 0.00131)/(2.3148 - 0.1299R))$$
$$- \log(1 - 0.001005S),$$

where S is the sample salinity, and R is the absorbance ratio calculated as:

$$R = (A_{616} - A_{730})/(A_{444} - A_{730}),$$

where A_i is the absorbance at wavelength i nm.

The measurement sequence such as system blank (phosphoric acid blank), 1.5% CO_2 gas in a nitrogen base, sea water samples (6) was programmed to repeat. The measurement of 1.5% CO_2 gas was undertaken to monitor the response of the coulometer solutions that either were from UIC Inc. or made in the laboratory.

(4) Performance

Replicate analysis was undertaken on approximately every fifth seawater sample. The repeatability for DIC and TA was estimated as 0.20 ± 2.49 (n = 108) and 0.63 ± 3.05 (n = 108) μmol kg^{-1}, respectively (based on data that have not undergone QC).

(5) Results

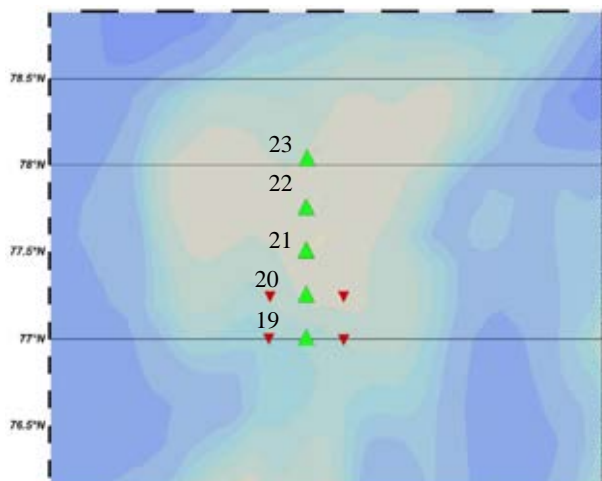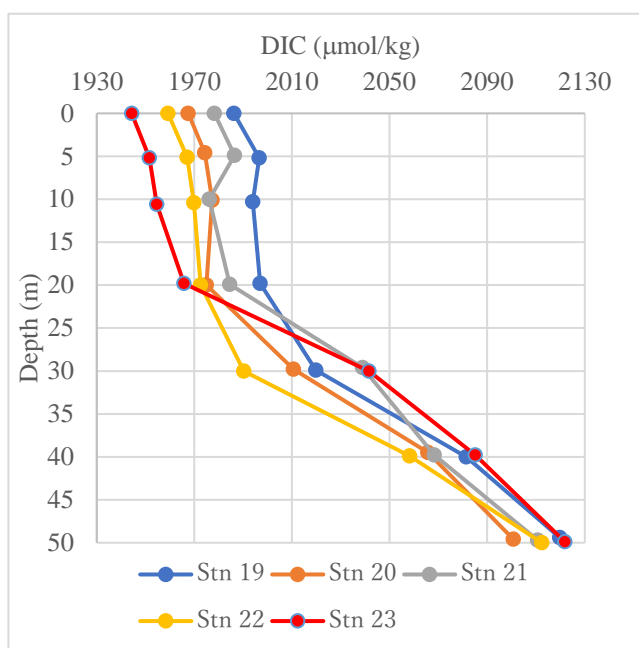Figure 4.3-1: Positions of repeat line stations (triangles).

Figure 4.3-2: Vertical distribution of DIC in upper 100 m at each of the repeat line stations.

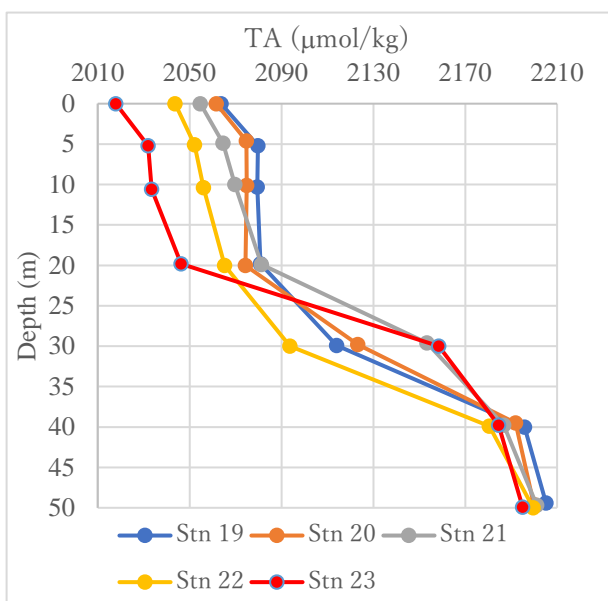Figure 4.3-3: Vertical distribution of TA in upper 100 m at each of the repeat line stations.

References

Yao W. and R. H. Byrne (1998) Simplified seawater alkalinity analysis: Use of linear array spectrometers. Deep-Sea Research I 45, 1383-1392.

4.4 CH$_4$

(1) Personnel

Akihiko Murata   JAMSTEC   - PI

Sohiko Kameyama   Hokkaido Univ.   - not on board

(2) Objectives

Methane (CH$_4$) is one of the most potent greenhouse gases and its concentration in the atmosphere has increased over past decades. Despite its importance, the marine contribution to the global CH$_4$ budget has substantial uncertainty because observations of oceanic CH$_4$ are limited. For the Arctic Ocean, it is known that the surface waters are usually supersaturated with respect to atmospheric CH$_4$, implying that the ocean acts as a source for atmospheric CH$_4$. However, the magnitude of CH$_4$ emission varies considerably over both time and space. This large variability reflects the complex biogeochemical dynamics of the Arctic Ocean. Our water column observations of CH$_4$ were undertaken to understand the processes that control the large spatiotemporal variability of CH$_4$ distribution within the Arctic Ocean.

(3) Parameters

Dissolved CH$_4$ concentration

Carbon isotopic composition of CH$_4$

(4) Instruments and methods

(4-1) Discrete bottle sampling

Discrete water samples for each station (Table 4.4) were collected at multiple depths using 12-L Niskin bottles mounted on a CTD system. For each sample, an aliquot of 100 mL seawater was transferred from the Niskin bottles to an amber vial (100 mL). The vial was filled smoothly from the bottom with seawater using a drawing tube that extended from the Niskin drain to the bottom of the vial. The seawater was allowed to overflow by an amount of approximately one and a half times the vial volume. After sampling, 0.5 mL saturated mercuric chloride was added to poison the sample. Then, the vial was crimp-sealed with a butyl-rubber stopper and aluminum cap.

(4-2) Sample storage

The samples were stored at 4 °C in the dark onboard the R/V Mirai, and transported chilled to laboratories on land for analysis when the R/V Mirai returned to Japan.

(4-3) Sample measurement

The samples will be measured using gas chromatography-isotope ratio mass spectrometry (GC-IRMS) coupled with a purge and trap extraction system in Nagoya University, Japan.

(5) Station list or Observation log

A list of the water sampling stations for CH$_4$ is presented in Table 4.4.

Table 4.4: List of sampling stations for water column CH_4

Stn.	Sampling date (UTC)	Latitude (N)	Longitude (W)
002	08 Oct.	66°-00.17"	168°-44.72"
004	08 Oct.	67°-00.13"	168°-44.26"
005	09 Oct.	69°-00.19"	168°-45.18"
007	09 Oct.	69°-59.96"	168°-45.03"
009	10 Oct.	71°-59.76"	163°-29.99"
011	10 Oct.	72°-60.00"	160°-00.20"
013	11 Oct.	72°-19.98"	155°-00.52"
015	12 Oct.	71°-59.99"	147°-29.98"
019-1	16 Oct.	76°-59.96"	164°-59.94"
020-1	16 Oct.	77°-15.04"	164°-59.71"
021-1	17 Oct.	77°-30.01"	165°-00.01"
022-1	17 Oct.	77°-45.00"	165°-00.01"
023	18 Oct.	78°-02.13"	164°-58.49"

(6) Data archives

The data obtained during the cruise will be submitted to the Data Management Group of JAMSTEC, and they will be made available to the public via the "Data Research System for Whole Cruise Information in JAMSTEC (DARWIN)" on the JAMSTEC website (http://www.godac.jamstec.go.jp/darwin/e)

4.5 Radiocesium (^{134}Cs and ^{137}Cs), radioradium (^{226}Ra and ^{228}Ra) and PAHs

(1) Personnel

Yuichiro Kumamoto　　　　　JAMSTEC　　　- not on board, PI

(2) Objective

Determination of activity concentrations of radiocesium (^{134}Cs and ^{137}Cs), radioradium (^{226}Ra and ^{228}Ra) and polycyclic aromatic hydrocarbons (PAHs) in the Arctic Ocean, Bering Sea and northern North Pacific Ocean.

(3) Parameters

^{134}Cs, ^{137}Cs, ^{226}Ra, ^{228}Ra, and PAHs

(4) Instruments and methods

a. Sampling

Surface seawater samples were collected from water pumped continuously from a depth of approximately 4 m. The sample volumes collected for analysis of radiocesium, radioradium and PAHs were 40 L (two 20-L plastic containers), 20 L (one 20-L plastic container) and 10 L (one 10-L stainless-steel container), respectively.

b. Preparation and analysis

The seawater samples collected for the radiocesium measurements were unfiltered and acidified by adding nitric acid. Radiocesium in the seawater samples was concentrated using ammonium phosphomolybdate, which forms an insoluble compound with cesium. The radiocesium (^{134}Cs and ^{137}Cs) in the derived compound was measured using Ge gamma ray spectrometers.

The seawater sample used for the radioradium measurements was unfiltered. Least Ra-contaminated barium carrier and SO_4^{2-} were added to the 20-L seawater sample to coprecipitate the radium with $BaSO_4$. After evaporating to dryness, the $BaSO_4$ fraction was compressed to a disc as a mixture of $Fe(OH)_3$ and NaCl for gamma ray spectrometry using Ge-detectors.

Particulate and dissolved phases of the 10-L seawater sample were separated by filtration through 0.5-µm glass-fiber filters. Dissolved organic compounds, including PAHs, were concentrated using C18 solid-phase extraction disks. Particulate and dissolved PAHs were extracted from the glass-fiber filters using an ultrasonic method and eluted from the C18 disks with dichloromethane, respectively. Dimethyl sulfoxide was added to both extracted solutions, following which the dichloromethane was evaporated to dryness and the residue of the dimethyl sulfoxide was dissolved in acetonitrile. The PAHs in the sample was quantified using the high-performance liquid chromatography (HPLC) system with a fluorescence detector.

(5) Sample list

We collected samples of seawater from nine stations for the analyses of radiocesium, radioradium and PAHs in the Arctic Ocean, Bering Sea and northern North Pacific Ocean during this cruise (Table 4.5).

(6) Data archives

The data obtained during the cruise will be submitted to the Data Management Group of JAMSTEC, and they will be made available to the public via the "Data Research System for Whole Cruise Information in JAMSTEC (DARWIN)" on the JAMSTEC website (http://www.godac.jamstec.go.jp/darwin/e)

Table 4.5: Seawater samples collected for the analyses of radiocesium, radioradium and PAHs

No.	Station	Depth (m)	Method	Latitude (N)	Longitude (E)	Date (UTC)
1	surface-1	4	pump	46.76	160.30	2019/10/2
2	surface-2	4	pump	52.47	170.02	2019/10/4
3	surface-3	4	pump	59.16	180.05	2019/10/6
4	surface-4	4	pump	64.67	190.08	2019/10/8
5	surface-5	4	pump	69.89	191.27	2019/10/9
6	surface-6	4	pump	72.97	200.18	2019/10/10
7	surface-7	4	pump	73.79	214.75	2019/10/13
8	surface-8	4	pump	75.52	204.26	2019/10/15
9	surface-9	4	pump	78.07	194.83	2019/10/18

4.6 ^{129}I

(1) Personnel

Yuichiro Kumamoto   JAMSTEC   - not on board, PI

(2) Objective

Determination of activity concentrations of ^{129}I in the Arctic Ocean, Bering Sea and northern North Pacific Ocean.

(3) Parameters

^{129}I

(4) Instruments and methods

a. Sampling

Seawater samples for ^{129}I were collected using 12-L Niskin-X bottles. Seawater for sampling was collected from the surface using a bucket or pumped continuously from a depth of approximately 4 m. The seawater samples were collected into 1-L plastic bottles that had been rinsed twice.

b. Preparation and analysis

Iodine in the seawater samples was extracted using the solvent extraction technique. Extracted iodine was then precipitated as silver iodide by the addition of silver nitrate. The iodine isotopic ratios (^{129}I/^{127}I) of the silver iodide were measured by accelerator mass spectrometry. To evaluate the ^{129}I concentration in the seawater samples, iodine concentration (^{127}I) will be measured using inductively coupled plasma mass spectrometry and/or voltammetry.

(5) Sample list

We collected 74 seawater samples for ^{129}I measurements from the Arctic Ocean, Bering Sea, and northern North Pacific Ocean during this cruise (Table 4.6).

(6) Data archives

The data obtained during the cruise will be submitted to the Data Management Group of JAMSTEC, and they will be made available to the public via the "Data Research System for Whole Cruise Information in JAMSTEC (DARWIN)" on the JAMSTEC website (http://www.godac.jamstec.go.jp/darwin/e)

Table 4.6: Seawater samples collected for the [129]I measurements

No.	Station	Depth (m)	Method	Latitude (N)	Longitude (E)	Date (UTC)
1	Stn.13	0	bucket	72.33	204.99	2019/10/11
2	Stn.13	20	niskin	72.33	204.99	2019/10/11
3	Stn.13	50	niskin	72.33	204.99	2019/10/11
4	Stn.13	100	niskin	72.33	204.99	2019/10/11
5	Stn.13	150	niskin	72.33	204.99	2019/10/11
6	Stn.13	200	niskin	72.33	204.99	2019/10/11
7	Stn.13	250	niskin	72.33	204.99	2019/10/11
8	Stn.13	300	niskin	72.33	204.99	2019/10/11
9	Stn.13	400	niskin	72.33	204.99	2019/10/11
10	Stn.13	600	niskin	72.33	204.99	2019/10/11
11	Stn.13	800	niskin	72.33	204.99	2019/10/11
12	Stn.13	1000	niskin	72.33	204.99	2019/10/11
13	Stn.13	1500	niskin	72.33	204.99	2019/10/11
14	Stn.13	1952	niskin	72.33	204.99	2019/10/11
15	Stn.15	0	bucket	71.20	212.50	2019/10/12
16	Stn.15	20	niskin	71.20	212.50	2019/10/12
17	Stn.15	50	niskin	71.20	212.50	2019/10/12
18	Stn.15	100	niskin	71.20	212.50	2019/10/12
19	Stn.15	150	niskin	71.20	212.50	2019/10/12
20	Stn.15	200	niskin	71.20	212.50	2019/10/12
21	Stn.15	250	niskin	71.20	212.50	2019/10/12
22	Stn.15	300	niskin	71.20	212.50	2019/10/12
23	Stn.15	400	niskin	71.20	212.50	2019/10/12
24	Stn.15	600	niskin	71.20	212.50	2019/10/12
25	Stn.15	800	niskin	71.20	212.50	2019/10/12
26	Stn.15	1000	niskin	71.20	212.50	2019/10/12
27	Stn.15	1500	niskin	71.20	212.50	2019/10/12
28	Stn.15	2000	niskin	71.20	212.50	2019/10/12
29	Stn.15	2500	niskin	71.20	212.50	2019/10/12
30	Stn.15	3000	niskin	71.20	212.50	2019/10/12
31	Stn.15	3505	niskin	71.20	212.50	2019/10/12
32	Stn.16	0	bucket	72.00	215.00	2019/10/12
33	Stn.16	20	niskin	72.00	215.00	2019/10/12
34	Stn.16	50	niskin	72.00	215.00	2019/10/12
35	Stn.16	100	niskin	72.00	215.00	2019/10/12
36	Stn.16	150	niskin	72.00	215.00	2019/10/12

Table 4.6: continued.

No.	Station	Depth (m)	Method	Latitude (N)	Longitude (E)	Date (UTC)
37	Stn.16	200	niskin	72.00	215.00	2019/10/12
38	Stn.16	250	niskin	72.00	215.00	2019/10/12
39	Stn.16	300	niskin	72.00	215.00	2019/10/12
40	Stn.16	400	niskin	72.00	215.00	2019/10/12
41	Stn.16	600	niskin	72.00	215.00	2019/10/12
42	Stn.16	800	niskin	72.00	215.00	2019/10/12
43	Stn.16	1000	niskin	72.00	215.00	2019/10/12
44	Stn.16	1500	niskin	72.00	215.00	2019/10/12
45	Stn.16	2000	niskin	72.00	215.00	2019/10/12
46	Stn.16	2500	niskin	72.00	215.00	2019/10/12
47	Stn.16	3000	niskin	72.00	215.00	2019/10/12
48	Stn.16	3306	niskin	72.00	215.00	2019/10/12
49	Stn.17	0	bucket	74.77	209.50	2019/10/14
50	Stn.17	20	niskin	74.77	209.50	2019/10/14
51	Stn.17	50	niskin	74.77	209.50	2019/10/14
52	Stn.17	100	niskin	74.77	209.50	2019/10/14
53	Stn.17	150	niskin	74.77	209.50	2019/10/14
54	Stn.17	200	niskin	74.77	209.50	2019/10/14
55	Stn.17	250	niskin	74.77	209.50	2019/10/14
56	Stn.17	300	niskin	74.77	209.50	2019/10/14
57	Stn.17	400	niskin	74.77	209.50	2019/10/14
58	Stn.17	600	niskin	74.77	209.50	2019/10/14
59	Stn.17	800	niskin	74.77	209.50	2019/10/14
60	Stn.17	1000	niskin	74.77	209.50	2019/10/14
61	Stn.17	1500	niskin	74.77	209.50	2019/10/14
62	Stn.17	2000	niskin	74.77	209.50	2019/10/14
63	Stn.17	2500	niskin	74.77	209.50	2019/10/14
64	Stn.17	3000	niskin	74.77	209.50	2019/10/14
65	Stn.17	3824	niskin	74.77	209.50	2019/10/14
66	surface-1	4	pump	46.76	160.30	2019/10/2
67	surface-2	4	pump	52.47	170.02	2019/10/4
68	surface-3	4	pump	59.16	180.05	2019/10/6
69	surface-4	4	pump	64.67	190.08	2019/10/8
70	surface-5	4	pump	69.89	191.27	2019/10/9
71	surface-6	4	pump	72.97	200.18	2019/10/10
72	surface-7	4	pump	73.79	214.75	2019/10/13

Table 4.6: continued.

No.	Station	Depth (m)	Method	Latitude (N)	Longitude (E)	Date (UTC)
73	surface-8	4	pump	75.52	204.26	2019/10/15
74	surface-9	4	pump	78.07	194.83	2019/10/18

4.7 DOC and FDOM

(1) Personnel

Masahito Shigemitsu   JAMSTEC   - not on board, PI

Akihiko Murata   JAMSTEC

(2) Objectives

The Arctic Ocean receives approximately 10% of global river runoff. The rivers draining into the Arctic Ocean have high concentrations of dissolved organic carbon (DOC) and consequently they supply a large amount of the DOC found there. The rates of supply of DOC must vary spatially and temporally, which should affect the quantity and composition of dissolved organic matter (DOM) within the Arctic Ocean. Changes in the quantity and composition of the DOM play an important role in the growth of microbes, and ultimately in the fate of the supplied DOM in the Arctic Ocean. To elucidate the quantity and composition of DOM in the Arctic Ocean, samples of surface water were collected for analysis of the DOC concentration and excitation–emission matrix (EEM) of fluorescent dissolved organic matter (FDOM).

(3) Parameters

DOC concentration

EEM of FDOM

(4) Instruments and methods

(4-1) Bottle sampling

Discrete samples of surface water at each sampling station (Table 4.7) were collected using 12-L Niskin bottles mounted on a CTD system. Each sample was filtered using a precombusted glass-fiber filter (GF/F, Whatman). The filtration was undertaken by connecting a spigot of the Niskin bottle through a silicone tube to an inline plastic filter holder. Filtrates for the analyses of DOC concentration and EEM of FDOM were collected in acid-washed 60-mL high-density polyethylene bottles and precombusted glass vials with acid-washed Teflon-lined caps after triple rinsing, respectively.

(4-2) Sample storage

The samples were stored frozen in the dark onboard the R/V Mirai until analysis.

(4-3) Sample measurement

The samples for DOC concentration and EEM of FDOM will be measured using a Shimadzu TOC-L system coupled with a Shimadzu Total N analyzer at JAMSTEC and by a Horiba Aqualog at JAMSTEC, respectively.

(5) Station list

A list of the water sampling stations for the analyses of DOC concentration and EEM of FDOM is presented in Table 4.7.

Table 4.7: List of sampling stations for analyses of DOC concentration and EEM of FDOM

CTD Stn.	Latitude	Longitude
002	66-00.17N	168-44.72W
004	67-00.13N	168-44.26W
005	69-00.19N	168-45.18W
007	69-59.96N	168-45.03W
009	71-59.76N	163-29.99W
011	72-60.00N	160-00.20W
013	72-19.98N	155-00.52W
014	72-09.43N	153-47.41W
015	71-59.99N	147-29.98W
016	72-00.00N	145-00.05W
017	74-46.09N	150-30.13W
018	76-27.95N	161-38.51W
019	76-59.96N	164-59.94W
020	77-15.04N	164-59.71W
021	77-30.01N	165-00.01W
022	77-45.00N	165-00.01W
023	78-02.13N	164-58.49W
024	77-15.00N	165-59.97W
025	77-00.37N	165-59.88W
026	77-00.01N	164-00.01W
027	77-15.00N	164-00.01W
028	77-00.22N	168-46.13W
029	74-00.01N	168-44.83W
030	73-30.00N	168-45.00W
031	73-00.03N	168-45.04W
032	72-30.03N	168-44.61W
033	70-30.00N	168-44.92W
034	70-00.00N	168-45.04W
035	69-30.19N	168-45.23W
036	68-59.99N	168-45.29W
037	68-00.88N	167-52.05W
038	67-46.99N	168-36.29W
039	67-30.07N	168-45.11W
040	67-00.06N	168-44.71W
041	66-29.99N	168-45.02W

(6) Data archives

The data obtained during the cruise will be submitted to the Data Management Group of JAMSTEC, and they will be made available to the public via the "Data Research System for Whole Cruise Information in JAMSTEC (DARWIN)" on the JAMSTEC website (http://www.godac.jamstec.go.jp/darwin/e)

4.8 Underway surface water monitoring

(1) Personnel

Akihiko Murata	JAMSTEC	- PI
Erii Irie	MWJ	- Operation leader
Yuko Miyoshi	MWJ	
Kanako Yoshida	MWJ	

(2) Objective

Our purpose was to obtain temperature, salinity, dissolved oxygen and fluorescence data continuously from near-sea surface water to reveal their spatiotemporal variations.

(3) Parameters

Temperature
Salinity
Dissolved oxygen
Fluorescence
Turbidity

(4) Instruments and Methods

The Continuous Sea Surface Water Monitoring System (Marine Works Japan Co., Ltd.) has four sensors that can automatically measure temperature, salinity, dissolved oxygen, fluorescence and turbidity in near-surface seawater every minute. Onboard the R/V Mirai, this system is located in the sea surface monitoring laboratory and connected to the ship's LAN. During the monitoring program, the measured data, time and location of the ship were stored in a PC-based data management system. Seawater was pumped continuously up to the laboratory from an intake placed approximately 4.5 m below the sea surface and it flowed into the system via a vinyl-chloride pipe. The flow rate of the surface seawater was adjusted to 10 dm^3 min^{-1}.

a. Instruments

Software

Seamoni Ver.1.2.0.0

Sensors

The specifications of each sensor in this system are listed below.

Temperature and Conductivity sensor

Model:	SBE-45, SEA-BIRD ELECTRONICS, INC.
Serial number:	4557820-0319
Measurement range:	Temperature -5 ºC - +35 ºC
	Conductivity 0 S m^{-1} - 7 S m^{-1}
Initial accuracy:	Temperature 0.002 ºC
	Conductivity 0.0003 S m^{-1}

Typical stability (per month):	Temperature 0.0002 ºC
	Conductivity 0.0003 S m^{-1}
Resolution:	Temperature 0.0001 ºC
	Conductivity 0.00001 S m^{-1}

Bottom of ship thermometer

Model:	SBE 38, SEA-BIRD ELECTRONICS, INC.
Serial number:	3852788-0457
Measurement range:	-5 ºC - +35 ºC
Initial accuracy:	±0.001 ºC
Typical stability (per 6 month):	0.001 ºC
Resolution:	0.00025 ºC

Dissolved oxygen sensor

Model:	RINKO II, JFE ADVANTECH CO. LTD.
Serial number:	0013
Measuring range:	0 mg L^{-1} - 20 mg L^{-1}
Resolution:	0.001 mg L^{-1} - 0.004 mg L^{-1} (25 ºC)
Accuracy:	Saturation ± 2 % F.S. (non-linear) (1 atm, 25 ºC)

Fluorescence & Turbidity sensor

Model:	C3, TURNER DESIGNS
Serial number:	2300384
Measuring range:	Chlorophyll in vivo 0 μg L^{-1} – 500 μg L^{-1}
Minimum Detection Limit:	Chlorophyll in vivo 0.03 μg L^{-1}
Measuring range:	Turbidity 0 NTU - 1500 NTU
Minimum Detection Limit:	Turbidity 0.05 NTU

(5) Observation log

The spatial and temporal distributions of each property are shown in Figure 4.8-1. We took samples of the surface seawater from this system once daily to compare the sensor data with bottle salinity, dissolved oxygen and chlorophyll a data. The results are shown in Figure 4.8-2. All the salinity samples were analyzed using the model 8400B "AUTOSAL" manufactured by Guildline Instruments Ltd. (see Chapter 3.2). The dissolved oxygen samples were analyzed using the Winkler method (see Chapter 4.1). Chlorophyll a was analyzed using the 10-AU manufactured by Turner Designs (see Chapter 4.11).
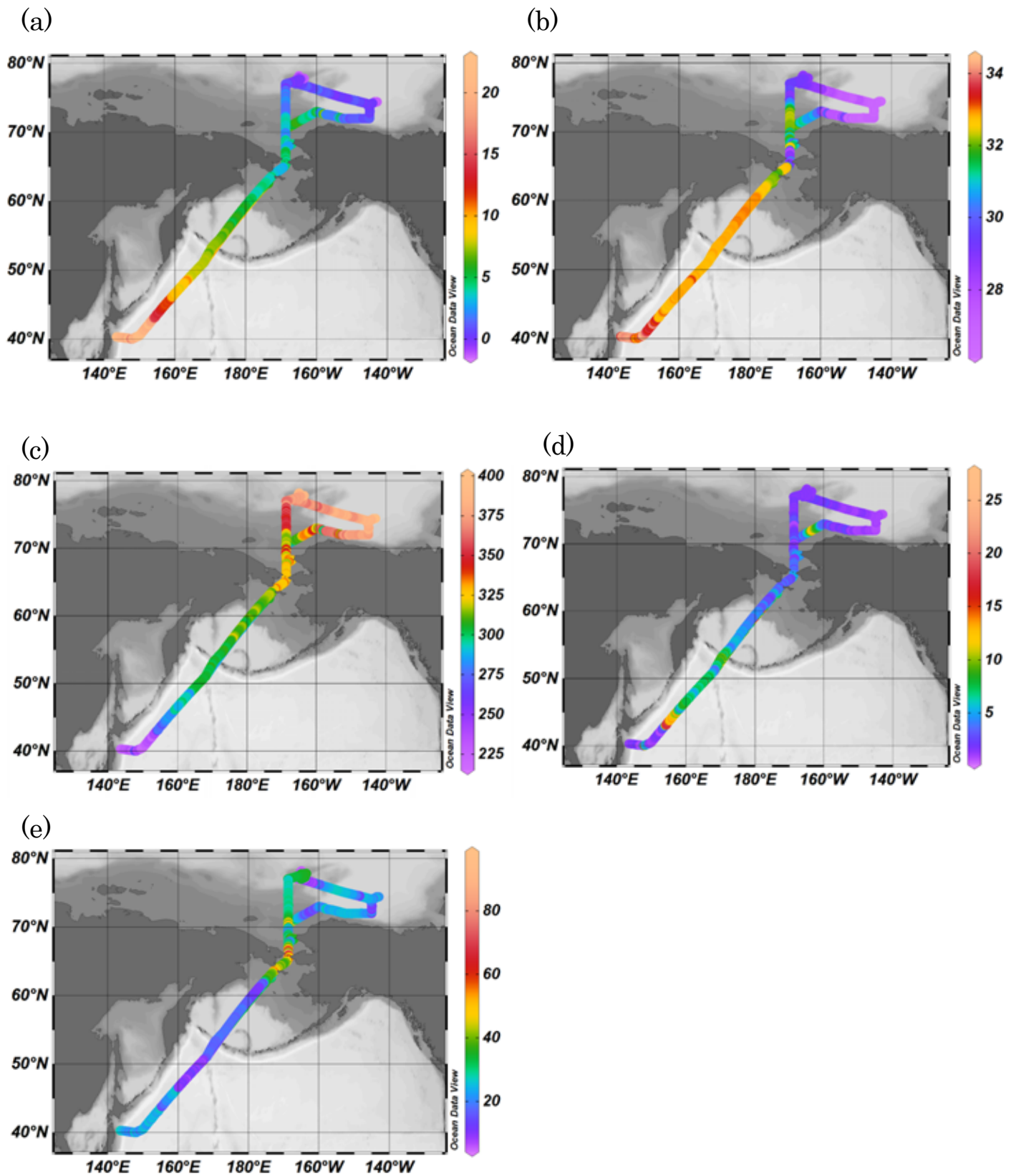
Figure 4.8-1: Spatial and temporal distributions of (a) temperature, (b) salinity, (c) dissolved oxygen, (d) fluorescence and (e) turbidity recorded during the MR19-03C cruise.
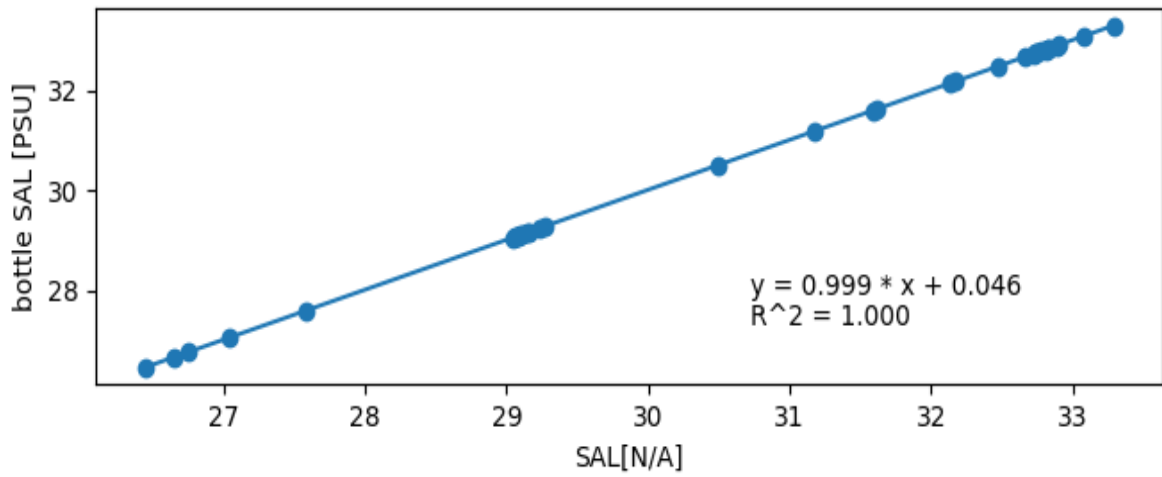
Figure 4.8-2: Correlation between salinity of sensor data and bottle data.
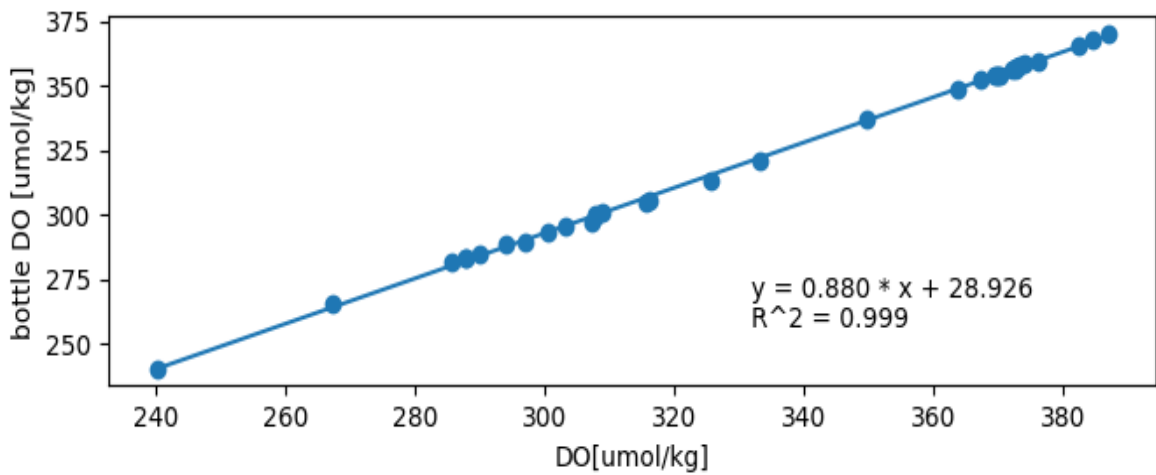
Figure 4.8-3: Correlation between dissolved oxygen of sensor data and bottle data.
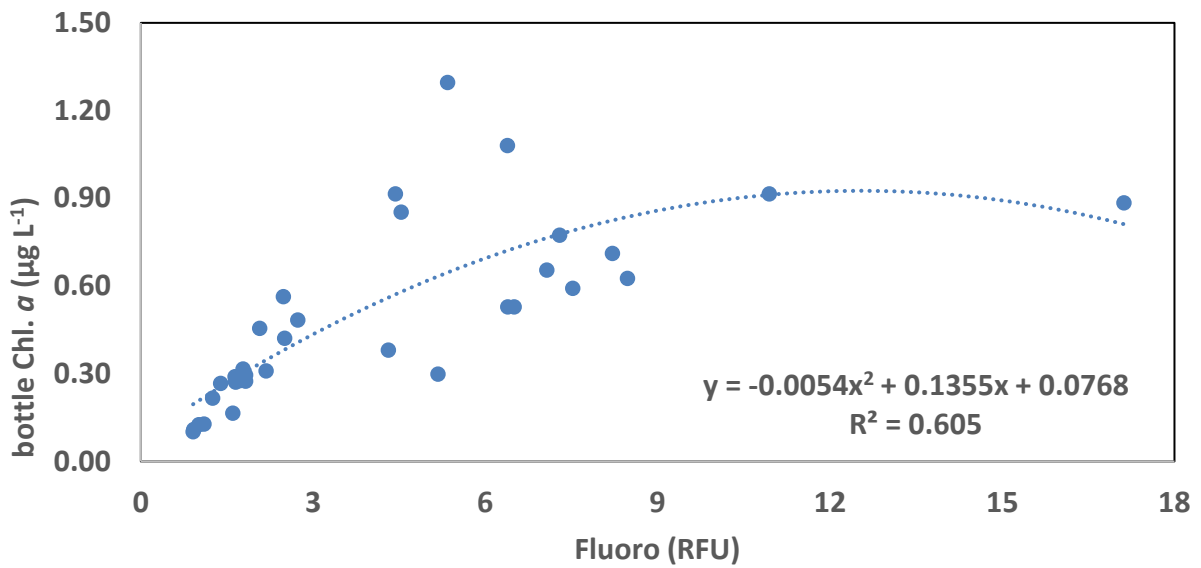
Figure 4.8-4: Correlation between fluorescence of sensor data and bottle data.

(6) Data archives

The data obtained during the cruise will be submitted to the Data Management Group of JAMSTEC, and they will be made available to the public via the "Data Research System for Whole Cruise Information in JAMSTEC (DARWIN)" on the JAMSTEC website (http://www.godac.jamstec.go.jp/darwin/e)

4.9 Continuous measurement of CO_2 and CH_4

(1) Personnel

Akihiko Murata   JAMSTEC   - PI

Atsushi Ono   MWJ

Masahiro Orui   MWJ

Hiroshi Hoshino   MWJ

Sohiko Kameyama   Hokkaido University

(2) Objective

Our purpose was to acquire in situ measurements of the concentrations of CO_2 and CH_4 in near-surface seawater.

(3) Methods, Apparatus and Performance

Using CO_2 and CH_4 standard gases (Table 4.9-1), the concentrations of CO_2 and CH_4 both in the atmosphere and in air equilibrated with surface seawater were analyzed using an automated system equipped with a nondispersive infrared gas analyzer (NDIR; LI-7000, Li-Cor) and an off-axis integrated-cavity output spectroscopy gas analyzer (Off-Axis ICOS; 911-0011, Los Gatos Research), which was developed based on cavity ringdown spectroscopy. Standard gases and atmospheric air taken from the bow of the ship (approximately13 m above sea level) were measured at approximately 2-h intervals. Seawater was taken from an intake placed approximately 4.5 m below the sea surface and pumped into the equilibrator at a flow rate of 4–5 L min^{-1}. The equilibrated air was circulated in a closed loop by a pump at a flow rate of 0.6–0.7 L min^{-1} through two electric cooling units, a starling cooler, the NDIR and the Off-Axis ICOS.

We also conducted discrete water sampling for surface seawater CH_4 for verification of the underway CH_4 measurements (Table 4.9-2)

(4) Preliminary result

The temporal variations of CO_2 and CH_4 concentrations are shown in Figures 4.9-1 and 4.9-2, respectively.

Table 4.9-1: Concentrations of CO_2 and CH_4 standard gases

	CO_2 (ppmv)	CH_4 (ppmv)
STD 1	249	-
STD 2	319	-
STD 3	390	-
STD 4	461	-
STD 5	241	1.62
STD 6	380	1.91
STD 7	-	2.13

Table 4.9-2: Sampling points of seawater CH_4 samples used to check for contamination

CTD Stn.	Sampling date (UTC)	Latitude (N)	Longitude (W)
002	08 Oct.	66°-00.17"	168°-44.72"
004	08 Oct.	67°-00.13"	168°-44.26"
005	09 Oct.	69°-00.19"	168°-45.18"
007	09 Oct.	69°-59.96"	168°-45.03"
009	10 Oct.	71°-59.76"	163°-29.99"
011	10 Oct.	72°-60.00"	160°-00.20"
013	11 Oct.	72°-19.98"	155°-00.52"
015	12 Oct.	71°-59.99"	147°-29.98"
019-1	16 Oct.	76°-59.96"	164°-59.94"
020-1	16 Oct.	77°-15.04"	164°-59.71"
021-1	17 Oct.	77°-30.01"	165°-00.01"
022-1	17 Oct.	77°-45.00"	165°-00.01"

The data obtained during the cruise will be submitted to the Data Management Group of JAMSTEC, and they will be made available to the public via the "Data Research System for Whole Cruise Information in JAMSTEC (DARWIN)" on the JAMSTEC website (http://www.godac.jamstec.go.jp/darwin/e)

Figure 4.9-1: Temporal variations of atmospheric and surface seawater CO_2. Blue and orange colors show atmospheric and surface seawater CO_2 concentrations, respectively. The x-axis shows sequential days starting from 1 January 2019.
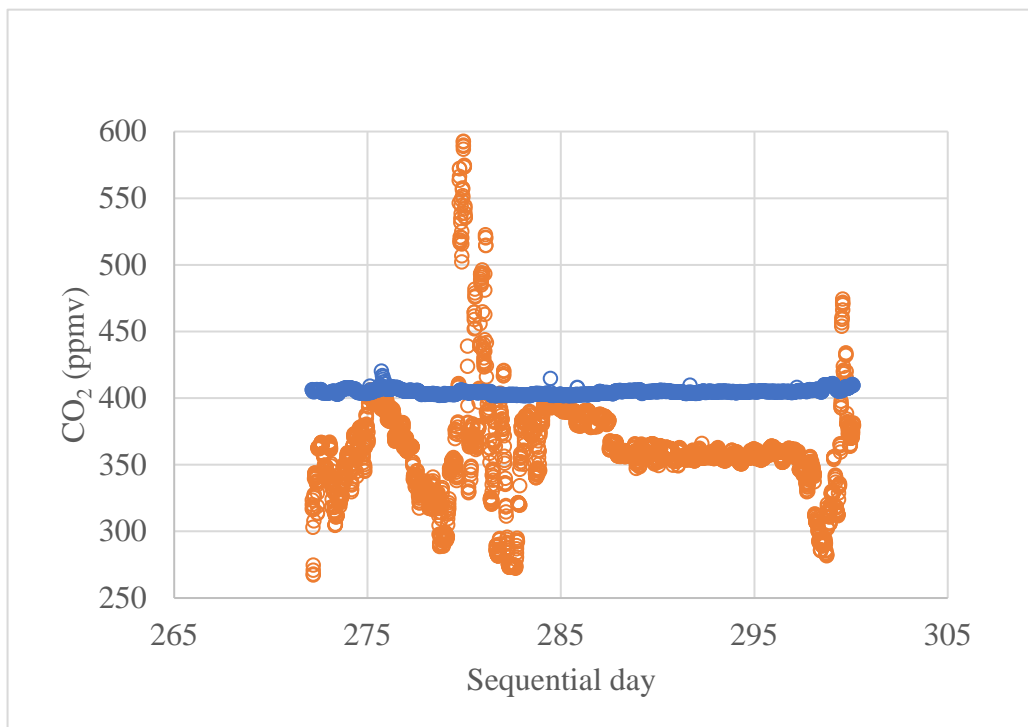

Figure 4.9-2: Temporal variations of atmospheric and surface seawater CH_4. Blue and orange colors show atmospheric and surface seawater CH_4 concentrations, respectively. The x-axis shows sequential days starting from 1 January 2019.
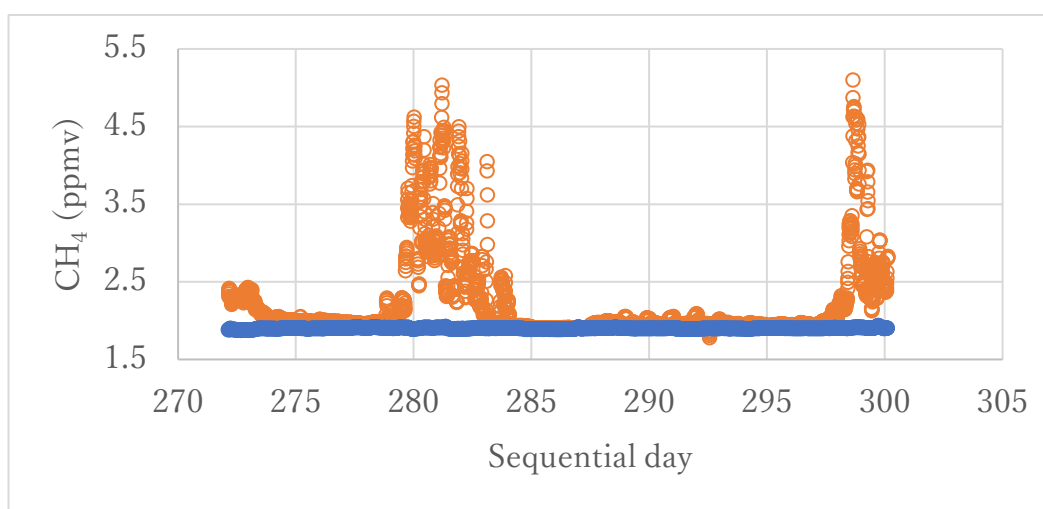
4.10 Underway DIC

(1) Personnel

Akihiko Murata   JAMSTEC   - PI

Hiroshi Hoshino   MWJ

Masahiro Orui   MWJ

Atsushi Ono   MWJ

(2) Objective

Our purpose was to measure the total DIC concentration in surface seawater and to reveal its spatiotemporal variations.

(3) Parameter

DIC

(4) Instruments and Methods

Continuous underway measurements of surface seawater C_T were made using the C_T measuring system (Nihon ANS, Inc.) installed onboard the R/V Mirai of JAMSTEC.

The underway water sampling device collects surface seawater in a ~300 mL borosilicate glass bottle automatically after allowing overflow of three times the bottle volume. Before measurement, the water samples were stored at 20 °C. The seawater is then transferred into a pipette (~15 mL) maintained at a temperature of 20 °C by a water jacket fed from a water bath set at 20 °C. The CO_2 dissolved in a seawater sample is extracted in a stripping chamber of the CO_2 extraction system by the addition of phosphoric acid (~10% v/v; approximately 2 mL). The stripping chamber is approximately 25-cm long and has a fine frit at the bottom. The acid is added to the stripping chamber from the bottom of the chamber by pressurizing an acid bottle for a given time that pushes out the correct amount of acid. The pressurizing is conducted using nitrogen gas (99.9999%). After the acid is transferred to the stripping chamber, the seawater sample in the pipette is introduced to the stripping chamber using the same method as for adding the acid. The seawater reacts with phosphoric acid and is stripped of its CO_2 by bubbling the nitrogen gas through the fine frit at the bottom of the stripping chamber. The CO_2 stripped in the chamber is carried by the nitrogen gas (flow rate: 140 mL min^{-1}) to the coulometer through a dehydrating module. The module consists of two electric dehumidifiers (maintained at ~2 °C) and a chemical desiccant (Mg(ClO$_4$)$_2$).

(5) Observation log

The cruise track during the underway DIC observation is shown in Figure 4.10-1.
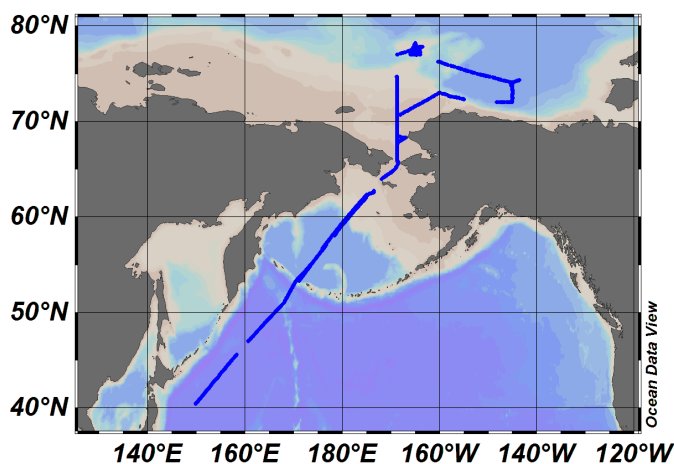
Figure 4.10-1: Cruise track during underway DIC observations.

(6) Results

The temporal variations of surface seawater DIC and salinity-normalized DIC are shown in Figure 4.10-2.
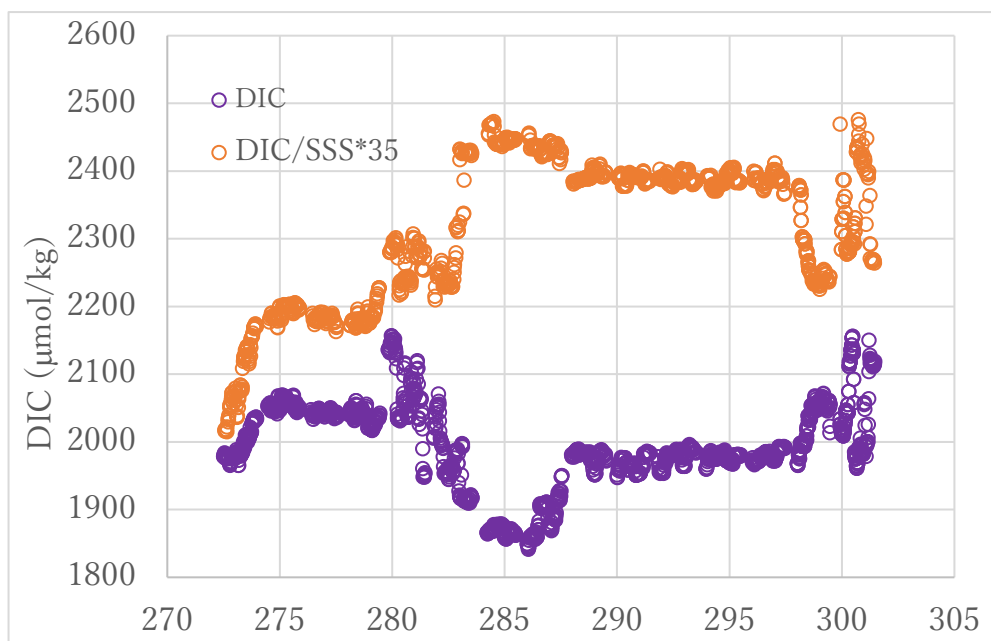
Figure 4.10-2: Temporal variations of surface seawater DIC and DIC normalized by salinity of 35.

(7) Date archives

The data obtained during the cruise will be submitted to the Data Management Group of JAMSTEC, and they will be made available to the public via the "Data Research System for Whole Cruise Information in JAMSTEC (DARWIN)" on the JAMSTEC website (http://www.godac.jamstec.go.jp/darwin/e)

4.11 Marine bioaerosol particles

(1) Personnel

Kaori Kawana	JAMSTEC	- not on board
Fumikazu Taketani	JAMSTEC	
Kazuhiko Matsumoto	JAMSTEC	- not on board
Yugo Kanaya	JAMSTEC	- not on board

(2) Objectives

Marine bioaerosol particles ejected from the sea surface affect climate change via cloud processes by acting as cloud condensation nuclei and ice nucleating particles. Marine bioaerosols are produced directly at the sea surface through wind–wave interaction. Organic matter becomes enriched in the surface microlayer in organic gels. Transparent exopolymer particles (TEPs), i.e., polysaccharide-rich microgels produced primarily by abiotic coagulation of phytoplankton exudates, and Coomassie stainable particles (CSPs) containing proteinaceous polymers released during cell lysis and decomposition, have been identified as organic gels within the ocean interior. To investigate the air–sea interaction of biological particles, the abundance of biological particles in seawater was measured at the sampling stations.

(3) Methods

i. Sampling and filtration for marine gel particles

Seawater samples were collected using a bucket and Niskin bottles or from a laboratory water outlet (Table 4.11). To estimate the CSP concentrations, triplicate water samples of 200 mL were filtered onto 0.4-μm polycarbonate filters, and the filters were stained with 1 mL Coomassie brilliant blue solution and rinsed five times with 1 mL of Milli-Q water. Stained filter samples were stored in a freezer until required for analysis. Water samples for the TEP analysis were preserved through addition of formalin to a final concentration of 1% in a refrigerator (4 °C). Preserved samples will be filtered in the same way as the CSP samples in the laboratory on land, and the filters will be stained with 1 mL Alcian blue solution and rinsed thrice with 1 mL of Milli-Q water.

ii. Colorimetric measurement for marine gel particles

For the colorimetric analysis of TEPs, the stained filter samples will be soaked for 2–5 h in 6 mL of 80% sulfuric acid (H_2SO_4) to elute the dye, following which the absorbance of the solution can be measured at 787 nm in a 1-cm cuvette. For the colorimetric analysis of CSPs, the stained filter samples will be soaked for 2 h in 4 mL of 3% sodium dodecyl sulfate (SDS) in 50% isopropyl alcohol with sonication to elute the dye, following which the absorbance of the solution can be measured at 615 nm in a 1-cm cuvette. All samples will be analyzed in the laboratory using the above methods.

iii. measurements for marine bioaerosols

For analysis of the marine bioaerosols, seawater samples were filtered through a membrane filter onto a gold-coated chip, and the abundance of bioaerosol particles (dead/alive) was counted using a Bioplorer (KB-VKH01, Koyo Sangyo Co., Ltd), based on fluorescence measurements with UV and green light excitation. Stained fluorescence measurements were also conducted with reagents of DAPI and Hoechst.

(4) Data archive

The data obtained during the cruise will be submitted to the Data Management Group of JAMSTEC, and they will be made available to the public via the "Data Research System for Whole Cruise Information in JAMSTEC (DARWIN)" on the JAMSTEC website (http://www.godac.jamstec.go.jp/darwin/e)

Table 4.11: Sampling locations

On board ID	Date Collected					Latitude			Longitude		
	YYYY	MM	DD	hh:mm:ss	UTC/JST	Deg.	Min.	N/S	Deg.	Min.	E/W
MR1903C-TEP-001	2019	10	05	2:20	UTC	55	48.49	N	174	47.96	E
MR1903C-TEP-002	2019	10	08	6:45	UTC	65	39.66	N	168	27.73	W
MR1903C-TEP-003	2019	10	09	5:10	UTC	69	00.00	N	168	45	W
MR1903C-TEP-004	2019	10	10	7:55	UTC	71	59.51	N	163	30.51	W
MR1903C-TEP-005	2019	10	11	6:55	UTC	72	30.00	N	156	17.79	W
MR1903C-TEP-006	2019	10	12	8:45	UTC	71	59.99	N	147	29.98	W
MR1903C-TEP-007	2019	10	15	16:48	UTC	76	27.95	N	161	38.51	W
MR1903C-TEP-008	2019	10	16	5:15	UTC	77	00.00	N	165	00.00	W
MR1903C-TEP-009	2019	10	18	6:35	UTC	77	15.00	N	165	00.03	W
MR1903C-TEP-010	2019	10	21	6:37	UTC	77	15.00	N	165	59.97	W
MR1903C-TEP-011	2019	10	21	6:37	UTC	77	15.00	N	165	59.97	W
MR1903C-TEP-012	2019	10	21	6:37	UTC	77	15.00	N	165	59.97	W
MR1903C-TEP-013	2019	10	21	6:37	UTC	77	15.00	N	165	59.97	W
MR1903C-TEP-014	2019	10	22	7:04	UTC	77	00.37	N	165	59.88	W
MR1903C-TEP-015	2019	10	23	6:30	UTC	77	00.01	N	164	00.01	W
MR1903C-TEP-016	2019	10	25	8:59	UTC	77	00.22	N	168	46.13	W
MR1903C-TEP-017	2019	10	26	5:39	UTC	74	00.01	N	168	44.83	W
MR1903C-TEP-018	2019	10	26	13:08	UTC	73	00.03	N	168	45.04	W
MR1903C-TEP-019	2019	10	26	16:51	UTC	72	30.00	N	168	44.61	W
MR1903C-TEP-020	2019	10	27	5:42	UTC	70	00.00	N	168	44.92	W
MR1903C-TEP-021	2019	10	27	13:00	UTC	69	30.19	N	168	45.23	W
MR1903C-TEP-022	2019	10	28	5:05	UTC	68	00.88	N	168	52.05	W
MR1903C-TEP-023	2019	10	28	10:42	UTC	67	30.07	N	168	45.11	W
MR1903C-TEP-024	2019	10	28	17:22	UTC	66	29.99	N	168	45.02	W
MR1903C-TEP-025	2019	11	03	0:10	UTC	50	00.00	N	166	08.00	E
MR1903C-TEP-026	2019	11	03	0:00	UTC	50	00.00	N	166	08.00	E
MR1903C-TEP-027	2019	11	03	0:00	UTC	50	00.00	N	166	08.00	E

4.12. Phytoplankton

(1) Personnel

Kohei Matsuno	Hokkaido University	- PI
Atsushi Yamaguchi	Hokkaido University	
Yoshiyuki Abe	Tokyo University	
Koki Tokuhiro	Hokkaido University	
Yuri Fukai	Hokkaido University	
Fumihiko Kimura	Hokkaido University	
Nao Sato	Hokkaido University	

(2) Objective

The goals of this study were as follows:

1) Clarify the horizontal distribution of the phytoplankton community analyzed using a multispectral excitation–emission fluorometer (MFL), HPLC and chlorophyll *a* in the surface water

2) Clarify the spatial distribution of the microprotist community analyzed by MFL, HPLC, chlorophyll *a* and microscopy

(3) Sampling and treatment

(3-1) Surface monitoring

An MFL was set in a black calibration bucket. Surface seawater from a branch line of the underway monitoring system flowed continuously into the bucket from 30 September to 11 November 2019. We took samples of the surface water from the underway system once daily to measure the chlorophyll *a* and for HPLC analysis. Seawater samples (0.25 L) for analysis of the total chlorophyll *a* were vacuum-filtrated (<0.013 MPa) through a Whatman GF/F filter (25-mm diameter). Phytoplankton pigments retained on the filters were extracted immediately in a cuvette tube immersed with 6 mL of *N,N*-dimethylformamide, then stored and extracted for >24 h. After extraction of the pigment, the fluorescence of the samples was measured using a Turner model 10-005-R Filter Fluorometer. To estimate the chlorophyll *a* concentration, we applied the fluorometric "Acidification method" (Holm-Hansen et al., 1965). The correlation of the fluorescence between the sensor data and the bottle data was determined, as shown in Figure 4.12-1. For the HPLC samples, seawater (2 L) was vacuum-filtrated (<0.013 MPa) through a Whatman GF/F filter (25-mm diameter); the filters were preserved at -80 °C.

(3-2) Spatial distribution by Niskin sampler and bucket

Seawater samples (1 L) were collected from depths of 0, 10, 20, 30, 40 and 50 m for determination of the chlorophyll *a* maximum layer using a bucket and the Niskin water sampler at 44 stations (Figure 4.12-2, Table 4.12). The water samples were fixed by acid lugol (1% final concentration). In the land laboratory, the samples will be concentrated to 20 mL with a syphon, and microprotists will be enumerated and identified under inverted microscopy. Additionally, seawater samples (0.25 L) for analysis of the total chlorophyll *a* were also vacuum-filtrated (<0.013 MPa) through a Whatman GF/F filter (25-mm diameter). After the filtering, the chlorophyll *a* was measured as mentioned above (see 3.1). An MFL (Multi-Exciter, JFE-Advantech Co. Ltd.) was attached to the CTD frame to measure the vertical profile of chlorophyll *a* fluorescence.

(4) Station list

Table 4.12: Log of water samples collected by Niskin sampler and bucket. Circles indicate an MFL was attached to the CTD frame. Chlorophyll *a* was measured at the same depth as the lugol samples for microscopy.

St.	Date	Latitude (N)		Longitude		Sampling depth (m)	MFL
St. 011 (CTD001)	2019/10/7	65	38.27	168	27.79 W	0,10,20,30,40	O
St. 013 (CTD003)	2019/10/8	66	30.03	168	45.12 W	0,10,20,30,40	O
St. 014 (CTD004)	2019/10/8	67	0.72	168	42.61 W	0,10,20,30,25	O
St. 018 (CTD005)	2019/10/8	69	0.62	168	45.63 W	0,10,20,30,40,5	O
St. 019 (CTD006)	2019/10/8	69	29.91	168	45.04 W	0,10,20,30,40,15	O
St. 021 (CTD008)	2019/10/9	70	29.81	168	46.26 W	0,10,20,30,15	O
St. 024 (CTD009)	2019/10/9	71	59.23	163	30.98 W	0,10,20,30	O
St. 025 (CTD010)	2019/10/10	72	29.94	161	44.83 W	0,10,20,30,13	O
St. 026 (CTD011)	2019/10/10	72	59.93	160	0.76 W	0,10,20,30,40,50,12	O
St. 029 (CTD012)	2019/10/10	72	30.01	156	15.16 W	0,10,20,30,40,50,27	
St. 030 (CTD013)	2019/10/11	72	19.94	155	0.4 W	0,10,20,30,40,50,18	
St. 031 (CTD014)	2019/10/11	72	9.84	153	45.51 W	0,10,20,30,40,50,13	
St. 034 (CTD015)	2019/10/11	72	0	147	30 W	0,10,20,30,40,50,33	
St. 035 (CTD016)	2019/10/12	71	59.94	144	59.79 W	0,10,20,30,40,50,45	
St. FP2 (CTD017)	2019/10/14	74	46.17	150	30.68 W	0,10,20,30,40,50,34	
St. FP3 (CTD018)	2019/10/15	76	28.18	161	37.53 W	0,10,20,30,40,50,5	
St. 39-01 (CTD019-01)	2019/10/15	76	59.98	164	59.99 W	0,10,20,30,40,50,43	
St. 40-02 (CTD020-02)	2019/10/16	77	14.95	164	59.57 W	0,10,20,30,40,50,38	O
St. 42-01 (CTD022-01)	2019/10/17	77	45.03	165	0 W	0,10,20,30,40,50,45	O
St. 40-03 (CTD020-03)	2019/10/17	77	15.14	164	59.8 W	0,10,20,30,40,50,15	O
St. 42-02 (CTD022-02)	2019/10/18	77	45.01	165	0.35 W	0,10,20,30,40,50,45	O
St. MIZ-03 (CTD023)	2019/10/18	78	2.63	164	57.41 W	0,10,20,30,40,50,25	O
St. 39-02 (CTD019-02)	2019/10/18	77	0.11	164	59.79 W	0,10,20,30,40,50,15	O
St. 41-03 (CTD021-03)	2019/10/19	77	30	165	0.04 W	0,10,20,30,40,50,12	O
St. 39-03 (CTD019-03)	2019/10/19	77	0.18	164	59.78 W	0,10,20,30,40,50,27	O
St. 41-04 (CTD021-04)	2019/10/20	77	30	164	59.99 W	0,10,20,30,40,50,15	O
St. 43 (CTD024)	2019/10/20	77	15.14	166	0.01 W	0,10,20,30,40,50,15	
St. 39-04 (CTD019-04)	2019/10/21	77	0.19	164	59.74 W	0,10,20,30,40,50,42	O
St. 44 (CTD025)	2019/10/21	77	0.32	166	0.09 W	0,10,20,30,40,50,34	
St. 39-05 (CTD019-05)	2019/10/22	77	0.08	164	59.78 W	0,10,20,30,40,50,36	O
St. 45 (CTD026)	2019/10/22	77	0.13	164	0.16 W	0,10,20,30,40,50,15	

St.	Date	Latitude (N)		Longitude		Sampling depth (m)	MFL
St. 39-06 (CTD019-06)	2019/10/22	77	0.02	164	59.75 W	0,10,20,30,40,50,15	O
St. 46 (CTD027)	2019/10/23	77	15.15	163	59.29 W	0,10,20,30,40,50,15	
St. 39-07 (CTD019-07)	2019/10/24	77	0.29	164	59.71 W	0,10,20,30,40,50,17	O
St. 49 (CTD028)	2019/10/24	77	0.13	168	45.56 W	0,10,20,30,40,50,15	
St. 52 (CTD029)	2019/10/25	74	0.02	168	44.46 W	0,10,20,30,40,50,15	O
St. 54 (CTD031)	2019/10/26	73	0	168	44.99 W	0,10,20,30,40,50,17	O
St. 60 (CTD034)	2019/10/26	70	0	168	44.98 W	0,10,20,30,40,50,15	
St. 61 (CTD035)	2019/10/27	69	30.04	168	45.26 W	0,10,20,30,40,50,15	
St. 62 (CTD036)	2019/10/27	69	0.09	168	41.27 W	0,10,20,30,40,50,12	
St. 68 (CTD037)	2019/10/27	68	0.83	167	52.23 W	0,10,20,30,40,50,15	
St. 70 (CTD038)	2019/10/27	67	47.02	168	36.15 W	0,10,20,30,40,50,15	
St. 71 (CTD039)	2019/10/27	67	30.03	168	45.08 W	0,10,20,30,40,50,12	
St. 72 (CTD040)	2019/10/28	67	0.03	168	44.69 W	0,10,20,30,40,50,12	

(5) Preliminary results

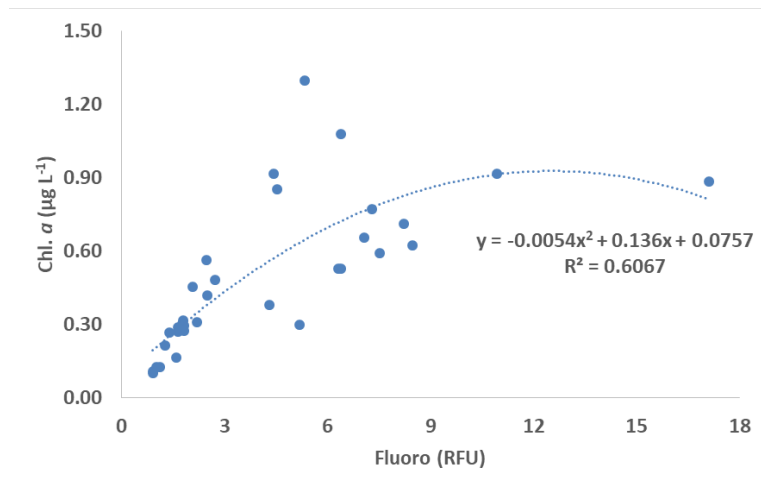As an indication of the preliminary results, we present following items.

Figure 4.12-1: Correlation of fluorescence between sensor data and bottle data.
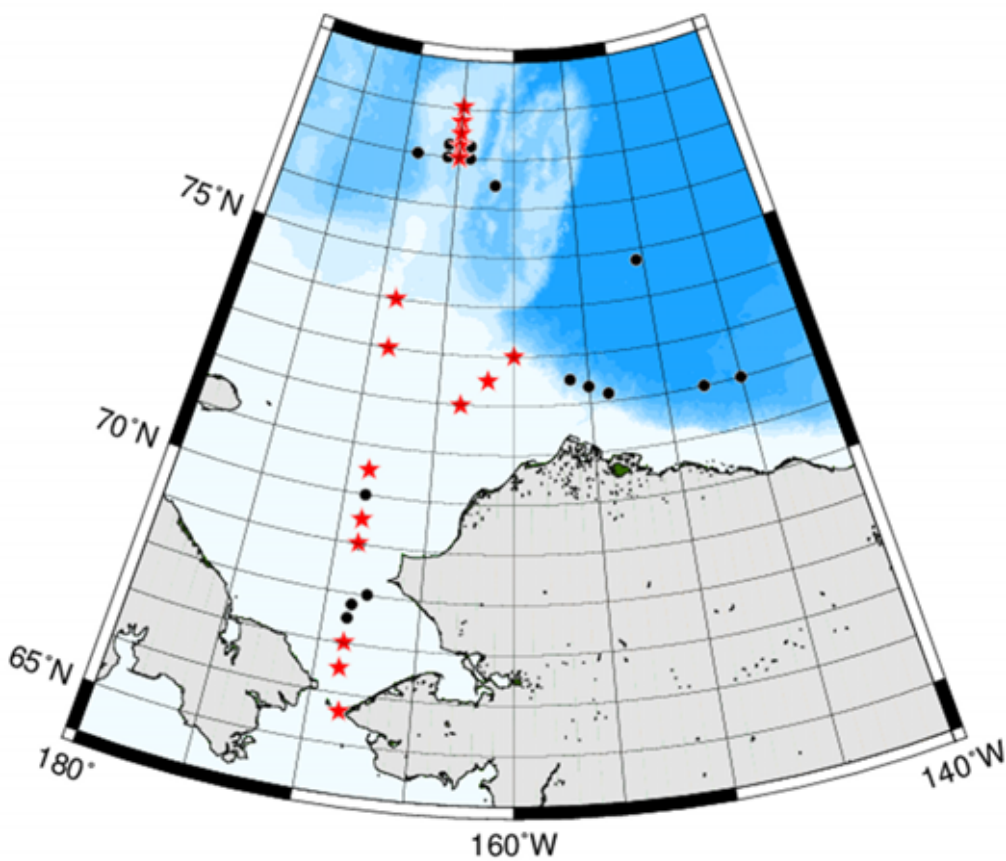

Figure 4.12-2: Locations of the water sampling and MFL stations in the Pacific sector of the Arctic Ocean (circles: CTD+bucket, stars: CTD+bucket+MFL).

4.13 Zooplankton net samplings

(1) Personnel

Kohei Matsuno	Hokkaido University	-PI
Atsushi Yamaguchi	Hokkaido University	
Yoshiyuki Abe	Tokyo University	
Koki Tokuhiro	Hokkaido University	
Yuri Fukai	Hokkaido University	
Fumihiko Kimura	Hokkaido University	
Nao Sato	Hokkaido University	

(2) Objective

The goals of this study were as follows:

1) Clarify the temporal changes of the plankton community in the pre-ice-covered season
2) Evaluate the physical conditions (gut pigments, DNA of fecal pellets, stable isotopes and lipid compositions) of Pacific and Arctic copepods in the Arctic Ocean
3) Estimate the amount of Pacific copepods transported into the Arctic Ocean
4) Clarify the grazing impact of Arctic copepods in the pre-ice-covered season

(3) Sampling

Zooplankton samples were collected by vertical haul of Quad-NORPAC nets at 58 stations in the Pacific sector of the Arctic Ocean. The Quad-NORPAC net (mesh sizes: 335, 150 and two of 63 µm [one is for a fixed sample and the other has a large-sized cod-end to collected fresh samples for incubation], mouth diameter: 45 cm) was towed between the surface and the depth of 150 m (or the bottom − 10 m at stations where the bottom was <150 m) at all stations (Figure 4.13 and Table 4.13-1). Zooplankton samples collected using the NORPAC net with 335, 150 and 63 µm mesh were immediately fixed with 5% buffered formalin for zooplankton structure analysis. In addition, samples collected with the 63-µm mesh were used for picking pterapods and evaluation of copepod physiological activity (i.e., gut pigments, DNA of fecal pellets, stable isotopes and lipid compositions). After sorting, the remaining subsamples were fixed with 99.5% ethanol for analysis of radiolaria (investigator: Dr. Yasuhide Nakamura [JSPS PD]). The volume of water filtered through the net was estimated based on readings from a flow meter mounted in the mouth ring of the net.

An 80-cm ring net (mesh: 335 µm, mouth diameter: 80 cm) was towed between the surface and the depth of 300 m (or the bottom − 10 m) at 32 stations (Figure 4.13 and Table 4.13-2). Fresh samples were used for picking pterapods and evaluation of copepod physiological activity (i.e., gut pigments, DNA of fecal pellets, stable isotope and lipid composition).

A closing PCP net (mesh size: 63 µm, mouth diameter: 45 cm) was towed at three shallow stations in two layers (i.e., 0–20 m and 20 to (bottom − 10) m) and at one deep station in five layers (0–50, 50–100, 100–250, 250–500 and 500–1000 m). The volume of water filtered through the net was estimated based on readings from a flow meter mounted in the mouth ring. Zooplankton samples collected by the closing PCP net were immediately fixed with 5% buffered formalin for zooplankton structure analysis (Figure 4.13 and Table 4.13-3).

(4) Onboard treatment

[gut pigments, DNA of fecal pellets, stable isotopes and lipid compositions]

Fresh zooplankton samples collected with a bucket net or ring net were divided roughly into two aliquots. We immediately added 10% soda water (CO_2 water) to one aliquot for use in the gut pigment and lipid composition analyses. We sorted the late copepodid stages of the Pacific copepods (*Neocalanus cristatus, N. plumchrus, N. flemingeri, Eucalanus bungii, Metridia pacifica*) and the Arctic copepods (*Calanus glacialis, C. hyperboreus, M. longa*). Some specimens were rinsed with Milli-Q water, transferred into a small plastic case (3 mL) and stored at -20 °C for lipid analysis. Other specimens were transferred into a cuvette tube immersed with 6 mL dimethylformamide, then stored and extracted for >24 h. After extraction of the pigment, the fluorescence of these samples was measured using a Turner model 10-005-R Filter Fluorometer. The other aliquot without soda water was used for the DNA analysis of fecal pellets and the stable isotope analysis. The identified species were targeted as much as possible (e.g., copepods, krill, chaetognaths, appendicularians and ostracods). The sorted animals were incubated in DNA-free seawater collected from the chlorophyll *a* maximum layer with a Niskin bottle. After several hours, the evacuated fecal pellets were picked up and preserved at -20 °C. The remaining animals were rinsed with Milli-Q water, transferred onto a microplate and stored at -20 °C for stable isotope analysis. Additionally, seawater (1–4 L) collected by a Niskin sampler from the chlorophyll *a* maximum layer was filtered through 100, 10 and 0.8 µm filters for in situ DNA analysis, and through 100 µm and GF/F filters for in situ stable isotope analysis. All filters were preserved at -20 °C.

(5) Station list

Table 4.13–1: Data on plankton samples collected by vertical hauls with a Quad-NORPAC net (GG54: 335 µm mesh)

Table 4.13–2: Data on plankton samples collected by vertical hauls with a ring net (mesh size: 335 µm)

Table 4.13–3: Data on plankton samples collected by vertical hauls with a closing net (mesh size: 63 µm)

Table 4.13-1. Data on plankton samples collected by vertical hauls with Quad-NORPAC net.
GG54: 0.335 mm mesh.

Station no.	Position Lat. (N)	Lon.	S.M.T. Date	Hour	Length of wire (m)	Angle of wire (°)	Depth estimated by wire angle (m)	Kind of cloth	Flowmeter No.	Reading	Estimated volume of water filtered (m³)	Remark
FP1	64 40.11	169 55.12 W	7 Oct	13:02	37	18	35	GG54	3994	408	5.68	no CTD cast
RINKO 001								150 µm	3993	449	6.81	UTC-11h
								63 µm	3998	378	5.20	
								63 µm				for experiment, remaining ethanol
St. 011	65 38.27	168 27.79 W	7 Oct	19:08	38	10	37	GG54	3994	403	5.61	
CTD001								150 µm	3993	370	5.61	
								63 µm	3998	289	3.98	1)
								63 µm				for experiment, remaining ethanol
St. 013	66 30.03	168 45.12 W	8 Oct	1:25	39	3	39	GG54	3994	362	5.04	
CTD003								150 µm	3993	311	4.72	
								63 µm	3998	134	1.84	1)
								63 µm				for experiment, remaining ethanol
St. 014	67 0.72	168 42.61 W	8 Oct	6:01	34	5	34	GG54	3994	400	5.57	
CTD004								150 µm	3993	328	4.97	
								63 µm	3998	275	3.79	1)
								63 µm				for experiment, remaining ethanol
St. 018	69 0.62	168 45.63 W	8 Oct	19:03	42	8	42	GG54	3994	444	6.18	2)
CTD005								150 µm	3993	376	5.70	2)
								63 µm	3998	295	4.06	2)
								63 µm				for experiment, remaining ethanol
St. 019	69 29.91	168 45.04 W	8 Oct	22:03	42	8	42	GG54	3994	350	4.87	
CTD006								150 µm	3993	281	4.26	
								63 µm	3998	230	3.17	
								63 µm				for experiment, remaining ethanol
St. 021	70 29.81	168 46.26 W	9 Oct	6:55	28	1	28	GG54	3994	375	5.22	
CTD008								150 µm	3993	300	4.55	
								63 µm	3998	235	3.24	
								63 µm				for experiment, remaining ethanol
St. 024	71 59.23	163 30.98 W	9 Oct	21:54	28	7	28	GG54	3994	435	6.06	
CTD009								150 µm	3993	399	6.05	
								63 µm	3998	389	5.36	
								63 µm				for experiment, remaining ethanol
St. 025	72 29.94	161 44.83 W	10 Oct	2:48	35	5	35	GG54	3994	609	8.48	
CTD010								150 µm	3993	499	7.57	
								63 µm	3998	435	5.99	
								63 µm				for experiment, remaining ethanol
St. 026	72 59.93	160 0.76 W	10 Oct	8:49	151	8	150	GG54	3994	1502	20.92	
CTD011								150 µm	3993	1263	19.15	
								63 µm	3998	941	12.96	
								63 µm				for experiment, remaining ethanol
St. 029	72 30.01	156 15.16 W	10 Oct	18:07	150	1	150	GG54	3994	1522	21.20	
CTD012								150 µm	3993	1318	19.99	
								63 µm	3998	939	12.93	
								63 µm				for experiment, remaining ethanol
St. 030	72 19.94	155 0.4 W	11 Oct	2:05	150	4	150	GG54	3994	1450	20.19	
CTD013								150 µm	3993	1271	19.27	
								63 µm	3998	897	12.35	
								63 µm				for experiment, remaining ethanol
St. 031	72 9.84	153 45.51 W	11 Oct	5:17	151	7	150	GG54	3994	1514	21.08	
CTD014								150 µm	3993	1323	20.06	
								63 µm	3998	1122	15.45	
								63 µm				for experiment, remaining ethanol
St. 034	72 0	147 30 W	11 Oct	22:26	150	4	150	GG54	3994	1408	19.61	
CTD015								150 µm	3993	1153	17.48	
								63 µm	3998	842	11.59	
								63 µm				for experiment, remaining ethanol
St. 035	71 59.94	144 59.79 W	12 Oct	3:15	154	13	150	GG54	3994	1541	21.46	
CTD016								150 µm	3993	1298	19.68	
								63 µm	3998	951	13.09	
								63 µm				for experiment, remaining ethanol
St. FP2	74 46.17	150 30.68 W	14 Oct	7:22	151	8	150	GG54	3994	1870	26.04	
CTD017								150 µm	3993	1573	23.85	
								63 µm	3998	1390	19.14	
								63 µm				for experiment, remaining ethanol
St. FP3	76 28.18	161 37.53 W	15 Oct	4:45	151	7	150	GG54	3994	1377	19.18	
CTD018								150 µm	3993	1185	17.97	
								63 µm	3998	910	12.53	
								63 µm				for experiment, remaining ethanol
St. 39-01	76 59.98	164 59.99 W	15 Oct	17:30	150	4	150	GG54	3994	1302	18.13	line observation start
CTD019								150 µm	3993	1174	17.80	
								63 µm	3998	916	12.61	
								63 µm				for experiment, remaining ethanol

S.M.T. is UTC-11h
1) phytoplankton abundant
2) clione&limacina abundant

185

Table 4.13-1. (Continued.)

Station no.	Position Lat. (N)		Lon.		S.M.T. Date	Hour	Length of wire (m)	Angle of wire (°)	Depth estimated by wire angle (m)	Kind of cloth	Flowmeter No.	Reading	Estimated volume of water filtered (m³)	Remark
St. MIZ-01 RINKO 011	78	3.95	164	53.66 W	16 Oct	13:20	160	20	150	GG54	3994	1496	20.83	
										150 µm	3993	1254	19.01	
										63 µm	3998	1050	14.46	
										63 µm				for experiment, remaining ethanol
St. 040-02 CTD020-02	77	14.95	164	59.57 W	16 Oct	19:22	150	0	150	GG54	3994	1345	18.73	
										150 µm	3993	1167	17.70	
										63 µm	3998	818	11.26	
										63 µm				for experiment, remaining ethanol
St. 042-01 CTD022	77	45.03	165	0 W	17 Oct	3:08	150	2	150	GG54	3994	1362	18.97	
										150 µm	3993	1173	17.79	
										63 µm	3998	878	12.09	
										63 µm				for experiment, remaining ethanol
St. MIZ-02 RINKO 013	78	0.26	164	59.61 W	17 Oct	11:35	153	12	150	GG54	3994	1315	18.31	
										150 µm	3993	1157	17.54	
										63 µm	3998	836	11.51	
										63 µm				for experiment, remaining ethanol
St. 040-03 CTD020-03	77	15.14	164	59.8 W	17 Oct	18:34	151	6	150	GG54	3994	1383	19.26	
										150 µm	3993	1179	17.88	
										63 µm	3998	870	11.98	
										63 µm				for experiment, remaining ethanol
St. 042-02 CTD022-02	77	45.01	165	0.35 W	18 Oct	1:35	155	14	150	GG54	3994	1430	19.91	
										150 µm	3993	1256	19.05	
										63 µm	3998	868	11.95	
										63 µm				for experiment, remaining ethanol
St. MIZ-03 CTD023	78	2.63	164	57.41 W	18 Oct	10:21	154	13	150	GG54	3994	1585	22.07	
										150 µm	3993	1317	19.97	
										63 µm	3998	966	13.30	
										63 µm				for experiment, remaining ethanol
St. 39-02 CTD019-02	77	0.11	164	59.79 W	18 Oct	20:24	150	0	150	GG54	3994	1320	18.38	
										150 µm	3993	1131	17.15	
										63 µm	3998	834	11.48	
										63 µm				for experiment, remaining ethanol
St. 41-03 CTD021-03	77	30	165	0.04 W	19 Oct	3:44	150	1	150	GG54	3994	1358	18.91	
										150 µm	3993	1147	17.39	
										63 µm	3998	870	11.98	
										63 µm				for experiment, remaining ethanol
St. MIZ-04 RINKO 017	78	3.40	164	57.68 W	19 Oct	13:23	155	14	150	GG54	3994	1485	20.68	
										150 µm	3993	1250	18.95	
										63 µm	3998	1019	14.03	
										63 µm				for experiment, remaining ethanol
St. 39-03 CTD019-03	77	0.18	164	59.78 W	19 Oct	21:03	151	8	150	GG54	3994	1430	19.91	
										150 µm	3993	1175	17.82	
										63 µm	3998	951	13.09	
										63 µm				for experiment, remaining ethanol
St. 41-04 CTD021-04	77	30	164	59.99 W	20 Oct	4:52	152	9	150	GG54	3994	1547	21.54	
										150 µm	3993	1322	20.05	
										63 µm	3998	1055	14.53	
										63 µm				for experiment, remaining ethanol
St. MIZ-05 RINKO 020	78	0.64	164	59.14 W	20 Oct	11:35	162	22	150	GG54	3994	1785	24.86	
										150 µm	3993	1455	22.06	
										63 µm	3998	1310	18.04	
										63 µm				for experiment, remaining ethanol
St. 43 CTD024	77	15.14	166	0.01 W	20 Oct	17:58	151	6	150	GG54	3994	1546	21.53	
										150 µm	3993	1302	19.74	
										63 µm	3998	1071	14.75	
										63 µm				for experiment, remaining ethanol
St. 39-04 CTD019-04	77	0.19	164	59.74 W	21 Oct	0:53	150	3	150	GG54	3994	1361	18.95	
										150 µm	3993	1173	17.79	
										63 µm	3998	888	12.23	
										63 µm				for experiment, remaining ethanol
St. MIZ-06 RINKO 022	78	1.17	164	58.78 W	21 Oct	11:40	164	24	150	GG54	3994	1694	23.59	
										150 µm	3993	1419	21.52	
										63 µm	3998	1383	19.04	
										63 µm				for experiment, remaining ethanol
St. 44 CTD025	77	0.32	166	0.09 W	21 Oct	19:10	150	0	150	GG54	3994	1525	21.24	
										150 µm	3993	1247	18.91	
										63 µm	3998	1052	14.48	
										63 µm				for experiment, remaining ethanol
St. 39-05 CTD019-05	77	0.08	164	59.78 W	22 Oct	0:39	153	12	150	GG54	3994	1493	20.79	
										150 µm	3993	1247	18.91	
										63 µm	3998	1020	14.04	
										63 µm				for experiment, remaining ethanol

S.M.T. is UTC-11h

1) phytoplankton abundant

2) clione&limacina abundant

Table 4.13-1. (Continued.)

Station no.	Position Lat. (N)		Lon.		S.M.T. Date	Hour	Length of wire (m)	Angle of wire (°)	Depth estimated by wire angle (m)	Kind of cloth	Flowmeter No.	Reading	Estimated volume of water filtered (m³)	Remark
St. MIZ-07	77	46.6	164	4.28 W	22 Oct	13:26	153	12	150	GG54	3994	1518	21.14	
RINKO 024										150 µm	3993	1292	19.59	
										63 µm	3998	1004	13.82	
										63 µm				for experiment, remaining ethanol
St. 45	77	0.13	164	0.16 W	22 Oct	18:42	150	3	150	GG54	3994	1336	18.61	
CTD026										150 µm	3993	1115	16.91	
										63 µm	3998	852	11.73	
										63 µm				for experiment, remaining ethanol
St. 39-06	77	0.02	164	59.75 W	22 Oct	23:44	152	9	150	GG54	3994	1363	18.98	
CTD019-06										150 µm	3993	1169	17.73	
										63 µm	3998	862	11.87	
										63 µm				for experiment, remaining ethanol
St. MIZ-08	77	47.02	163	35.49 W	23 Oct	11:38	160	20	150	GG54	3994	1598	22.25	
RINKO 026										150 µm	3993	1295	19.64	
										63 µm	3998	1119	15.41	
										63 µm				for experiment, remaining ethanol
St. 46	77	15.15	163	59.29 W	23 Oct	16:28	153	12	150	GG54	3994	1530	21.31	
CTD027										150 µm	3993	1263	19.15	
										63 µm	3998	1047	14.42	
										63 µm				for experiment, remaining ethanol
St. 39-07	77	0.29	164	59.71 W	24 Oct	0:19	151	6	150	GG54	3994	1412	19.66	
CTD019-07										150 µm	3993	1196	18.14	
										63 µm	3998	938	12.91	
										63 µm				for experiment, remaining ethanol
St. MIZ-09	77	50	163	0 W	24 Oct	13:44	153	12	150	GG54	3994	1445	20.12	line observation end
RINKO 028										150 µm	3993	1464	22.20	
										63 µm	3998	1088	14.98	
										63 µm				for experiment, remaining ethanol
St. 49	77	0.13	168	45.56 W	24 Oct	23:57	151	6	150	GG54	3994	1381	19.23	
CTD028										150 µm	3993	1227	18.61	
										63 µm	3998	850	11.70	
										63 µm				for experiment, remaining ethanol
St. FT18	74	41.77	168	46.67 W	25 Oct	13:24	150	0	150	GG54	3994	1500	20.89	
RINKO 029										150 µm	3993	1282	19.44	
										63 µm	3998	1032	14.21	
										63 µm				for experiment, remaining ethanol
St. 52	74	0.02	168	44.46 W	25 Oct	17:52	151	6	150	GG54	3994	1417	19.73	
CTD029										150 µm	3993	1165	17.67	
										63 µm	3998	884	12.17	
										63 µm				for experiment, remaining ethanol
St. 54	73	0	168	44.99 W	26 Oct	2:41	51	10	50	GG54	3994	565	7.87	
CTD031										150 µm	3993	462	7.01	
										63 µm	3998	376	5.18	
										63 µm				for experiment, remaining ethanol
St. 56	72	0.01	168	44.95 W	26 Oct	9:27	40	14	39	GG54	3994	392	5.46	
RINKO 030										150 µm	3993	308	4.67	
										63 µm	3998	239	3.29	
										63 µm				for experiment, remaining ethanol
St. 58	70	59.99	168	45.03 W	26 Oct	15:44	34	3	34	GG54	3994	398	5.54	
RINKO 032										150 µm	3993	349	5.29	
										63 µm	3998	294	4.05	
										63 µm				for experiment, remaining ethanol
St. 60	70	0	168	44.98 W	26 Oct	22:22	30	12	29	GG54	3994	304	4.23	
CTD034										150 µm	3993	237	3.59	
										63 µm	3998	181	2.49	
										63 µm				for experiment, remaining ethanol
St. 61	69	30.04	168	45.26 W	27 Oct	1:35	41	0	41	GG54	3994	571	7.95	
CTD035										150 µm	3993	459	6.96	
										63 µm	3998	413	5.69	
										63 µm				for experiment, remaining ethanol
St. 62	69	0.09	168	41.27 W	27 Oct	5:48	42	13	41	GG54	3994	541	7.53	2)
CTD036										150 µm	3993	446	6.76	2)
										63 µm	3998	425	5.85	2)
										63 µm				for experiment, remaining ethanol
St. 63	68	30.15	168	45.17 W	27 Oct	9:02	43	7	43	GG54	3994	669	9.32	
RINKO 033										150 µm	3993	522	7.92	
										63 µm	3998	540	7.44	
										63 µm				for experiment, remaining ethanol
St. 64	68	17.97	166	56.32 W	27 Oct	14:02	24	13	23	GG54	3994	357	4.97	
RINKO 034										150 µm	3993	284	4.31	
										63 µm	3998	307	4.23	
										63 µm				for experiment, remaining ethanol

S.M.T. is UTC-11h
1) phytoplankton abundant
2) clione&limacina abundant

Table 4.13-1. (Continued.)

Station no.	Position Lat. (N)	Lon.		S.M.T. Date	Hour	Length of wire (m)	Angle of wire (°)	Depth estimated by wire angle (m)	Kind of cloth	Flowmeter No.	Reading	Estimated volume of water filtered (m³)	Remark
St. 68	68	0.83	167 52.23 W	27 Oct	16:35	41	8	41	GG54	3994	798	11.11	
CTD037									150 μm	3993	650	9.86	
									63 μm	3998	578	7.96	
									63 μm				for experiment, remaining ethanol
St. 70	67	47.02	168 36.15 W	27 Oct	21:10	40	4	40	GG54	3994	552	7.69	
CTD038									150 μm	3993	469	7.11	
									63 μm	3998	400	5.51	
									63 μm				for experiment, remaining ethanol
St. 71	67	30.03	168 45.08 W	27 Oct	23:22	39	2	39	GG54	3994	480	6.68	
CTD039									150 μm	3993	400	6.07	
									63 μm	3998	370	5.09	
									63 μm				for experiment, remaining ethanol
St. 72	67	0.03	168 44.69 W	28 Oct	3:26	35	9	35	GG54	3994	498	6.94	
CTD040									150 μm	3993	419	6.35	
									63 μm	3998	359	4.94	
									63 μm				for experiment, remaining ethanol

S.M.T. is UTC-11h

1) phytoplankton abundant

2) clione&limacina abundant

Table 4.13-2. Data on plankton samples collected by vertical hauls with 80 cm ring net.

GG54: 0.335 mm mesh.

Station no.	Position Lat. (N)	Lon.		S.M.T. Date	Hour	Length of wire (m)	Angle of wire (°)	Depth estimated by wire angle (m)	Kind of cloth	Remark
St. 39-01 (CTD019)	77	0.01	164 59.86 W	15 Oct	17:43	300	1	300	GG54	for experiments
St. MIZ-01 (RINKO 011)	78	3.95	164 53.66 W	16 Oct	13:20	300	5	299	GG54	for experiments
St. 040-02 (CTD020-02)	77	14.95	164 59.57 W	16 Oct	19:34	300	1	300	GG54	for experiments
St. MIZ-02 (RINKO 013)	78	0.26	164 59.61 W	17 Oct	11:47	300	0	300	GG54	for experiments
St. 040-03 (CTD020-03)	77	15.14	164 59.8 W	17 Oct	18:46	300	6	298	GG54	for experiments
St. MIZ-03 (CTD023)	78	2.63	164 57.41 W	18 Oct	10:21	300	15	290	GG54	for experiments
St. 39-02 (CTD019-02)	77	0.11	164 59.79 W	18 Oct	20:37	300	0	300	GG54	for experiments
St. MIZ-04 (RINKO 017)	78	3.40	164 57.68 W	19 Oct	13:36	300	13	292	GG54	for experiments
St. 39-03 (CTD019-03)	77	0.18	164 59.78 W	19 Oct	21:17	600	7	596	GG54	for experiments
St. MIZ-05 (RINKO 020)	78	0.64	164 59.14 W	20 Oct	11:49	300	14	291	GG54	for experiments
St. 43 (CTD024)	77	15.14	166 0.01 W	20 Oct	18:13	710	3	709	GG54	for experiments
St. 39-04 (CTD019-04)	77	0.19	164 59.74 W	21 Oct	1:06	300	5	299	GG54	for experiments
St. MIZ-06 (RINKO 022)	78	1.17	164 58.78 W	21 Oct	11:55	300	8	297	GG54	for experiments
St. 44 (CTD025)	77	0.32	166 0.09 W	21 Oct	19:26	500	8	495	GG54	for experiments
St. 39-05 (CTD019-05)	77	0.08	164 59.78 W	22 Oct	0:52	300	0	300	GG54	for experiments
St. MIZ-07 (RINKO 024)	77	46.6	164 4.28 W	22 Oct	13:39	250	0	250	GG54	for experiments
St. 45 (CTD026)	77	0.13	164 0.16 W	22 Oct	18:56	400	0	400	GG54	for experiments
St. 39-06 (CTD019-06)	77	0.02	164 59.75 W	22 Oct	23:59	300	0	300	GG54	for experiments
St. MIZ-08 (RINKO 026)	77	47.02	163 35.49 W	23 Oct	11:50	250	0	250	GG54	for experiments
St. 46 (CTD027)	77	15.15	163 59.29 W	23 Oct	16:42	300	0	300	GG54	for experiments
St. 39-07 (CTD019-07)	77	0.29	164 59.71 W	24 Oct	0:32	300	2	300	GG54	for experiments
St. MIZ-09 (RINKO 028)	77	50	163 0 W	24 Oct	13:55	250	9	247	GG54	for experiments
St. 49 (CTD028)	77	0.13	168 45.56 W	25 Oct	0:09	300	1	300	GG54	for experiments
St. 52 (CTD029)	74	0.02	168 44.46 W	25 Oct	18:06	150	4	150	GG54	for experiments
St. 54 (CTD031)	73	0	168 44.99 W	26 Oct	2:48	51	2	51	GG54	for experiments
St. 58 (RINKO 032)	70	59.99	168 45.03 W	26 Oct	15:52	34	4	34	GG54	for experiments
St. 60 (CTD034)	70	0	168 44.98 W	26 Oct	22:31	30	2	30	GG54	for experiments
St. 61 (CTD035)	69	30.04	168 45.26 W	27 Oct	1:43	41	3	41	GG54	for experiments
St. 62 (CTD036)	69	0.09	168 41.27 W	27 Oct	5:56	42	7	42	GG54	for experiments
St. 63 (RINKO 033)	68	30.15	168 45.17 W	27 Oct	9:12	43	2	43	GG54	for experiments
St. 68 (CTD037)	68	0.83	167 52.23 W	27 Oct	16:44	41	0	41	GG54	for experiments
St. 70 (CTD038)	67	47.02	168 36.15 W	27 Oct	21:20	40	3	40	GG54	for experiments

S.M.T. is UTC-11h

188

Table 4.13-3. Data on plankton samples collected by vertical hauls with closing PCP net. The number in the parenthesis means the number of sorted from the sample.

Station no.	Position		S.M.T.		Length of wire (m)	Angle of wire (°)	Depth estimated by wire angle (m)	Closed net depth (m)	Kind of cloth	Flowmeter		Estimated volume of water filtered (m³)	Remark
	Lat. (N)	Lon.	Date	Hour						No.	Reading		
St.014	67 0.72	168 42.61 W	8 Oct	6:10	20	3	20	0	63 µm	2374	169	2.54	No record of sorted species
CTD004				6:16	34	2	34	21	63 µm	2374	274	4.12	No record of sorted species
St. 021	70 29.81	168 46.26 W	9 Oct	7:02	20	3	20	0	63 µm	2374	205	3.09	
CTD008				7:07	28	10	28	18	63 µm	2374	142	2.14	
St. 024	71 59.23	163 30.98 W	9 Oct	22:05	20	1	20	0	63 µm	2374	202	3.04	Sorted *L. helicina* (1)
CTD009				22:11	28	5	28	18	63 µm	2374	179	2.69	
St. FP2	74 46.19	150 30.79 W	14 Oct	7:42	50	6	50	0	63 µm	2374	593	8.92	Sorted *Themisto libellua* (1)
CTD017				7:51	100	4	100	50	63 µm	2374	443	6.67	Sorted *P. glacialis* C5F (1), C4F (2), C3 (3)
				8:03	250	0	250	103	63 µm	2374	890	13.39	Sorted *Aetideopsis multiserrata* C5F (1), *Chiridius obtusifrons* C6F (1), *C. hyperboreus* C6F (1), *Gaetanus tenuispinus* C5M (1), *Heterorhabdus norvegicus* C6F (1), C6M (1), *Scaphocalanus magnus* C5M (1), Appendicularia (1)
				8:19	500	2	500	259	63 µm	2374	1505	22.65	Sorted *C. obtusifrons* C6F (3), *C. hyperboreus* C6F (2), *H. norvegicus* C6F (3), C6M (2), *S. magnus* C6F (1), C5F (4), C5M (2), Amphipoda (1), *Boroecia maxima* (15), *Eukrohnia hamata* (2)
				8:41	1001	1	1001	503	63 µm	2374	2809	42.27	Sorted *A. multiserrata* C6F (1), *G. brevispinus* C6F (2), *S. magnus* C5M (1), Appendicularia (5), Amphipoda (4), Decapoda (1)

S.M.T. is UTC-11h

(6) Preliminary results

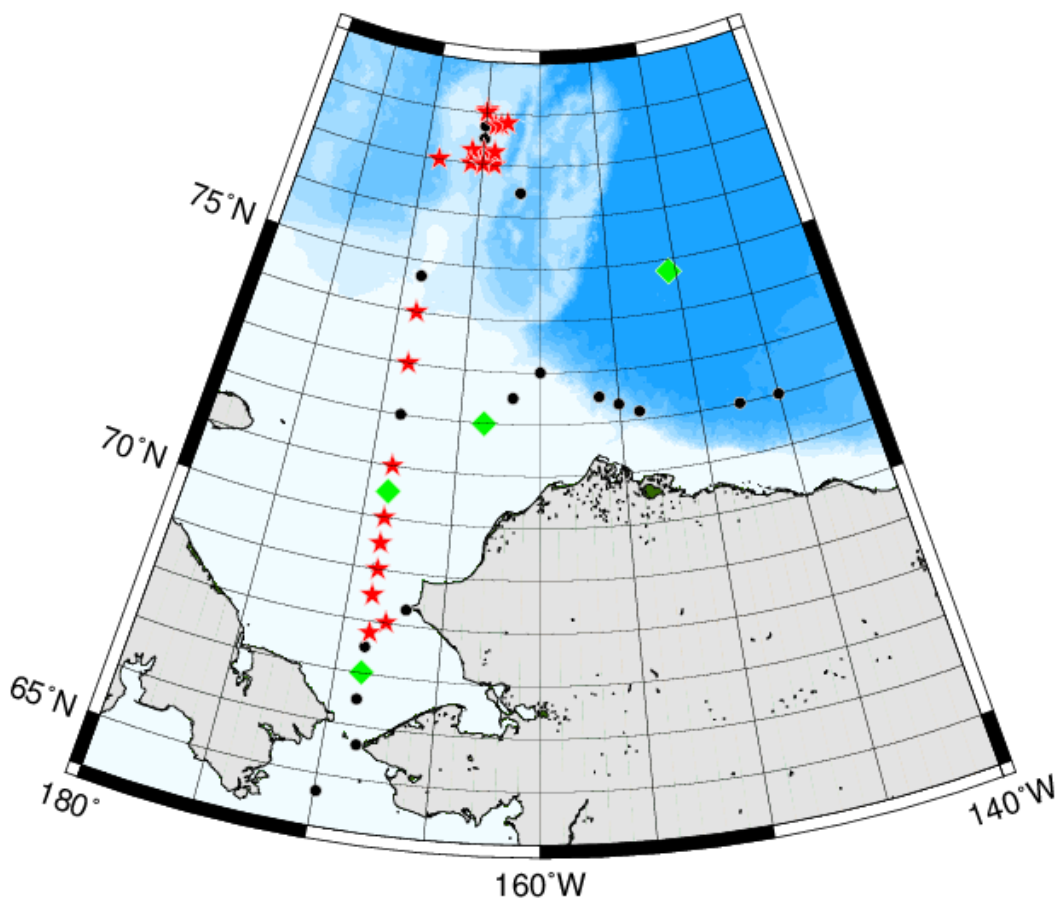As an indication of the preliminary results, we present the following item.

Figure 4.13: Locations of the sampling stations in the Pacific sector of Arctic Ocean (circles: NORPAC net, diamonds: NORPAC net+closing nets, stars: NORPAC net+ring net).

4.14 Zooplankton incubation

(1) Personnel

Kohei Matsuno	Hokkaido University	- PI
Atsushi Yamaguchi	Hokkaido University	
Yoshiyuki Abe	Tokyo University	
Koki Tokuhiro	Hokkaido University	
Yuri Fukai	Hokkaido University	
Fumihiko Kimura	Hokkaido University	
Nao Sato	Hokkaido University	

(2) Objective

The goals of this study were as follows:

1) Evaluate the effect of temperature on growth rate and Sr/Ca ratio of pteropods in the Arctic Ocean

(3) Sampling and treatment

Fresh pterapods (Figure 4.14) were collected by bucket net with a large-sized cod-end (mesh: 63 µm, mouth diameter: 45 cm) or ring net (mesh: 335 µm, mouth diameter: 80 cm) in the Pacific sector of the Arctic Ocean. The bucket net and ring net were towed between the surface and depths of 150–300 m or a depth of the (bottom − 10) m (at stations where the bottom was shallower than 150 m) at 58 and 32 stations, respectively (Tables 4.13-1 and 4.13-2). Fresh pteropod specimens (*Limacina helicina*) were immediately sorted and poured into a 500 mL bottle filled with filtered seawater for acclimation. At the same station, water samples from the chlorophyll *a* maximum layer were collected with a Niskin sampler for analysis of the reference in situ Sr/Ca ratio and oxygen stable isotope (Table 4.14). After acclimation, live pteropods were incubated in seawater with calcein (50 mg L^{-1}) for 1 h. Then, the specimens were rinsed gently with Milli-Q water and placed in incubators in 500 mL bottles filled with filtered seawater at 3, 4, 5 and 6 °C. After incubation for three weeks, the specimens were checked to ascertain whether they were alive or dead, and preserved at -80 °C.

In the land laboratory, the shell growth will be measured under an epifluorescence microscope with UV light excitation, and the Sr/Ca ratio and stable isotopes in that part will be measured.

(4) Station list

Logs of the stations of net samplings are presented in Tables 4.13-1 and 4.13-2 in the previous section.

Table 4.14: List of water samples obtained for analyses of the Sr/Ca ratio and oxygen stable isotope.

Date	St.	Sampling depth (m)
2019/10/8	St. 011 (CTD001)	30
2019/10/8	St. 014 (CTD004)	10,30
2019/10/8	St. 021 (CTD008)	10,30
2019/10/9	St. 024 (CTD009)	10,30
2019/10/14	St. FT2 (CTD017)	30,75,150
2019/10/19	St. 39-03 (CTD019-03)	5,10
2019/10/20	St. 41-04 (CTD021-04)	5
2019/10/20	St. 43 (CTD024)	5
2019/10/20	St. 39-04 (CTD019-04)	5
2019/10/21	St. 44 (CTD025)	20
2019/10/22	St. 39-05 (CTD019-05)	20
2019/10/22	St. 45 (CTD026)	10,20
2019/10/23	St. 46 (CTD027)	10
2019/10/24	St. 49 (CTD028)	20
2019/10/25	St. 52 (CTD029)	20
2019/10/26	St. 54 (CTD031)	20
2019/10/26	St. 60 (CTD034)	20
2019/10/27	St. 61 (CTD035)	20
2019/10/27	St. 62 (CTD036)	20
2019/10/27	St. 68 (CTD037)	20

(5) Preliminary results

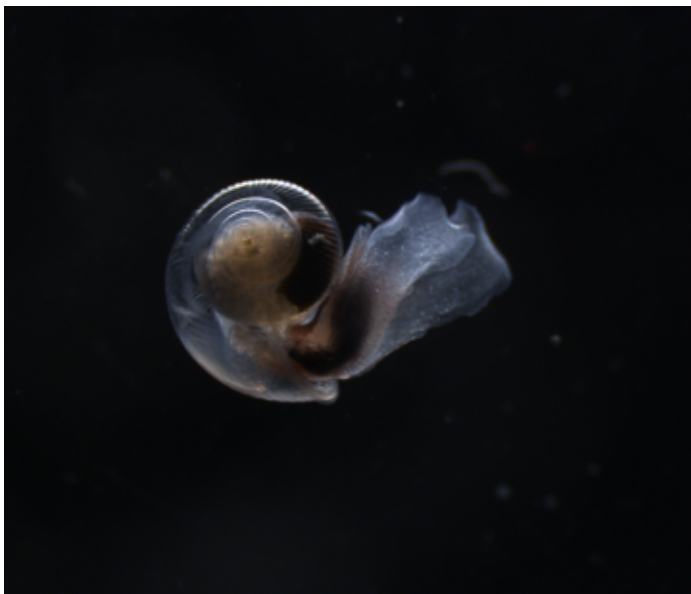As an indication of the preliminary results, we present the following item.

Figure 4.14: Photograph of a live pterapod.

4.15. Sea bottom sediments

(1) Personnel

Kohei Matsuno	Hokkaido University	-PI
Atsushi Yamaguchi	Hokkaido University	
Yoshiyuki Abe	Tokyo University	
Koki Tokuhiro	Hokkaido University	
Yuri Fukai	Hokkaido University	
Fumihiko Kimura	Hokkaido University	
Nao Sato	Hokkaido University	

(2) Objective

The goals of this study were as follows:

1) Clarify the spatial distribution of diatom resting cells in the sediment of the Pacific sector of the Arctic Ocean

(3) Sampling

Sea bottom sediments were collected using a Smith–McIntyre sampler at eight stations in the Pacific sector of the Arctic Ocean (Figure 4.15). We inserted a liner tube (diameter: 3.6 cm) and cut the sediment from the surface to the depth of 3 cm; all samples were sorted in dark cool (~4 °C) conditions. After a period of more than one month, their containing resting cells will be quantified by incubation (most probable number method). Another aliquot (depth: 0–1 cm) was cut and preserved in dark cool conditions for analysis of dinoflagellates (investigator: Dr. So-Young Kim [KOPRI]). Additionally, surface sediments (depth: 0–3 cm) and short core samples (depth: 0–3–6 cm) were cut and sorted in dark cool conditions for isolation of the diatom *Skeletonema* spp. (investigator: Dr. Satoshi Nagai [AFFRC]).

(4) Station list

Table 4.15: List of stations for sediment samples collected using a Smith–McIntyre sampler in the Pacific sector of the Arctic Ocean during October 2019.

St.	Date	Latitude (N)		Longitude		Bottom depth (m)
FP1 (RINKO 001)	2019/10/7	64	40.11	169	55.12 W	47
St. 14 (CTD 004)	2019/10/8	67	0.72	168	42.61 W	44
St. 18 (CTD 005)	2019/10/8	69	0.62	168	45.63 W	52
St. 21 (CTD 008)	2019/10/9	70	29.81	168	46.26 W	38
St. 24 (CTD 009)	2019/10/9	71	59.23	163	30.98 W	38
St. 60 (CTD 034)	2019/10/26	70	0	168	44.98 W	40
St. 68 (CTD 037)	2019/10/27	68	0.83	167	52.23 W	51
St. 70 (CTD 038)	2019/10/27	67	47.02	168	36.15 W	50

(5) Preliminary results

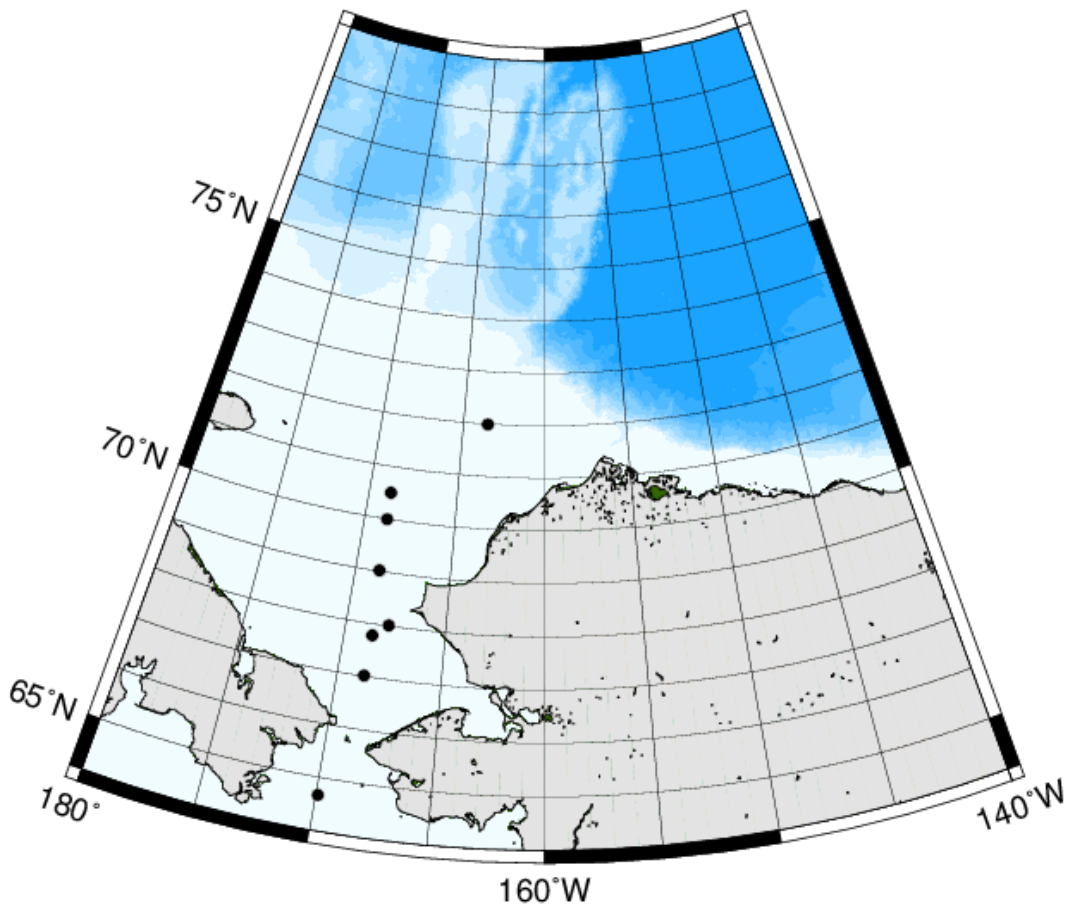As an indication of preliminary results, we present the following item.

Figure 4.15: Locations of the sampling stations for the collection of bottom sediments in the Pacific sector of the Arctic Ocean during October 2019. Black dots indicate sampling stations.

5. Geology

5.1. Sea Bottom Topography Measurement

(1) Personnel

Kazutoshi Sato	KIT	-PI
Ryo Ohyama	NME	
Souichiro Sueyoshi	NME	
Shinya Okumura	NME	
Kazuho Yoshida	NME	
Yutaro Murakami	NME	
Takehito Hattori	MIRAI Crew	

(2) Objective

The R/V Mirai is equipped with a multibeam echo sounding system (MBES; SEABEAM 3012, L3 Communications ELAC Nautik). The objective of using the MBES was to achieve continuous collection of bathymetric data along the ship's track (except in shallow depths) to contribute to regional geological and geophysical studies.

(3) Instruments and Methods

The "SEABEAM 3012" onboard the R/V Mirai was used for bathymetry mapping during this cruise. To obtain accurate sound velocity of the water column for ray-path correction of acoustic beams, we determined sound velocities at the depth of 6.62 m (the bottom of the ship) using a surface sound velocimeter. We produced sound velocity profiles using the equation of Del Grosso (1974) based on CTD, XCTD and Argo float data acquired during the cruise.

The system configuration and details of its performance are shown in Table 5.1.

Table 5.1: SEABEAM 3012 system configuration and performance

Frequency:	12 kHz
Transmit beam width:	2.0 degree
Transmit power:	4 kW
Transmit pulse length:	2 to 20 msec.
Receive beam width:	1.6 degree
Depth range:	50 to 11,000 m
Number of beams:	301 beams (Spacing mode: Equi-angle)
Beam spacing:	1.5 % of water depth (Spacing mode: Equi-distance)
Swath width:	60 to 150 degrees
Depth accuracy:	< 1 % of water depth (average across the swath)

(4) Preliminary Results

The results will be published after primary processing.

(5) Data archives

The data obtained during the cruise will be submitted to the Data Management Group of JAMSTEC, and they will be made available to the public via the "Data Research System for Whole Cruise Information in JAMSTEC (DARWIN)" on the JAMSTEC website (http://www.godac.jamstec.go.jp/darwin/e)

(6) Remarks

1. During the following periods, data acquisition was suspended owing to difficulties with the workstation.

     13:07 UTC on 06 November 2019 to 13:23 UTC on 06 November 2019

     19:17 UTC on 06 November 2019 to 19:24 UTC on 06 November 2019

2. During the following periods, data acquisition was suspended owing to the R/V Mirai track passing through areas of shallow sea.

     01:00 UTC on 07 October 2019 to 23:43 UTC on 10 October 2019

     09:49 UTC on 26 October 2019 to 07:10 UTC on 30 October 2019

3. During the following periods, data acquisition was suspended owing to the observation of microstructure measurements (T-MAP).

     18:00 UTC on 18 October 2019 to 18:20 UTC on 18 October 2019

     23:24 UTC on 18 October 2019 to 00:09 UTC on 19 October 2019

     06:43 UTC on 19 October 2019 to 07:13 UTC on 19 October 2019

     10:18 UTC on 19 October 2019 to11:10 UTC on 19 October 2019

     14:58 UTC on 19 October 2019 to 15:29 UTC on 19 October 2019

     23:44 UTC on 19 October 2019 to 00:09 UTC on 20 October 2019

     07:15 UTC on 20 October 2019 to 08:08 UTC on 20 October 2019

     11:13 UTC on 20 October 2019 to 12:18 UTC on 20 October 2019

     16:08 UTC on 20 October 2019 to 16:33 UTC on 20 October 2019

     21:56 UTC on 20 October 2019 to 22:22 UTC on 20 October 2019

     04:17 UTC on 21 October 2019 to 04:42 UTC on 20 October 2019

     09:57 UTC on 21 October 2019 to 10:30 UTC on 20 October 2019

     14:59 UTC on 21 October 2019 to 15:28 UTC on 20 October 2019

     16:59 UTC on 21 October 2019 to 17:21 UTC on 20 October 2019

     05:29 UTC on 22 October 2019 to 05:55 UTC on 22 October 2019

     09:31 UTC on 22 October 2019 to 10:06 UTC on 22 October 2019

     14:53 UTC on 22 October 2019 to 15:18 UTC on 22 October 2019

     16:45 UTC on 22 October 2019 to 17:09 UTC on 22 October 2019

     23:45 UTC on 22 October 2019 to 00:12 UTC on 23 October 2019

     05:00 UTC on 23 October 2019 to 05:41 UTC on 23 October 2019

     08:39 UTC on 23 October 2019 to 09:16 UTC on 23 October 2019

     12:38 UTC on 23 October 2019 to 13:09 UTC on 23 October 2019

     15:46 UTC on 23 October 2019 to 16:13 UTC on 23 October 2019

     21:59 UTC on 23 October 2019 to 22:26 UTC on 23 October 2019

02:53 UTC on 24 October 2019 to 03:16 UTC on 24 October 2019

09:14 UTC on 24 October 2019 to 09:51 UTC on 24 October 2019

14:29 UTC on 24 October 2019 to 14:50 UTC on 24 October 2019

16:18 UTC on 24 October 2019 to 16:43 UTC on 24 October 2019

00:02 UTC on 25 October 2019 to 00:29 UTC on 25 October 2019

08:03 UTC on 25 October 2019 to 08:44 UTC on 25 October 2019

00:02 UTC on 25 October 2019 to 00:29 UTC on 25 October 2019

23:45 UTC on 25 October 2019 to 00:06 UTC on 26 October 2019

22:58 UTC on 02 November 2019 to 23:29 UTC on 02 November 2019

5.2. Sea Surface Gravity Measurement

(1) Personnel

Kazutoshi Sato	KIT	-PI
Ryo Oyama	NME	
Souichiro Sueyoshi	NME	
Shinya Okumura	NME	
Kazuho Yoshida	NME	
Yutaro Murakami	NME	
Takehito Hattori	MIRAI Crew	

(2) Objective

Local gravity is an important parameter in geophysics and geodesy. We collected gravity data during this cruise.

(3) Parameters

Relative Gravity [CU: Counter Unit]

[mGal] = (coefl: 0.9946) * [CU]

(4) Instruments and Methods

We measured relative gravity using a LaCoste and Romberg air–sea gravity meter S-116 (Micro-g LaCoste, LLC) during the cruise. To convert relative gravity to absolute gravity, we measured gravity using a portable gravity meter (Scintrex gravity meter CG-5) at the ports of Sekinehama and Hachinohe as reference points.

(5) Preliminary Results

Absolute gravity measured at the ports of Sekinehama and Hachinohe is shown in Table 5.2.

Table 5.2: Absolute gravity of the MR19-03C cruise

No.	Date	UTC	Port	Absolute Gravity [mGal]	Sea Level [cm]	Ship Draft [cm]	Gravity at Sensor * [mGal]	S-116 Gravity [mGal]
#1	26-Sep-19	06:50	Sekinehama	980371.86	248	622	980372.83	12655.67
#2	11-Nov-19	00:24	Hachinohe	980353.29	262	618	980354.30	12632.49

*:   Gravity at Sensor

= Absolute Gravity + Sea Level*0.3086/100 + (Draft-530)/100*0.2222

(6) Observation Log

26 Sep. 2019 to 11 Nov. 2019

(7) Data archives

The data obtained during the cruise will be submitted to the Data Management Group of JAMSTEC, and they will be made available to the public via the "Data Research System for Whole Cruise Information in JAMSTEC (DARWIN)" on the JAMSTEC website (http://www.godac.jamstec.go.jp/darwin/e)

(8) Remarks

i)   At the following times, the Depth and Gyro values in the GRV data were invalid because of server error.

05:36 UTC on 29 September 2019

21:48 UTC on 14 October 2019

ii)   During the following period, data acquisition was suspended owing to difficulties with operation of the PC.

07:43 UTC on 04 October 2019 to 08:45 UTC on 04 October 2019

iii)   During the following period, data were invalid owing to Spring Motor trouble.

15:29 UTC on 08 October 2019 to 01:00 UTC 09 October 2019

5.3. Surface Magnetic Field Measurement

(1) Personnel

Kazutoshi Sato	KIT	-PI
Ryo Oyama	NME	
Souichiro Sueyoshi	NME	
Shinya Okumura	NME	
Kazuho Yoshida	NME	
Yutaro Murakami	NME	
Takehito Hattori	MIRAI Crew	

(2) Objective

Measurement of magnetic force on the sea is required for geophysical investigations of marine magnetic anomalies caused by magnetization in upper-crustal structures. We measured the geomagnetic field using a three-component magnetometer during this cruise.

(3) Instruments and Methods

A shipboard three-component magnetometer system (SFG2018, Tierra Tecnica) is installed onboard the R/V Mirai. Three-axis flux-gate sensors with ring-cored coils are fixed on the foremast. Outputs from the sensors are digitized by a 20-bit A/D converter (1 nT/LSB) and sampled eight times per second. Yaw (heading), pitch and roll are measured by the Inertial Navigation System (INS) used for controlling the attitude of the Doppler radar. The ship's position (differential GNSS), speed over ground and gyro data are taken from the LAN every second.

The relation between a magnetic field vector observed onboard, H_{ob}, (in the ship's fixed coordinate system) and the geomagnetic field vector, F, (in the Earth's fixed coordinate system) can be expressed as follows:

$$\mathbf{H}_{ob} = \widetilde{\mathbf{A}} \ \widetilde{\mathbf{R}} \ \widetilde{\mathbf{P}} \ \widetilde{\mathbf{Y}} \ \mathbf{F} + \mathbf{H}_p \qquad \text{(a)}$$

where $\widetilde{\mathbf{R}}$, $\widetilde{\mathbf{P}}$ and $\widetilde{\mathbf{Y}}$ are the matrices of rotation due to roll, pitch and heading of the ship, respectively. $\widetilde{\mathbf{A}}$ is a 3×3 matrix that represents the magnetic susceptibility of the ship, and $\mathbf{H}_p$ is a magnetic field vector produced by a permanent magnetic moment of the ship's body. Rearrangement of Eq. (a) gives the following:

$$\widetilde{\mathbf{B}} \ \mathbf{H}_{ob} + \mathbf{H}_{bp} = \widetilde{\mathbf{R}} \ \widetilde{\mathbf{P}} \ \widetilde{\mathbf{Y}} \ \mathbf{F} \qquad \text{(b)}$$

where $\widetilde{\mathbf{B}} = \widetilde{\mathbf{A}}^{-1}$ and $\mathbf{H}_{bp} = -\widetilde{\mathbf{B}} \ \mathbf{H}_p$. The magnetic field, F, can be obtained by measuring , $\widetilde{\mathbf{R}}$, $\widetilde{\mathbf{P}}$, $\widetilde{\mathbf{Y}}$ and $\mathbf{H}_{ob}$, if $\widetilde{\mathbf{B}}$ and $\mathbf{H}_{bp}$ are known. Twelve constants in $\widetilde{\mathbf{B}}$ and $\mathbf{H}_{bp}$ can be determined by measuring the variation of $\mathbf{H}_{ob}$ with $\widetilde{\mathbf{R}}$, $\widetilde{\mathbf{P}}$ and $\widetilde{\mathbf{Y}}$ at a place where the geomagnetic field, F, is known.

(4) Preliminary Results

The results will be published after primary processing.

(5) Data archives

The data obtained during the cruise will be submitted to the Data Management Group of JAMSTEC, and they will be made available to the public via the "Data Research System for Whole Cruise Information in JAMSTEC (DARWIN)" on the JAMSTEC website (http://www.godac.jamstec.go.jp/darwin/e)

(6) Remarks

1. For calibration of the ship's magnetic effect, we conducted "figure-of-eight" turns (a pair of clockwise and anticlockwise rotations) for the following periods at the listed positions.

05:45–06:15 UTC on 12 October 2019 at around 73-46°N, 145-10°W

04:46–05:15 UTC on 24 October 2019 at around 77-15°N, 164-00°W

04:00–04:20 UTC on 07 November 2019 at around 40-18°N, 145-59°E

2. During the following period, navigational data (i.e., Position, COG, SOG LOG, Heading and Depth) were not updated owing to server error.

05:36:11–05:36:24 UTC on 29 September 2019

3. During the following periods, data acquisition was stopped.

19:39:54–19:40:16 UTC on 14 October 2019

23:41:03–23:42:17 UTC on 14 October 2019

6. Notice on using

This cruise report is preliminary but it represents final documentation as of the end of the cruise. This report might not be corrected even if changes regarding its content (e.g., taxonomic classifications) are found after its publication. Moreover, this report might also be changed without notice. Data in this cruise report might be raw or unprocessed. If you intend to use or to refer to the data presented in this report, please ask the Chief Scientist for the latest information. Users of the data or results presented in this cruise report are requested to submit their results to the Planning Group, Research Fleet Department, Marine Technology and Engineering Center of JAMSTEC.

E-mail: submit-rv-cruise@jamstec.go.jp